

THE WAS JUNI JUNI

LIBRARY Michigan State University

This is to certify that the thesis entitled

Preliminary Investigation of Negative Impedance Converters with Microstrip Lines

presented by

Rodolph Sanon, Jr.

has been accepted towards fulfillment of the requirements for the

Master of Science

degree in

Electrical and Computer Engineering

Major Professor's Signature

02 Hay 2008

Date

MSU is an affirmative-action, equal-opportunity employer

PLACE IN RETURN BOX to remove this checkout from your record.

TO AVOID FINES return on or before date due.

MAY BE RECALLED with earlier due date if requested.

DATE DUE	DATE DUE	DATE DUE

5/08 K:/Proj/Acc&Pres/CIRC/DateDue.indd

Preliminary Investigation of Negative Impedance Converters with Microstrip Lines

By

Rodolph Sanon, Jr.

A THESIS

Submitted to
Michigan State University
in partial fulfillment of the requirements
for the degree of

MASTER OF SCIENCE

Department of Electrical and Computer Engineering

2008

ABSTRACT

Preliminary Investigation of Negative Impedance Converters with Microstrip Lines

By

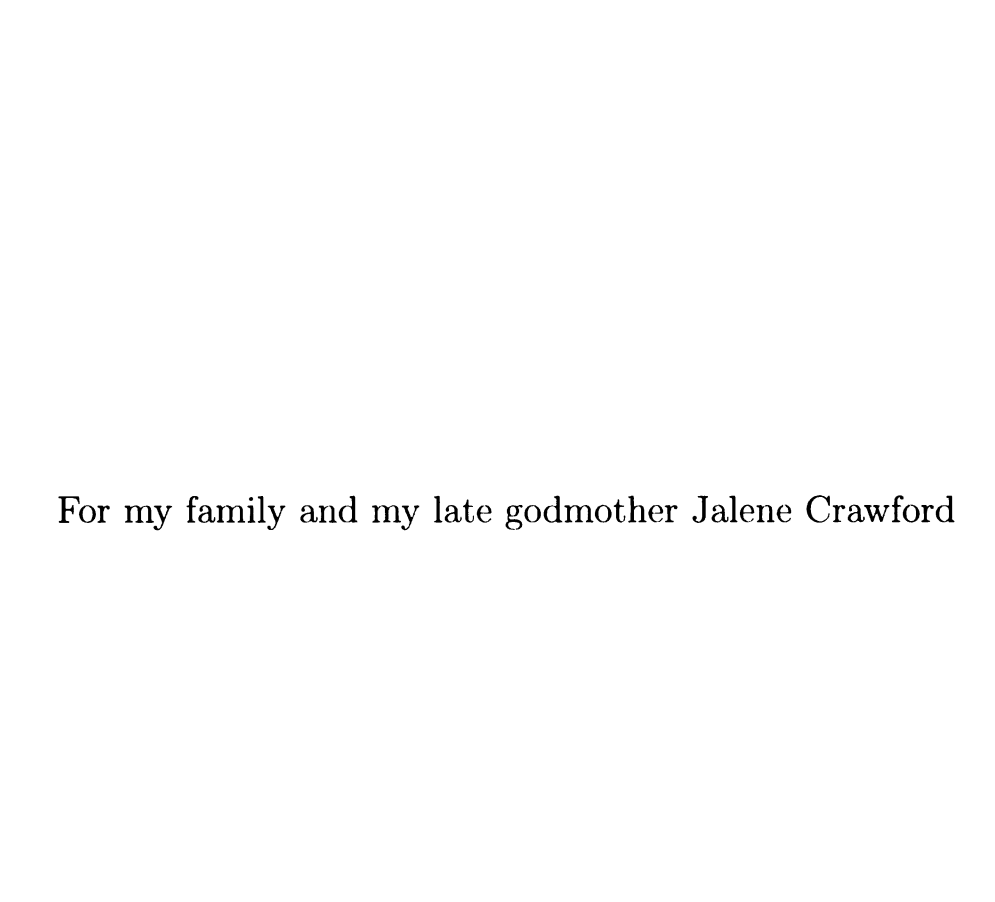
Rodolph Sanon, Jr.

The purpose of this thesis is to design a negative impedance converter (NIC) such that it functions as a load to a microstrip transmission line. Like other transmission lines, the performance of the microstrip depends on its load impedance which determines the reflection of a wave traveling along the line at the load. The wave characteristics of the microstrip for a traditional – positive – load impedance, a short circuit, and an open circuit are already known. However, the predictability of the performance of a microstrip with negative load impedance is not well understood.

In order to observe the behavior of a microstrip with a negative load impedance, an electronic device must be designed, built, implemented, and integrated to the microstrip. In this thesis, a theoretical model of a NIC will be simulated with a microstrip such that it behaves as its load impedance. Since microstrip lines are generally observed at high frequencies, the NIC must be designed to optimally perform at the desired frequency bandwidth of interest, in this case C-band (6-8 GHz).

A technique called de-embedding will be used to attach the NIC to a microstrip line. This process will detail how the NIC affects the microstrip's performance. The means of how it will be done is through the *Thru-Reflect-Line* (TRL) calibration technique. The microstrip will be modeled such that it will be de-embedded using the calibration technique. In addition, a parameter study will be performed to characterize the behavior of the microstrip with a NIC.

Copyright by
Rodolph Sanon, Jr.
2008



ACKNOWLEDGMENTS

A lot of people have been involved directly and indirectly for their contributions for the work displayed here in this thesis and many other things during my time at Michigan State. I would first like to thank my advisor Dr. Leo Kempel for helping me in all phases in conducting this work. I am thankful to work as your student and to find a project as stimulating and challenging as this one. You also gave me a valuable perspective in exploring opportunities in industry and academia and will be a valuable resource in my future endeavors. To Dr. Edward J. Rothwell, my surrogate advisor, who helped me understand what it takes to be a graduate student and the daily struggles that come with it. To Dr. Shanker B. for helping me establish a means to think critically, even though my head split in two in the process. To the students of the Electromagnetics Research Group for making my time as a graduate special. We had some fun times at the Engineering Library.

Thanks to Dr. Percy Pierre and Dr. Barbara O'Kelly for their support through the Sloan Fellowship Program. To Sheryl Hulet, Vanessa Mitchner, and members of the staff of the Department of Electrical and Computer Engineering for their support. To Michael Archbold for providing an opportunity to go to graduate school when no opportunity existed due to unfortunate circumstances.

A special thank you to friends and family around the country for their love and support during my time in graduate school at Michigan State. A personal thanks to the family of my late godmother Jalene Crawford who helped me establish discipline when my parents were watching over me in my youth.

TABLE OF CONTENTS

LIST O	F TABI	LES	ii
LIST O	F FIGU	RES	ix
KEY TO	O SYM	BOLS AND ABBREVIATIONS xi	١V
CHAPT Introduc			1
CHAPT Negative		lance Converters	3
2.1	Foster' 2.1.1 2.1.2 2.1.3	The Complex Poynting Theorem	3 4 6 9
2.2	Operate 2.2.1 2.2.2 2.2.3 2.2.4	Voltage Inversion NICs vs. Current Inversion NICs	12 13 15 17
CHAPT De-Emb		Test Fixtures and Microstrip Circuits	29
3.1	Micros 3.1.1 3.1.2	Transmission Line Theory	31 32 34 38 39 40
3.2	3.2.1	Scattering, Transmission, and ABCD Parameters53.2.1.1 The Transmission Matrix53.2.1.2 The Scattering Matrix53.2.1.3 The ABCD Transmission Matrix53.2.1.4 Transformation between Parameters5	45 50 55 56 57
	3.2.2	3.2.2.1 The Thru Measurement 6 3.2.2.2 The Reflect Measurement 6 3.2.2.3 The Line Measurement 6	59 50 51 54

CHAP	ΓER 4	
Designi	ng and Modeling the Microstrip and the NIC	73
4.1	Microstrip Design	73
4.2	Negative Impedance Converter Circuit Design	7 5
4.3	De-embedding the Test Port Cables and the Microstrip	88 89 89
4.4	4.4.1 Modeling the Test Fixture	92 93 104 115
4.5	Comparing Computational Results with Simulated Results	119
CHAPT Conclus	ΓER 5 sions and Future Work	164
BIBLIC	OGRAPHY	167

LIST OF TABLES

Table 4.1	Values of Z_{in} for negative capacitor with load capacitance of 10 pF in C-band	117
Table 4.2	Values of Z_{in} for negative inductor with load inductance of 0.1 nH in C-band	118

LIST OF FIGURES

Figure 2.1	Two-port network hybrid parameter model [1]	13
Figure 2.2	Hybrid parameter model for VINIC [1]	14
Figure 2.3	Hybrid parameter model for CINIC [1]	15
Figure 2.4	GNIC circuit [7]	16
Figure 2.5	FNIC circuit [7]	16
Figure 2.6	Open-circuit stable NIC [7]	17
Figure 2.7	Short-circuit stable NIC [7]	18
Figure 2.8	NIC terminated at both its ports [7]	19
Figure 2.9	npn and pnp BJT [10]	20
Figure 2.10	The BJT in active mode viewed as two diodes [12]	22
Figure 2.11	The Early effect [11]	23
Figure 2.12	Voltage-current relationship for both BJTs [10]	24
Figure 2.13	n-channel and p-channel MOSFET [12]	26
Figure 2.14	Voltage-current relationship for n -channel MOSFET [11]	27
Figure 3.1	Test fixture diagram locating the measurement and device planes	30
Figure 3.2	Transmission line model [5] \dots	31
Figure 3.3	Transmission line terminated with load impedance $[5]$	35
Figure 3.4	Wave reflection and transmission at intersection of transmission lines with different characteristic impedances [5]	38
Figure 3.5	Transmission line terminated with an open circuit $[5]$	40
Figure 3.6	Transmission line terminated with a short circuit [5]	41
Figure 3.7	Microstrip geometry [5, 20]	42
Figure 3.8	Field lines due to microstrip [5]	43
Figure 3.9	Flow chart describing the de-embedding process [19]	47
Figure 3.10	Two-port S-parameter network [18]	48
Figure 3.11	Two-port S-parameter network represented as a signal flow graph [5]	48
Figure 3.12	Signal flow graph representing the test fixture halves and the DUT [16]	50
Figure 3.13	Schematic representing the test fixture halves and the DUT $[5]$.	54
Figure 3.14	Two-port ABCD-parameter network for series impedance $[5]$	57
Figure 3.15	Schematic of Thru Standard Connection [5, 18]	60

Figure 3.16	Signal flow graph of <i>Thru</i> Standard Connection [5]	61
Figure 3.17	Schematic of Reflect Standard Connection [5, 18]	62
Figure 3.18	Signal flow of Reflect Standard Connection [5]	63
Figure 3.19	Schematic of <i>Line</i> Standard Connection [5, 18]	65
Figure 3.20	Schematic of <i>Line</i> Standard Connection [5]	65
Figure 4.1	Negative impedance converter with capacitively terminated load [7, 9]	75
Figure 4.2	Negative impedance converter with inductively terminated load [7, 9]	76
Figure 4.3	High frequency small-signal equivalent circuit of a BJT [10]	77
Figure 4.4	High frequency small-signal equivalent circuit of a MOSFET [10]	77
Figure 4.5	Typical frequency response of a BJT [11]	78
Figure 4.6	Ebers-Moll model of npn BJT [10]	80
Figure 4.7	Basic common-emitter amplifier [24]	81
Figure 4.8	Input voltage-current relationship of common-emitter amplifier [24]	83
Figure 4.9	Output voltage-current relationship of common-emitter amplifier [24]	83
Figure 4.10	Transfer characteristic of common-emitter amplifier [11]	84
Figure 4.11	Basic common-base amplifier [24]	84
Figure 4.12	Input voltage-current relationship of common-base amplifier $[24]$.	86
Figure 4.13	Output voltage-current relationship of common-base amplifier [24]	86
Figure 4.14	Transfer characteristic of common-base amplifier [11]	87
Figure 4.15	Test fixture modeled as a lossy transmission line [16]	93
Figure 4.16	Test fixture modeled as a lossless transmission line [16]	94
Figure 4.17	Magnitude of transmission coefficient for <i>Thru</i> standard of the test fixture	98
Figure 4.18	Phase of transmission coefficient for Thru standard of the test fixture	99
Figure 4.19	Magnitude of reflection coefficient for <i>Reflect</i> standard of the test fixture	100
Figure 4.20	Phase of reflection coefficient for Reflect standard of the test fixture	101
Figure 4.21	Magnitude of transmission coefficient for <i>Line</i> standard of the test fixture	102
Figure 4.22	Phase of transmission coefficient for <i>Line</i> standard of the test fixture?	103
Figure 4.23	Magnitude of reflection coefficient for <i>Thru</i> standard of the microstrip (Sonnet vs. Ansoft Designer)	105

Figure 4.24	Phase of reflection coefficient for <i>Thru</i> standard of the microstrip (Sonnet vs. Ansoft Designer)	.06
Figure 4.25	Magnitude of reflection coefficient for <i>Reflect</i> standard of the microstrip (Sonnet vs. Ansoft Designer)	.07
Figure 4.26	Phase of reflection coefficient for <i>Reflect</i> standard of the microstrip (Sonnet vs. Ansoft Designer)	.08
Figure 4.27	Magnitude of reflection coefficient for <i>Line</i> standard of the microstrip (Sonnet vs. Ansoft Designer)	.09
Figure 4.28	Phase of reflection coefficient for <i>Line</i> standard of the microstrip (Sonnet vs. Ansoft Designer)	.10
Figure 4.29	Magnitude of transmission coefficient for <i>Thru</i> standard of the microstrip (Sonnet vs. Ansoft Designer)	11
Figure 4.30	Phase of transmission coefficient for <i>Thru</i> standard of the microstrip (Sonnet vs. Ansoft Designer)	.12
Figure 4.31	Magnitude of transmission coefficient for <i>Line</i> standard of the microstrip (Sonnet vs. Ansoft Designer)	.13
Figure 4.32	Phase of transmission coefficient for <i>Line</i> standard of the microstrip (Sonnet vs. Ansoft Designer)	.14
Figure 4.33	Negative impedance converter with capacitively terminated load . $$ 1	.16
Figure 4.34	Negative impedance converter with inductively terminated load $$. $$ 1	16
Figure 4.35	Magnitude of reflection coefficient of full-length microstrip vs. cascaded half-length microstrips (Sonnet vs. Ansoft Designer) 1	.21
Figure 4.36	Phase of reflection coefficient of full-length microstrip vs. cascaded half-length microstrips (Sonnet vs. Ansoft Designer)	.22
Figure 4.37	Magnitude of transmission coefficient of full-length microstrip vs. cascaded half-length microstrips (Sonnet vs. Ansoft Designer) 1	.23
Figure 4.38	Phase of transmission coefficient of full-length microstrip vs. cascaded half-length microstrips (Sonnet vs. Ansoft Designer) 1	.24
Figure 4.39	Magnitude of reflection coefficient of cascaded half-length microstrips with 50 - Ω resistor in between (Sonnet vs. Ansoft Designer) 1	.27
Figure 4.40	Phase of reflection coefficient of cascaded half-length microstrips with $50-\Omega$ resistor in between (Sonnet vs. Ansoft Designer)	128
Figure 4.41	Magnitude of transmission coefficient of cascaded half-length microstrips with 50 - Ω resistor in between (Sonnet vs. Ansoft Designer) 1	29
Figure 4.42	Phase of transmission coefficient of cascaded half-length microstrips with $50-\Omega$ resistor in between (Sonnet vs. Ansoft Designer) 1	30

Figure 4.43	Magnitude of reflection coefficient of cascaded half-length microstrips with 75- Ω resistor in between (Sonnet vs. Ansoft Designer)131
Figure 4.44	Phase of reflection coefficient of cascaded half-length microstrips with 75- Ω resistor in between (Sonnet vs. Ansoft Designer) 132
Figure 4.45	Magnitude of transmission coefficient of cascaded half-length microstrips with 75- Ω resistor in between (Sonnet vs. Ansoft Designer)133
Figure 4.46	Phase of transmission coefficient of cascaded half-length microstrips with 75- Ω resistor in between (Sonnet vs. Ansoft Designer)134
Figure 4.47	Magnitude of reflection coefficient of cascaded half-length microstrips with 100- Ω resistor in between (Sonnet vs. Ansoft Designer)135
Figure 4.48	Phase of reflection coefficient of cascaded half-length microstrips with 100- Ω resistor in between (Sonnet vs. Ansoft Designer) 136
Figure 4.49	Magnitude of transmission coefficient of cascaded half-length microstrips with 100 - Ω resistor in between (Sonnet vs. Ansoft Designer) 137
Figure 4.50	Phase of transmission coefficient of cascaded half-length microstrips with 100- Ω resistor in between (Sonnet vs. Ansoft Designer)138
Figure 4.51	Magnitude of reflection coefficient of cascaded half-length microstrips with 10-pF capacitor in between (Sonnet vs. Ansoft Designer)
Figure 4.52	Phase of reflection coefficient of cascaded half-length microstrips with 10-pF capacitor in between (Sonnet vs. Ansoft Designer) 140
Figure 4.53	Magnitude of transmission coefficient of cascaded half-length microstrips with 10-pF capacitor in between (Sonnet vs. Ansoft Designer)
Figure 4.54	Phase of transmission coefficient of cascaded half-length microstrips with 10-pF capacitor in between (Sonnet vs. Ansoft Designer)
Figure 4.55	Magnitude of reflection coefficient of cascaded half-length microstrips with 0.1-nH inductor in between (Sonnet vs. Ansoft Designer)
Figure 4.56	Phase of reflection coefficient of cascaded half-length microstrips with 0.1-nH inductor in between (Sonnet vs. Ansoft Designer) 144
Figure 4.57	Magnitude of transmission coefficient of cascaded half-length microstrips with 0.1-nH inductor in between (Sonnet vs. Ansoft Designer)
Figure 4.58	Phase of transmission coefficient of cascaded half-length microstrips with 0.1-nH inductor in between (Sonnet vs. Ansoft Designer)

Figure 4.59	Magnitude of reflection coefficient of cascaded half-length microstrips with -10 -pF capacitor in between (Sonnet vs. Ansoft Designer)	147
Figure 4.60	Phase of reflection coefficient of cascaded half-length microstrips with -10 -pF capacitor in between (Sonnet vs. Ansoft Designer) .	148
Figure 4.61	Magnitude of transmission coefficient of cascaded half-length microstrips with -10 -pF capacitor in between (Sonnet vs. Ansoft Designer)	149
Figure 4.62	Phase of transmission coefficient of cascaded half-length microstrips with -10 -pF capacitor in between (Sonnet vs. Ansoft Designer)	150
Figure 4.63	Magnitude of reflection coefficient of cascaded half-length microstrips with -0.1 -nH inductor in between (Sonnet vs. Ansoft Designer)	151
Figure 4.64	Phase of reflection coefficient of cascaded half-length microstrips with -0.1 -nH inductor in between (Sonnet vs. Ansoft Designer) .	152
Figure 4.65	Magnitude of transmission coefficient of cascaded half-length microstrips with -0.1 -nH inductor in between (Sonnet vs. Ansoft Designer)	153
Figure 4.66	Phase of transmission coefficient of cascaded half-length microstrips with -0.1 -nH inductor in between (Sonnet vs. Ansoft Designer)	154
Figure 4.67	Magnitude of reflection coefficient of parameter study of cascaded system with capacitor varied from 10 pF to -10 pF	156
Figure 4.68	Phase of reflection coefficient of parameter study of cascaded system with capacitor varied from 10 pF to -10 pF \dots	157
-	Magnitude of transmission coefficient of parameter study of cascaded system with capacitor varied from 10 pF to -10 pF	158
Figure 4.70	Phase of transmission coefficient of parameter study of cascaded system with capacitor varied from 10 pF to -10 pF	159
Figure 4.71	Magnitude of reflection coefficient of parameter study of cascaded system with inductor varied from $0.1~\mathrm{nH}$ to $-0.1~\mathrm{nH}$	160
Figure 4.72	Phase of reflection coefficient of parameter study of cascaded system with inductor varied from $0.1~\text{nH}$ to $-0.1~\text{nH}$	161
Figure 4.73	Magnitude of transmission coefficient of parameter study of cascaded system with inductor varied from 0.1 nH to -0.1 nH	162
Figure 4.74	Phase of transmission coefficient of parameter study of cascaded system with inductor varied from 0.1 nH to -0.1 nH	163

KEY TO SYMBOLS AND ABBREVIATIONS

AC: Alternating Current

BJT: Bipolar-Junction Transistor

CINIC: Current Inversion Negative Impedance Converter

DC: Direct Current

DUT: Device Under Test

EM: Electromagnetic

FET: Field-Effect Transistor

FNIC: Floating Negative Impedance Converter

GNIC: Grounded Negative Impedance Converter

JFET: Junction Field-Effect Transistor

MESFET: Metal-Semiconductor Field-Effect Transistor

MOSFET: Metal-Oxide Semiconductor Field-Effect Transistor

NIC: Negative Impedance Converter

PCB: Printed Circuit Board

RF: Radio Frequency

RMS: Root-Mean-Square

SMT: Surface Mount Technology

SWR: Standing Wave Ratio

TE: Transverse Electric

TEM: Transverse Electromagnetic

TM: Transverse Magnetic

TRL: Thru-Reflect-Line

VINIC: Voltage Inversion Negative Impedance Converter

VNA: Vector Network Analyzer

VSWR: Voltage Standing Wave Ratio

CHAPTER 1

INTRODUCTION

In recent decades, the electronic industry has manufactured and sold products that use high frequency technology. More importantly, radio-frequency (RF) and circuit design engineers have designed, built, and tested devices that can be used for microwave and RF applications. One type of high frequency device that is commonly integrated with electrical circuit components is the microstrip transmission line. In this thesis, a theoretical negative impedance converter will be connected to a microstrip transmission line such that the negative impedance converter acts as a load to the microstrip. Its characteristics will be observed in C-band or the frequency range of 6 to 8 Gigahertz (GHz).

Like other transmission lines, the performance of the microstrip is dependent on its load impedance. The load impedance of the microstrip impacts how the a wave traveling along the line will reflect at the load. Transmission line theory has shown how a traditional – positive – load impedance, a short circuit, and an open circuit will affect the wave characteristic of the microstrip. These wave characteristics include the input impedance and the dimensions of the microstrip. However, the predictability of the performance of a microstrip with negative load impedance is not well understood.

When conducting microstrip analysis with a negative load impedance, an electronic device must be designed, built, implemented, and integrated to the microstrip. In this case the negative load impedance will be realized through a negative impedance converter (NIC). Constructing a negative impedance converter requires knowledge of Foster's reactance theorem, its relation to NICs, the types of negative impedance converters that exist, and the active and passive circuit elements needed to implement them. Chapter 2 covers these concepts.

Chapter 3 describes the theory of designing a microstrip circuit. Topics also included are transmission line theory and microwave network analysis. In addition, it also shows the reader how to integrate the microstrip line with the NIC. The process which it take is called de-embedding and it will be done by using *Thru-Reflect-Line* (TRL) calibration. This is important because although microstrip lines can be integrated with electrical circuit components, the high frequency properties if the NIC must be inferred from measurements that include a device-under-test (DUT) and a test fixture (e.g. the microstrip line).

Chapter 4 displays the design and operation of the type of NIC that will be used for testing. It also has a design procedure for performing the TRL calibration standards using a HP 8510 vector network analyzer (VNA). In addition, data will be collected to compare computational results using circuit design software simulation programs. These results explain how the NIC affects the microstrip's performance.

CHAPTER 2

NEGATIVE IMPEDANCE CONVERTERS

In order to know how a NIC works, one must know the concept of Foster's reactance theorem. The relation between Foster's reactance theorem and NICs is that negative impedance converters are composed of non-Foster circuit elements. Aberle and Loepsinger-Romak [1] state that NICs are circuits that do not obey Foster's reactance theorem; hence, these type of circuits are classified as non-Foster circuits [1]. This chapter will describe Foster's reactance theorem, how NICs are implemented and operated, different models of NICs, and the types of classifications of NICs that exist.

2.1 Foster's Reactance Theorem

Comprehending Foster's reactance theorem requires deriving the complex Poynting theorem by applying Maxwell's equations in the frequency (phasor) domain and using microwave network analysis. Rothwell [2] does point out, however, that if Maxwell's equations are applied to obtain Poynting's theorem, it must be assumed that the fields are linked to an energy flux that propagates at the speed of light and the region of space that is observed is symmetric [2]. In addition, it is postulated that the electromagnetic (EM) fields are time-harmonic [3]. Using the complex Poynting vector, $\vec{S} = \frac{1}{2}\Re[\vec{E}\times\vec{H}^*]$, where the asterisk (*) denotes the complex conjugate of the vector field, the complex Poynting theorem can be evaluated. The $\frac{1}{2}$ term arises from the fact that the time-harmonic fields are the root-mean-square (RMS) values of the instantaneous fields (e.g., $peak = rms\sqrt{2}$); the instantaneous fields correspond to peak values of the EM fields [4].

2.1.1 The Complex Poynting Theorem

Using Faraday's Law and Ampere's Law,

$$\nabla \times \overrightarrow{E} = -j\omega \mu \overrightarrow{H} \tag{2.1a}$$

$$\nabla \times \overrightarrow{H} = \overrightarrow{J} + j\omega \epsilon \overrightarrow{E} \tag{2.1b}$$

the complex average power density can be evaluated.

By dotting (2.1a) by \overrightarrow{H}^* and the conjugate of (2.1b) by \overrightarrow{E} and using $\overrightarrow{J} = \overrightarrow{J}_i + \overrightarrow{J}_c$ where \overrightarrow{J}_i is the impressed current density due to an external source and $\overrightarrow{J}_c = \sigma \overrightarrow{E}$ is the conduction current density, the following equation is obtained

$$\overrightarrow{H}^* \cdot (\nabla \times \overrightarrow{E}) = -j\omega \mu \overrightarrow{H} \cdot \overrightarrow{H}^*$$
 (2.2a)

$$\overrightarrow{E} \cdot (\nabla \times \overrightarrow{H}^*) = \overrightarrow{E} \cdot \overrightarrow{J}_i^* + \sigma \overrightarrow{E} \cdot \overrightarrow{E}^* + j\omega \epsilon \overrightarrow{E} \cdot \overrightarrow{E}$$
 (2.2b)

Subtracting (2.2a) from (2.2b) gives

$$\overrightarrow{E} \cdot (\nabla \times \overrightarrow{H}^*) - \overrightarrow{H}^* \cdot (\nabla \times \overrightarrow{E}) = \overrightarrow{E} \cdot \overrightarrow{J}_i^* + \sigma \overrightarrow{E} \cdot \overrightarrow{E}^* - j\omega \epsilon \overrightarrow{E} \cdot \overrightarrow{E}^* + j\omega \mu \overrightarrow{H} \cdot \overrightarrow{H}^* \quad (2.3)$$

Using the vector identity

$$\nabla \cdot (\overrightarrow{A} \times \overrightarrow{B}) = \overrightarrow{B} \cdot (\nabla \times \overrightarrow{A}) - \overrightarrow{A} \cdot (\nabla \times \overrightarrow{B}) \tag{2.4}$$

and dividing by 2, (2.3) is reduced to

$$\frac{1}{2} \left[\nabla \cdot (\overrightarrow{H}^* \times \overrightarrow{E}) \right] = \frac{1}{2} \overrightarrow{E} \cdot \overrightarrow{J}_i^* + \frac{1}{2} \sigma |\overrightarrow{E}|^2 + \frac{1}{2} j \omega \mu |\overrightarrow{H}|^2 - \frac{1}{2} j \omega \epsilon |\overrightarrow{E}|^2$$
 (2.5a)

or

$$-\frac{1}{2}\left[\nabla\cdot(\overrightarrow{E}\times\overrightarrow{H}^*)\right] = \frac{1}{2}\overrightarrow{E}\cdot\overrightarrow{J}_i^* + \frac{1}{2}\sigma|\overrightarrow{E}|^2 + j2\omega\left[\frac{1}{4}(\mu|\overrightarrow{H}|^2 - \epsilon|\overrightarrow{E}|^2)\right]$$
(2.5b)

Equation (2.5) characterizes energy conservation in point (differential) form. To express (2.5) in integral form, it has to be integrated over a volume region of space V and the divergence theorem needs to be applied to the left side of (2.5) to apply the energy conservation equation to an entire region

$$-\iiint_{V} \nabla \cdot \frac{1}{2} [\overrightarrow{E} \times \overrightarrow{H}^{*}] = \frac{1}{2} \oiint_{S} (\overrightarrow{E} \times \overrightarrow{H}^{*}) \cdot \widehat{n} dS = \frac{1}{2} \iiint_{V} (\overrightarrow{E} \cdot \overrightarrow{J}_{i}^{*}) dV + \frac{1}{2} \iiint_{V} \sigma |\overrightarrow{E}|^{2} dV + j2\omega \iiint_{V} \frac{1}{4} \left[\mu |\overrightarrow{H}|^{2} - \epsilon |\overrightarrow{E}|^{2} \right] dV$$
(2.6)

or

$$-\frac{1}{2}\iiint_{V}(\overrightarrow{E}\cdot\overrightarrow{J}_{i}^{*})dV = \frac{1}{2}\iint_{S}(\overrightarrow{E}\times\overrightarrow{H}^{*})\cdot\widehat{n}dS + \frac{1}{2}\iiint_{V}\sigma|\overrightarrow{E}|^{2}dV + j2\omega\iiint_{V}\frac{1}{4}\left[\mu|\overrightarrow{H}|^{2} - \epsilon|\overrightarrow{E}|^{2}\right]dV$$
(2.7)

which can be written as

$$P_{s} = P_{f} + P_{d} + j\omega(\overline{W_{m}} - \overline{W_{e}}) \text{ where}$$

$$P_{s} = -\frac{1}{2} \iiint_{V} (\overrightarrow{E} \cdot \overrightarrow{J}_{i}^{*}) dV = \text{complex power supplied by } \overrightarrow{J}^{i}$$
(2.8a)

$$P_f = \frac{1}{2} \oiint_S (\overrightarrow{E} \times \overrightarrow{H}^*) \cdot \widehat{n} dS = \text{complex power exiting } V$$
 (2.8b)

$$P_d = \frac{1}{2} \iiint_V \sigma |\overrightarrow{E}|^2 dV = \text{real power dissipated in lossy medium}$$
 (2.8c)

$$\overline{W_m} = \frac{1}{4} \iiint_V \mu |\overrightarrow{H}|^2 dV = \text{time-average magnetic energy}$$
 (2.8d)

$$\overline{W_e} = \frac{1}{4} \iiint_V \epsilon |\overrightarrow{E}|^2 dV = \text{time-average electric energy}$$
 (2.8e)

Equation (2.7) is referred to as the *complex Poynting theorem* and is valid only for lossless (non-dissipative) materials. The real part of (2.7) or (2.8) characterizes

a time-average power balance while the imaginary part of the (2.7) or (2.8) refers to reactive power [2, 3].

2.1.2 Microwave Network Analysis

Microwave network analysis must be applied to (2.7) or (2.8) for a N-port network to derive Foster's reactance theorem. For this particular case, a two-port network will be observed to derive Foster's reactance theorem. It is assumed that the two-port network is bounded within a perfect electric conductor except at the terminal port cross sections. It is also postulated that only the principal waveguide mode propagates in each terminal due to the fact that the terminals are far away from the network resulting in all higher-order waveguide modes decaying to an amplitude that is negligible at the reference planes. Describing the parameters for the two-port network will be described later.

Using (2.7) or (2.8) and introducing mode vectors $\hat{e} = -\hat{n} \times \hat{h}$ and $\hat{h} = \hat{n} \times \hat{e}$, mode voltage V, and mode current I (all of which are real), the transverse electric and magnetic fields can be expressed in terms of modal functions, voltages, and currents by modal expansion.

$$\overrightarrow{E}_t = \sum_{i=1}^N \widehat{e}_i V_i \tag{2.9a}$$

$$\overrightarrow{H}_t = \sum_{i=1}^N \widehat{h}_i I_i \tag{2.9b}$$

Equation (2.9) represents modal expansions of the general electric and magnetic fields of the waveguide terminal. By establishing orthogonality and using normalization for the modal fields, (2.9) is dot multiplied by arbitrary mode vectors and integrated over the cross section to get

$$\iint_{CS} \widehat{e}_i \cdot \widehat{e}_j dS = \iint_{S} \widehat{h}_i \cdot \widehat{h}_j dS = \delta_{ij}$$
(2.10)

and

$$\iint_{CS} \overrightarrow{E}_t \cdot \widehat{e}_i dS = V_i \tag{2.11a}$$

$$\iint_{CS} \overrightarrow{H}_t \cdot \widehat{h}_i dS = I_i \tag{2.11b}$$

where V_i and I_i are the modal expansion coefficients of the microwave network, CS is designated as the closed surface of the terminal, and

$$\delta_{ij} = \begin{cases} 0 & \text{if } i \neq j \\ 1 & \text{if } i = j. \end{cases}$$
 (2.12)

is the Kronecker delta function. Using (2.7), (2.10), (2.11), and the vector identity

$$\overrightarrow{A} \cdot (\overrightarrow{B} \times \overrightarrow{C}) = \overrightarrow{B} \cdot (\overrightarrow{C} \times \overrightarrow{A}) = \overrightarrow{C} \cdot (\overrightarrow{A} \times \overrightarrow{B})$$
 (2.13)

the modal power transport for ports 1 and 2 is

$$P_{in} = -P_{f}$$

$$= -\frac{1}{2} \oint_{S} (\overrightarrow{E} \times \overrightarrow{H}^{*}) \cdot \widehat{n} dS = -\frac{1}{2} \oint_{S} (\widehat{n} \times \overrightarrow{E}) \times \overrightarrow{H}^{*} dS$$

$$= -\frac{1}{2} \iint_{CS} (\overrightarrow{E} \times \overrightarrow{H}^{*}) \cdot \widehat{n} dS = \iint_{CS} \sum_{i=1}^{N} (\widehat{e}_{i} V_{i}) \times \sum_{j=1}^{N} (\widehat{h}_{j} I_{j}^{*}) \cdot \widehat{n} dS$$

$$= \sum_{i=1}^{N} \sum_{j=1}^{N} \frac{1}{2} V_{i} I_{j}^{*} \iint_{CS} \widehat{e}_{i} \cdot (-\widehat{n} \times \widehat{h}_{j}) dS = \sum_{i=1}^{N} \sum_{j=1}^{N} \frac{1}{2} V_{i} I_{j}^{*} \iint_{CS} \widehat{e}_{i} \cdot \widehat{e}_{j} dS$$

$$= \sum_{i=1}^{N} \sum_{j=1}^{N} \frac{1}{2} V_{i} I_{j}^{*} \delta_{ij} = \frac{1}{2} V_{i} I_{i}^{*} = P_{d} + j 2\omega (\overline{W_{m}} - \overline{W_{e}})$$

$$(2.14)$$

The reason why there is no P_s term in (2.14) is because there the microwave network that is being observed is a source-free region. Now knowing the power entering

ports 1 and 2, the input impedance and admittance can be computed.

$$Z_{in} = R + jX = \frac{P_{in}}{|I|^2} = \frac{P_d + j2\omega(\overline{W_m} - \overline{W_e})}{|I|^2}$$
 (2.15)

$$Y_{in} = G + jB = \frac{P_{in}^*}{|V|^2} = \frac{P_d - j2\omega(\overline{W_m} - \overline{W_e})}{|V|^2}$$
 (2.16)

By examining equations (2.14), (2.15), and (2.16), the following observations can be made:

- 1. There is no dissipated power in a lossless network resulting in no input resistance and no input conductance (R=0, G=0 and $P_d=0$).
- 2. The input resistance R (or conductance G) is always positive for a lossy network.
- 3. At resonance, the input reactance X and input susceptance B are zero.
- 4. The input resistance (or conductance) is an even function of ω while the input reactance (or susceptance) is an odd function of ω where they both depend on frequency.

The relation for frequency is $\omega = 2\pi f$ where ω is the radial frequency and f is the more commonly used temporal frequency.

Since the lossless case is only being considered, (2.14) will be imaginary making V out of phase with I^* by 90 degrees (90°). The boundary conditions ($\widehat{n} \times \overrightarrow{E} = 0$ and $\widehat{n} \times \overrightarrow{H} = \overrightarrow{J}$ for a perfect electric conductor) and the source-free Maxwell curl equations where $\overrightarrow{J} = 0$ from (2.1) associated with the microwave network are only satisfied when \overrightarrow{E} is real and \overrightarrow{H} is imaginary over the surface area S and within the volume region of space V. The uniqueness theorem requires this particular solution to be the only solution and making the EM fields \overrightarrow{E} and \overrightarrow{H} in phase quadrature within the network.

2.1.3 Verifying Foster's Reactance Theorem

Theorem 2.1 (Foster's Reactance Theorem) The slope of the reactance or susceptance with respect to frequency of a lossless n-port network is always positive. In other words,

$$\frac{dX}{d\omega} > 0 \quad and \quad \frac{dB}{d\omega} > 0$$
 (2.17)

Proving Foster's reactance theorem requires examination how the source-free Maxwell curl equations change with frequency. Taking the derivative of (2.1) with respect to ω and setting \overrightarrow{J} to zero, (2.1) becomes

$$\nabla \times \frac{\partial \overrightarrow{E}}{\partial \omega} = -j\mu \overrightarrow{H} - j\omega \mu \frac{\partial \overrightarrow{H}}{\partial \omega}$$
 (2.18a)

$$\nabla \times \frac{\partial \overrightarrow{H}}{\partial \omega} = -j\epsilon \overrightarrow{E} - j\omega\epsilon \frac{\partial \overrightarrow{E}}{\partial \omega}$$
 (2.18b)

Dot multiplying (2.18a) by \overrightarrow{H}^* and the conjugate of (2.18b) by $\frac{\partial \overrightarrow{E}}{\partial \omega}$ and subtract the two results in

$$\nabla \cdot \left(\frac{\partial \overrightarrow{E}}{\partial \omega} \times \overrightarrow{H}^* \right) = -j\mu |\overrightarrow{H}|^2 - j\omega\mu \overrightarrow{H}^* \cdot \frac{\partial \overrightarrow{H}}{\partial \omega} + j\omega\epsilon \overrightarrow{E}^* \cdot \frac{\partial \overrightarrow{E}}{\partial \omega}$$

$$\nabla \cdot \left(\frac{\partial \overrightarrow{H}}{\partial \omega} \times \overrightarrow{E}^* \right) = -j\epsilon |\overrightarrow{E}|^2 - j\omega\mu \frac{\partial \overrightarrow{E}}{\partial \omega} \cdot \overrightarrow{E}^* + j\omega \overrightarrow{H}^* \cdot \frac{\partial \overrightarrow{H}}{\partial \omega}$$

$$\nabla \cdot \left[\frac{\partial \overrightarrow{E}}{\partial \omega} \times \overrightarrow{H}^* - \frac{\partial \overrightarrow{H}}{\partial \omega} \times \overrightarrow{E}^* \right] = -j\mu |\overrightarrow{H}|^2 - j\epsilon |\overrightarrow{E}|^2$$
(2.19)

Integrating (2.19) throughout the region of space, in this case the microwave network, and applying the divergence theorem to the left-hand side of (2.19) creates the

following expression

$$\iiint_{V} \nabla \cdot \left[\frac{\partial \overrightarrow{E}}{\partial \omega} \times \overrightarrow{H}^{*} - \frac{\partial \overrightarrow{H}}{\partial \omega} \times \overrightarrow{E}^{*} \right] dV = \oiint_{S} \left[\frac{\partial \overrightarrow{E}}{\partial \omega} \times \overrightarrow{H}^{*} - \frac{\partial \overrightarrow{H}}{\partial \omega} \times \overrightarrow{E}^{*} \right] \cdot \widehat{n} dS$$

$$= -j \iiint_{V} \left[\mu |\overrightarrow{H}|^{2} + \epsilon |\overrightarrow{E}|^{2} \right] dV \qquad (2.20)$$

where the right-hand side of (2.20) is proportional to the total EM energy enclosed in the network. Performing modal expansion using (2.9) to (2.20) and using (2.13) and the vector identity $\hat{e} \times \hat{h} = -\hat{h} \times \hat{e}$ creates the following equation.

$$\iint_{S} \left[\frac{\partial \overrightarrow{E}}{\partial \omega} \times \overrightarrow{H}^{*} - \frac{\partial \overrightarrow{H}}{\partial \omega} \times \overrightarrow{E}^{*} \right] \cdot \widehat{n} dS = \iint_{S} \left[\left(\sum_{i=1}^{N} \frac{\partial (\widehat{c}_{i} V_{i})}{\partial \omega} \times \sum_{j=1}^{N} (\widehat{h}_{j} I_{j}^{*}) \right) - \left(\sum_{i=1}^{N} \frac{\partial (\widehat{h}_{i} I_{i})}{\partial \omega} \times \sum_{j=1}^{N} (\widehat{e}_{j} V_{j}^{*}) \right) \right] \cdot \widehat{n} dS$$

$$= \sum_{i=1}^{N} \sum_{j=1}^{N} \left[\frac{\partial V_{i}}{\partial \omega} I_{j}^{*} + \frac{\partial I_{i}}{\partial \omega} V_{j}^{*} \right] \iint_{S} (\widehat{e} \times \widehat{h}) \cdot \widehat{n} dS$$

$$= \sum_{i=1}^{N} \sum_{j=1}^{N} \left[\frac{\partial V_{i}}{\partial \omega} I_{j}^{*} + \frac{\partial I_{i}}{\partial \omega} V_{j}^{*} \right] \iint_{CS} (\widehat{e} \cdot (-\widehat{n} \times \widehat{e})) dS$$

$$= \sum_{i=1}^{N} \sum_{j=1}^{N} \left[\frac{\partial V_{i}}{\partial \omega} I_{j}^{*} + \frac{\partial I_{i}}{\partial \omega} V_{j}^{*} \right] \iint_{CS} -(\widehat{e} \cdot \widehat{e}) dS$$

$$= -\sum_{i=1}^{N} \sum_{j=1}^{N} \left[\frac{\partial V_{i}}{\partial \omega} I_{j}^{*} + \frac{\partial I_{i}}{\partial \omega} V_{j}^{*} \right] \delta_{ij}$$

$$= -\sum_{i=1}^{N} \left[I_{i}^{*} \frac{\partial V_{i}}{\partial \omega} + V_{i}^{*} \frac{\partial I_{i}}{\partial \omega} \right]$$
(2.21)

Substituting (2.21) into (2.20),

$$\sum_{i=1}^{N} \left[I_{i}^{*} \frac{\partial V_{i}}{\partial \omega} + V_{i}^{*} \frac{\partial I_{i}}{\partial \omega} \right] = j \iiint_{V} [\mu |\overrightarrow{H}|^{2} + \epsilon |\overrightarrow{E}|^{2}] dV = j2(\overline{W_{m}} - \overline{W_{e}})$$
 (2.22)

Since $\Im[Z_{in}] = \Im\left[\frac{V}{I}\right] = X = \frac{1}{B}$, it can be concluded that the frequency derivatives are

$$\frac{dX}{d\omega} = \frac{1}{jI} \frac{\partial V}{\partial \omega} \Big|_{I=constant} = \frac{4}{|I|^2} (\overline{W_m} - \overline{W_e}) > 0$$

$$\frac{dB}{d\omega} = \frac{1}{jV} \frac{\partial I}{\partial \omega} \Big|_{V=constant} = \frac{4}{|V|^2} (\overline{W_m} - \overline{W_e}) > 0 \tag{2.23}$$

and from (2.15)

$$X = \frac{4\omega}{|I|^2} (\overline{W_m} - \overline{W_e}) \tag{2.24}$$

and

$$B = \frac{4\omega}{|V|^2} (\overline{W_e} - \overline{W_m}) \tag{2.25}$$

validating Foster's reactance theorem with (2.23). The effect that results from (2.23) is that all poles and zeros of the reactance or susceptance function are simple and must alternate with respect to ω [1, 3]. In addition, $\frac{dX}{d\omega} > \frac{X}{\omega}$ and $\frac{dB}{d\omega} > \frac{B}{\omega}$ since [3]

$$\overline{W_e} = \frac{|I|^2}{8} \left[\frac{dX}{d\omega} - \frac{X}{\omega} \right] = \frac{|V|^2}{8} \left[\frac{dB}{d\omega} + \frac{B}{\omega} \right] > 0 \tag{2.26}$$

$$\overline{W_m} = \frac{|I|^2}{8} \left[\frac{dX}{d\omega} + \frac{X}{\omega} \right] = \frac{|V|^2}{8} \left[\frac{dB}{d\omega} - \frac{B}{\omega} \right] > 0$$
 (2.27)

If a network device had an impedance and admittance function that does not obey (2.23), it is classified as a "non-Foster" element. Typical non-Foster circuit elements contain active circuit components such as capacitors and inductors to produce negative inductors and negative capacitors, respectively. The negative capacitor has an input impedance function $Z_{in} = -\frac{1}{j\omega C_L}$ and the negative inductor has an input impedance function $Z_{in} = -j\omega L_L$. The negative capacitor has a load capacitance value of C_L and the negative inductor has a load inductance value of L_L . An application that is best used to visualize how negative capacitors, negative inductors and

other non-Foster circuits operate are negative impedance converters.

2.2 Operation of Negative Impedance Converters

A practical application for the theory behind non-Foster circuits are NICs. Ideally it is defined as a two-port device where the input impedance of the network is the negative impedance of the load impedance attached to the network, i.e., a capacitor or inductor, that is usually scaled by a constant creating a negative element [7]. Negative impedance converters were originally going to be used for reduction of resistive loss in electrical circuits 80 years ago [1, 6]. In the 1950s, NICs were used to develop a new type of telephone repeater that was cost-effective [6]. Recently, NICs have been used to eliminate resistive loss in amplifier-speaker systems and for impedance matching for electrically small antennas [1, 9]. Although the means of how NICs are modeled has been revolutionized, building NICs that are stable, lossless, and broadband have been quite a challenge.

In order to model an NIC, examine Figure 2.1 where $Z_{in} = -kZ_L$ with k > 0. If k = 1, the following parameters must be set

$$h_{11} = 0 (2.28)$$

$$h_{22} = 0 (2.29)$$

$$h_{12} \cdot h_{21} = 1 \tag{2.30}$$

The types of NICs that exist fall into several classifications: the type of inversion of the NIC (voltage inversion vs. current inversion), the reference level (grounded vs. floating), the stability of the NIC (open-circuit stable vs. short-circuit stable), and the type of transistor models that exist [bipolar-junction transistor (BJT) vs. field-effect transistor (FET)].

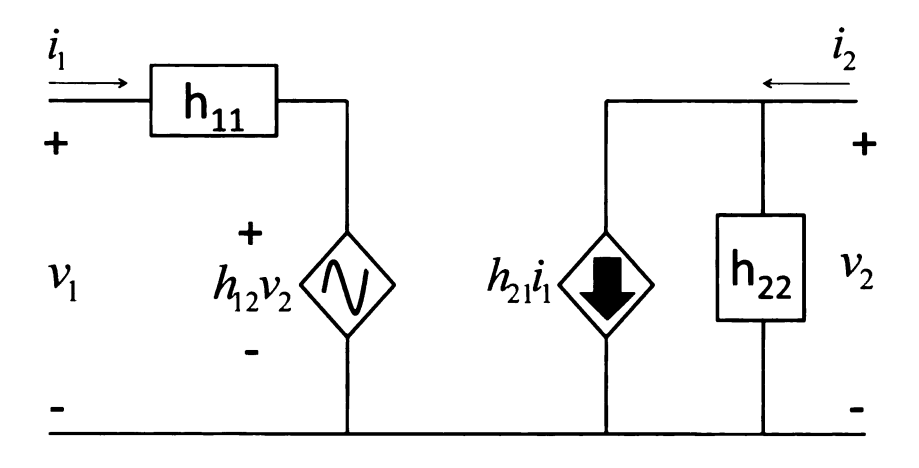


Figure 2.1. Two-port network hybrid parameter model [1]

2.2.1 Voltage Inversion NICs vs. Current Inversion NICs

Revisiting Figure 2.1, if $h_{12} = h_{21} = -1$, the NIC is categorized as a voltage inversion NIC (VINIC) while the NIC is a current inversion NIC (CINIC) if $h_{12} = h_{21} = 1$. Analyzing the hybrid parameter models for the VINIC shown in Figure 2.2 and the CINIC displayed in Figure 2.3, the following relationships are established for the VINIC

$$v_{in} = v_1 = -v_2 = -v_L (2.31a)$$

$$i_{in} = i_1 = -i_2 = i_L (2.31b)$$

$$Z_{in} = \frac{v_{in}}{i_{in}} = \frac{-v_L}{i_L} = -Z_L$$
 (2.31c)

and the CINIC

$$v_{in} = v_1 = v_2 = -v_L (2.32a)$$

$$i_{in} = i_1 = i_2 = -i_L (2.32b)$$

$$Z_{in} = \frac{v_{in}}{i_{in}} = \frac{v_L}{-i_L} = -Z_L$$
 (2.32c)

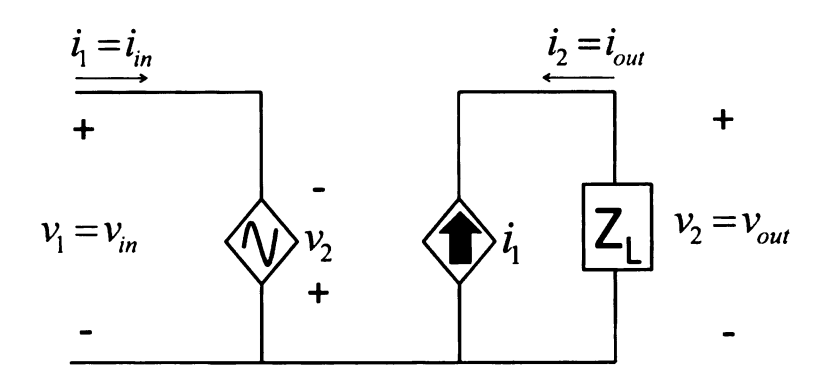


Figure 2.2. Hybrid parameter model for VINIC [1]

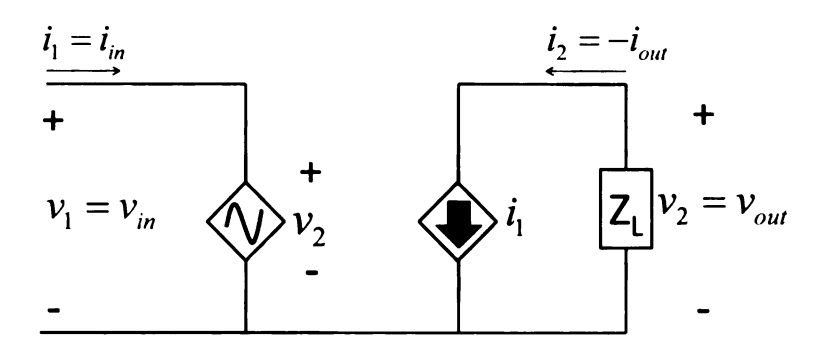


Figure 2.3. Hybrid parameter model for CINIC [1]

where v_{in} is the input voltage, i_{in} is the input current, v_L is the load voltage, and i_L is the load current of the NIC network. In the VINIC, the input voltage is inverted while the input current remains unchanged at the load. In the CINIC, the opposite takes place. VINICs and CINICs are also known as series NICs and shunt NICs, respectively [6].

2.2.2 Grounded NICs vs. Floating NICs

If the load impedance of the NIC network is connected to ground, it is called a grounded NIC (GNIC). Otherwise, it is called a floating NIC (FNIC). Figure 2.4 displays the GNIC while Figure 2.5 displays both the FNIC [1].

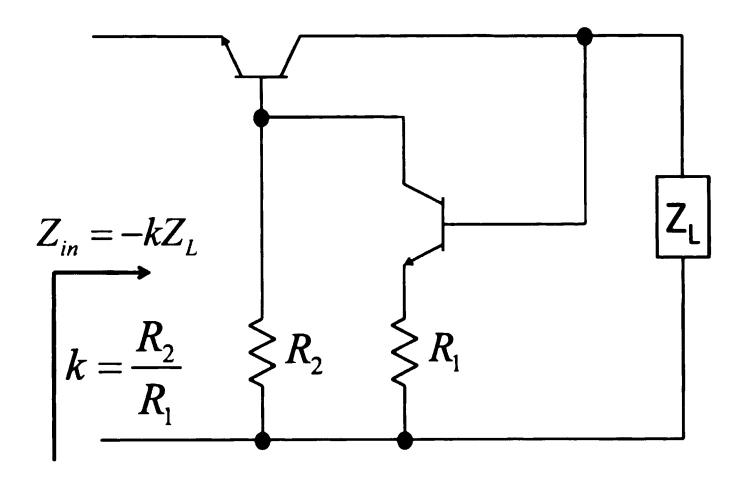


Figure 2.4. GNIC circuit [7]

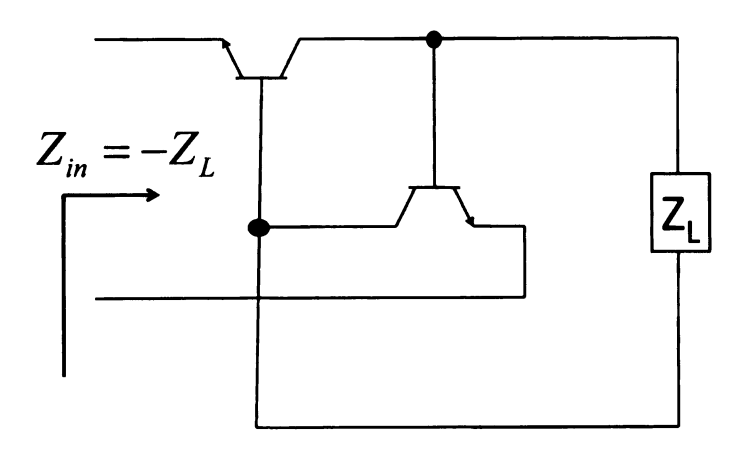


Figure 2.5. FNIC circuit [7]

2.2.3 Open-circuit Stable vs. Short-circuit Stable

One of the difficult things in observing a NIC is that the computational analysis does not always correlate with the physical characteristics of the negative impedance converter. The cause of this is that NICs are only stable provided that certain conditions are satisfied. Another term for this is conditional stability [1]. Even though the predictability of implementing a stable NIC can be complex at times, one thing is common among all NICs: they are open-circuit stable at one port and short-circuit stable at the other port [7].

Examining Figure 2.6, if a load impedance Z_L is attached to port 2, the NIC network is stable if port 1 is an open circuit. The restriction for the NIC being open-circuit stable is that $|Z_{L1}| \geq |Z_{in1}|$.

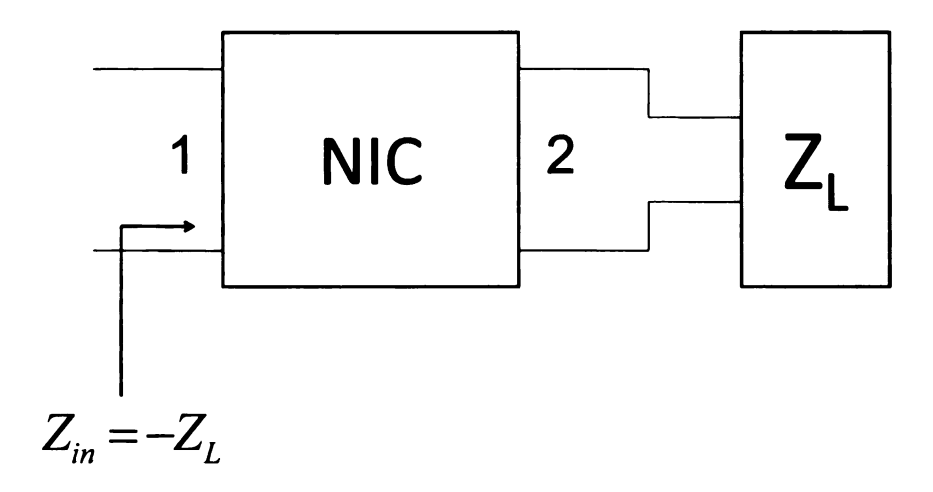


Figure 2.6. Open-circuit stable NIC [7]

Analyzing Figure 2.7, if a load impedance is attached to port 1, the NIC network is stable if port 2 is short-circuited. The constraint for the NIC being short-circuit stable is that $|Z_{L2}| \leq |Z_{in2}|$.

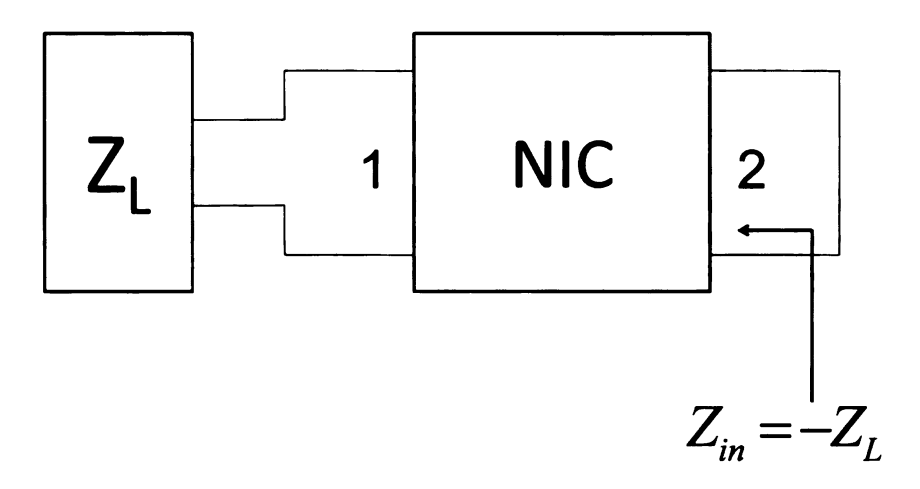


Figure 2.7. Short-circuit stable NIC [7]

The limitations which the magnitude of the load impedance with relation to the magnitude of the input impedance is the result of the inherent conditional stability of NICs. The load impedances will determine how large or how the small it will be with respect to the input impedance of the network. Figure 2.8 depicts a NIC terminated with load impedances at both ports to help visualize the relationships of conditional stability for both cases.

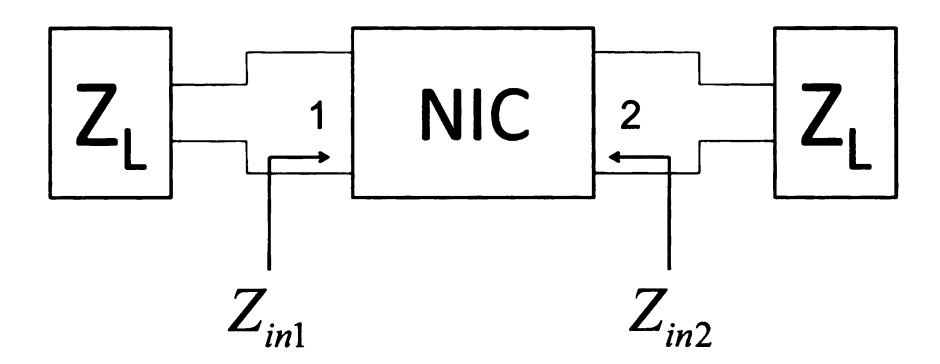


Figure 2.8. NIC terminated at both its ports [7]

2.2.4 BJT vs. FET

Negative impedance converters can be built using operational amplifiers (op-amps), BJTs, and FETs. However, since the NIC that will be built will operate in C-band, op-amps will not be considered because they are generally used for low frequency and audio frequency applications. Most NICs that are transistor-based are VINICs because the transistors operate as dependent current sources resulting in the input current of the NIC network to not invert at the load.

The BJT is a three terminal device (base, collector, and emitter) that is controlled by the current flowing into one terminal. Two types of BJTs exist: the *npn* transistor and the *pnp* transistor; the voltage-current characteristics of each type of BJT are the same except that the polarities for each type of transistor are different. Typically npn transistors are used more often than pnp transistors due to better performance in most circuit applications. As a result, only npn transistors will be considered from this point forward. Figure 2.9 displays circuit symbols for both npn and pnp transistors.

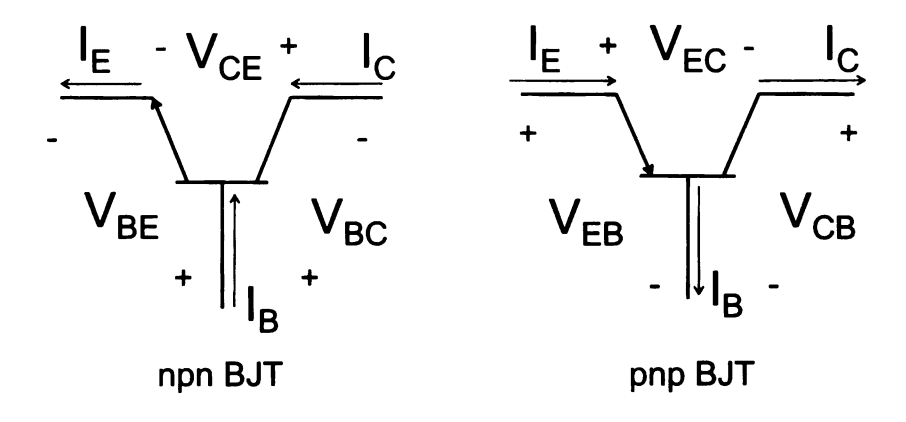


Figure 2.9. npn and pnp BJT [10]

The voltage relationship for each junction of the BJT is

$$V_{BE} = V_{BC} + V_{CE} \quad (npn) \tag{2.33a}$$

$$V_{EB} = V_{CB} + V_{EC} \quad \text{(pnp)} \tag{2.33b}$$

while the current relationship for each terminal of the BJT is

$$I_E = I_B + I_C \tag{2.34}$$

Three circuit configurations are most common with BJTs: common-emitter, common-base, and common-collector. Most BJT circuits are of the common-emitter configuration where the input voltage is V_{BE} (base-emitter voltage) and the output voltage is V_{CE} (collector-emitter voltage). The common-base configuration is used for special applications where the input voltage is V_{BE} and the output voltage is V_{BC} (base-collector voltage). The common-collector configuration is rarely, if ever, used where the input voltage is V_{BC} and the output voltage is V_{CE} .

There are four modes of operation for the BJT: cutoff, inversion (reverse-active), saturation, and active. In cutoff mode, the base-emitter and base-collector junctions are reverse biased. No current is flowing into the input terminal of the transistor no matter what the output voltage is. In reverse-active mode, the base-emitter junction is reverse biased and the base-collector is forward biased. There is still no current flowing from the input terminal of the BJT. The BJT undergoes saturation when the base-emitter junction is forward biased and the base-collector junction is reverse biased. The output voltage is small enough for the BJT to function and the output terminal is almost but not entirely grounded since typical voltages in this mode of operation are typically around $V_{sat}=0.2$ volts (V) where V_{sat} corresponds to the saturation voltage of the BJT. The BJT is active if the base-emitter junction is forward biased and the base-collector is reverse biased. In active mode, the BJT can be visualized as two diodes sharing an anode (npn) or a cathode (pnp) as shown in Figure 2.10 and $V_{BE}\approx 0.7$ volts for the npn BJT and $V_{EB}\approx 0.7$ volts for the pnp BJT.

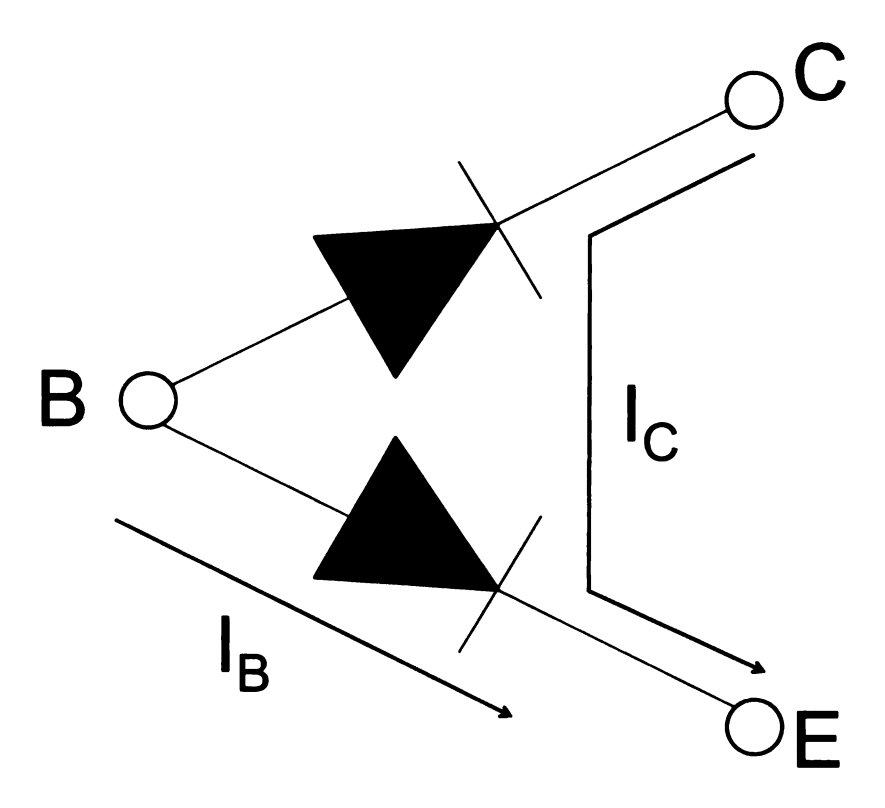


Figure 2.10. The BJT in active mode viewed as two diodes [12]

In addition, the output current goes through a small change with the base-emitter voltage for a known input current where the output current increases with input current. This is due to the *Early effect*. The slope of the voltage-current relationship due to the Early effect shown in Figure 2.11 is

$$\frac{di_{out}}{dv_{out}} = \frac{i_{out}}{V_A} \tag{2.35}$$

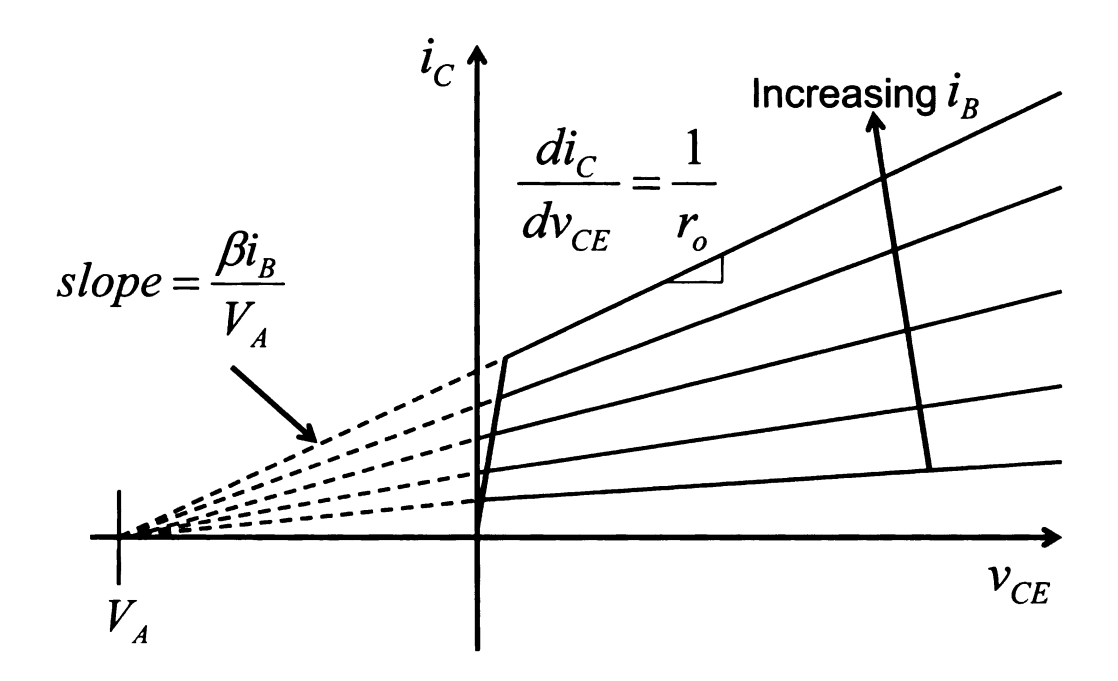


Figure 2.11. The Early effect [11]

where V_A is the Early voltage of the transistor for a BJT operating in the common-emitter configuration. Values of (2.35) typically fall anywhere between 0.01 to 0.05 milliamperes per volt (mA/V). The reciprocal of (2.35) is known as the *output resistance* of the BJT ($\frac{di_{out}}{dv_{out}} = \frac{1}{r_o}$). Another mode of operation that the BJT can undergo is *avalanche breakdown*. This mode will not be considered too much since the application that will be needed in making a NIC does not require a very large applied voltage [10, 11]. The voltage-current relationship for each the *npn* and *pnp* BJT is shown in Figure 2.12

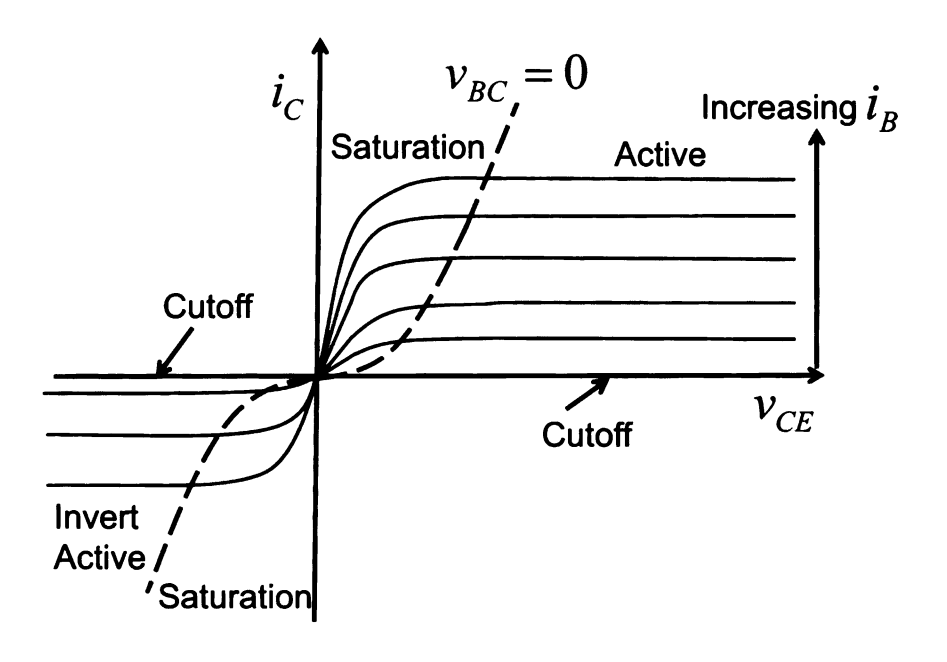


Figure 2.12. Voltage-current relationship for both BJTs [10]

using the relation

$$I_C = I_{C0}(e^{V_{BE}/\eta V_T} - 1) \approx \beta_F I_B$$
 common-emitter configuration (2.36a)

$$I_C = I_{C0}(e^{V_{BE}/\eta V_T} - 1) \approx \alpha_F I_E$$
 common-base configuration (2.36b)

where $\beta_F = \frac{\alpha_F}{(1-\alpha_F)} \approx \frac{I_C}{I_B}$ is the common-emitter direct current (DC) gain which has a typical value of approximately 100, α_F is the common-base DC gain, $I_{C0} = \alpha_F I_{E0}$ where I_{E0} is the is the saturation current of the base-emitter junction, η is the emission coefficient that has a value of 1 or 2 depending on the physics of the junction, $V_T = \frac{kT}{q}$ is the thermal voltage with k designated as Boltzman's constant $(1.381 \times 10^{-23} \text{ Joules per degree Kelvin (J/K))}$, T corresponding to the temperature in

degrees Kelvin, and q being the electric charge (1.602 × 10¹⁹ Coulombs) [$V_T \approx 25 \ mV$ at 300 K (room temperature)]. The first equalities of (2.36) is better known as the Ebers-Moll equation.

The BJT is sometimes viewed as a current-controlled current device as is shown in the second equalities of (2.36). However, this is not an accurate way of depicting how a BJT operates. Modeling BJT circuits based on the common emitter current DC gain makes it a bad circuit due to the fact that the value of β_F can vary from 20 to 1000 depending on what type of BJT that the designer uses, the collector current, the collector-emitter voltage, and the temperature of the transistor [12]. Looking at the first equality of (2.36), it can be shown that the BJT is better modeled as a transconductance device. Details of this will be explained later, but it should be noted that the BJT can be visualized better as a transconductance device rather than a current controlled current device from (2.36) where the input voltage determines the output current. Examples of NICs composed of BJTs are shown in [1], [7], [8], [9], and [13].

The FET is a four-terminal device (body, gate, drain, source) that is controlled by the amount of voltage applied to it. Generally the body is connected directly to the substrate. Three common types of FETs exist: the junction field-effect transistor (JFET), the metal-oxide semiconductor field-effect transistor (MOSFET), and the metal semiconductor field-effect transistor (MESFET). Most NICs that have been built using FETs have been made from MOSFETs. Circuit symbols for each FET are shown in figures Figure 2.13. The NICs that are made from FETs use MOSFETs and examples are shown in [14] and [15].

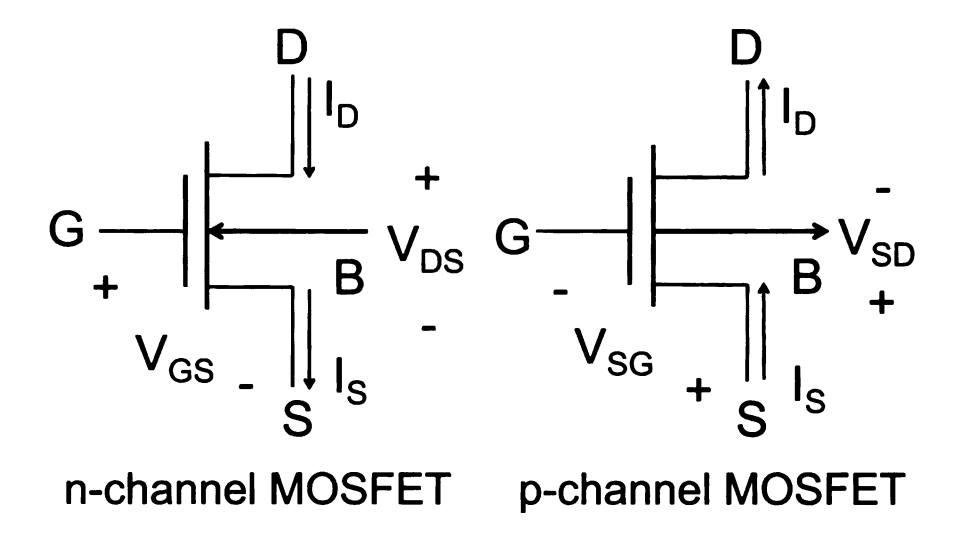


Figure 2.13. n-channel and p-channel MOSFET [12]

Two types of MOSFETs exist: n-channel and p-channel MOSFETs. Both types of MOSFETs can be classified as either enhancement-mode or depletion-mode. Unlike BJTs, no current flows into the gate terminal of the MOSFET. The voltage current characteristics of the n-channel and p-channel MOSFETs are the same except that the polarities are different and the enhancement-mode and depletion-mode MOSFETs have the same voltage-current relationship except that the enhancement-mode MOSFET has a positive (n-channel) or negative (p-channel) threshold voltage V_{TR} while the depletion-mode MOSFET has the opposite threshold voltage with respect to the enhancement-mode MOSFET. The voltage-current relationship for the n-channel enhancement-mode MOSFET is shown in Figure 2.14.

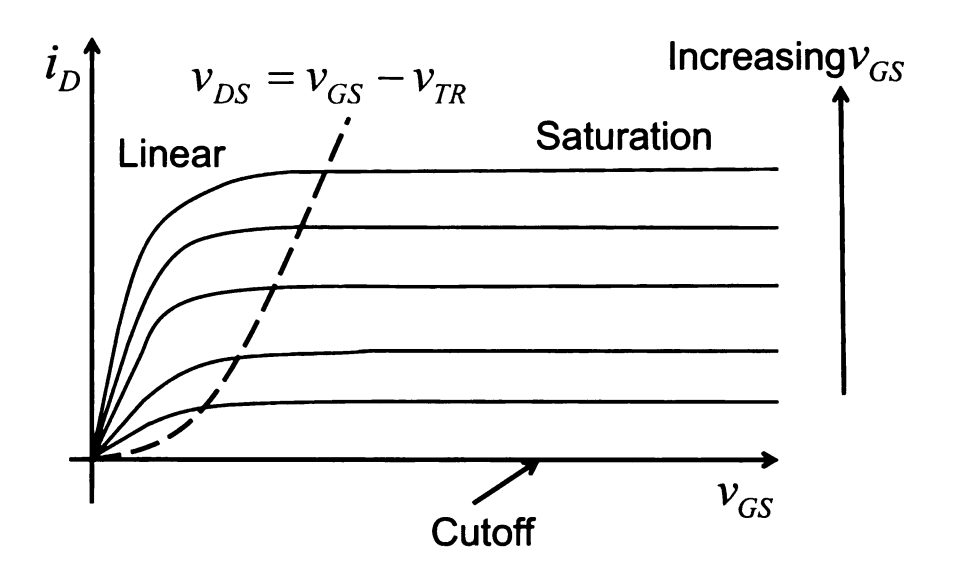


Figure 2.14. Voltage-current relationship for *n-channel MOSFET* [11]

Although the MOSFET and other FETs can be considered as a voltage controlled current device, like the BJT, it is better to consider them as transconductance devices. There are four modes of operation for the MOSFET: cutoff, subthreshold, linear (ohmic), and saturation where the voltage-current relationship is defined as

$$I_D = \begin{cases} 0 & \text{cutoff (for } V_{GS} \ll V_{TR}), \\ Ke^{V_{GS} - V_{TR}} & \text{subthreshold (for } V_{GS} < V_{TR}), \\ K[2(V_{GS} - V_{TR})V_{DS} - V_{DS}^2] & \text{linear (for } V_{GS} > V_{TR} \text{ and } 0 < V_{DS} < V_{GS} - V_{TR}), \\ K(V_{GS} - V_{TR})^2 & \text{saturation (for } V_{GS} > V_{TR} \text{ and } V_{DS} \ge V_{GS} - V_{TR}), \end{cases}$$

$$(2.37)$$

where $K = \frac{\mu_n}{2} \frac{\epsilon_{ox}}{t_{ox}} \frac{W}{L} = \frac{\mu_n}{2} C_{ox} \frac{W}{L}$ is the conductance parameter with a value of

around 0.5 mA/V², μ_n is the electron mobility, $C_{ox} = \frac{\epsilon_{ox}}{t_{ox}}$ is the gate oxide-layer capacitance per unit area, ϵ_{ox} is the dielectric constant of the oxide material within the MOSFET, $V_{GS} - V_{TR} = V_{DS}$, sat is the voltage at which the MOSFET operates in saturation, and the gate dimensions t_{ox} , W, and L correspond to the gate thickness, width, and length, respectively. V_{GS} is the gate-to-source voltage, and V_{DS} is the drain-to-source voltage and Figure 2.14 displays where each mode of operation is located.

CHAPTER 3

DE-EMBEDDING TEST FIXTURES AND MICROSTRIP CIRCUITS

Attaching the NIC to a microstrip transmission line such that it acts as its load is not as simple as one thinks. Recording measurements of the NIC will not be accurate because the instrument will account for the microstrip, the NIC, and the coaxial cables connected from the equipment to the system. This is a problem since most RF circuits use printed circuit board (PCB or PC board) or surface mount technologies (SMT). A test fixture will be needed to connect the cables to the microstrip which is not a coaxial transmission line. Essentially, the instrument will account for the coaxial cables, the test fixture, the microstrip, and the NIC.

Other errors will occur due to improper calibration of the instrument and other external or internal sources that are unpredictable. Errors due to improper calibration can be fixed and removed using proper calibration techniques. Random errors are harder to eliminate due to their unpredictability and can result from unidentified sources of noise within the system, equipment testing the system, or the environment of where the data will be taken. Such errors form an important component in the uncertainty of the measurement.

One solution that removes the effects of the coaxial cables connected from the equipment measuring the system, the test fixture, and the microstrip from the features of the NIC is to perform a step-by-step process called *de-embedding*. This process will undergo two stages [16]:

- 1. In the first stage, the instrument measuring the composite system of the microstrip and the NIC moves the reference plane from the coaxial interface to the input port of the composite system producing accurate data.
- 2. In the second stage, the instrument measuring the device under test (DUT)

moves the reference plane from the microstrip interface to the input port of the DUT – the NIC – producing accurate data.

The type of de-embedding that will be conducted is called two-stage de-embedding. Figure 3.1 gives a visualization of where the measurement and device planes are located on the overall system. The means of how the test fixture and microstrip will be de-embedded is through TRL calibration. This calibration technique will manipulate scattering parameter (S-parameter) and transmission parameter (T-parameter) matrices to allow the user to obtain the measurements of the NIC.

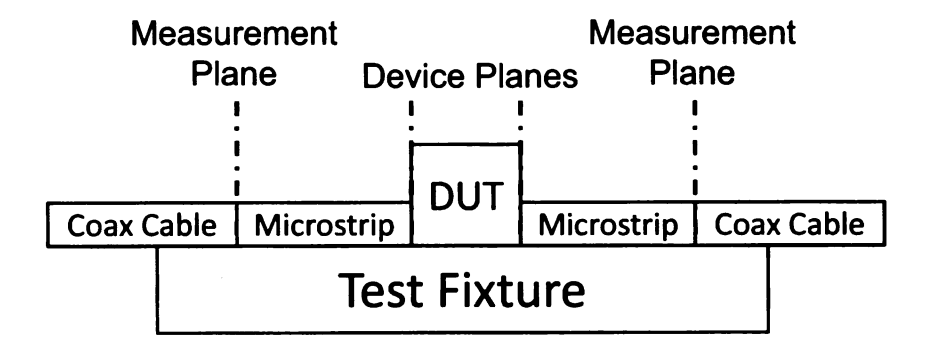


Figure 3.1. Test fixture diagram locating the measurement and device planes

This chapter will describe the operation of a microstrip transmission line through a brief overview of transmission line theory and microwave network analysis contributing to the microstrip. It will also show the user how to de-embed the test fixture and microstrip using TRL calibration. Once the test fixture and microstrip are de-embedded, the NIC will be able to be attached to the line and measurements can be taken without the microstrip, test fixture, cables connected to the circuit, or any other external sources of interference impeding accurate measurements of the NIC.

3.1 Microstrip Circuits

The best way to illustrate how a microstrip works is to introduce transmission line theory. The figure shown below displays a lumped circuit model of a transmission line. The wave that propagates along the line is a transverse-electromagnetic (TEM) wave in the \hat{z} -direction; in other words, the field components along the \hat{z} -direction are zero [5].

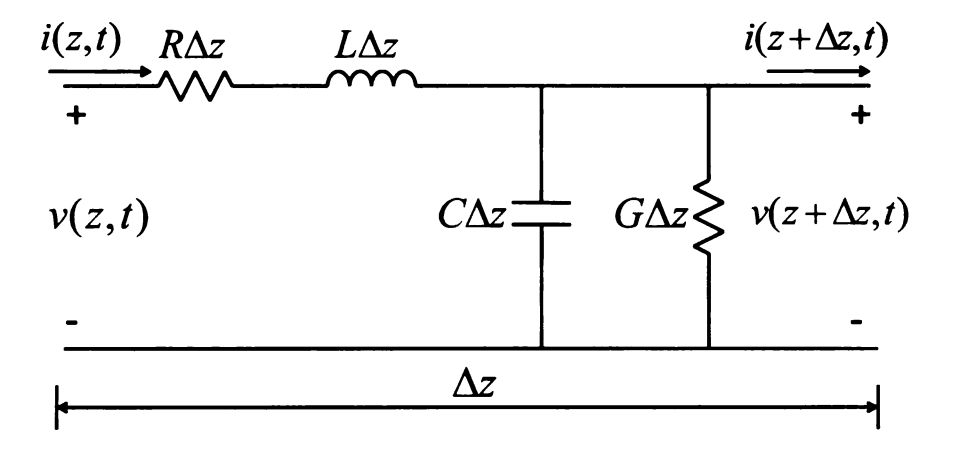


Figure 3.2. Transmission line model [5]

3.1.1 Transmission Line Theory

The quantity R (series resistance per unit length) characterizes the series resistance due to the finite conductivity of the conducting wall of the line, G (shunt conductance per unit length) corresponds to the shunt conductance due to the dielectric loss of the material between the conducting wall, L (series inductance per unit length) signifies the total self-inductance of the conducting wall, and C (shunt capacitance per unit length) is the capacitance due to the conducting wall.

Constructing a loop for Figure 3.2 and applying Kirchhoff's voltage and current laws yields the following equations.

$$v(z,t) - v(z + \Delta z, t) = R\Delta z i(z,t) + L\Delta z \frac{\partial i(z,t)}{\partial t}$$
(3.1a)

$$i(z,t) - i(z + \Delta z, t) = G\Delta z v(z,t) + C\Delta z \frac{\partial v(z,t)}{\partial t}$$
 (3.1b)

Dividing (3.1) by Δz and taking the limit $\Delta z \to 0$ obtains the following equations.

$$\frac{\partial v(z,t)}{\partial z} = -Ri(z,t) - L\frac{i(z,t)}{\partial t}$$
(3.2a)

$$\frac{\partial i(z,t)}{\partial z} = -Gv(z,t) - C\frac{v(z,t)}{\partial t}$$
(3.2b)

Equation 3.2a represents the transmission line or telegraph equations in the time domain. If the assumption is taken that the TEM waves are time-harmonic, v(z,t) and i(z,t) can be expressed in phasor form

$$v(z,t) = \Re[V(z)e^{j\omega t}]$$

$$i(z,t) = \Re[I(z)e^{j\omega t}]$$

and (3.2a) reduces from a partial differential equation to an ordinary differential

equation such that

$$\frac{dV(z)}{dz} = -(R + j\omega L)I(z)$$
(3.4a)

$$\frac{dI(z)}{dz} = -(G + j\omega C)V(z)$$
(3.4b)

If the propagation constant $\gamma = \alpha + j\beta = \sqrt{(R + j\omega L)(G + j\omega C)}$ is introduced where α is the attenuation constant and β is the phase constant, the equations of (3.4) can be solved simultaneously to acquire the wave equations for V(z) and I(z).

$$\frac{d^2V(z)}{dz^2} = \gamma^2V(z) \tag{3.5a}$$

$$\frac{d^2I(z)}{dz^2} = \gamma^2I(z) \tag{3.5b}$$

The solutions for (3.5) are

$$V(z) = V^{+}e^{-\gamma z} + V^{-}e^{\gamma z}$$
 (3.6a)

$$I(z) = I^{+}e^{-\gamma z} + I^{-}e^{\gamma z}$$
 (3.6b)

where $e^{-\gamma z}$ characterizes a TEM wave propagating in the $+\hat{z}$ direction while $e^{\gamma z}$ characterizes a TEM wave propagating in the $-\hat{z}$ direction. Substituting (3.6) into (3.4a) and solving for I(z) gives

$$\gamma[-V^{+}e^{-\gamma z} + V^{-}e^{\gamma z}] = -(R + j\omega L)I(z)$$

$$I(z) = \frac{\gamma}{R + i\omega L}[V^{+}e^{-\gamma z} - V^{-}e^{\gamma z}]$$
(3.7)

reducing (3.6) into only one unknown

$$V(z) = V^{+}e^{-\gamma z} + V^{-}e^{\gamma z}$$
 (3.8a)

$$I(z) = \frac{1}{Z_0} [V^+ e^{-\gamma z} - V^- e^{\gamma z}]$$
 (3.8b)

and comparing the equations of (3.6) defines the characteristic impedance Z_0 as

$$Z_0 = \frac{R + j\omega L}{\gamma} = \sqrt{\frac{R + j\omega L}{G + j\omega C}} = \frac{V^+}{I^+} = -\frac{V^-}{I^-}$$
(3.9)

If the transmission line is lossless, $R=G=0,\,\gamma=j\beta=j\omega\sqrt{LC},\,\alpha=0,\,\beta=\omega\sqrt{LC},$ and $Z_0=\sqrt{\frac{L}{C}}.$

If a load impedance is attached to one end of the transmission line, the TEM wave propagating along the line will reflect back. How much the wave reflects back is determined by what type of load impedance is at the end of the line. Three cases will be considered: an arbitrary load, an open circuit, and a short circuit. For convenience, it is assumed that the transmission line is lossless.

3.1.1.1 Arbitrary Load Impedance

For an arbitrary load where $Z_L \neq Z_0$ shown in Figure 3.3, the impedance at the load will be Z_L and the voltage and current of the line will be the sum of the incident and reflected waves expressed by (3.8) with $\gamma = j\beta$ [5]. Using this relation, the load impedance can be found at z = 0 where

$$Z_L = \frac{V(0)}{I(0)} = \frac{V^+ + V^-}{V^+ - V^-} Z_0 \tag{3.10}$$

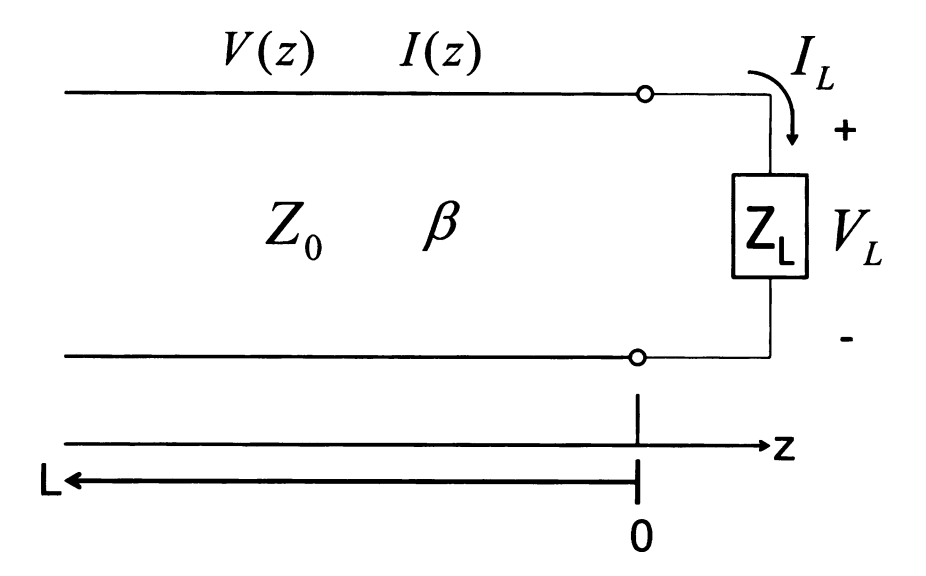


Figure 3.3. Transmission line terminated with load impedance [5]

Using (3.10), the reflection coefficient Γ_L can be computed when solving for V^- .

$$V^{-} = \frac{Z_{L} - Z_{0}}{Z_{L} + Z_{0}} V^{+}$$

$$\Gamma_{L} = \frac{V^{-}}{V^{+}} = \frac{Z_{L} - Z_{0}}{Z_{L} + Z_{0}}$$
(3.11)

and (3.8) for the lossless case can be expressed as

$$V(z) = V^{+}[e^{-j\beta z} + \Gamma_L e^{j\beta z}]$$
(3.12a)

$$I(z) = \frac{V^{+}}{Z_0} [e^{-j\beta z} - \Gamma_L e^{j\beta z}]$$
 (3.12b)

It can be concluded that from looking at (3.12) that the waves propagating along

the transmission line are standing waves if an arbitrary load is attached one end of the transmission line. If $Z_L = Z_0$, the load impedance is matched and $\Gamma_L = 0$ by (3.11). Physically, no reflection occurs anywhere along the line.

Using (3.12), the time-average power flow along the point z anywhere along the line will be

$$P_{av} = \frac{1}{2} \Re[V(z)I(z)^*]$$

$$= \frac{1}{2} \Re[1 - \Gamma_L^* e^{-j2\beta z} + \Gamma_L e^{j2\beta z} - |\Gamma_L|^2]$$

$$= \frac{1}{2} \frac{|V^+|^2}{Z_0} (1 - |\Gamma_L|^2)$$
(3.13)

since $\Gamma_L^* e^{-j2\beta z} + \Gamma_L e^{j2\beta z} = j2\Im[\Gamma_L e^{j2\beta z}]$ which is purely imaginary and does not contribute to (3.13) since P_{av} is purely real and constant [5]. The total power delivered to the load is

$$P_{av} = \frac{|V^+|^2}{2Z_0} - \frac{|V|^2 |\Gamma_L|^2}{2Z_0}$$
 (3.14)

Maximum power is delivered to the load if it is a matched load since $\Gamma=0$ no power is delivered to the load for a short-circuited and open-circuited transmission line since $|\Gamma_L|=1$.

Evaluating the standing wave ratio (SWR) of the line requires first taking the magnitude of (3.12a)

$$|V(z)| = |V^{+}||1 + \Gamma_{L}e^{j2\beta z}|$$

$$= |V^{+}||1 + |\Gamma_{L}|e^{j(\theta - 2\beta l)}|$$
(3.15)

where l=-z represents the distance measured from the load impedance at z=0 and θ is the phase of the reflection coefficient $\Gamma_L=|\Gamma_L|e^{j\theta}$. From (3.15), the maximum voltage occurs when $e^{j(\theta-2\beta l)}=1$ and minimum voltage occurs when $e^{j(\theta-2\beta l)}=-1$

where

$$V_{max} = |V^{+}|(1 + |\Gamma_{L}|) \tag{3.16a}$$

$$V_{min} = |V^{+}|(1 - |\Gamma_{L}|) \tag{3.16b}$$

and the SWR can be found from (3.16).

$$SWR = \frac{V_{max}}{V_{min}} = \frac{1 + |\Gamma_L|}{1 - |\Gamma_L|}$$
 (3.17)

Since $-1 < \Gamma_L < 1$, the voltage SWR (VSWR) is a real number such that $1 \le SWR \le \infty$ where SWR = 1 corresponds to a matched load.

Referring back to (3.12) and applying (3.11) for anywhere along the line, the reflection coefficient can be calculated at any point l.

$$\Gamma_L(l) = \frac{V^- e^{-j\beta l}}{V^+ e^{j\beta l}} = \Gamma_L e^{-j2\beta l}$$
(3.18)

The *input impedance* of the transmission line is found by analyzing the line at distance z = -l by applying (3.11).

$$Z_{in} = \frac{V(-l)}{I(-l)} = Z_0 \frac{V^+[e^{-j\beta l} + \Gamma_L e^{-j\beta l}]}{V^+[e^{-j\beta l} - \Gamma_L e^{-j\beta l}]}$$

$$= Z_0 \frac{e^{-j\beta l} + \Gamma_L e^{-j\beta l}}{e^{-j\beta l} - \Gamma_L e^{-j\beta l}} = Z_0 \frac{e^{j\beta l} + \frac{Z_L - Z_0}{Z_L + Z_0} e^{-j\beta l}}{e^{j\beta l} - \frac{Z_L - Z_0}{Z_L + Z_0} e^{-j\beta l}}$$

$$= Z_0 \frac{(Z_L + Z_0)e^{j\beta l} + (Z_L - Z_0)e^{-j\beta l}}{(Z_L + Z_0)e^{j\beta l} - (Z_L - Z_0)e^{-j\beta l}}$$

$$= Z_0 \frac{Z_L \cos(\beta l) + jZ_0 \sin(\beta l)}{Z_0 \cos(\beta l) + jZ_L \sin(\beta l)}$$

$$= Z_0 \frac{Z_L + jZ_0 \tan(\beta l)}{Z_0 + iZ_L \tan(\beta l)}$$
(3.19)

If the length of the transmission line is half of a wavelength $(l=\frac{\lambda}{2})$, the input impedance is equal to the load impedance from (3.19), i.e., $Z_{in}=Z_L$. If the length of the transmission line is quarter of a wavelength $(l=\frac{\lambda}{4} \text{ or } \frac{2n\lambda+1}{4})$, the input impedance is inversely proportional to the load impedance of the transmission line. To be more precise, $Z_{in}=\frac{Z_0^2}{Z_L}$ and the transmission line is known as a quarter-wave transformer [5].

3.1.1.2 Arbitrary Characteristic Impedance

Looking at Figure 3.4, if transmission line of characteristic impedance Z_0 is feeding a line of an arbitrary characteristic impedance $Z_{arb} \neq Z_0$, the input impedance seen by the feed line is Z_{arb} , i.e., $Z_{in} = Z_{arb}$ and (3.11) is now expressed as

$$\Gamma_L = \frac{Z_{arb} - Z_0}{Z_{arb} + Z_0} \tag{3.20}$$

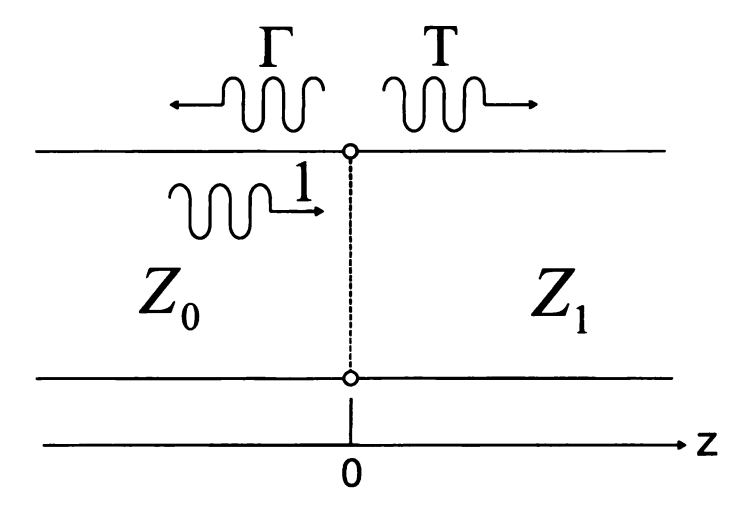


Figure 3.4. Wave reflection and transmission at intersection of transmission lines with different characteristic impedances [5]

The incident voltage of the feed line is expressed from (3.12) for z < 0. Assuming that no reflections are present in the feed line, the transmitted voltage of the line is

$$V(z) = V^{+} T e^{-j\beta z}$$
 where
$$T = 1 + \Gamma_{L} = \frac{2Z_{arb}}{Z_{arb} + Z_{0}} = transmission \ coefficient \ of the line \eqno(3.21)$$

The transmission and reflection coefficients are often expressed in decibels (dB) as the *insertion loss* and *return loss*, respectively where

$$IL = -20\log_{10}(|T|) = \text{insertion loss}$$
 (3.22a)

$$RL = -20\log_{10}(|\Gamma_L|) = \text{return loss}$$
 (3.22b)

with the insertion loss relating to mismatched characteristic impedances of a transmission line and the return loss relating to mismatched loads at the end of a transmission line.

3.1.1.3 Open-circuited Load Impedance

For an open-circuited load impedance, $Z_L = \infty$ as shown in Figure 3.5, the following relation from (3.11) occurs.

$$\lim_{Z_L \to \infty} \Gamma_L = \frac{Z_L}{Z_L} = 1 \tag{3.23}$$

The voltage and current of the line from (3.12) become

$$V(z) = V^{+}[e^{-j\beta z} + e^{j\beta z}] = 2V^{+}\cos(\beta z)$$
 (3.24a)

$$I(z) = \frac{V^{+}}{Z_0} [e^{-j\beta z} - e^{j\beta z}] = \frac{-j2V^{+}}{Z_0} \sin(\beta z)$$
 (3.24b)

and the input impedance is

$$Z_{in} = -jZ_0 \cot(\beta l) \tag{3.25}$$

The standing wave ratio for an open circuit without the transmission line varies over the line.

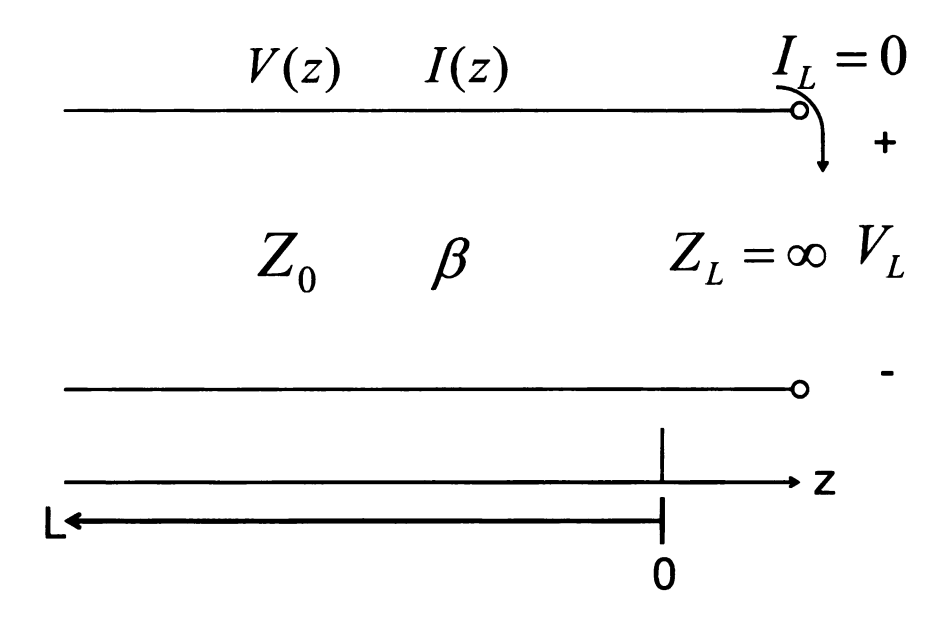


Figure 3.5. Transmission line terminated with an open circuit [5]

3.1.1.4 Short-circuited Load Impedance

For a short-circuited load impedance, $Z_L=0$ as shown in Figure 3.6, the following relation from (3.11) occurs.

$$\lim_{Z_L \to 0} \Gamma_L = \frac{-Z_0}{Z_0} = -1 \tag{3.26}$$

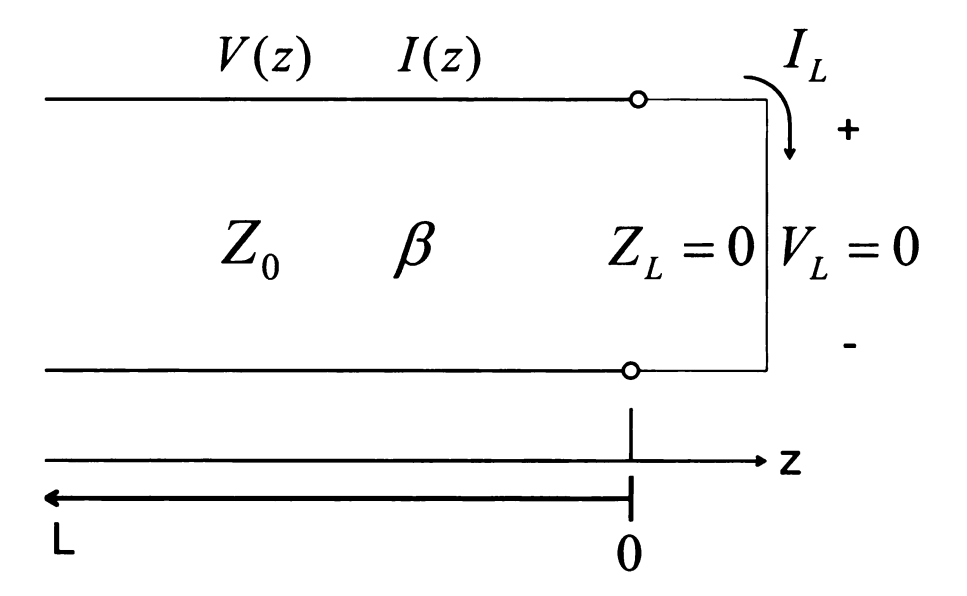


Figure 3.6. Transmission line terminated with a short circuit [5]

The voltage and current of the line from (3.12) become

$$V(z) = V^{+} [e^{-j\beta z} - e^{j\beta z}] = -j2V^{+} \sin(\beta z)$$
 (3.27a)

$$I(z) = \frac{V^{+}}{Z_{0}} \left[e^{-j\beta z} + e^{j\beta z} \right] = \frac{2V^{+}}{Z_{0}} \cos(\beta z)$$
 (3.27b)

and the input impedance is

$$Z_{in} = jZ_0 \tan(\beta l) \tag{3.28}$$

The standing wave ratio for a short circuit by itself without a transmission line is $SWR = \infty$ from (3.17).

3.1.2 Microstrip

A microstrip is best defined as a rectangular waveguide consisting of a metallic strip of width W and thickness t mounted on top of a dielectric substrate of height h with a relative permittivity ϵ_T sitting on a conducting plate operating in the microwave spectrum of a frequency range of 100 MHz to 300 GHz [20]. Figure 3.7 and Figure 3.8 show a diagram of the geometry of the microstrip with the fields distributed accordingly.

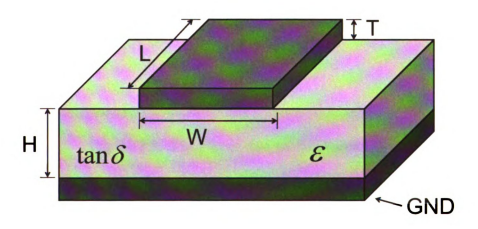


Figure 3.7. Microstrip geometry [5, 20]

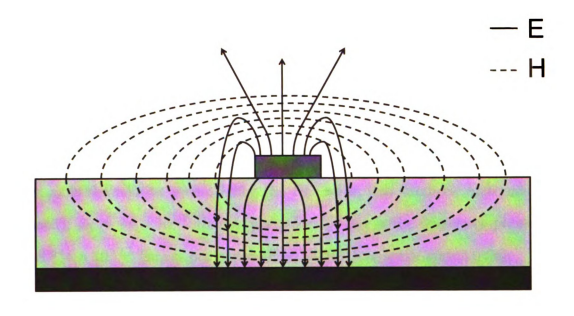


Figure 3.8. Field lines due to microstrip [5]

Due to the presence of the dielectric substrate, the fields due to the microstrip are not TEM waves but hybrid transverse electric-transverse magnetic (TE-TM or HE-HM) mode because most of the fields are concentrated within the substrate between the conducting strip and the ground plane although these are fringing fields. The phase velocity at which the waves propagate in the substrate is less than $c \approx 3 \times 10^8$ meters per second (m/s), which is the phase velocity of the wave in the air [5]. Since the thickness of the dielectric substrate is very thin and much smaller than a wavelength λ ($h \ll \lambda$) at any frequency f, the hybrid mode can be considered as a quasi-TEM wave allowing for very accurate approximations of the phase velocity v_0 , propagation

constant β , and characteristic impedance Z_0 where for a given aspect ratio $\frac{W}{h}$

$$c = \frac{1}{\sqrt{\mu_0 \epsilon_0}} = \frac{\omega}{\beta} \tag{3.29a}$$

$$k_0 = \frac{2\pi}{\lambda} = \omega \sqrt{\mu_0 \epsilon_0} = \frac{\omega}{c}$$
 (3.29b)

$$v_p = \frac{\lambda}{f} = \frac{c}{\sqrt{\mu_r \epsilon_{eff}}} \tag{3.29c}$$

$$\beta = k_0 \sqrt{\epsilon_{eff}} \tag{3.29d}$$

where μ_r is the relative permeability (for this work, non-magnetic materials will be assumed), $\mu_0 \approx 4\pi \times 10^{-7}$ Henrys per meter (H/m) is the free-space permeability, $\epsilon_0 \approx 8.854 \times 10^{-12}$ Farads per meter (F/m) is the free-space permittivity,

$$\epsilon_{eff} = \frac{\epsilon_r + 1}{2} \left[1 + \frac{1}{\sqrt{1 + 12\frac{h}{W}}} \right],\tag{3.30}$$

and

$$Z_{0} = \begin{cases} \frac{60}{\sqrt{\epsilon_{eff}}} \ln\left[\frac{8h}{W} + \frac{W}{4h}\right] & \text{for } \frac{W}{h} \leq 1\\ \frac{120\pi}{\sqrt{\epsilon_{eff}}\left[\frac{W}{h} + 1.393 + 0.667 \ln\left(\frac{W}{h} + 1.444\right)\right]} & \text{for } \frac{W}{h} \geq 1 \end{cases}$$
(3.31)

where ϵ_{eff} is the effective dielectric constant of the microstrip and $1 < \epsilon_{eff} < \epsilon_r$. The effective dielectric constant can be viewed as the dielectric constant of a homogeneous medium consisting of both the dielectric and air regions of the microstrip [5]. If a

specific characteristic impedance (Z_0) is required, then

$$\frac{W}{h} = \begin{cases}
\frac{8e^{A}}{e^{2A} - 2} & \text{for } \frac{W}{h} < 2 \\
\frac{2}{\pi} \left[B - 1 - \ln(2B - 1) + \frac{\epsilon_{r} - 1}{2\epsilon_{r}} \left[\ln(B - 1) + 0.39 - \frac{0.61}{\epsilon_{r}} \right] \right] & \text{for } \frac{W}{h} > 2
\end{cases}$$
(3.32)

where

$$A = \frac{Z_0}{60} \sqrt{\frac{\epsilon_r + 1}{2}} + \frac{\epsilon_r - 1}{\epsilon_r + 1} \left(0.23 + \frac{0.11}{\epsilon_r} \right)$$
$$B = \frac{377\pi}{2Z_0 \sqrt{\epsilon_r}}$$

can be used to design the microstrip line. Provided that the microstrip is postulated to be a quasi-TEM line, the attenuation due to dielectric loss and conductor loss are, respectively,

$$\alpha_d = \frac{k_0 \epsilon_r \tan \delta}{2} \frac{\epsilon_r (\epsilon_{eff} - 1)}{\epsilon_{eff} (\epsilon_r - 1)}$$
(3.33a)

$$\alpha_c = \frac{R_s}{Z_0 W} \tag{3.33b}$$

where $R_s = \sqrt{\frac{\omega \mu_0}{2\sigma}}$ is the conductor surface resistivity.

3.2 TRL Calibration

It was previously mentioned that taking measurements of the NIC attached to the microstrip for a calibrated instrument will not be fairly easy because it cannot discern the measurements due to the test fixture, the microstrip, and the DUT as a complete system and the components individually [19]. S-parameters and T-parameters are circuit representations in matrix form that will be considered for the de-embedding process. In this process, the S-parameters of the NIC can be found — or de-embedded

- from the overall system. Rhonda Franklin states that the method where the test fixture is illustrated by evaluating its S-parameters and T-parameters separately is called *unterminating* [19].

Two types of de-embedding exist: one-tier de-embedding and two-tier de-embedding. If two-tier de-embedding is used, the equipment needs to be calibrated by standards for the VNA. The test fixture and all other external devices with respect to the DUT are described by using the calibration standards of the DUT. The two-tier de-embedding method uses data transfer of standard measurements, test fixture description, and DUT de-embedding. If one-tier de-embedding is used, the calibration standards of the DUT can be found by taking measurements of the instrument after calibration. One-tier de-embedding is preferred over two-tier de-embedding for three reasons:

- Propagation of measurement discrepancies are reduced creating more accurate data of the device being tested.
- 2. The VNA offers de-embedded S-parameters without extra data processing.
- 3. The de-embedded data can be seen directly via a better graphical illustration on the VNA.

The only problem is that data can only be shown for one data point of the DUT [19]. The only case where two-tier de-embedding is preferred over one-tier de-embedding is if measurements need to be repeated over and over again therefore saving time when different test fixtures are used. Figure 3.9 shows a flow chart of how to de-embed the test fixture and all other external devices of the DUT.

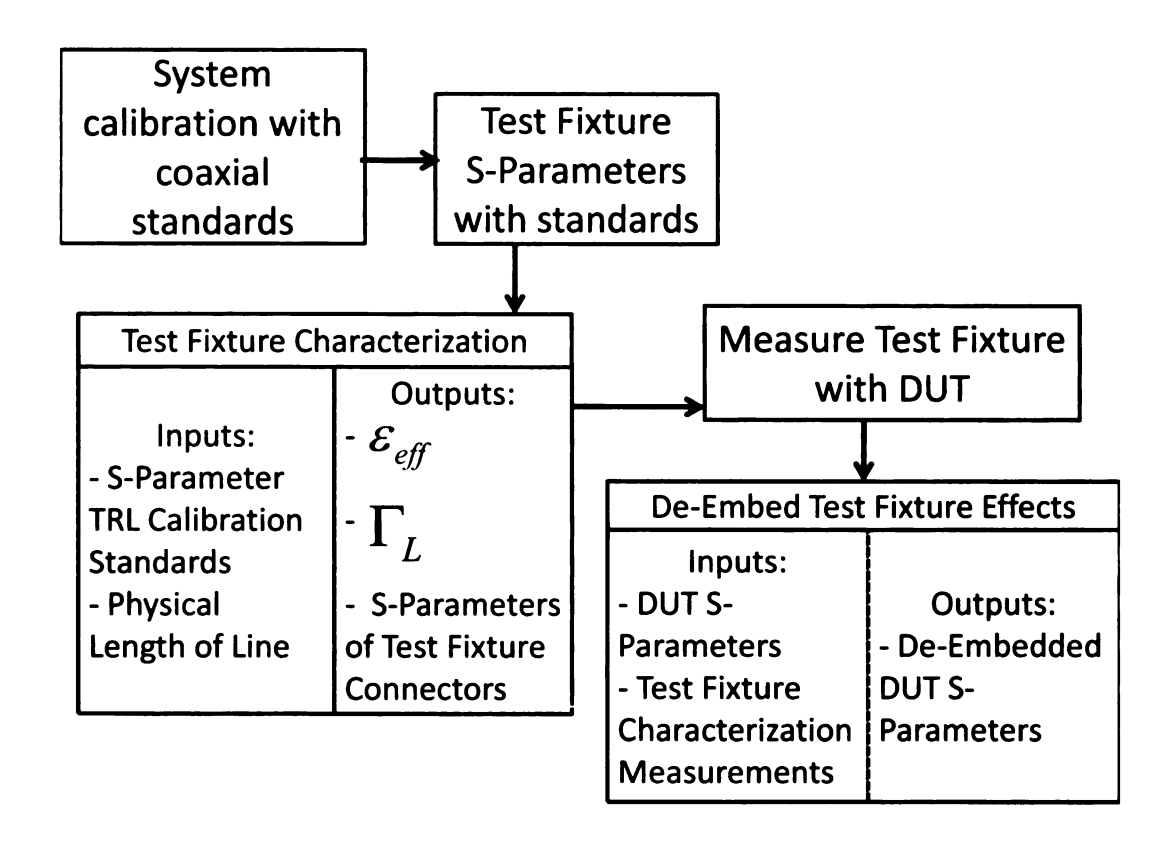


Figure 3.9. Flow chart describing the de-embedding process [19]

With the information provided, it can be concluded that the type of de-embedding that will be used will be one-tier de-embedding. The type of one-tier de-embedding that will be used is called *TRL calibration*. This calibration technique has been used for nearly thirty years to de-embed the DUT from the test fixture and other external devices using T-parameters [18, 21, 22]. A two-port network can be represented by a schematic or a signal flow graph as shown in Figure 3.10 and Figure 3.11.



Figure 3.10. Two-port S-parameter network [18]

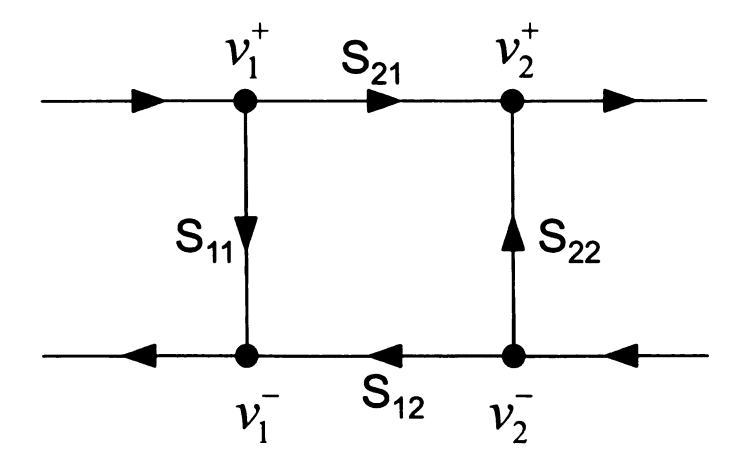


Figure 3.11. Two-port S-parameter network represented as a signal flow graph [5]

Each component of the composite system can be represented as a two-port network. The total network is composed of a DUT placed in between connectors A and B where each connector is viewed as a two-port error-box placed in between the actual measurement plane and the device plane of the DUT. Since two-stage de-embedding will be used to measure the S-parameters of the DUT, connectors A and B are designated as the test port cables of the instrument analyzing the composite system in the first stage and characterized as two segments of the microstrip divided evenly in the second stage. If a network is constructed as such, the TRL calibration technique will identify the characteristics of each connector before any measurements are taken then it will relocate the reference planes from the test cable ports of the VNA to the boundaries of the DUT [5, 16, 17, 18].

Figure 3.12 depicts how the cascaded system would look like using a series of signal flow graphs. Data that needs to be taken using this calibration method are the three standards of TRL calibration and the measurements of the composite system. These standards are:

- 1. Thru this standard takes measurements where connectors A and B are connected together with no device placed in between them.
- 2. Reflect this standard collects data where either connector A or connector B is terminated with a short circuit or open circuit.
- 3. Line this standard records measurements where an empty transmission line of a given, specified length is connected in between connectors A and B.

Before implementing this method for the necessary application, it is best to understand the concept of S-parameters, T-parameters, and ABCD parameters.

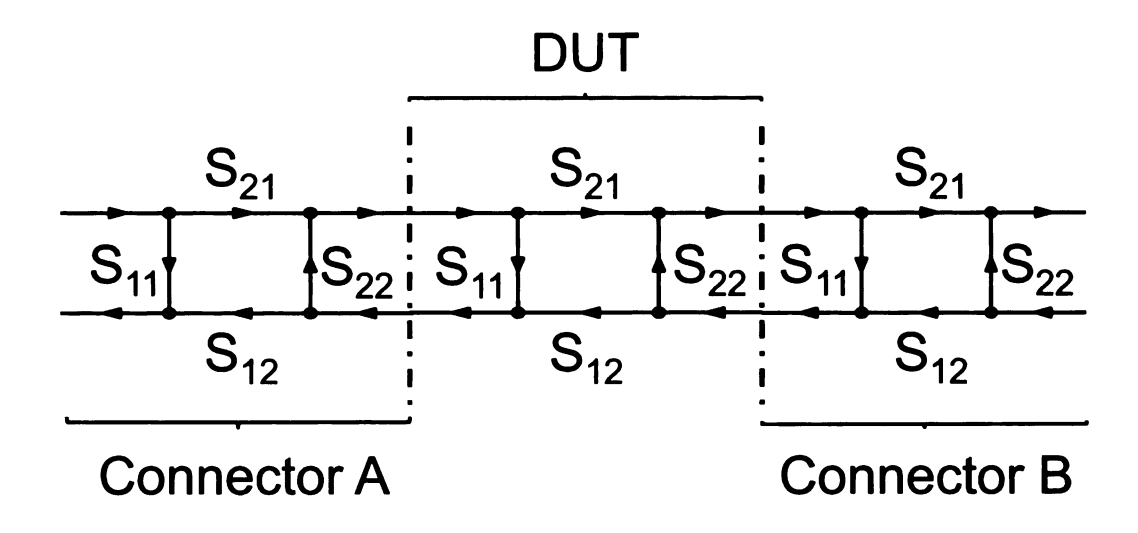


Figure 3.12. Signal flow graph representing the test fixture halves and the DUT [16]

3.2.1 Scattering, Transmission, and ABCD Parameters

Referring back to Section 2.1.2 for a N-port network and applying it to a two-port network, it was assumed that for a microwave network, $\hat{n} \times \vec{E} = 0$ over the surface of the enclosed network except over the cross sections of the terminal ports. If the transverse fields are known at each port of the network, then all modal voltages or currents of the network will be known [3]. Specified I_i or V_i at each port leads to a specified transverse magnetic or electric field \vec{H}_t or \vec{E}_t , respectively. As a consequence, mixed tangential fields \vec{E}_{tang} and \vec{H}_{tang} are specified over the enclosed network surface S and the EM fields within the network volume V established by the

uniqueness theorem. Since the microwave network is linear, the impedance matrix [z] for a N-port network is defined by

$$V_i = \sum_{j=1}^{N} z_{ij} I_j \text{ for } i = 1, 2, \dots, N$$
 (3.34a)

$$z_{ij} = \frac{V_i}{I_j} \bigg|_{I_k = 0, \ k \neq j} \tag{3.34b}$$

$$\begin{bmatrix} V_1 \\ V_2 \\ \vdots \\ V_N \end{bmatrix} = \begin{bmatrix} z_{11} & z_{12} & \cdots & z_{1N} \\ z_{21} & z_{22} & \cdots & z_{2N} \\ \vdots & \vdots & \ddots & \vdots \\ z_{N1} & z_{N2} & \cdots & z_{NN} \end{bmatrix} \begin{bmatrix} I_1 \\ I_2 \\ \vdots \\ I_N \end{bmatrix}$$
(3.34c)

$$[V] = [z][I] \tag{3.34d}$$

where V_i and I_i are the mode voltage and mode current in the i^{th} port, z_{ij} is the open-circuit transfer impedance, and z_{ii} is the open-circuit input impedance seen looking into port i. The inverse of (3.34) is the admittance matrix defined by

$$I_i = \sum_{j=1}^{N} y_{ij} V_j \text{ for } i = 1, 2, \dots, N$$
 (3.35a)

$$y_{ij} = \frac{I_i}{V_j} \bigg|_{V_k = 0, \ k \neq j} \tag{3.35b}$$

$$\begin{bmatrix} I_1 \\ I_2 \\ \vdots \\ I_N \end{bmatrix} = \begin{bmatrix} y_{11} & y_{12} & \cdots & y_{1N} \\ y_{21} & y_{22} & \cdots & y_{2N} \\ \vdots & \vdots & \ddots & \vdots \\ z_{N1} & y_{N2} & \cdots & y_{NN} \end{bmatrix} \begin{bmatrix} V_1 \\ V_2 \\ \vdots \\ V_N \end{bmatrix}$$
(3.35c)

$$[I] = [y][V] \tag{3.35d}$$

where $[y] = [z]^{-1}$, y_{ij} is the short-circuit transfer admittance, and y_{ii} is the short-circuit input admittance. To show that an isotropic network is reciprocal, the *Lorentz* reciprocity theorem will be used. For fields $(\overrightarrow{E}^a, \overrightarrow{H}^b)$ and $(\overrightarrow{E}^b, \overrightarrow{H}^a)$ in a linear and isotropic bounded medium

$$\oint_{S} (\overrightarrow{E}^{a} \times \overrightarrow{H}^{b} - \overrightarrow{E}^{b} \times \overrightarrow{H}^{a}) \cdot \widehat{n} dS = \int_{V} (-\overrightarrow{E}^{a} \cdot \overrightarrow{J}^{b} - \overrightarrow{H}^{b} \cdot \overrightarrow{J}^{a}_{m} + \overrightarrow{E}^{b} \cdot \overrightarrow{J}^{a} + \overrightarrow{H}^{a} \cdot \overrightarrow{J}^{b}_{m}) dV$$

$$= \oint_{S} [(\widehat{n} \times \overrightarrow{E}^{a}) \cdot \overrightarrow{H}^{b} - (\widehat{n} \times \overrightarrow{E}^{b}) \cdot \overrightarrow{H}^{a}] dS = 0$$
(3.36)

since a source-free region is observed and $\hat{n} \times \vec{E}^a = \hat{n} \times \vec{E}^b = 0$ on the conducting surface of the network.

If (2.9) is substituted into (3.36) and the second term is moved to the right side of the equation

$$\sum_{n=1}^{N} V_n^a I_n^b \int_{CS_n} (\widehat{e}_n \times \widehat{h}_n) \cdot \widehat{n} dS = \sum_{n=1}^{N} V_n^b I_n^a \int_{CS_n} (\widehat{e}_n \times \widehat{h}_n) \cdot \widehat{n} dS$$
 (3.37a)

$$\sum_{n=1}^{N} V_n^a I_n^b = \sum_{n=1}^{N} V_n^b I_n^a$$
 (3.37b)

Substituting (3.34a) into (3.37a) verifies that isotropic networks are reciprocal

$$\sum_{n=1}^{N} I_{n}^{b} \sum_{m=1}^{N} z_{nm} I_{m}^{a} = \sum_{n=1}^{N} I_{n}^{a} \sum_{m=1}^{N} z_{nm} I_{m}^{b}$$

$$= \sum_{m=1}^{N} I_{m}^{b} \sum_{n=1}^{N} z_{mn} I_{n}^{a} = \sum_{n=1}^{N} I_{n}^{a} \sum_{m=1}^{N} z_{nm} I_{m}^{b} \qquad (3.38a)$$

$$\sum_{m=1}^{N} \sum_{n=1}^{N} (z_{mn} - z_{nm}) I_m^b I_n^a = 0$$
(3.38b)

where (3.38b) is true only when $z_{mn} = z_{nm}$. Similarly, substituting (3.35a) into (3.37a) yields $y_{mn} = y_{nm}$. If the network is lossless, z_{mn} and y_{mn} are purely imagi-

nary [5]. For a two-port network, N=2.

While it is good to use these matrices to derive microwave networks analysis for Nport networks, it is better to use matrices that describe the waveguide characteristics
for each terminal port [3]. The voltages and currents of each port can expressed as a
form of (3.8) or (3.12) for lossless networks where the first is the incident wave and
the second term is the reflected wave.

$$V_n = V_n^+ + V_n^- (3.39a)$$

$$I_n = I_n^+ + I_n^- = \frac{1}{Z_{0n}} (V_n^+ - V_n^-)$$
 (3.39b)

3.2.1.1 The Transmission Matrix

The *T-parameter matrix* is derived from (3.39) with respect to traveling waves. These matrices are best used for cascaded networks. For TRL calibration, T-parameter matrices are used for the composite system consisting of both connectors A and B and the DUT. This also applies to two-stage de-embedding. Using (3.39) for a two-port network

$$\begin{bmatrix} V_2^- \\ V_2^+ \end{bmatrix} = \begin{bmatrix} T_{11} & T_{12} \\ T_{21} & T_{22} \end{bmatrix} \begin{bmatrix} V_1^+ \\ V_1^- \end{bmatrix}$$
(3.40)

where

$$T_{11} = \frac{V_2^-}{V_1^+} \bigg|_{V_1^- = 0} \tag{3.41a}$$

$$T_{12} = \frac{V_2^-}{V_1^-} \bigg|_{V_1^+ = 0} \tag{3.41b}$$

$$T_{21} = \frac{V_2^+}{V_1^+} \bigg|_{V_1^- = 0} \tag{3.41c}$$

$$T_{22} = \frac{V_2^+}{V_1^-} \bigg|_{V_1^+ = 0} \tag{3.41d}$$

Examining Figure 3.13, the incident and reflected waves at the input of the DUT are the reflected and incident waves, respectively at the output of connector A. The same applies for connector B with respect to the DUT. In general, the incident and reflected waves at the output of network N are the reflected and incident waves, respectively at the input of network N+1 [3]. For a cascaded network, the T-parameter matrix is the product of each individual network, i.e.,

$$[\mathbf{T}] = [\mathbf{T}_N][\mathbf{T}_{N-1}] \cdots [\mathbf{T}_2][\mathbf{T}_1] \tag{3.42}$$

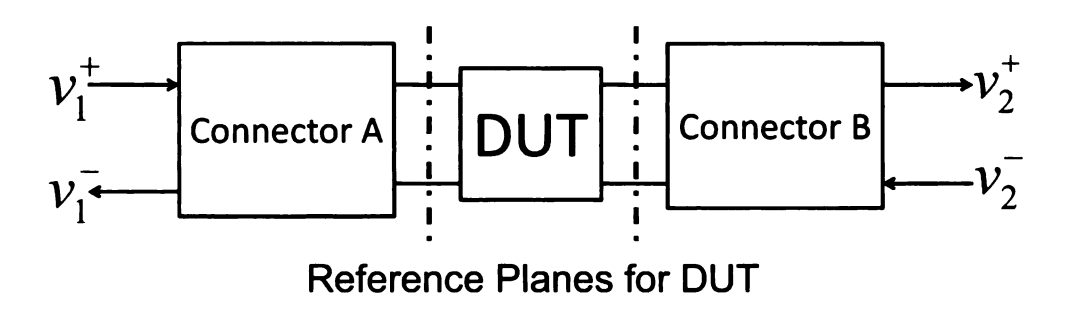


Figure 3.13. Schematic representing the test fixture halves and the DUT [5]

3.2.1.2 The Scattering Matrix

The S-parameter matrix is also derived from (3.39) with respect to traveling waves. S-parameters are the reported quantity from a VNA. In the case of TRL calibration, S-parameters are evaluated from the T-parameter matrices for each individual component of the composite system. Using (3.39) for a two-port network

$$\begin{bmatrix} V_1^- \\ V_2^- \end{bmatrix} = \begin{bmatrix} S_{11} & S_{12} \\ S_{21} & S_{22} \end{bmatrix} \begin{bmatrix} V_1^+ \\ V_1^+ \end{bmatrix}$$
(3.43)

where

$$S_{11} = \frac{V_1^-}{V_1^+} \bigg|_{V_2^+ = 0} \tag{3.44a}$$

$$S_{12} = \frac{V_1^-}{V_2^+} \bigg|_{V_1^+ = 0} \tag{3.44b}$$

$$S_{21} = \frac{V_2^-}{V_1^+} \bigg|_{V_2^+ = 0} \tag{3.44c}$$

$$S_{22} = \frac{V_2^-}{V_2^+} \bigg|_{V_1^+ = 0} \tag{3.44d}$$

and the general expression for a N-port network is

$$S_{ij} = \frac{V_i^-}{V_j^+} \bigg|_{V_k^+ = 0, \ k \neq j} \tag{3.45}$$

with S_{11} being the port 1 reflection coefficient with port 2 matched, S_{12} designated as the transmission coefficient from port 2 to port 1, S_{21} corresponding to the transmission coefficient from port 1 to port 2, S_{22} representing the port 2 reflection coefficient with port 1 matched, S_{ii} known as the port *i* reflection coefficient with all other ports are terminated with matched loads, and S_{ij} being the transmission coefficient from port *j* to port *i* and all other ports are terminated with matched loads [5]. If the microwave network is symmetric, then $[S]^t = [S]$, where $[S]^t$ is the transposed S-parameter matrix. If the network is lossless, $[S]^t[S]^* = [U]$ where $[S]^* = ([S]^t)^{-1}$ is the unitary matrix and [U] is the identity matrix where

$$[\mathbf{U}] = \begin{bmatrix} 1 & 0 & \cdots & 0 \\ 0 & 1 & \cdots & \vdots \\ \vdots & 0 & \ddots & 0 \\ 0 & 0 & \cdots & 1 \end{bmatrix}$$
 (3.46)

3.2.1.3 The ABCD Transmission Matrix

The ABCD-parameter transmission matrix is closely related to (3.12) with respect to total voltages and currents. Like T-parameter matrices, these matrices are best used for cascaded networks. ABCD-parameter matrices will not be needed for the TRL calibration method, but they will be needed to visualize the NIC connected to the microstrip such that the parameter Z shown in Figure 3.14 is the series impedance of the two-port network corresponding to the input impedance of the NIC. Using (3.39) for a two-port network

$$\begin{bmatrix} V_1 \\ I_1 \end{bmatrix} = \begin{bmatrix} \mathbf{A} & \mathbf{B} \\ \mathbf{C} & \mathbf{D} \end{bmatrix} \begin{bmatrix} V_2 \\ I_2 \end{bmatrix}$$
 (3.47)

where

$$A = \frac{V_1}{V_2} \bigg|_{I_2 = 0} = \frac{V_1}{V_1} = 1 \tag{3.48a}$$

$$B = \frac{V_1}{I_2} \bigg|_{V_2 = 0} = \frac{V_1}{V_1/Z} = Z \tag{3.48b}$$

$$C = \frac{I_1}{V_2} \bigg|_{I_2 = 0} = 0 \tag{3.48c}$$

$$D = \frac{I_1}{I_2} \bigg|_{V_2 = 0} = \frac{I_1}{I_1} = 1 \tag{3.48d}$$

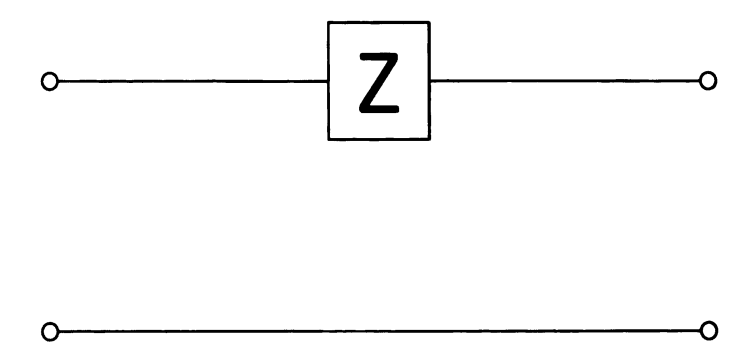


Figure 3.14. Two-port ABCD-parameter network for series impedance [5]

In order to analyze two-port networks based on ABCD-parameters, the current is flowing out of port 2 where Figure 3.10 has current flowing into port 2. In general, the input and output voltages and currents at the output of network N are the input and output voltages and currents waves at the input of network N+1. As was done for T-parameters, the ABCD-parameter matrix for a cascaded network is the product of the individual networks of the system being analyzed. It can be shown that AD - BC = 1 for a reciprocal network [5].

3.2.1.4 Transformation between Parameters

Expressing S-parameters in terms of impedance parameters yields

$$[\mathbf{S}] = [z - z_0][z + z_0]^{-1} \tag{3.49}$$

where

$$[z_0] = \begin{bmatrix} z_{01} & 0 \\ 0 & z_{02} \end{bmatrix}$$

where z_{01} and z_{02} are the characteristic impedances for ports 1 and 2, respectively, and for a two-port network

$$\begin{bmatrix} S_{11} & S_{12} \\ S_{21} & S_{22} \end{bmatrix} = \frac{1}{\Delta Z} \begin{bmatrix} (z_{11} - Z_0)(z_{22} + Z_0) - z_{12}z_{21} & 2z_{12}Z_0 \\ 2z_{21}Z_0 & (z_{11} + Z_0)(z_{22} - Z_0) - z_{12}z_{21} \end{bmatrix}$$
(3.50)

where $\Delta Z = (z_{11} + Z_0)(z_{22} + Z_0) - z_{12}z_{21}$. Expressing T-parameters in terms of S-parameters for a two-port network yields

$$[\mathbf{T}] = \begin{bmatrix} T_{11} & T_{12} \\ T_{21} & T_{22} \end{bmatrix} = \frac{1}{S_{21}} \begin{bmatrix} S_{12}S_{21} - S_{11}S_{22} & S_{11} \\ -S_{22} & 1 \end{bmatrix}$$
(3.51)

and performing the inverse relationship gives

$$[\mathbf{S}] = \begin{bmatrix} S_{11} & S_{12} \\ S_{21} & S_{22} \end{bmatrix} = \frac{1}{T_{22}} \begin{bmatrix} T_{12} & T_{11}T_{22} - T_{12}T_{21} \\ 1 & -T_{21} \end{bmatrix}$$
(3.52)

Using (3.52), reciprocity for a two-port network holds when

$$T_{11}T_{22} - T_{12}T_{21} = \frac{z_{02}}{z_{01}} = 1 \quad \text{or} \quad S_{12} = S_{21}$$
 (3.53)

Expressing ABCD-parameters in terms of S-parameters yields

$$\begin{bmatrix} \mathbf{A} & \mathbf{B} \\ \mathbf{C} & \mathbf{D} \end{bmatrix} = \frac{1}{2S_{21}} \begin{bmatrix} (1+S_{11})(1-S_{12}) + S_{12}S_{21} & Z_0[(1+S_{11})(1+S_{12}) - S_{12}S_{21}] \\ [(1-S_{11})(1-S_{12})/Z_0 - S_{12}S_{21}] & (1-S_{11})(1-S_{12}) + S_{12}S_{21} \\ (3.54) \end{bmatrix}$$

and performing the inverse relationship gives

$$\begin{bmatrix} S_{11} & S_{12} \\ S_{21} & S_{22} \end{bmatrix} = \frac{\begin{bmatrix} A + \frac{B}{Z_0} - CZ_0 - D & 2(AD - BC) \\ 2 & -A + \frac{B}{Z_0} - CZ_0 + D \end{bmatrix}}{A + \frac{B}{Z_0} + CZ_0 + D}$$
(3.55)

3.2.2 Deriving the Thru-Reflect-Line Calibration Method

With the knowledge obtained for the scattering, transmission, and the ABCD parameters, signal flow graphs can be used to derive a set of equations for each TRL calibration standard. This technique has been used by Barba via Matthews and Song and Pozar [5, 18, 21]. This section of the thesis is essentially a recasting of material in [18] and [21]. Using (3.51) and (3.52), the scattering and transmission parameters can be evaluated for each individual component of the composite system using the following formula

$$[\mathbf{T_{comp}}] = [\mathbf{T_A}] \cdot [\mathbf{T_{DUT}}] \cdot [\mathbf{T_B}]$$
(3.56)

(3.57d)

where

$$[\mathbf{T_{comp}}] = \begin{bmatrix} T_{comp11} & T_{comp12} \\ T_{comp21} & T_{comp22} \end{bmatrix} = \mathbf{T}\text{-matrix of composite system}$$
(3.57a)
$$[\mathbf{T_A}] = \begin{bmatrix} T_{A11} & T_{A12} \\ T_{A21} & T_{A22} \end{bmatrix} = \mathbf{T}\text{-matrix of connector A}$$
(3.57b)
$$[\mathbf{T_B}] = \begin{bmatrix} T_{B11} & T_{B12} \\ T_{B21} & T_{B22} \end{bmatrix} = \mathbf{T}\text{-matrix of connector B}$$
(3.57c)

$$\begin{bmatrix} \mathbf{T_A} \end{bmatrix} = \begin{bmatrix} T_{A11} & T_{A12} \\ T_{A21} & T_{A22} \end{bmatrix} = \text{T-matrix of connector A}$$
(3.57b)

$$[\mathbf{T_B}] = \begin{bmatrix} T_{B11} & T_{B12} \\ T_{B21} & T_{B22} \end{bmatrix} = \text{T-matrix of connector B}$$
 (3.57c)

$$[\mathbf{T_{DUT}}] = \begin{bmatrix} T_{DUT11} & T_{DUT12} \\ T_{DUT21} & T_{DUT22} \end{bmatrix}$$
$$= [\mathbf{T_A}]^{-1} \cdot [\mathbf{T_{comp}}] \cdot [\mathbf{T_B}]^{-1} = \text{T-matrix of the DUT}$$

3.2.2.1 The *Thru* Measurement

The *Thru* measurement is realized by having connectors A and B directly connected to each other as shown by a schematic in Figure 3.15 and a signal flow graph in Figure 3.16. Using (3.51), the T-parameter matrix for the *Thru* standard is

$$[\mathbf{T}_{\mathbf{T}}] = \begin{bmatrix} T_{T11} & T_{T12} \\ T_{T21} & T_{T22} \end{bmatrix} = [\mathbf{T}_{\mathbf{A}}] \cdot [\mathbf{T}_{\mathbf{THRU}}] \cdot [\mathbf{T}_{\mathbf{B}}] = [\mathbf{T}_{\mathbf{A}}] \cdot [\mathbf{T}_{\mathbf{B}}]$$
(3.58)

where the ideal transmission matrix for the *Thru* standard is the identity matrix given by

$$[\mathbf{T_{THRU}}] = \begin{bmatrix} 1 & 0 \\ 0 & 1 \end{bmatrix} \tag{3.59}$$

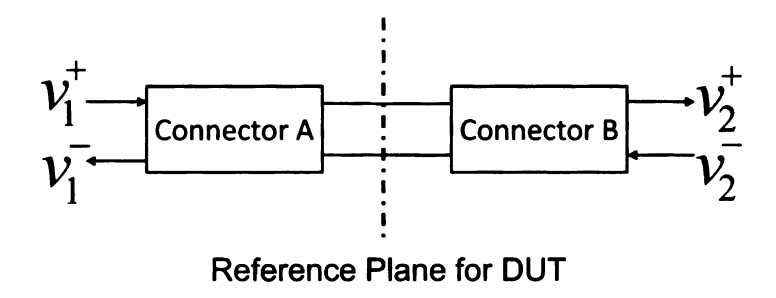


Figure 3.15. Schematic of *Thru* Standard Connection [5, 18]

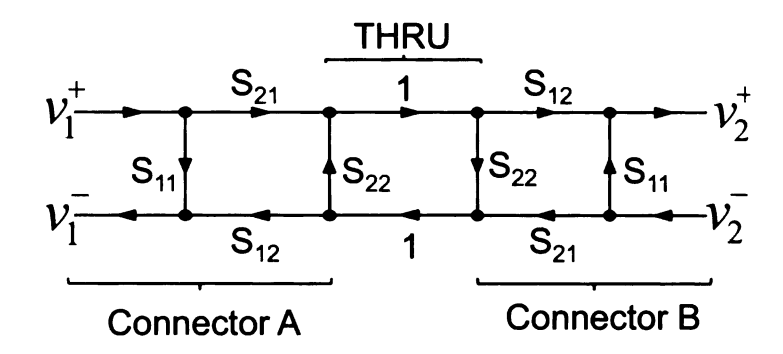


Figure 3.16. Signal flow graph of *Thru* Standard Connection [5]

3.2.2.2 The Reflect Measurement

The *Reflect* measurement is realized by placing a short circuit or open circuit at one end of connector A or B as shown by a schematic in Figure 3.17 and a signal flow graph in Figure 3.18.

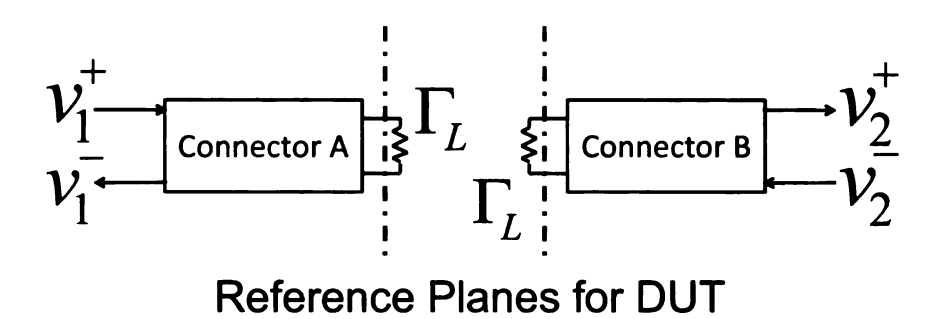


Figure 3.17. Schematic of Reflect Standard Connection [5, 18]

The reflection coefficient seen by the VNA will be a function of the reflection coefficient Γ_L and the S-parameters of the connector by the following equation

$$S_{R11} = S_{A11} + \frac{S_{A12}S_{A21}\Gamma_L}{1 - S_{A22}\Gamma_L} = \frac{\frac{T_{A12}}{T_{A22}} + \frac{T_{A11}}{T_{A22}} \cdot \Gamma_L}{1 + \frac{T_{A21}}{T_{A22}} \cdot \Gamma_L}$$
(3.60)

and using (3.60), the ratio $\frac{T_{A11}}{T_{A22}}$ is found.

$$\frac{T_{A11}}{T_{A22}} = \frac{1}{\Gamma_L} \cdot \frac{S_{R11} - \frac{T_{A12}}{T_{A22}}}{1 - \frac{T_{A21}}{T_{A11}} \cdot S_{R11}}$$
(3.61)

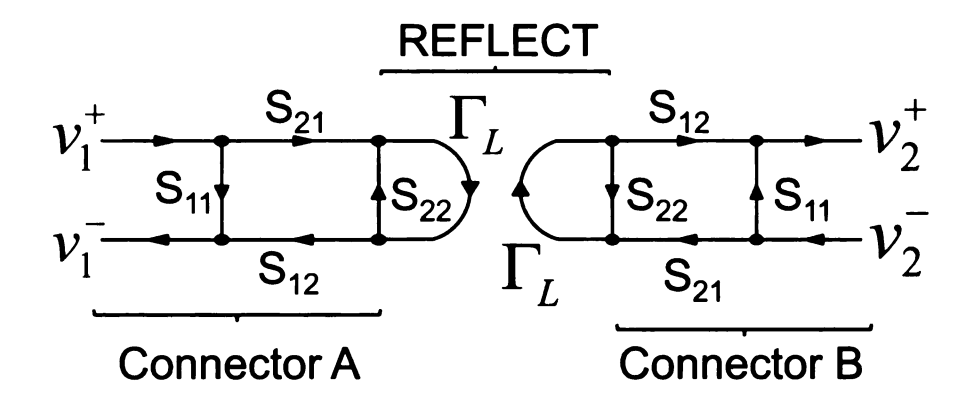


Figure 3.18. Signal flow of *Reflect* Standard Connection [5]

The same method applies to connector B using the same reflection coefficient Γ_L .

$$S_{R22} = S_{B22} + \frac{S_{B12}S_{B21}\Gamma_L}{1 - S_{B11}\Gamma_L} = \frac{-\frac{T_{B21}}{T_{B22}} + \frac{T_{B11}}{T_{B22}} \cdot \Gamma_L}{1 - \frac{T_{B12}}{T_{B22}} \cdot \Gamma_L}$$
(3.62)

Using (3.62) to find the ratio $\frac{T_{B11}}{T_{B22}}$

$$\frac{T_{B11}}{T_{B22}} = \frac{1}{\Gamma_L} \cdot \frac{S_{R22} + \frac{T_{B21}}{T_{B22}}}{1 + \frac{T_{B12}}{T_{B11}} \cdot S_{R22}}$$
(3.63)

then taking the product of (3.61) and (3.63) yields

$$\frac{T_{A11}}{T_{A22}} \cdot \frac{T_{B11}}{T_{B22}} = \frac{\left(S_{R11} - \frac{T_{A12}}{T_{A22}}\right) \left(1 + \frac{T_{B12}}{T_{B11}} \cdot S_{R22}\right)}{\left(S_{R22} + \frac{T_{B21}}{T_{B22}}\right) \left(1 - \frac{T_{B12}}{T_{B22}}\right)}$$
(3.64)

3.2.2.3 The *Line* Measurement

The *Line* measurement is realized by having an empty transmission line of known length ℓ placed in between connectors A and B as shown by a schematic and in Figure 3.19 and a signal flow graph in Figure 3.20. The S-parameters for this system will be measured and using (3.51), the T-parameter matrix for the *Line* standard is

$$[\mathbf{T_L}] = \begin{bmatrix} T_{L11} & T_{L12} \\ T_{L21} & T_{L22} \end{bmatrix} = [\mathbf{T_A}] \cdot [\mathbf{T_{LINE}}] \cdot [\mathbf{T_B}]$$
(3.65)

where the ideal transmission matrix for the Line standard is a phase-shifted identity matrix given by

$$[\mathbf{T_{LINE}}] = \begin{bmatrix} e^{-\gamma\ell} & 0\\ 0 & e^{\gamma\ell} \end{bmatrix}$$
 (3.66)

and (3.65) becomes

$$[\mathbf{T_L}] = [\mathbf{T_A}] \cdot [\mathbf{T_{LINE}}] \cdot [\mathbf{T_A}]^{-1} \cdot [\mathbf{T_T}]$$
(3.67)

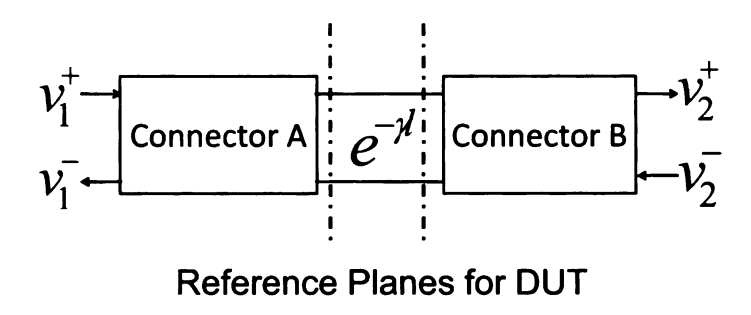


Figure 3.19. Schematic of Line Standard Connection [5, 18]

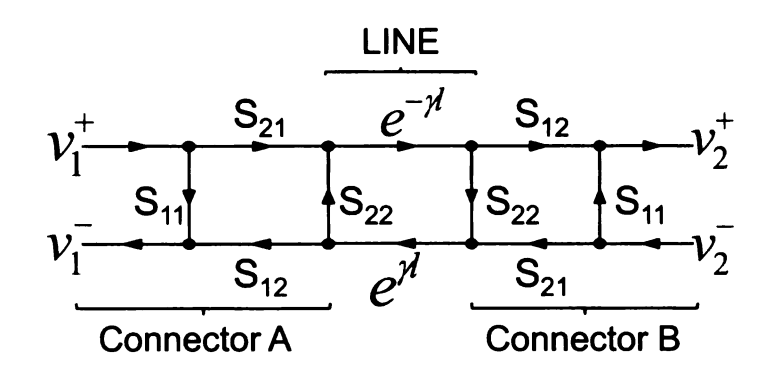


Figure 3.20. Schematic of *Line* Standard Connection [5]

If $[\mathbf{T_{LT}}]$ is defined by

$$[\mathbf{T_{LT}}] = [\mathbf{T_L}] \cdot [\mathbf{T_T}]^{-1} = \begin{bmatrix} T_{LT11} & T_{LT12} \\ T_{LT21} & T_{LT22} \end{bmatrix}$$

$$= \frac{1}{|\mathbf{T_T}|} \begin{bmatrix} T_{L11}T_{T22} - T_{L12}T_{T21} & T_{L12}T_{T11} - T_{L11}T_{T12} \\ T_{L21}T_{T22} - T_{L22}T_{T21} & T_{L22}T_{T11} - T_{L21}T_{T12} \end{bmatrix}$$
(3.68)

where $|\mathbf{T_T}|$ is the determinant of $[\mathbf{T_T}]$. Using (3.68), (3.67) can now be expressed as

$$[\mathbf{T_{LT}}] \cdot [\mathbf{T_A}] = [\mathbf{T_A}] \cdot [\mathbf{T_{LINE}}] \tag{3.69}$$

and expressing each component of (3.69) in linear form,

$$T_{LT11}T_{A11} + T_{LT12}T_{A21} = T_{A11}e^{-\gamma\ell}$$
(3.70a)

$$T_{LT11}T_{A12} + T_{LT12}T_{A22} = T_{A12}e^{\gamma\ell}$$
 (3.70b)

$$T_{LT21}T_{A11} + T_{LT22}T_{A21} = T_{A21}e^{-\gamma\ell}$$
(3.70c)

$$T_{LT21}T_{A12} + T_{LT22}T_{A22} = T_{A22}e^{\gamma\ell} \tag{3.70d}$$

then taking the ratios of (3.70a) to (3.70c) and (3.70b) to (3.70d), a pair of quadratic

equations are evaluated such that they have the same solutions.

$$T_{LT11} \left(\frac{T_{A11}}{T_{A21}}\right)^{2} + (T_{LT22} - T_{LT11}) \frac{T_{A11}}{T_{A21}} - T_{LT12} = 0$$

$$(3.71a)$$

$$T_{LT21} \left(\frac{T_{A12}}{T_{A22}}\right)^{2} + (T_{LT22} - T_{LT11}) \frac{T_{A12}}{T_{A22}} - T_{LT12} = 0$$

$$(3.71b)$$

$$\frac{T_{A11}}{T_{A21}}, \frac{T_{A12}}{T_{A22}} = \frac{1}{2T_{LT21}} [T_{LT11} - T_{LT22} \pm \sqrt{(T_{LT22} - T_{LT11})^{2} + 4(T_{LT21}T_{LT12})}]$$

$$(3.71c)$$

The roots of (3.71c) are determined by choosing a value of Γ_L . If a metallic plate is placed at the load of the microstrip and the experimentalist is aware that the reflection coefficient seen by the VNA is $S_{A11} = \frac{T_{A12}}{T_{A22}}$, it can be shown that this root has a larger magnitude and thus is assigned the reflection coefficient.

Referring back to (3.58) and solving for $[T_B]$

$$[\mathbf{T}_{\mathbf{B}}] = [\mathbf{T}_{\mathbf{A}}]^{-1} \cdot [\mathbf{T}_{\mathbf{T}}] \tag{3.72}$$

expanding (3.72) in matrix form

$$\begin{bmatrix} T_{B11} & T_{B12} \\ T_{B21} & T_{B22} \end{bmatrix} = \frac{1}{|\mathbf{T_A}|} \begin{bmatrix} T_{T11}T_{A22} - T_{T21}T_{A12} & T_{T12}T_{A22} - T_{T22}T_{A12} \\ T_{T21}T_{A11} - T_{T11}T_{A21} & T_{T22}T_{A11} - T_{T12}T_{A21} \end{bmatrix}$$
(3.73a)

and taking the ratios of T_{B21} to T_{B22} and T_{B12} to T_{B11} yielding

$$\frac{T_{B21}}{T_{B22}} = \frac{T_{T21} - \frac{T_{A21}}{T_{A11}} \cdot T_{T11}}{T_{T22} - \frac{T_{A21}}{T_{A11}} \cdot T_{T12}}$$

$$\frac{T_{B12}}{T_{B11}} = \frac{T_{T12} - \frac{T_{A12}}{T_{A22}} \cdot T_{T22}}{T_{T11} - \frac{T_{A12}}{T_{A22}} \cdot T_{T21}}$$
(3.74a)

$$\frac{T_{B12}}{T_{B11}} = \frac{T_{T12} - \frac{T_{A12}}{T_{A22}} \cdot T_{T22}}{T_{T11} - \frac{T_{A12}}{T_{A22}} \cdot T_{T21}}$$
(3.74b)

and taking the products of (3.74a) and (3.74b) to get

$$\frac{T_{A11}}{T_{A22}} \cdot \frac{T_{B11}}{T_{B21}} = \frac{T_{T11} - \frac{T_{A12}}{T_{A22}} \cdot T_{T21}}{T_{T22} - \frac{T_{A21}}{T_{A11}} \cdot T_{T12}}$$
(3.75)

Integrating the TRL Standards Together

Once all the measurements for each standard of the TRL calibration technique have been computed and defined, the results are put together and the S-parameters of the DUT are evaluated from (3.57d). Using both (3.64) and (3.75) creates a new expression for $\frac{T_{A11}}{T_{A22}}$

$$\frac{T_{A11}}{T_{A22}} = \pm \sqrt{\frac{\left(T_{T11} - \frac{T_{A12}}{T_{A22}} \cdot T_{T21}\right) \left(S_{R11} - \frac{T_{A12}}{T_{A22}}\right) \left(1 + \frac{T_{B12}}{T_{B11}} \cdot S_{R22}\right)}{\left(T_{T22} - \frac{T_{A21}}{T_{A11}} \cdot T_{T12}\right) \left(S_{R22} + \frac{T_{B21}}{T_{B22}}\right) \left(1 + \frac{T_{A21}}{T_{A11}} \cdot S_{R11}\right)}}$$
(3.76)

The sign of the ratio of (3.76) is selected with the condition that the value of Γ_L produces the same numerical value for (3.61) and (3.76). Another relation found from (3.76) is

$$\frac{T_{B11}}{T_{B22}} = \frac{T_{T11} - \frac{T_{A12}}{T_{A22}} \cdot T_{T21}}{T_{T22} - \frac{T_{A21}}{T_{A11}} \cdot T_{T12}} \left(\frac{T_{A11}}{T_{A22}}\right)^{-1}$$
(3.77)

and using (3.51) to produce the S-parameters of connector A with the reflection coefficients being

$$S_{A11} = \frac{T_{A12}}{T_{A22}} \tag{3.78a}$$

$$S_{A22} = -\frac{T_{A21}}{T_{A22}} = -\frac{T_{A21}}{T_{A11}} \cdot \frac{T_{A11}}{T_{A22}}$$
 (3.78b)

and referring to (3.52) and calculating the product $S_{A12}S_{A21}$

$$S_{A12}S_{A21} = \frac{T_{A11}}{T_{A22}} \left[1 - \frac{T_{A12}}{T_{A22}} \cdot \frac{T_{A21}}{T_{A11}} \right]$$
 (3.79)

For connector B, (3.51) and (3.73) can be used to find its reflection coefficients at for ports 1 and 2

$$S_{B11} = \frac{T_{B12}}{T_{B22}} = \frac{T_{T12} - \frac{T_{A12}}{T_{A11}} \cdot \frac{T_{A11}}{T_{A22}} \cdot T_{T22}}{\frac{T_{A11}}{T_{A22}} \cdot T_{T22} - \frac{T_{A21}}{T_{A22}} \cdot T_{T12}}$$
(3.80a)

$$S_{B22} = \frac{\frac{T_{A11}}{T_{A22}} \cdot T_{T21} - \frac{T_{A21}}{T_{A22}} \cdot T_{T11}}{\frac{T_{A11}}{T_{A22}} \cdot T_{T22} - \frac{T_{A21}}{T_{A22}} \cdot T_{T12}}$$
(3.80b)

Calculating the determinant of $|S_{\bf B}|$ and using (3.80) yields the product $S_{B12}S_{B21}$

$$|\mathbf{S_B}| = S_{B11}S_{B22} - S_{B12}S_{B21} = -\frac{T_{B12}S_{T21}}{S_{B22}S_{B22}} - \frac{T_{B11}}{T_{B22}} + \frac{T_{B12}S_{T21}}{S_{B22}S_{B22}}$$
(3.81a)

$$S_{B12}S_{B21} = \frac{T_{B11}}{T_{B22}} + S_{B11}S_{B22} \tag{3.81b}$$

When separating the off-diagonal elements of $[S_A]$ and $[S_B]$, two postulates are made: (1) The determinants of the T-parameter matrices for the *Thru* and *Line* standards are equal to each other and (2) the determinants for the T-parameter

matrices of the connectors A and B are equal to each other

$$|\mathbf{T_T}| = |\mathbf{T_L}| = \frac{S_{A12}}{S_{A21}} \cdot \frac{S_{B12}}{S_{B21}}$$
 (3.82)

$$|\mathbf{T_A}| = |\mathbf{T_B}|\tag{3.83}$$

Now using the assumptions made from above via (3.82) and (3.83), the ratios and $\frac{S_{B12}}{S_{B21}}$ are found

$$\frac{S_{A12}}{S_{A21}} = \frac{S_{B12}}{S_{B21}} = \sqrt{\frac{S_{T12}}{S_{T21}}} \tag{3.84}$$

and evaluating $S_{A12},\,S_{A21},\,S_{B12},\,$ and S_{B21} yield

$$S_{A12} = \sqrt{S_{A12} \cdot S_{A21} \sqrt{\frac{S_{T12}}{S_{T21}}}}$$
 (3.85a)

$$S_{A21} = \frac{S_{A12}S_{A21}}{S_{A12}} \tag{3.85b}$$

$$S_{A21} = \frac{S_{A12}S_{A21}}{S_{A12}}$$

$$S_{B12} = \sqrt{S_{B12} \cdot S_{B21} \sqrt{\frac{S_{T12}}{S_{T21}}}}$$
(3.85c)

$$S_{B21} = \frac{S_{B12}S_{B21}}{S_{B12}} \tag{3.85d}$$

Now everything needed to evaluate the elements of $[\mathbf{T}_{\mathbf{DUT}}]$ from (3.57) can be expressed using (3.51) and (3.52) and applying it to $[\mathbf{S}_{\mathbf{A}}]$ and $[\mathbf{S}_{\mathbf{B}}]$ where the T- parameters of the DUT are

$$\mathbf{T_{DUT11}} = \frac{T_{A22}(T_{comp11}T_{B22} - T_{comp12}T_{B21}) - T_{A12}(T_{comp21}T_{B22} - T_{comp22}T_{B21})}{(T_{A11}T_{A22} - T_{A12}T_{A21})(T_{B11}T_{B22} - T_{B12}T_{B21})}$$
(3.86a)
$$\mathbf{T_{DUT12}} = \frac{T_{A22}(T_{comp12}T_{B11} - T_{comp11}T_{B12}) - T_{A12}(T_{comp22}T_{B11} - T_{comp21}T_{B12})}{(T_{A11}T_{A22} - T_{A12}T_{A21})(T_{B11}T_{B22} - T_{B12}T_{B21})}$$
(3.86b)
$$\mathbf{T_{DUT21}} = \frac{T_{A11}(T_{comp21}T_{B22} - T_{comp22}T_{B21}) - T_{A21}(T_{comp11}T_{B22} - T_{comp12}T_{B21})}{(T_{A11}T_{A22} - T_{A12}T_{A21})(T_{B11}T_{B22} - T_{B12}T_{B21})}$$
(3.86c)
$$\mathbf{T_{DUT22}} = \frac{T_{A11}(T_{comp22}T_{B11} - T_{comp21}T_{B12}) - T_{A21}(T_{comp12}T_{B22} - T_{comp11}T_{B12})}{(T_{A11}T_{A22} - T_{A12}T_{A21})(T_{B11}T_{B22} - T_{B12}T_{B21})}$$
(3.86d)

and the S-parameters of the DUT are

$$\mathbf{S_{DUT11}} = \frac{S_{B11}(S_{A11}S_{comp22} - |\mathbf{S_{comp}}|) + (S_{comp11} - S_{A11})|\mathbf{S_{B}}|}{S_{B11} \cdot (S_{comp22} \cdot |\mathbf{S_{A}}| - S_{A22} \cdot |\mathbf{S_{comp}}|) + (S_{comp11}S_{A22} - |\mathbf{S_{A}}|) \cdot |\mathbf{S_{B}}|}$$

$$\mathbf{S_{DUT12}} = \frac{-S_{comp12}S_{A21}S_{B21}}{S_{B11} \cdot (S_{comp22} \cdot |\mathbf{S_{A}}| - S_{A22} \cdot |\mathbf{S_{comp}}|) + (S_{comp11}S_{A22} - |\mathbf{S_{A}}|) \cdot |\mathbf{S_{B}}|}$$

$$\mathbf{S_{DUT21}} = \frac{-S_{comp21}S_{A12}S_{B12}}{S_{B11} \cdot (S_{comp22} \cdot |\mathbf{S_{A}}| - S_{A22} \cdot |\mathbf{S_{comp}}|) + (S_{comp11}S_{A22} - |\mathbf{S_{A}}|) \cdot |\mathbf{S_{B}}|}$$

$$\mathbf{S_{DUT22}} = \frac{S_{B22}(S_{A22}S_{comp11} - |\mathbf{S_{A}}|) + S_{comp22}|\mathbf{S_{A}}| - S_{A22}|\mathbf{S_{comp}}|}{S_{B11} \cdot (S_{comp22} \cdot |\mathbf{S_{A}}| - S_{A22} \cdot |\mathbf{S_{comp}}|) + (S_{comp11}S_{A22} - |\mathbf{S_{A}}|) \cdot |\mathbf{S_{B}}|}$$

$$(3.87c)$$

$$\mathbf{S_{DUT22}} = \frac{S_{B22}(S_{A22}S_{comp11} - |\mathbf{S_{A}}|) + S_{comp22}|\mathbf{S_{A}}| - S_{A22}|\mathbf{S_{comp}}|}{S_{B11} \cdot (S_{comp22} \cdot |\mathbf{S_{A}}| - S_{A22} \cdot |\mathbf{S_{comp}}|) + (S_{comp11}S_{A22} - |\mathbf{S_{A}}|) \cdot |\mathbf{S_{B}}|}$$

$$(3.87d)$$

Considering that the de-embedding process will have two stages, here is how the process will be conducted for the test fixture and the microstrip [16]:

1. Construct a simulated model of the test fixture using S-parameter and T-

- parameter matrices to represent connectors A and B of the test fixture.
- 2. Collect the data for the S-parameters of the composite system of the test fixture, microstrip, and NIC and convert them to T-parameters.
- 3. Perform TRL calibration and apply (3.57d) and (3.86) to the measured T-parameters and convert them to S-parameters using (3.87) to remove the effects of the S-parameters due to the test fixture to obtain the S-parameters of the integrated system of the microstrip and the NIC.
- 4. Construct a simulated model of the microstrip using S-parameter and T-parameter matrices to represent two segments of the microstrip divided evenly.
- 5. Collect the data for the S-parameters of the integrated system of the microstrip and NIC and convert them to T-parameters.
- 6. Perform TRL calibration and apply (3.57d) and (3.86) to the measured T-parameters and convert them to S-parameters using (3.87) to remove the effects of the S-parameters due to the microstrip to obtain the S-parameters of the NIC (DUT).

CHAPTER 4

DESIGNING AND MODELING THE MICROSTRIP AND THE NIC

All the parameters have been gathered to construct the components of the composite system for two-stage de-embedding. These parameters must be chosen such that the most optimal results are produced. The microstrip will be constructed by the properties of a Rogers RT/Duroid 5870 high frequency laminate. The NIC that will be chosen for this particular project is a grounded, open-circuit stable VINIC consisting of BJTs. The type of transistor that will be used is the RF *npn* silicon-germanium (Si-Ge) NESG204619 BJT. Unfortunately there is no way to create a simulated model of the NIC using this transistor with the software available. Therefore, the RF *npn* silicon (Si) NESG2107M33 transistor will be considered.

This chapter depicts the dimensions of the microstrip, analyzes the NIC circuit, and shows how to perform one-tier de-embedding using the TRL calibration technique given the parameters of the system that will be observed for both stages of the de-embedding process. It also compares and contrasts simulated designs of the NIC with computational analysis the composite system and the DUT via TRL calibration.

4.1 Microstrip Design

Referring back to Section 3.1.2, for a Rogers RT/Duroid 5870 high frequency laminate with a known characteristic impedance $Z_0=50$ Ohms (Ω) and a dielectric constant $\epsilon_r=2.33$, the aspect ratio can be calculated. The initial guess is to use the case for $\frac{W}{h}<2$. From (3.32), A=1.18601 and $\frac{W}{h}=3.00401$. Therefore $\frac{W}{h}>2$, B=7.75913 and $\frac{W}{h}=2.97028$ with the effective dielectric constant $\epsilon_{eff}=2.40665$. If the thickness of the dielectric substrate is 0.7874 millimeters (0.031 inches), the width of the conducting strip is 2.3388 millimeters (mm).

The electrical length, ℓ , of the microstrip that is a quarter of a wavelength long operating at 7 GHz is

$$\phi = \beta \ell = k_0 \sqrt{\epsilon_{eff}} \ell = 90^\circ = \frac{2\pi}{\lambda} \frac{\lambda}{4} = \frac{\pi}{2}$$
 (4.1a)

$$k_0 = \frac{2\pi}{\lambda} = \omega \sqrt{\mu_0 \epsilon_0} = \frac{2\pi f}{c} = 146.709 \text{ radians per meter (rad/m)}$$
 (4.1b)

$$\ell = \frac{90^{\circ} \frac{\pi}{180^{\circ}}}{k_0 \sqrt{\epsilon_e f f}} = 6.90171 \text{ mm}$$
(4.1c)

These measurements are only estimates of the what the dimensions of the microstrip should be. Using a program called LineGauge by Zeland Software, more precise dimensions of the microstrip can be made using h=0.7874 mm, t=0.004 mm, $Z_0=90~\Omega,~\phi=90^{\circ},~\epsilon_r=2.33,~f=7$ GHz, W=2.33227 mm, $\ell=7.6354$ mm, $\epsilon_{eff}=1.96908$, and $\lambda=30.5213$ mm. With the given width and thickness of the microstrip, the aspect ratio is now $\frac{W}{h}=2.96199$. The reason for choosing the operating frequency to be 7 GHz is that this frequency lies in the middle of the frequency bandwidth of interest.

While these parameters produce the most optimal results, one should consider making the microstrip longer. In this case, the length of the microstrip will be 150 mm ($\ell=150$ mm) making the microstrip nearly two and a half wavelengths long. It is necessary to have a microstrip long enough for use of practical applications as the length of $\ell=7.6354$ mm is too small.

The attenuation constants due to dielectric and conductor loss can also be calculated knowing that the loss tangent of the laminate is $\tan(\delta) = 0.0012$ and the surface resistivity is $R_s = 2 \times 10^8$ megaohms (M Ω), (3.33a) and (3.33b) will have values of $\alpha_d = 0.126018$ nepers per meter (Np/m) and $\alpha_c = 1.71501 \times 10^{15}$ Np/m, respectively.

4.2 Negative Impedance Converter Circuit Design

A schematic of the NIC is displayed in Figure 4.1 and Figure 4.2. In this design, the NIC is composed of BJTs. For high frequency applications, BJTs are preferred over MOSFETs because the transconductance $g_m = \frac{i_{out}}{v_{in}}$, which is proportional to the unity-gain frequency f_T , is significantly much larger for BJTs than MOSFETs making BJTs more useful for high frequency amplifier design [12]. For this thesis, it is necessary to have a higher unity-gain frequency to have the BJT to maintain its expected performance when operating in the active region and the MOSFET to maintain its anticipated performance when operating in saturation. Otherwise, the transistors will not function properly.

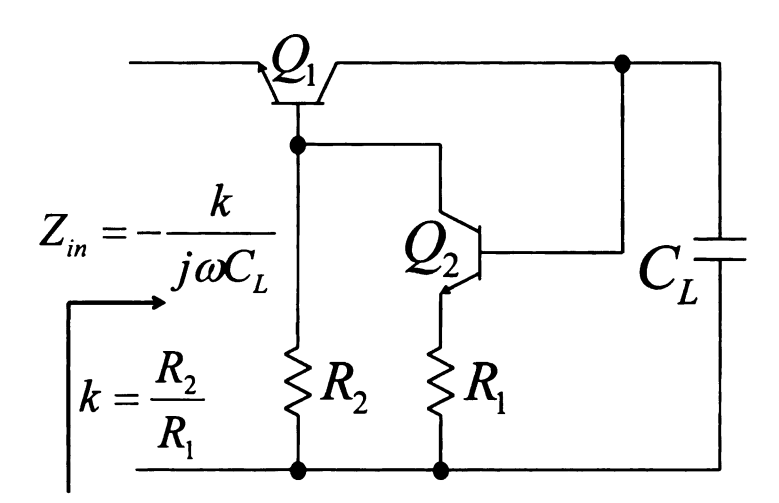


Figure 4.1. Negative impedance converter with capacitively terminated load [7, 9]

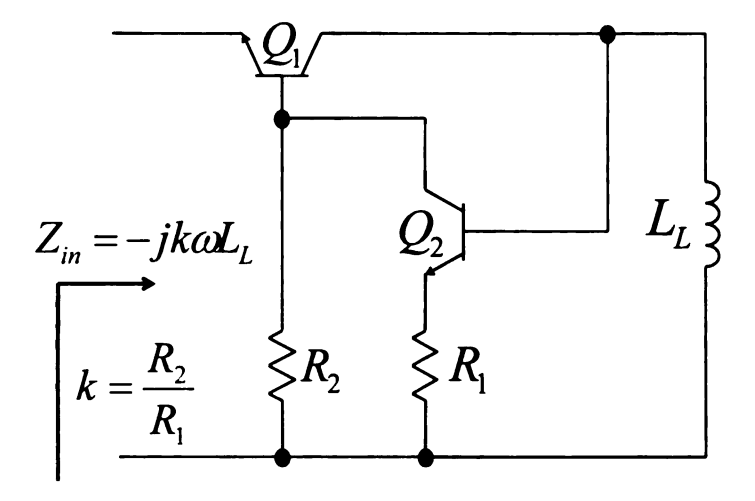


Figure 4.2. Negative impedance converter with inductively terminated load [7, 9]

The unity-gain frequency

$$f_T = \begin{cases} \frac{g_m}{2\pi (C_{BC} + C_{BE})} & \text{BJT} \\ \frac{g_m}{2\pi C_{OX}} & \text{MOSFET} \end{cases}$$
(4.2)

is the frequency where the small-signal current gain is equal to one or

$$\beta_F(\omega) \approx \frac{g_m r_\pi}{1 + j\omega r_\pi (C_{BE} + C_{BC})} = 1 \tag{4.3}$$

where C_{BC} is the base-collector junction capacitance, C_{BE} is the base-emitter capacitance, and $C_{OX} = C_{ox} \cdot Area_{gate}$ is the gate oxide-layer capacitance [10, 11, 12]. These parameters are found using alternating current (AC) small-signal equivalent circuit analysis. The small-signal models for the BJT and MOSFET are shown in Figure 4.3 and Figure 4.4.

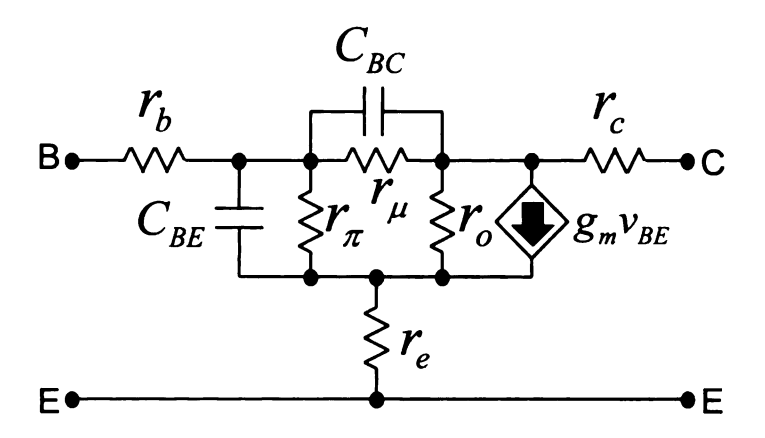


Figure 4.3. High frequency small-signal equivalent circuit of a BJT [10]

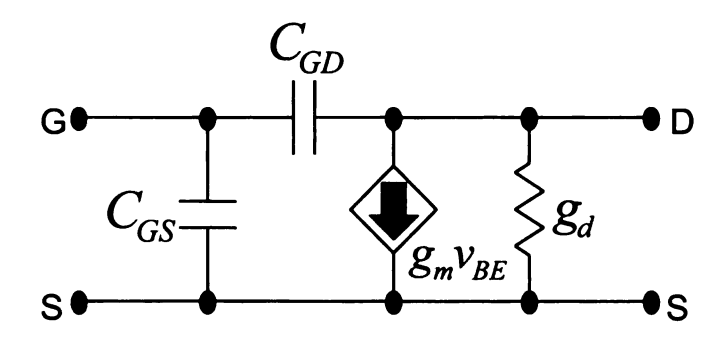


Figure 4.4. High frequency small-signal equivalent circuit of a MOSFET [10]

The unity-gain frequency represents the largest frequency that a transistor can operate to produce gain [11]. The given specifications require that the unity-gain frequency be much larger than 8 GHz. Since BJTs will be used to construct the NIC, $\beta_F(\omega) \gg 1$ in C-Band. It should also noted that frequency bandwidth of interest must be greater than the break frequency ω_B (e.g., $f_B <$ C-Band $< f_T$). This frequency is the point where the small-signal current gain falls by 3 dB. Figure 4.5 illustrates the trend for a transistor as the frequency increases.

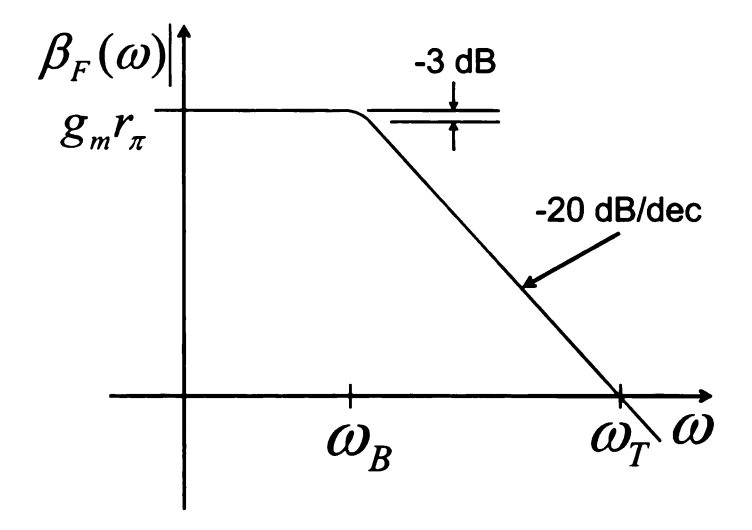


Figure 4.5. Typical frequency response of a BJT [11]

The transconductance for a BJT operating in the active region is

$$g_{m} = \frac{\partial I_{C}}{\partial V_{BE}} \bigg|_{V_{CE} = constant} - \frac{\partial I_{B}}{\partial V_{CE}} \bigg|_{V_{BE} = constant} \approx \frac{\partial I_{C}}{\partial V_{BE}} \bigg|_{V_{CE} = constant} \approx \frac{qI_{C}}{kT} = \frac{I_{C}}{V_{T}}$$

$$(4.4)$$

and the transconductance for a MOSFET operating in saturation is

$$g_m = \frac{\partial I_D}{\partial V_{GS}} \bigg|_{V_{DS} = constant} = 2K(V_{GS} - V_{TR}) = 2\sqrt{KI_D}$$
 (4.5)

It was previously mentioned in Section 2.2.4 that NICs composed of BJTs are VINICs because BJTs are transconductance devices. In other words, transistors are dependent current sources whose the input voltage controls the output current. It should also be noted that the NIC is grounded and open-circuit stable. Achieving the required specifications of the NIC make it necessary to favor the GNIC over the FNIC since most NIC designs are GNICs and this type of classification of NIC will be considered for this particular design. The NIC is open-circuit stable because the port that is not terminated with the load impedance is an open-circuit.

Revisiting Figure 4.1 and Figure 4.2, circuit analysis will show that the NIC is a VINIC. The transistors Q_1 and Q_2 have different configurations. Transistor Q_1 is operating as a common-base current follower and transistor Q_2 is operating as a common-emitter inverter. The load impedance Z_L is connected at the output of Q_1 and is connected in between the base and emitter resistor R_1 of Q_2 . It will be shown that $V_{out} = V_{Z_L} = -V_{in}$, the voltage at the base of Q_1 is in phase with V_{in} , and the input impedance is equal to the negative of the load impedance, i.e, $Z_{in} = -Z_L$.

Looking back to (2.36), the Ebers-Moll equations will be expanded to observe all modes of operation of the BJT mentioned in Section 2.2.4 using Figure 4.6

$$I_E = I_{E0}(e^{V_{BE}/\eta V_T} - 1) - \alpha_R I_{C0}(e^{V_{BC}/\eta V_T} - 1)$$
(4.6a)

$$I_C = \alpha_F I_{E0} (e^{V_{BE}/\eta V_T} - 1) - I_{C0} (e^{V_{BC}/\eta V_T} - 1)$$
(4.6b)

$$I_B = (1 - \alpha_F)I_{E0}(e^{V_{BE}/\eta V_T} - 1) + (1 - \alpha_R)I_{C0}(e^{V_{BC}/\eta V_T} - 1)$$
(4.6c)

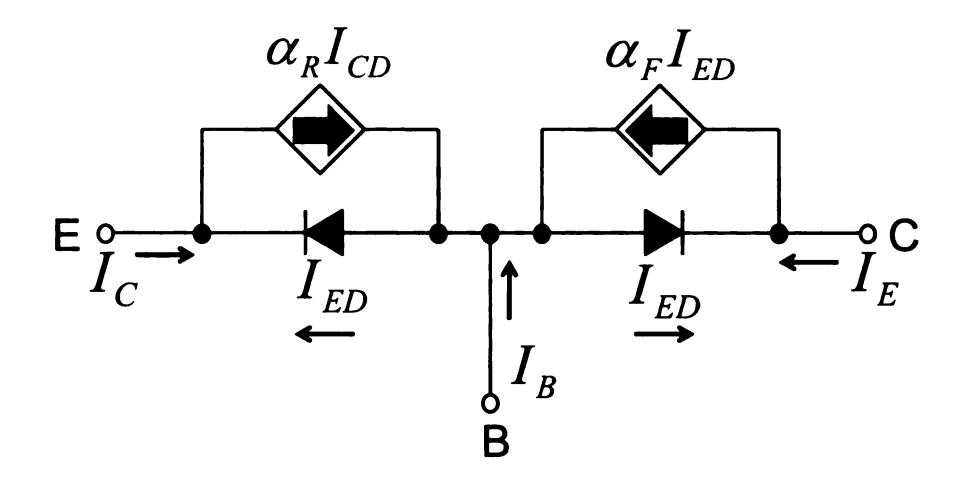


Figure 4.6. Ebers-Moll model of npn BJT [10]

where I_{E0} is the forward saturation current of the base-emitter junction, $I_{C0} = \alpha_F I_{E0}$ is the reverse saturation current of the base-collector junction, α_F is the forward common-base DC gain, α_R is the reverse common-base DC gain, $\beta_F = \frac{\alpha_F}{(1-\alpha_F)} \approx \frac{I_C}{I_B}$ is the forward-active common-emitter DC gain, and $\beta_R = \frac{\alpha_R}{(1-\alpha_R)} \approx -\frac{I_E}{I_B}$ is the reverse-active common-emitter direct current (DC) gain [10, 11]. The transconductance characteristics can be observed for the common-base current follower Q_1

$$I_{inQ_1} = I_{EQ_1} = I_{E0}(e^{V_{BEQ_1}/\eta V_T} - 1) - \alpha_R I_{C0}(e^{V_{BCQ_1}/\eta V_T} - 1)$$
(4.7a)

$$I_{outQ_1} = I_{CQ_1} = \alpha_F I_{E0} - (1 - \alpha_F \alpha_R) I_{C0} (e^{V_{BCQ_1}/\eta V_T} - 1)$$
(4.7b)

and the common-emitter inverter Q_2 [10]

$$I_{inQ_2} = I_{BQ_2}$$

$$= (1 - \alpha_F)I_{E0}(e^{V_{BEQ_2}/\eta V_T} - 1) + (1 - \alpha_R)I_{C0}(e^{(V_{BCQ_2} - V_{CEQ_2})/\eta V_T} - 1)$$
(4.8a)

$$I_{outQ_{2}} = I_{CQ_{2}}$$

$$= \frac{(\alpha_{F}I_{E0} - I_{C0}e^{-V_{CEQ_{2}}/\eta V_{T}})[I_{BQ_{2}} + (1 - \alpha_{F})I_{E0} + (1 - \alpha_{R})I_{C0}]}{(1 - \alpha_{F})I_{E0} + (1 - \alpha_{R})I_{C0}e^{-V_{CEQ_{2}}/\eta V_{T}}} + I_{C0} - \alpha_{F}I_{E0}$$

$$= \frac{I_{C0}(1 - e^{-V_{CEQ_{2}}/\eta V_{T}})[I_{BQ_{2}} + (1 - \alpha_{F})I_{E0} + (1 - \alpha_{R})I_{C0}]}{(1 - \alpha_{F})I_{E0} + (1 - \alpha_{R})I_{C0}e^{-V_{CEQ_{2}}/\eta V_{T}}}$$

$$(4.8b)$$

Since the *active* mode of the BJT is only being considered, the input-output transfer characteristics must be observed for all modes of operation to determine the range of which transistors Q_1 and Q_2 need to operate in the *active* region.

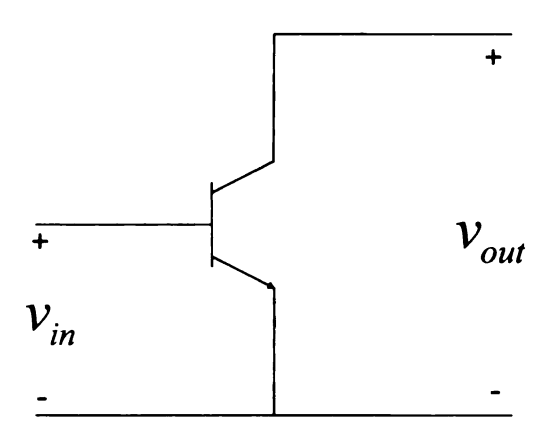


Figure 4.7. Basic common-emitter amplifier [24]

If only Q_2 is observed, then it is an inverter with an emitter resistor R_1 which is a common-emitter amplifier as shown in Figure 4.7. Considering AC sources, if Q_2 is

operating in the active region,

$$i_{EQ_2} = \frac{v_{out} - V_{BEQ_2}}{R_1}$$
 (4.9a)

$$i_{BQ_2} = i_{CQ_1} - i_{out} = \alpha_F i_{in} - \frac{v_{out}}{Z_L} = \frac{i_{EQ_2}}{\beta_F + 1} = \frac{v_{out} - V_{BEQ_2}}{(\beta_F + 1)R_1}$$
 (4.9b)

$$i_{CQ_2} = \beta_F i_{BQ_2} = \alpha_F i_{EQ_2} = \frac{\alpha_F}{R_1} (v_{out} - V_{BEQ_2})$$
 (4.9c)

$$v_{inQ_2} = v_{out} \tag{4.9d}$$

$$v_{outQ_2} = V_{CEQ_2} = V_{CQ_2} - i_{CQ_2}R_1$$

$$= V_{CQ_2} - (\beta_F + 1)i_{BQ_2}R_1$$

$$= V_{BQ_1} - (v_{out} - V_{BEQ_2}) = -v_{out} + (V_{BQ_1} + V_{BEQ_2})$$
(4.9e)

while transfer characteristics for the saturation region are

$$\begin{aligned} v_{outQ_2,min} &= V_{CEQ_2,sat} = V_{BQ_1} - (\beta_F + 1)i_{BQ_2,max}R_1 \\ &= V_{BQ_1} - (v_{out,max} - V_{BEQ_2}) = -v_{out,max} + (V_{BQ_1} + V_{BEQ_2}) \end{aligned} \tag{4.10a}$$

$$v_{out,max} = (V_{BQ_1} + V_{BEQ_2}) - V_{CEQ_2,sat}$$
(4.10b)

$$i_{BQ_2,sat} = i_{BQ_2,max} = \frac{v_{out,max} - V_{BEQ_2}}{(\beta_F + 1)R_1}$$
 (4.10c)

$$i_{CQ_2,sat} = i_{CQ_2,max} = \beta_F i_{BQ_2,sat} = \frac{\alpha_F}{R_1} (v_{out,max} - V_{BEQ_2})$$
 (4.10d)

The inverter is in cutoff mode when $v_{out} < V_{BEQ_2}$ and $v_{outQ_2} = V_{BQ_1}$. The voltage-current relationship at the input and output of the inverter is shown in Figure 4.8 and Figure 4.9, respectively. The input-output voltage relationship of the inverter is shown in Figure 4.10 where the applied input and output voltage ranges needed for Q_2 to operate in the active region are $V_{BEQ_2} < v_{inQ_2} = v_{out} < (V_{BQ_1} + V_{BEQ_2}) - V_{CEQ_2,sat}$ and $-v_{out,max} + (V_{BQ_1} + V_{BEQ_2}) < v_{outQ_2} = V_{CEQ_2} < V_{BQ_1}$, respectively.

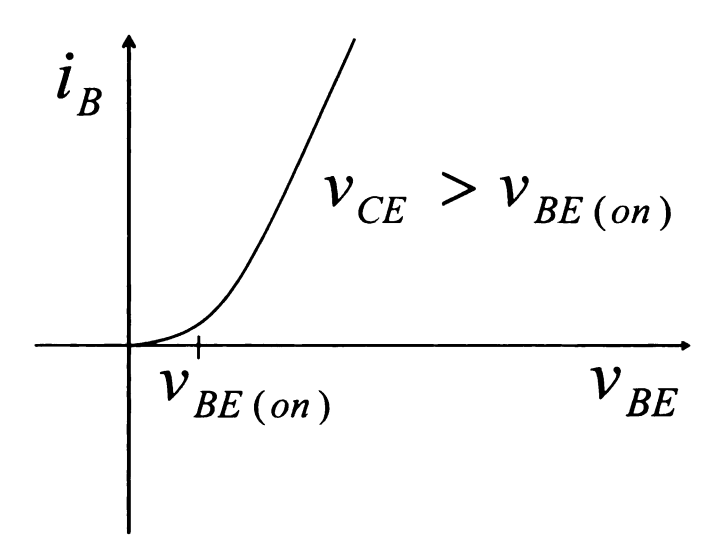


Figure 4.8. Input voltage-current relationship of common-emitter amplifier [24]

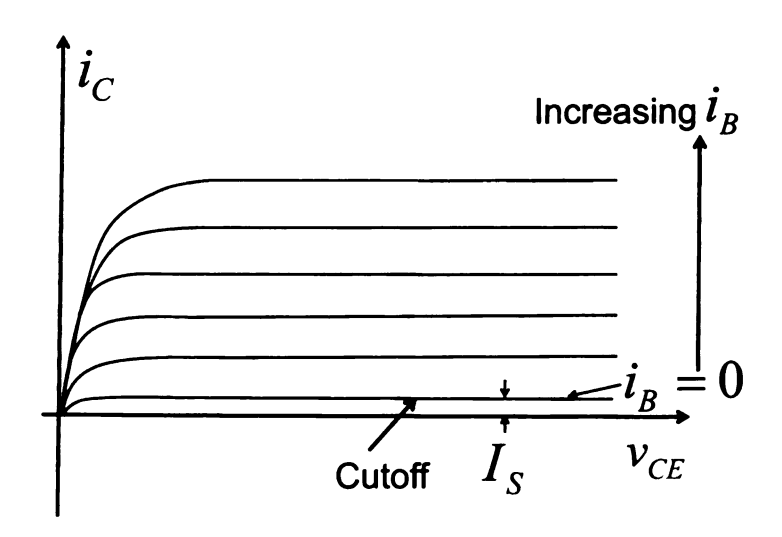


Figure 4.9. Output voltage-current relationship of common-emitter amplifier [24]

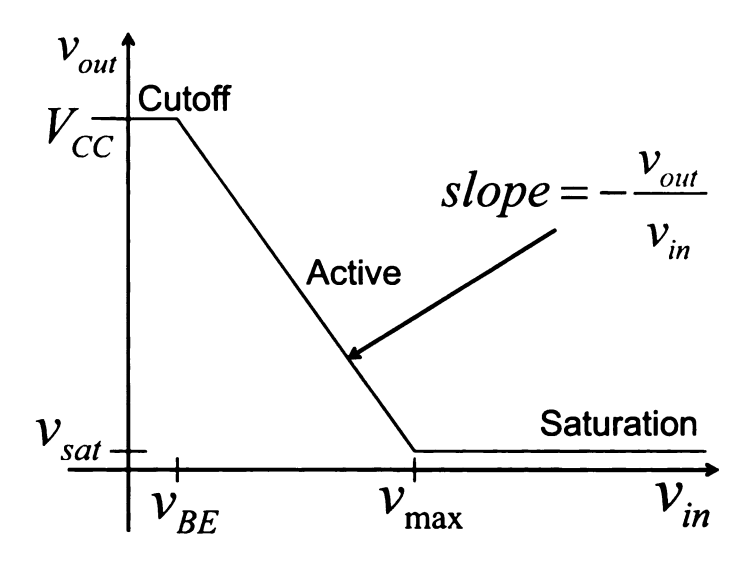


Figure 4.10. Transfer characteristic of common-emitter amplifier [11]

If Q_2 and R_1 are removed from the NIC circuit, the circuit will be a current follower with a base resistor R_2 and a load capacitor C_L of impedance $Z_L = \frac{1}{j\omega C_L}$ or a load inductor L_L of impedance $Z_L = j\omega L_L$ which is a common-base amplifier as shown in Figure 4.11.

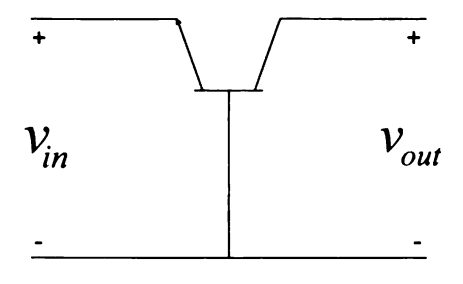


Figure 4.11. Basic common-base amplifier [24]

Considering AC sources, if the BJT is operating in the active region,

$$i_{EQ_1} = i_{in} \tag{4.11a}$$

$$i_{BQ_1} = \frac{i_{in}}{\beta_F + 1} = i_{CQ_2} + i_{R_2} = i_{CQ_2} + \frac{V_{BQ_1}}{R_2}$$
 (4.11b)

$$i_{CQ_1} = \frac{\beta_F}{\beta_F + 1} i_{in} = \alpha_F i_{in} = i_{BQ_2} + i_{out} = \frac{v_{out} - V_{BEQ_2}}{(\beta_F + 1)R_1} + \frac{v_{out}}{Z_L}$$
(4.11c)

$$v_{inQ_{1}} = v_{in} = V_{R_{2}} - V_{BEQ_{1}} = i_{R_{2}}R_{2} - V_{BEQ_{1}} = (i_{BQ_{1}} - i_{CQ_{2}})R_{2} - V_{BEQ_{1}}$$

$$= \left[\frac{i_{in}}{\beta_{F} + 1} - \frac{\alpha_{F}}{R_{1}}(v_{out} - V_{BEQ_{2}})\right]R_{2} - V_{BEQ_{1}}$$

$$= -\frac{\alpha_{F}R_{2}}{R_{1}}v_{out} + \left[\frac{i_{in}R_{2}}{\beta_{F} + 1} + \frac{\alpha_{F}R_{2}}{R_{1}}V_{BEQ_{2}}\right] - V_{BEQ_{1}}$$

$$(4.11d)$$

$$v_{outQ_1} = v_{out} = V_{BCQ_1} = V_{CEQ_1} - V_{BEQ_1} = i_{out} Z_L$$
(4.11e)

while transfer characteristics for the saturation region are

$$v_{out,min} = V_{CEQ_1,sat} - V_{BEQ_1} = -\alpha_F Z_L i_{in,sat}$$
(4.12a)

$$i_{in,sat} = i_{in,max} (4.12b)$$

and $v_{out} = 0$ in *cutoff* mode. The voltage-current relationship at the input and output of the current follower is shown in Figure 4.12 and Figure 4.13, respectively, where the input current range is $0 < i_{in} < i_{in,sat}$ and the output voltage range needed for Q_2 to operate in the active region is $-\alpha_F Z_L i_{in,sat} < v_{out} Q_1 = V_{BCQ_1} < 0$.

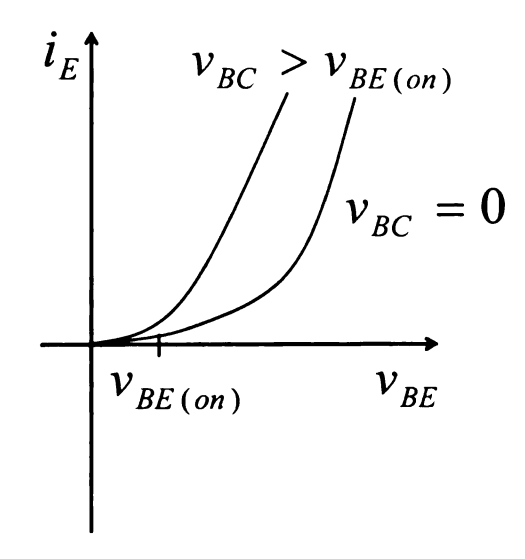


Figure 4.12. Input voltage-current relationship of common-base amplifier [24]

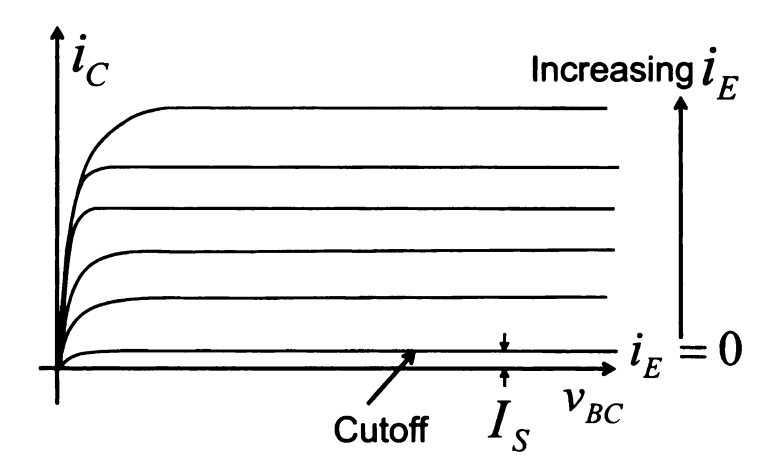


Figure 4.13. Output voltage-current relationship of common-base amplifier [24]

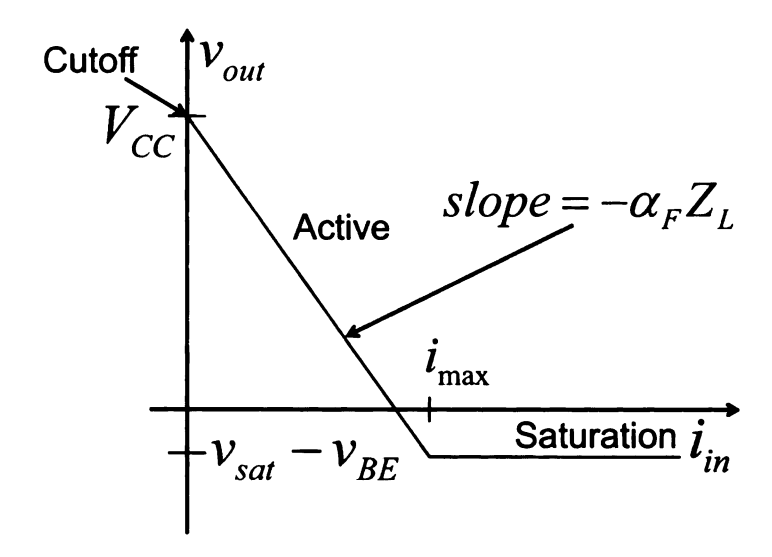


Figure 4.14. Transfer characteristic of common-base amplifier [11]

Equation (4.11d) can be used to find v_{in} in terms of v_{out} only

$$v_{in} = -\frac{\alpha_F R_2}{R_1} v_{out} + \left[\frac{i_{in} R_2}{\beta_F + 1} + \frac{\alpha_F R_2}{R_1} V_{BEQ_2} \right] - V_{BEQ_1} \approx -\frac{\alpha_F R_2}{R_1} v_{out}$$

$$\approx -\frac{R_2}{R_1} v_{out} = -\frac{R_2}{R_1} i_{out} Z_L = -\frac{R_2}{R_1} (i_{CQ_1} - i_{BQ_2}) Z_L$$

$$= -\frac{R_2}{R_1} \left[\alpha_F i_{in} - \frac{v_{out} - V_{BEQ_2}}{(\beta_F + 1)R_1} \right] Z_L \approx -\frac{R_2}{R_1} \alpha_F i_{in} Z_L$$

$$\approx -\frac{R_2}{R_1} i_{in} Z_L$$
(4.13)

since the last three terms are negligible compared to the first term by order of magnitude, $\alpha_F \approx 1$, and $\beta_F \gg 1$ in the first and last expressions of (4.13), respectively. Utilizing this information, it can be shown from (4.13) that $Z_{in} = \frac{v_{in}}{i_{in}} = -\frac{R_2}{R_1} Z_L$ where $k = \frac{R_2}{R_1}$. It is also shown from (4.9) that the voltage at the base of Q_1 is in phase with the input voltage v_{in} and that $v_{out} = -v_{in}$ from (4.13).

To simplify things, here is how the NIC works:

- 1. An input current flows out of the voltage source v_{in} and through the commonbase current follower Q_1 generating an output voltage $v_{out} = -Z_L i_{in}$ at load impedance Z_L .
- 2. The output voltage produces feedback through the collector-emitter stage via the base of the common-emitter inverter Q_2 inverting v_{out} at the base of Q_1 resulting in the voltage at the base of Q_1 to be in phase with v_{in} .
- 3. Since v_{out} = -v_{in}, the input impedance of the NIC is the negative of the load impedance of the NIC multiplied by a scaling factor, i.e., Z_{in} = -kZ_L where k is the scaling factor defined by how the NIC is implemented. For this particular circuit, k = R₂/R₁ [9].

Even though all the design parameters have been computed for the NIC design, there are a few precautions that need to be taken when operating this circuit [12]:

- 1. As the collector current I_C increases by a factor of 10, the base-emitter voltage V_{BE} increases 60 millivolts (mV). The general relationship between the change of collector current and base-emitter voltage is $\Delta V_{BE} = V_T \ln \left(\frac{I_{C2}}{I_{C1}} \right)$.
- 2. As the temperature T of the transistor increases, the base-emitter V_{BE} decreases 2.1 mV per degree Celsius (mV/°C).

4.3 De-embedding the Test Port Cables and the Microstrip

The test port cables and microstrip will be de-embedded using TRL calibration. Connectors A and B will be designated as the test port cables of the VNA for the first stage of two-stage de-embedding. It will be assumed that the test port cables will have equal length. In the second stage of the de-embedding process, the microstrip will be cut evenly in two, i.e., the lengths of connectors A and B are half the electrical length of the microstrip and they are equal to each other. If this is the case for both

stages of the de-embeding proces, then from (3.56) and (3.57)

$$[\mathbf{T_A}] = [\mathbf{T_B}]$$
 and $[\mathbf{S_A}] = [\mathbf{S_B}]$ (4.14)

Referring back to Sections 3.2.2.1, 3.2.2.2, and 3.2.2.3, the measurements for each standard of both stages of the de-embedding process will be conducted.

4.3.1 The Thru Measurement Revisited

From (3.58), $[\mathbf{T_T}]$ can be evaluated as

$$[\mathbf{T}_{\mathbf{T}}] = [\mathbf{T}_{\mathbf{A}}] \cdot [\mathbf{T}_{\mathbf{B}}] = [\mathbf{T}_{\mathbf{A}}] \cdot [\mathbf{T}_{\mathbf{A}}] \tag{4.15}$$

4.3.2 The Reflect Measurement Revisited

In the first stage of two-stage de-embedding, it will be assumed that the test port cables have low loss and the characteristic impedance of the test fixture connectors are matched with the microstrip. Details will be explained in Section 4.4.1. In the second stage of two-stage de-embedding, it will be assumed that the microstrip is lossless. If the connectors are terminated with a short circuit, $S_{11} = S_{22}$, $S_{21} = S_{12}$, and $\Gamma_L = -1$ making new expressions for equations (3.60) to (3.64)

$$S_{R11} = S_{A11} - \frac{S_{A21}^2}{1 + S_{A11}} = \frac{\frac{T_{A12}}{T_{A22}} - \frac{T_{A11}}{T_{A22}}}{1 - \frac{T_{A21}}{T_{A22}}}$$
(4.16)

where the ratio $\frac{T_{A11}}{T_{A22}}$ is expressed in (3.61). For connector B, (3.62) becomes

$$S_{R22} = S_{R11} = S_{B22} - \frac{S_{B12}S_{B21}}{1 + S_{B11}}$$

$$= S_{B11} - \frac{S_{B21}^2}{1 + S_{B11}} = \frac{-\frac{T_{B21}}{T_{B22}} - \frac{T_{B11}}{T_{B22}}}{1 + \frac{T_{B12}}{T_{B22}}}$$

$$(4.17)$$

and the ratio expressed in (3.63) becomes

$$\frac{T_{B11}}{T_{B22}} = \frac{T_{A11}}{T_{A22}} = -\frac{S_{R11} + \frac{T_{A21}}{T_{A22}}}{1 + \frac{T_{A12}}{T_{A11}} \cdot S_{R11}}$$
(4.18)

The product of (3.61) and (3.63) is now

$$\frac{T_{A11}}{T_{A22}} \cdot \frac{T_{B11}}{T_{B22}} = \frac{T_{A11}}{T_{A22}} \cdot \frac{T_{A11}}{T_{A22}} = \left(\frac{T_{A11}}{T_{A22}}\right)^{2}$$

$$= \frac{\left(S_{R11} - \frac{T_{A12}}{T_{A22}}\right) \left(1 + \frac{T_{B12}}{T_{B11}} \cdot S_{R22}\right)}{\left(S_{R22} + \frac{T_{B21}}{T_{B22}}\right) \left(1 - \frac{T_{B12}}{T_{B22}}\right)}$$

$$= \frac{\left(S_{R11} - \frac{T_{A12}}{T_{A22}}\right) \left(1 + \frac{T_{A12}}{T_{A11}} \cdot S_{R11}\right)}{\left(S_{R11} + \frac{T_{A21}}{T_{A22}}\right) \left(1 - \frac{T_{A12}}{T_{A22}}\right)} \tag{4.19}$$

4.3.3 The *Line* Measurement Revisited

To produce the best results for this standard, the length of the empty transmission line in the first stage and the electrical length of the empty, lossless microstrip in the second stage, ℓ , must be a quarter of a wavelength (e.g., $\ell = \frac{\lambda}{4}$) [17]. This makes $\gamma = j\beta$ in (3.66) where $\beta_{t-line} = \omega \sqrt{LC}$ from Section 3.1.1 for the test port cables and $\beta_{microstrip} = \frac{2\pi}{\lambda} \sqrt{\epsilon_{eff}}$ from (3.29) for the microstrip. Equation (3.72) is converted to

$$[\mathbf{T}_{\mathbf{B}}] = [\mathbf{T}_{\mathbf{A}}] = [\mathbf{T}_{\mathbf{A}}]^{-1} \cdot [\mathbf{T}_{\mathbf{T}}] \tag{4.20}$$

and is expanded in the same way shown in (3.73) and the ratios of (3.74) which remain the same

$$\frac{T_{B21}}{T_{B22}} = \frac{T_{A21}}{T_{A22}} = \frac{T_{T21} - \frac{T_{A21}}{T_{A11}} \cdot T_{T11}}{T_{T22} - \frac{T_{A21}}{T_{A11}} \cdot T_{T12}}$$

$$\frac{T_{B12}}{T_{B11}} = \frac{T_{A12}}{T_{A11}} = \frac{T_{T12} - \frac{T_{A12}}{T_{A22}} \cdot T_{T22}}{T_{T11} - \frac{T_{A12}}{T_{A22}} \cdot T_{T21}}$$
(4.21a)

$$\frac{T_{B12}}{T_{B11}} = \frac{T_{A12}}{T_{A11}} = \frac{T_{T12} - \frac{T_{A12}}{T_{A22}} \cdot T_{T22}}{T_{T11} - \frac{T_{A12}}{T_{A22}} \cdot T_{T21}}$$
(4.21b)

and (3.75) is now

$$\frac{T_{A11}}{T_{A22}} \cdot \frac{T_{B11}}{T_{B21}} = \frac{T_{A11}}{T_{A22}} \cdot \frac{T_{A11}}{T_{A21}} = \frac{T_{T11} - \frac{T_{A12}}{T_{A22}} \cdot T_{T21}}{T_{T22} - \frac{T_{A21}}{T_{A11}} \cdot T_{T12}}$$
(4.22)

The S-parameters of the DUT are recalculated from (3.57d). Using both (3.64) and (3.75) creates a new expression for $\frac{T_{A11}}{T_{A22}}$ using (4.14)

$$\frac{T_{A11}}{T_{A22}} = \pm \sqrt{\frac{\left(T_{T11} - \frac{T_{A12}}{T_{A22}} \cdot T_{T21}\right) \left(S_{R11} - \frac{T_{A12}}{T_{A22}}\right) \left(1 + \frac{T_{A12}}{T_{A11}} \cdot S_{R11}\right)}{\left(T_{T22} - \frac{T_{A21}}{T_{A11}} \cdot T_{T12}\right) \left(S_{R11} + \frac{T_{A21}}{T_{A22}}\right) \left(1 + \frac{T_{A21}}{T_{A11}} \cdot S_{R11}\right)}}$$
(4.23)

Following the same procedure to evaluate the S-parameters the DUT as shown in (3.87) through equations (3.77) to (3.85) obtains new expressions for (3.86) and (3.87)

where the T-parameters of the DUT are

$$\mathbf{T_{DUT11}} = \frac{T_{A22}(T_{comp11}T_{A22} - T_{comp12}T_{A21}) - T_{A12}(T_{comp21}T_{A22} - T_{comp22}T_{A21})}{(T_{A11}T_{A22} - T_{A12}T_{A21})(T_{A11}T_{A22} - T_{A12}T_{A21})}$$
(4.24a)
$$\mathbf{T_{DUT12}} = \frac{T_{A22}(T_{comp12}T_{A11} - T_{comp11}T_{A12}) - T_{A12}(T_{comp22}T_{A11} - T_{comp21}T_{A12})}{(T_{A11}T_{A22} - T_{A12}T_{A21})(T_{A11}T_{A22} - T_{A12}T_{A21})}$$
(4.24b)
$$\mathbf{T_{DUT21}} = \frac{T_{A11}(T_{comp21}T_{A22} - T_{comp22}T_{A21}) - T_{A21}(T_{comp11}T_{A22} - T_{comp12}T_{A21})}{(T_{A11}T_{A22} - T_{A12}T_{A21})(T_{A11}T_{A22} - T_{A12}T_{A21})}$$
(4.24c)
$$\mathbf{T_{DUT22}} = \frac{T_{A11}(T_{comp22}T_{A11} - T_{comp21}T_{A12}) - T_{A21}(T_{comp12}T_{A22} - T_{comp11}T_{A12})}{(T_{A11}T_{A22} - T_{A12}T_{A21})(T_{A11}T_{A22} - T_{A12}T_{A21})}$$
(4.24d)

and the S-parameters of the DUT are

$$\mathbf{S_{DUT11}} = \frac{S_{A11}(S_{A11}S_{comp11} - |\mathbf{S_{comp}}|) + (S_{comp11} - S_{A11})|\mathbf{S_{A}}|}{S_{A11} \cdot (S_{comp11} \cdot |\mathbf{S_{A}}| - S_{A11} \cdot |\mathbf{S_{comp}}|) + (S_{comp11}S_{A11} - |\mathbf{S_{A}}|) \cdot |\mathbf{S_{A}}|}$$

$$-S_{comp21}S_{A01}^{2}$$
(4.25a)

$$\mathbf{S_{DUT12}} = \frac{-S_{comp21}S_{A21}^2}{S_{A11} \cdot (S_{comp11} \cdot |\mathbf{S_A}| - S_{A11} \cdot |\mathbf{S_{comp}}|) + (S_{comp11}S_{A11} - |\mathbf{S_A}|) \cdot |\mathbf{S_A}|}$$

$$(4.25b)$$

$$\mathbf{S_{DUT21}} = \frac{-S_{comp21}S_{A12}^2}{S_{A11} \cdot (S_{comp11} \cdot |\mathbf{S_A}| - S_{A11} \cdot |\mathbf{S_{comp}}|) + (S_{comp11}S_{A11} - |\mathbf{S_A}|) \cdot |\mathbf{S_A}|}$$

$$(4.25c)$$

$$\mathbf{S_{DUT22}} = \frac{S_{A11}(S_{A11}S_{comp11} - |\mathbf{S_A}|) + S_{comp11}|\mathbf{S_A}| - S_{A11}|\mathbf{S_{comp}}|}{S_{A11} \cdot (S_{comp11} \cdot |\mathbf{S_A}| - S_{A11} \cdot |\mathbf{S_{comp}}|) + (S_{comp11}S_{A11} - |\mathbf{S_A}|) \cdot |\mathbf{S_A}|}$$

$$(4.25d)$$

4.4 Modeling the Test Fixture, Microstrip and NIC

With all the necessary measurements needed, the test fixture, microstrip, and NIC can be modeled using equations (4.14) to (4.25). Each component will be modeled accord-

ing to their physical parameters. It must be noted that the S-parameter, T-parameter, and ABCD-parameter matrices have to be represented as complex numbers.

4.4.1 Modeling the Test Fixture

The type of test fixture that will be used is an Anritsu 3680-20 Universal Test Fixture and will be modeled according to Figure 4.15.

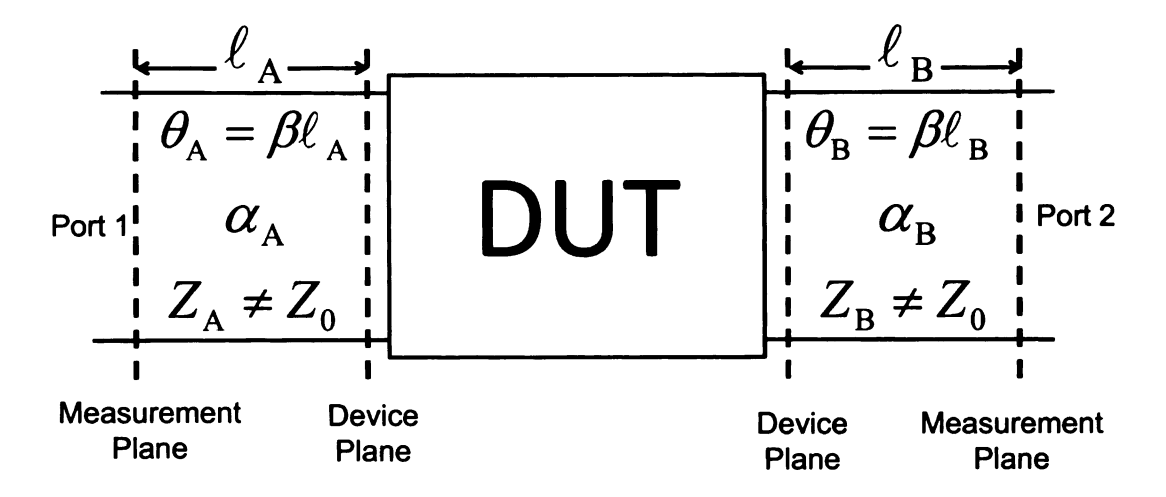


Figure 4.15. Test fixture modeled as a lossy transmission line [16]

The ideal case would be to model each side of the test fixture as a lossless transmission line with a characteristic impedance of 50 Ω as shown in Figure 4.16.

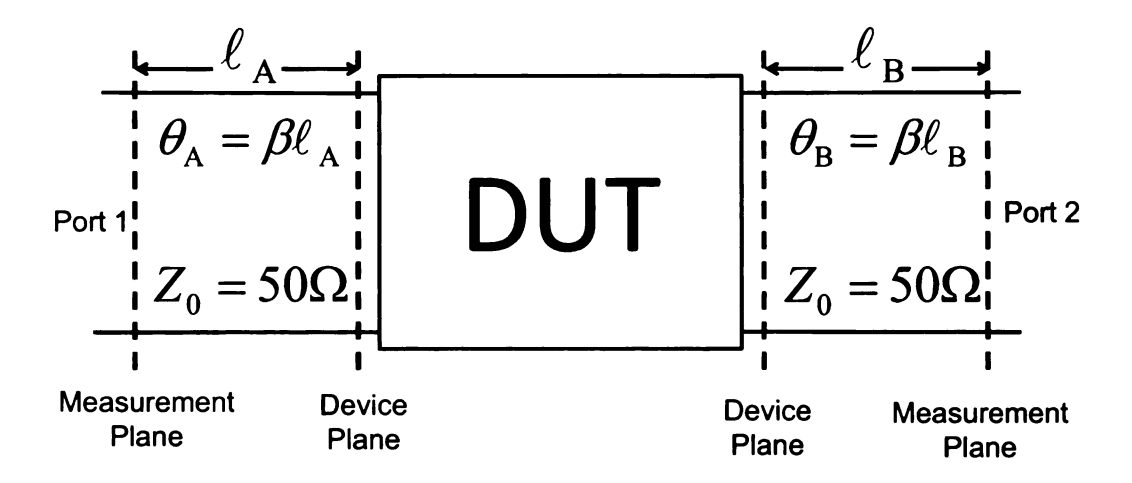


Figure 4.16. Test fixture modeled as a lossless transmission line [16]

However, since an accurate model needs to account for insertion loss and return loss, it will be first assumed that the test fixture is a lossy transmission line with an arbitrary characteristic impedance Z_{arb} and a return loss of -30 dB ($|\Gamma_L| = 10^{30/20} = 10^{-1.5} = 0.0316228$) [16, 23]. In this case, the magnitude of the reflection coefficient was found from (3.22b)

$$|\Gamma_L| = 10^{RL/20} \tag{4.26}$$

and the magnitude of the transmission coefficient can be found from (3.22a)

$$|T| = 10^{IL/20} (4.27)$$

For the first stage of the de-embedding process, the measurement plane is located at the ends of the cables while the device plane is located at the ends of integrated system of the microstrip and the NIC. The distance between these two planes will be designated as ℓ_A for connector A and ℓ_B for connector B of the test fixture. Since the signal sent from the VNA to the integrated system via the test port cables will encounter dispersion (the signal sent from the cables will be distorted as it propagates down the line), the propagation constant expressed in Section 3.1.1 is expanded to [5]

$$\gamma = \alpha + j\beta = \sqrt{(R + j\omega L)(G + j\omega C)}$$

$$= \sqrt{j\omega L \cdot j\omega C} \sqrt{\left(1 + \frac{R}{j\omega L}\right) \left(1 + \frac{G}{j\omega C}\right)}$$

$$= j\omega \sqrt{LC} \sqrt{1 - j\left(\frac{R}{\omega L} + \frac{G}{\omega C}\right) - \frac{RG}{\omega^2 LC}}$$
(4.28)

Suppose now that return loss of the cables is small. This goes under the condition that $R \ll \omega L$ and $G \ll \omega C$ making the conductor and the dielectric loss of the cables very small. This makes $RG \ll \omega^2 LC$ and

$$\gamma = j\omega\sqrt{LC}\sqrt{1 - j\left(\frac{R}{\omega L} + \frac{G}{\omega C}\right)}$$

$$\approx j\omega\sqrt{LC}\left[1 - \frac{j}{2}\left(\frac{R}{\omega L} + \frac{G}{\omega C}\right)\right]$$
(4.29a)

$$\alpha \approx \frac{1}{2} \left[R \sqrt{\frac{C}{L}} + G \sqrt{\frac{L}{C}} \right] = \frac{1}{2} \left[\frac{R}{Z_0} + G Z_0 \right]$$
 (4.29b)

$$\beta \approx \omega \sqrt{LC} \tag{4.29c}$$

$$Z_0 = \frac{R + j\omega L}{G + j\omega C} \approx \sqrt{LC}$$
 (4.29d)

If the signal propagating along the line is not dispersive, the ideal case is presented

where
$$\frac{R}{L} = \frac{G}{C}$$
 and

$$\gamma = j\omega\sqrt{LC}\sqrt{1 - 2j\frac{R}{\omega L} - \left(\frac{R}{\omega L}\right)^2}$$

$$= j\omega\sqrt{LC}\left[1 - j\frac{R}{\omega L}\right]$$

$$= R\sqrt{\frac{C}{L}} + j\omega\sqrt{LC} = \alpha + j\beta$$
(4.30a)

$$\alpha = R\sqrt{\frac{C}{L}} = \frac{R}{Z_0} \tag{4.30b}$$

$$\beta = \omega \sqrt{LC} \tag{4.30c}$$

Using this information, it can be concluded that the conductor and dielectric losses for connectors A and B will be chiefly due to the test fixture. For simplicity, since characteristic impedance of the test port cables and the test fixture cannot be directly obtained without measuring the characteristic impedances of the cables and the test fixture, it will be presumed from (4.29) that the test port cables are lossless and the input impedance at the device plane ($Z_0 = 50~\Omega$) is matched with the characteristic impedance of the cables ($Z_0 = 50~\Omega$) because the loss of the transmission line is small. This makes the reflection coefficient between the test port cables and the connectors of the test fixture zero. Since the distance between the two planes for each connector are equal and 3.5 mm long ($\ell_A = \ell_B = 3.5$ mm) as specified by [23], equations (4.16) to (4.25) can be applied to the test fixture to evaluate the S-parameters of the composite system of the microstrip and the NIC where they are defined by [16] for the C-band frequency bandwidth

$$[\mathbf{S_A}] = [\mathbf{S_B}] = \begin{bmatrix} S_{A11} & S_{A12} \\ S_{A21} & S_{A22} \end{bmatrix} = \begin{bmatrix} 0 & e^{-j\beta\ell_A} \\ e^{-j\beta\ell_A} & 0 \end{bmatrix} = \begin{bmatrix} 0 & e^{-j(2\pi f/c)\ell_A} \\ e^{-j(2\pi f/c)\ell_A} & 0 \end{bmatrix}$$
(4.31)

where $\beta=\frac{\omega}{c}=\frac{2\pi f}{c}$ and Figures 4.17 to 4.22 model the S-parameters of the test port cables for each TRL calibration standard. The TRL calculations were performed using MATLAB developed by The MathWorks. It is shown from these figures that the coax cables and the test fixture connectors have low loss. For purposes here, it will be assumed that the coaxial cables and test fixture connectors are lossless. Therefore, performing de-embedding in the first stage is not necessary. However, if the characteristic impedances of the cables and the test fixture connectors are not the same, then this stage of the de-embedding process needs to be performed.

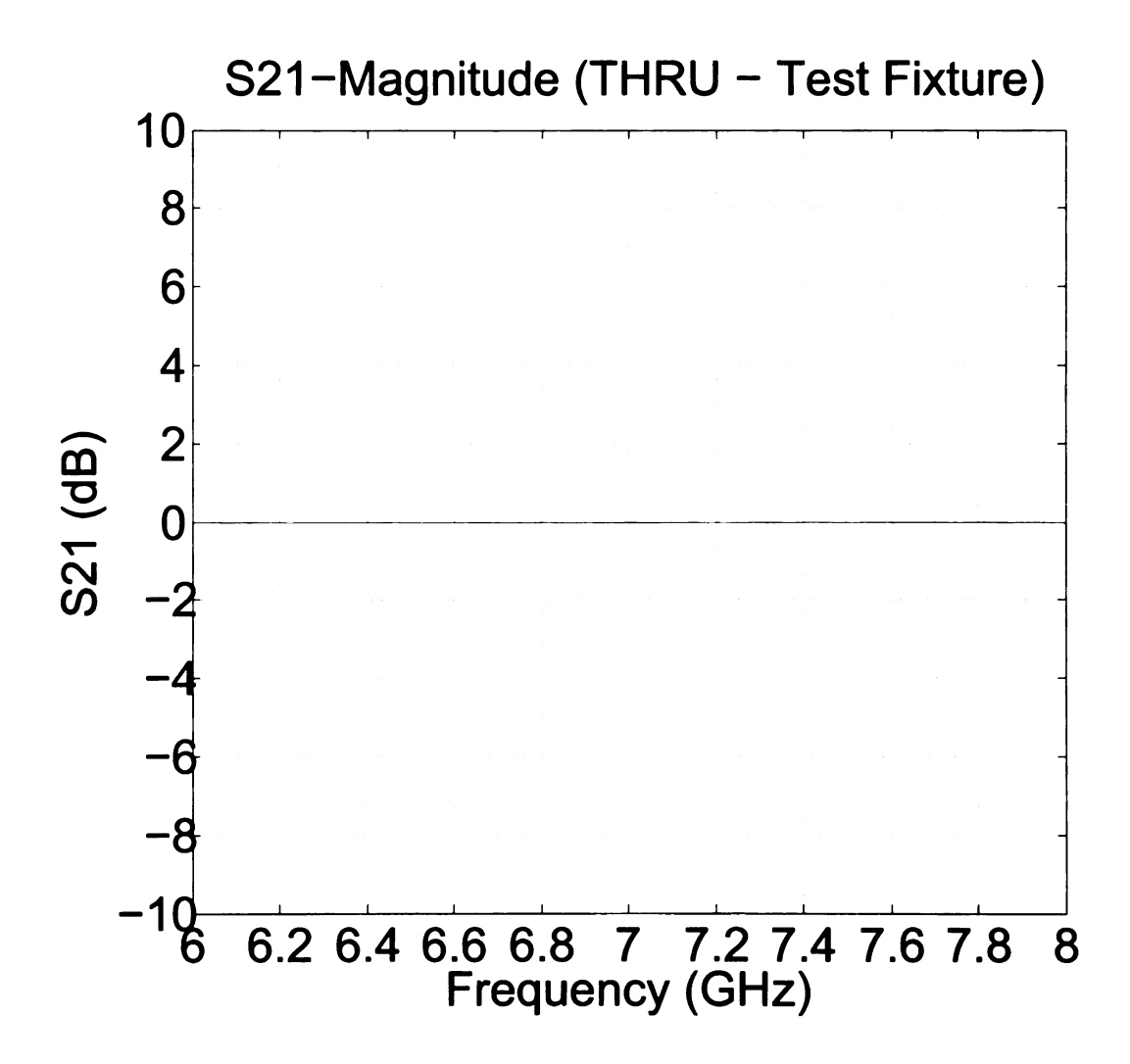


Figure 4.17. Magnitude of transmission coefficient for *Thru* standard of the test fixture

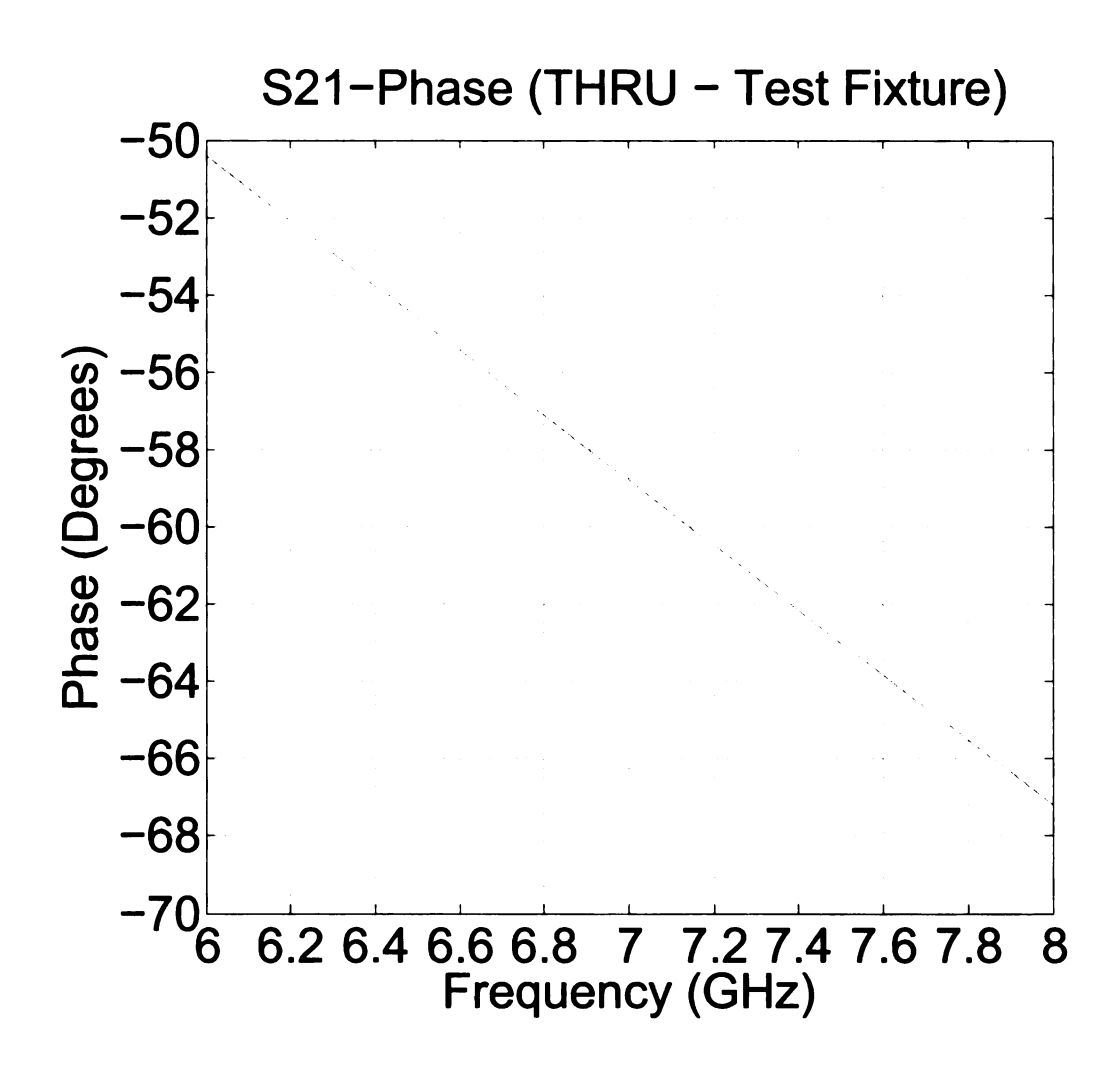


Figure 4.18. Phase of transmission coefficient for Thru standard of the test fixture

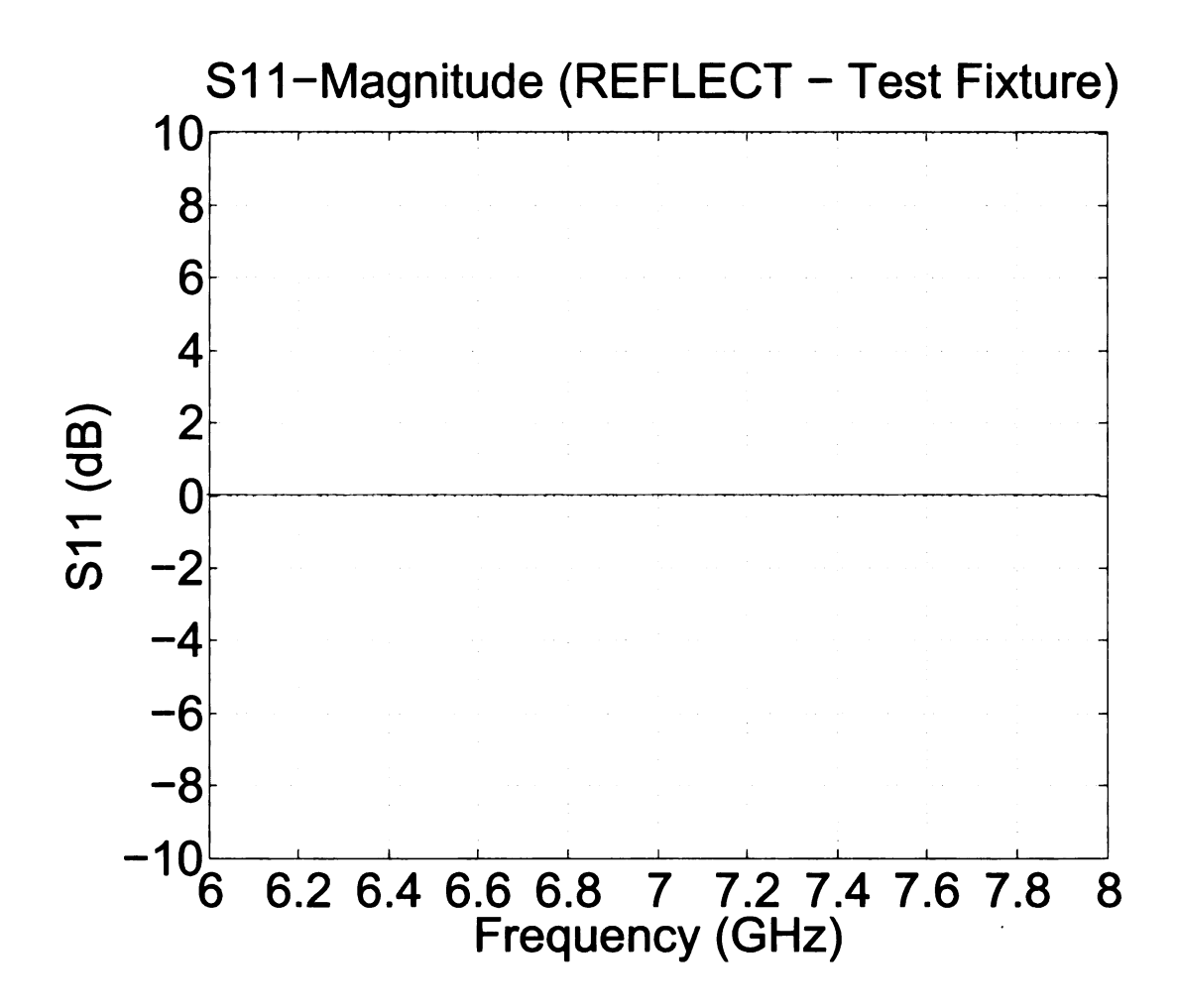


Figure 4.19. Magnitude of reflection coefficient for Reflect standard of the test fixture

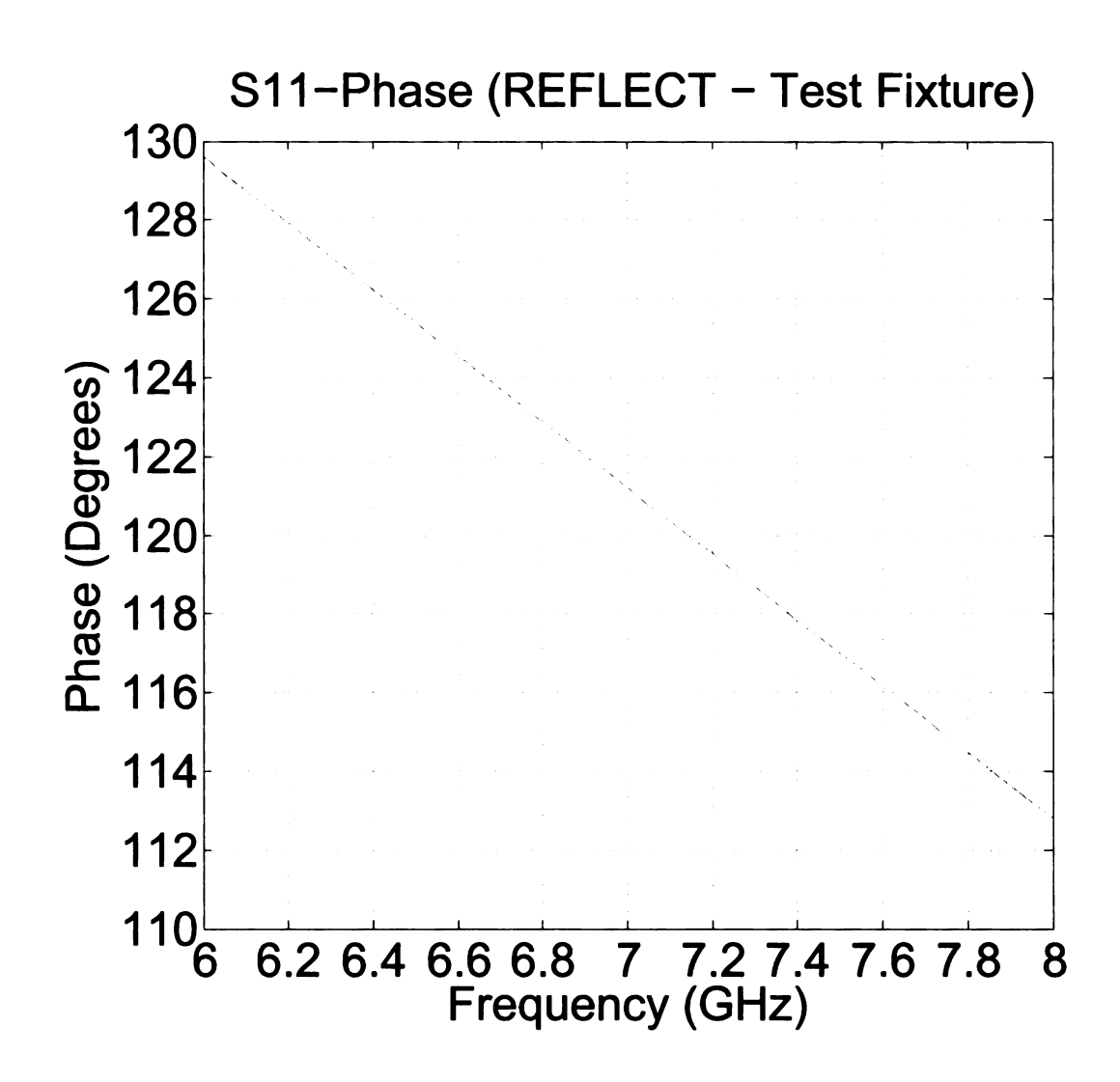


Figure 4.20. Phase of reflection coefficient for Reflect standard of the test fixture

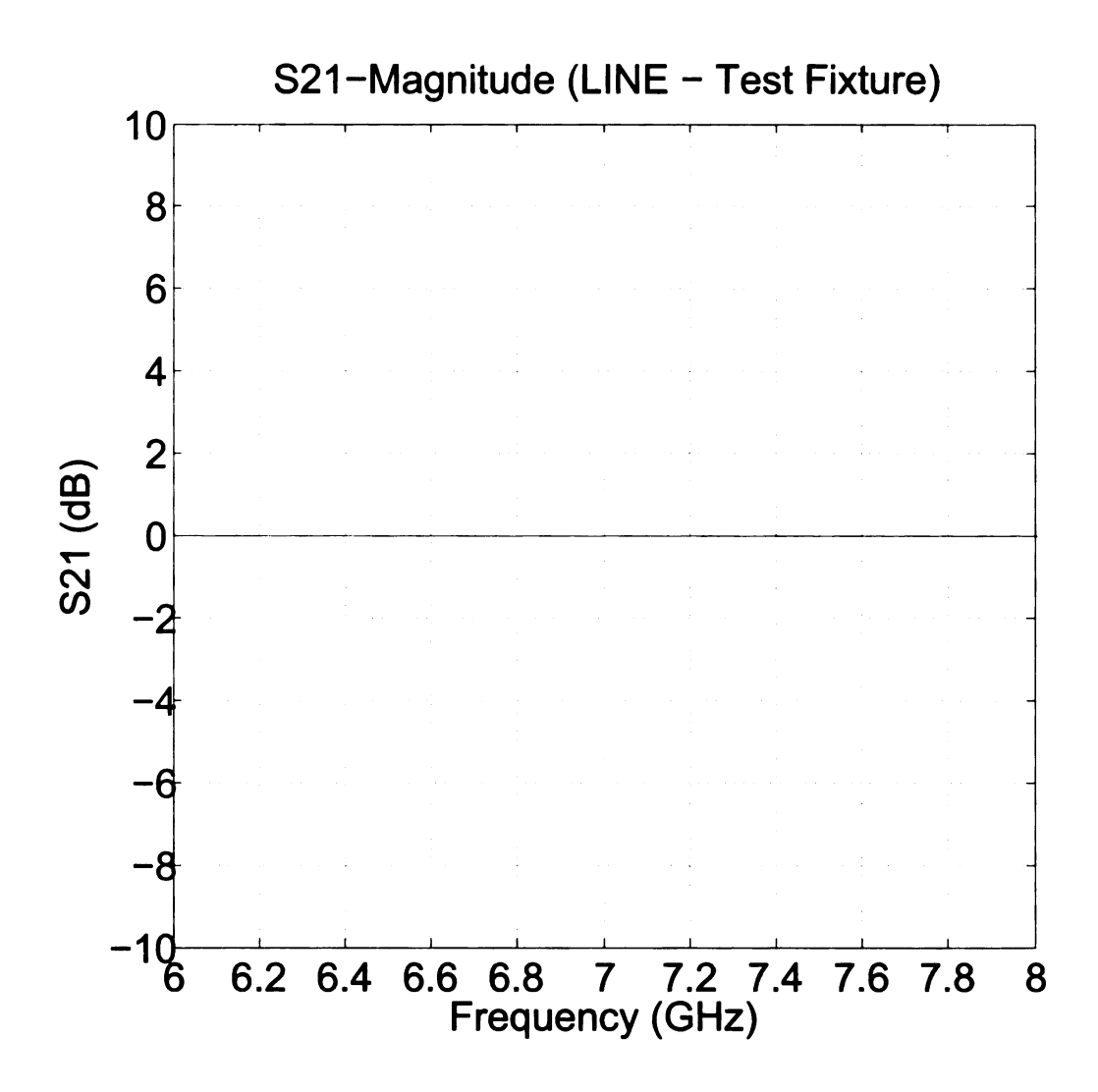


Figure 4.21. Magnitude of transmission coefficient for *Line* standard of the test fixture

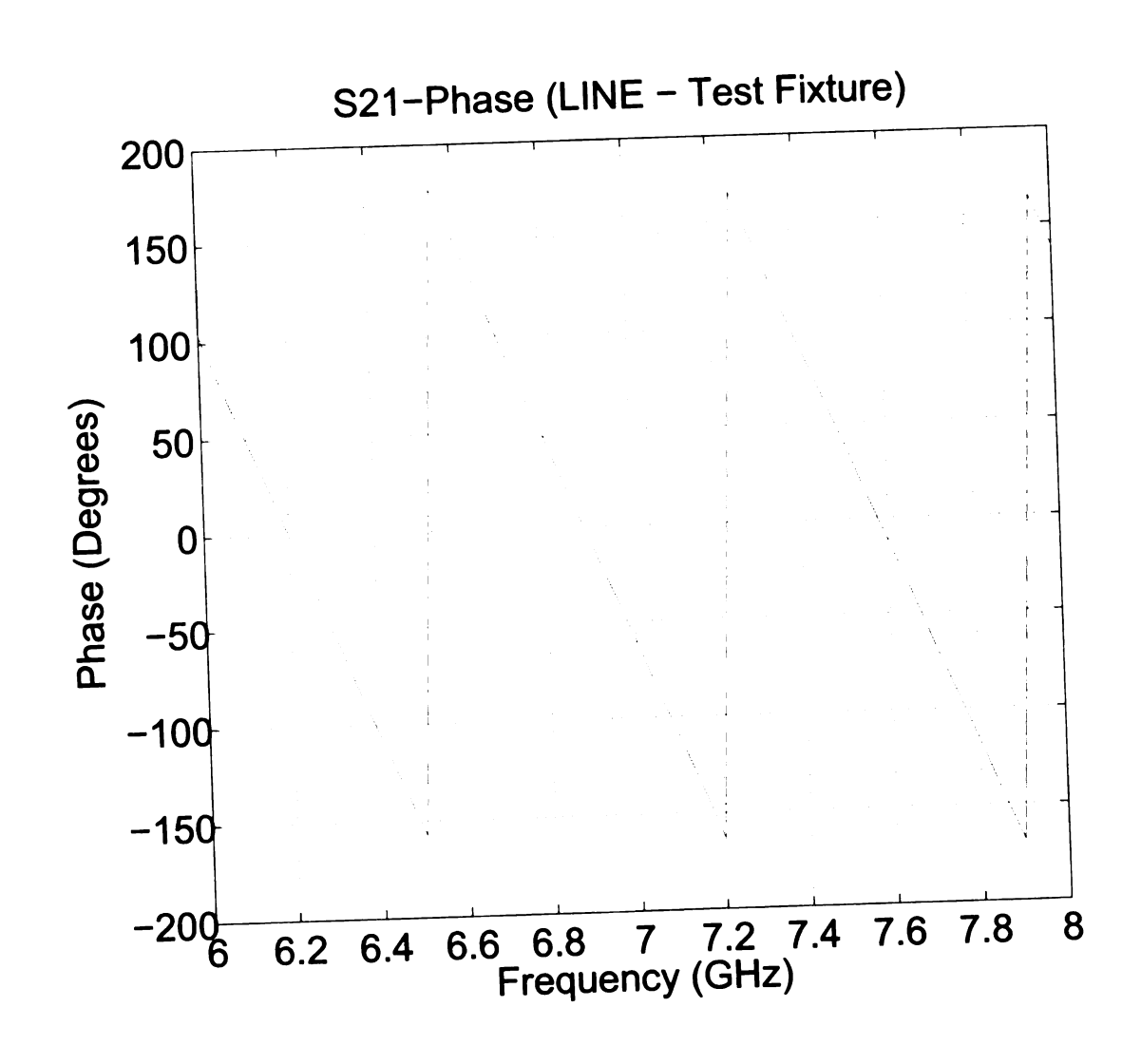


Figure 4.22. Phase of transmission coefficient for Line standard of the test fixture

4.4.2 Modeling the Microstrip

Referring back to Section 4.1, the S-parameters of the microstrip will be modeled for the second stage of the de-embedding process. The S-parameters for a lossless microstrip of a length $\ell=150$ mm and a phase constant analyzed in the frequency band of 6 GHz to 8 GHz in 50 MHz increments can be modeled from [16]

$$[\mathbf{S_A}] = [\mathbf{S_B}] = \begin{bmatrix} S_{A11} & S_{A12} \\ S_{A21} & S_{A22} \end{bmatrix} = \begin{bmatrix} 0 & e^{-j\beta\ell_A} \\ e^{-j\beta\ell_A} & 0 \end{bmatrix} = \begin{bmatrix} 0 & e^{-j(2\pi f/c)\ell_A} \\ e^{-j(2\pi f/c)\ell_A} & 0 \end{bmatrix}$$
(4.32)

where $e^{-j(2\pi f/c)\ell_A}$ with $\ell_A=\ell_B=\frac{\ell}{2}=75$ mm. A model can be made to visualize how the microstrip will behave. However, an EM simulator called Sonnet by Sonnet Software models more precise data of the microstrip since it is a full-wave Maxwell's equation solver. Another simulation program called Ansoft Designer by Ansoft Corporation can also be used to describe how the microstrip will behave using TRL calibration. Figures 4.23 to 4.32 model the S-parameters of the microstrip for each TRL calibration standard using the S-parameters of the half-length microstrip modeled in Sonnet and Ansoft Designer. The TRL calculations for each simulation program was performed using MATLAB.

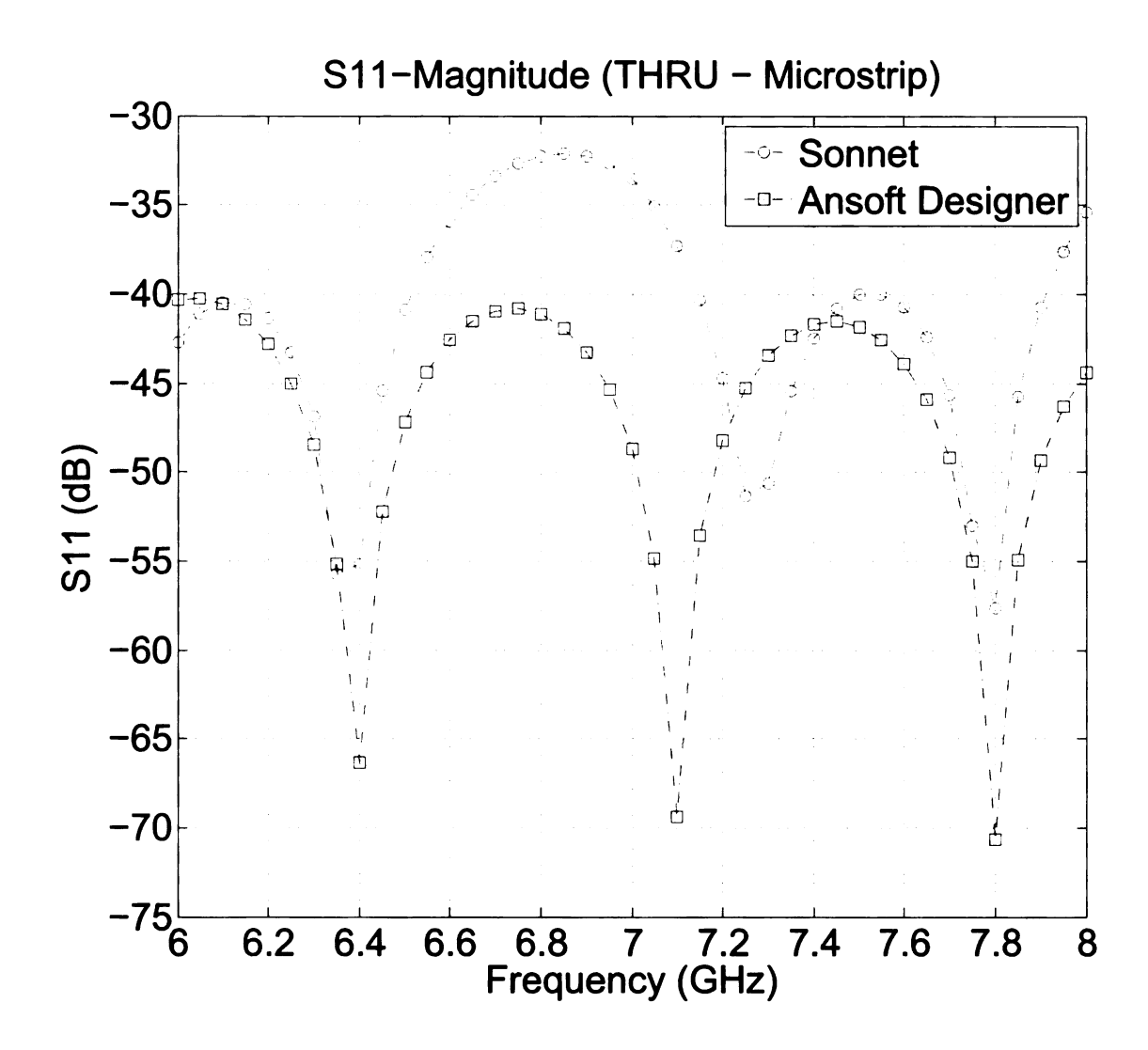


Figure 4.23. Magnitude of reflection coefficient for Thru standard of the microstrip (Sonnet vs. Ansoft Designer)

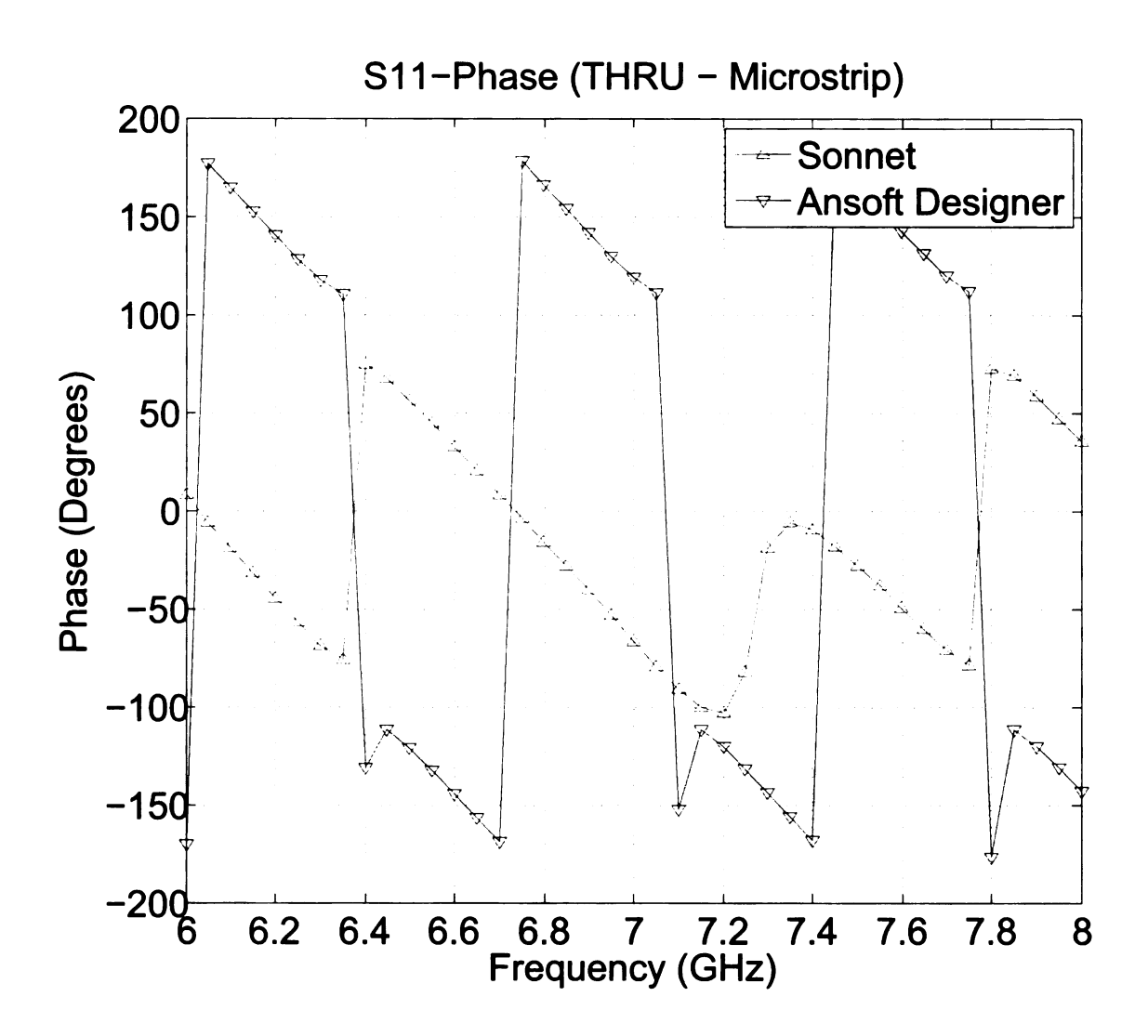


Figure 4.24. Phase of reflection coefficient for *Thru* standard of the microstrip (Sonnet vs. Ansoft Designer)

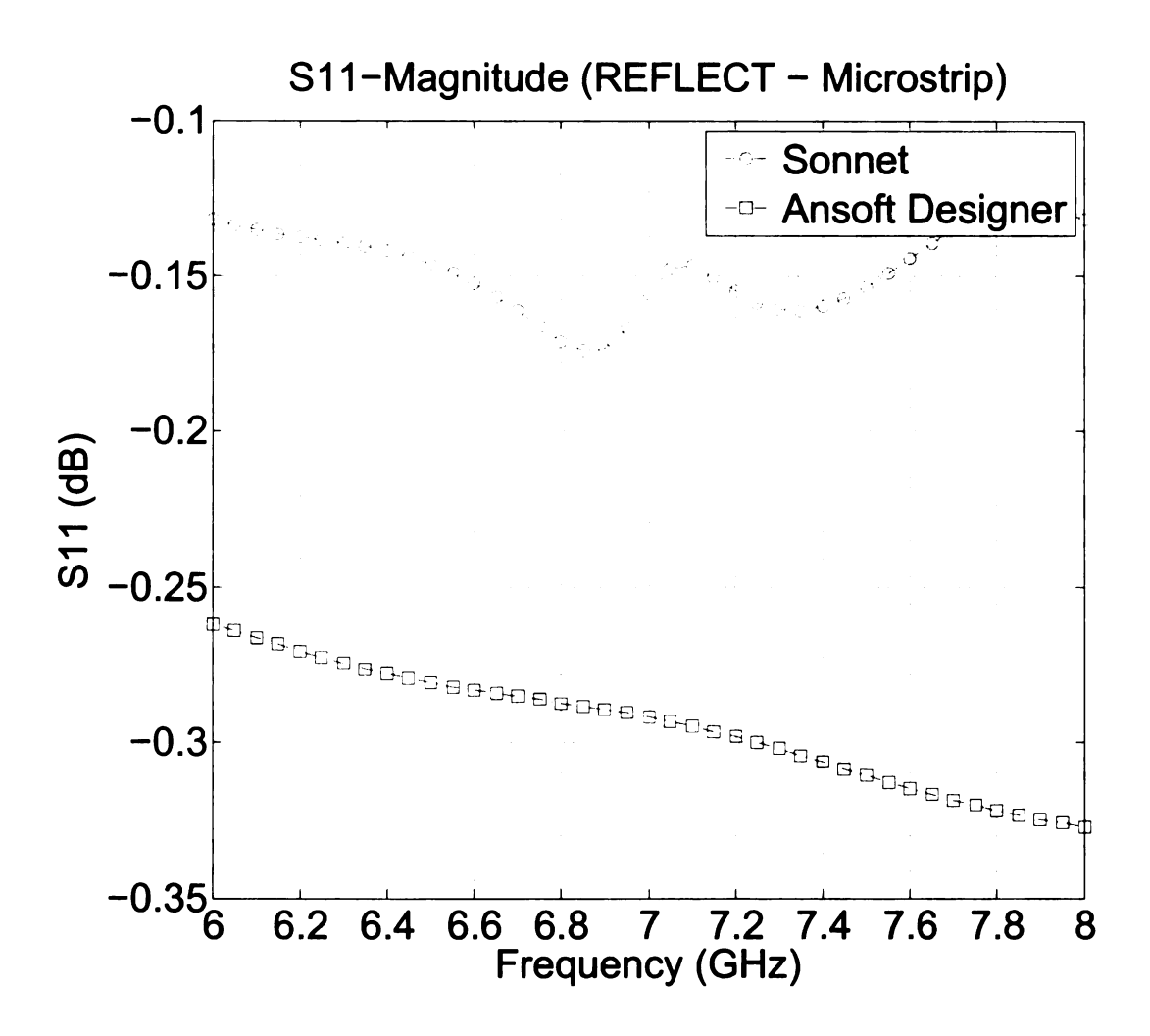


Figure 4.25. Magnitude of reflection coefficient for *Reflect* standard of the microstrip (Sonnet vs. Ansoft Designer)

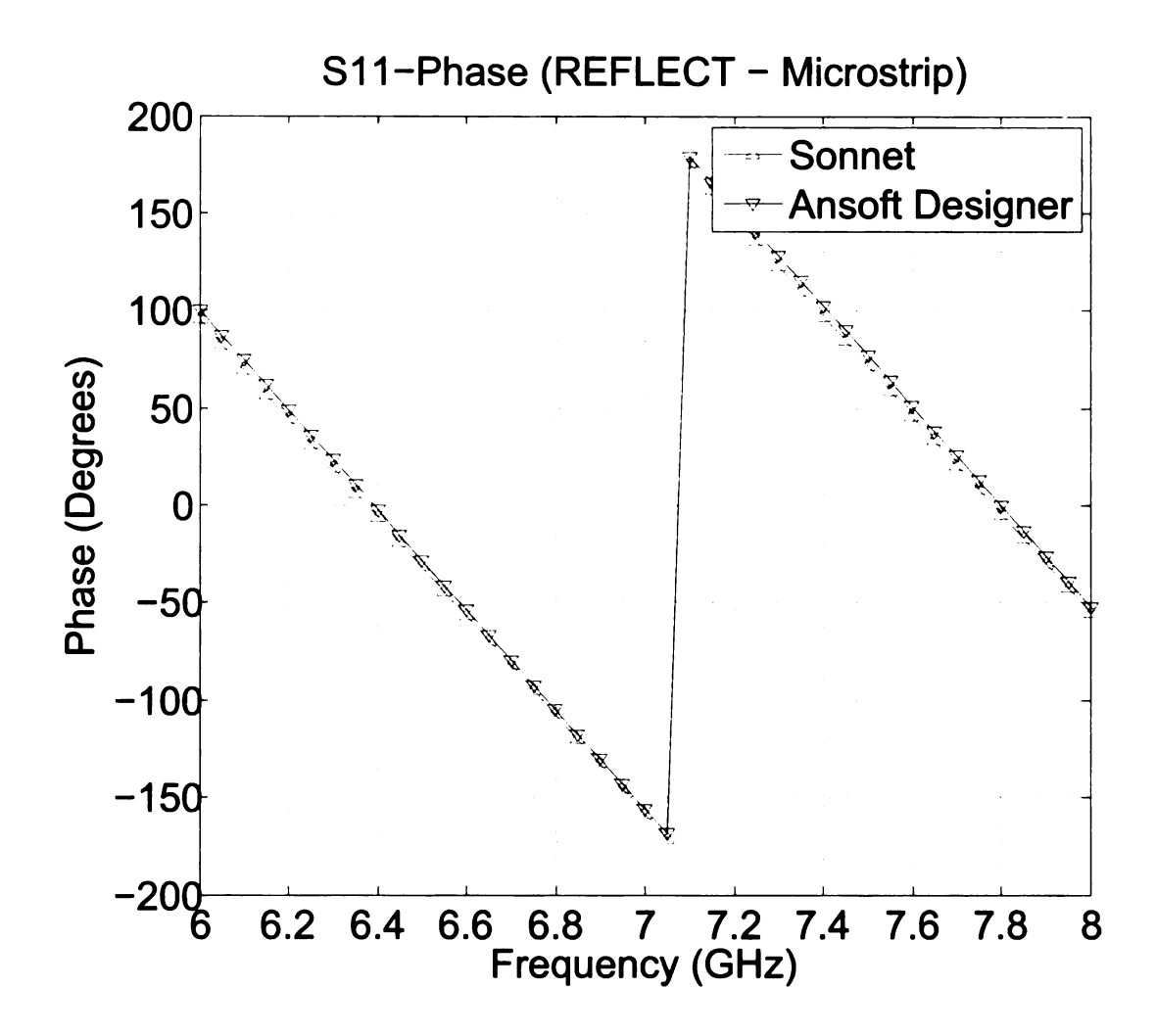


Figure 4.26. Phase of reflection coefficient for *Reflect* standard of the microstrip (Sonnet vs. Ansoft Designer)

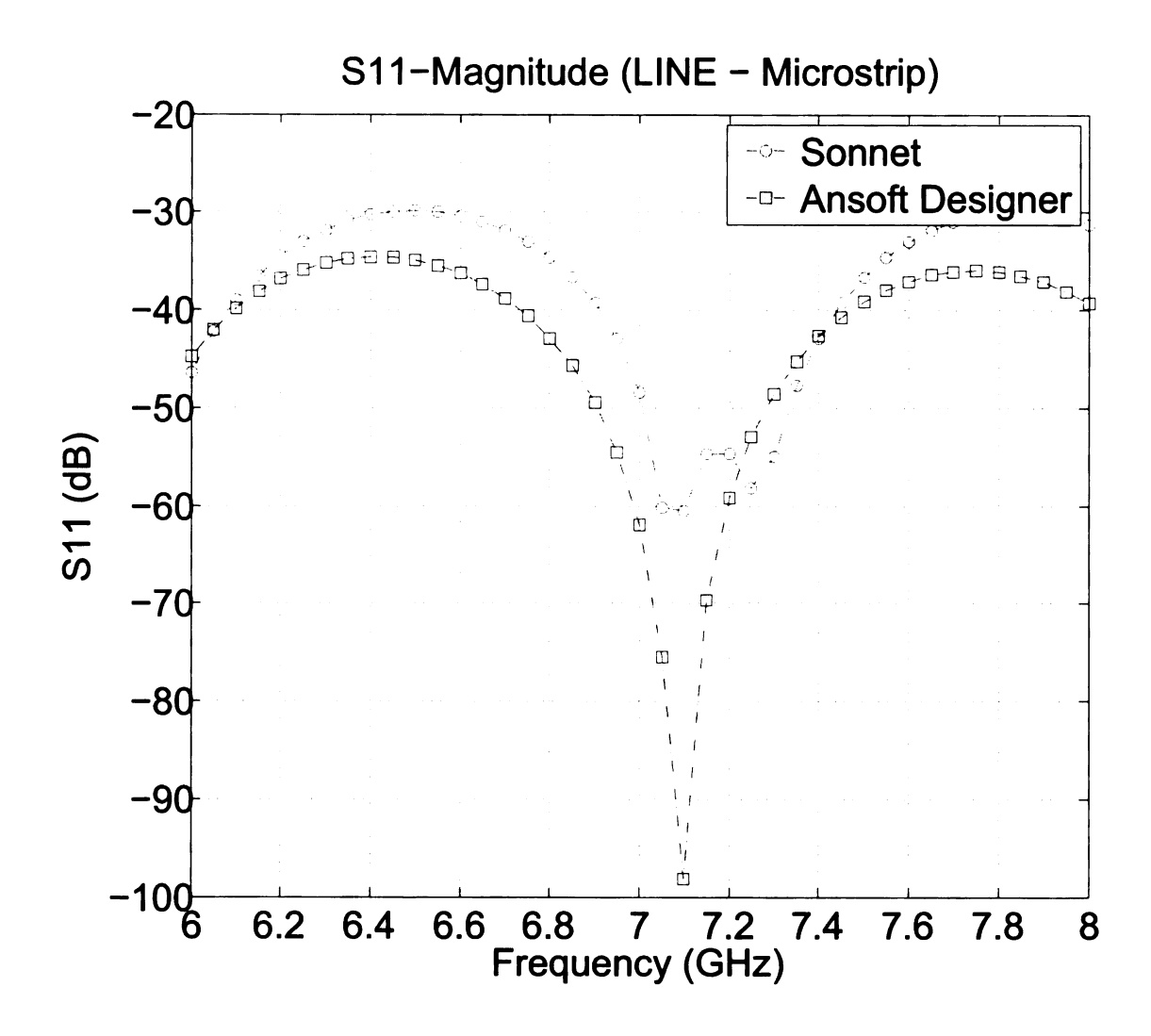


Figure 4.27. Magnitude of reflection coefficient for *Line* standard of the microstrip (Sonnet vs. Ansoft Designer)

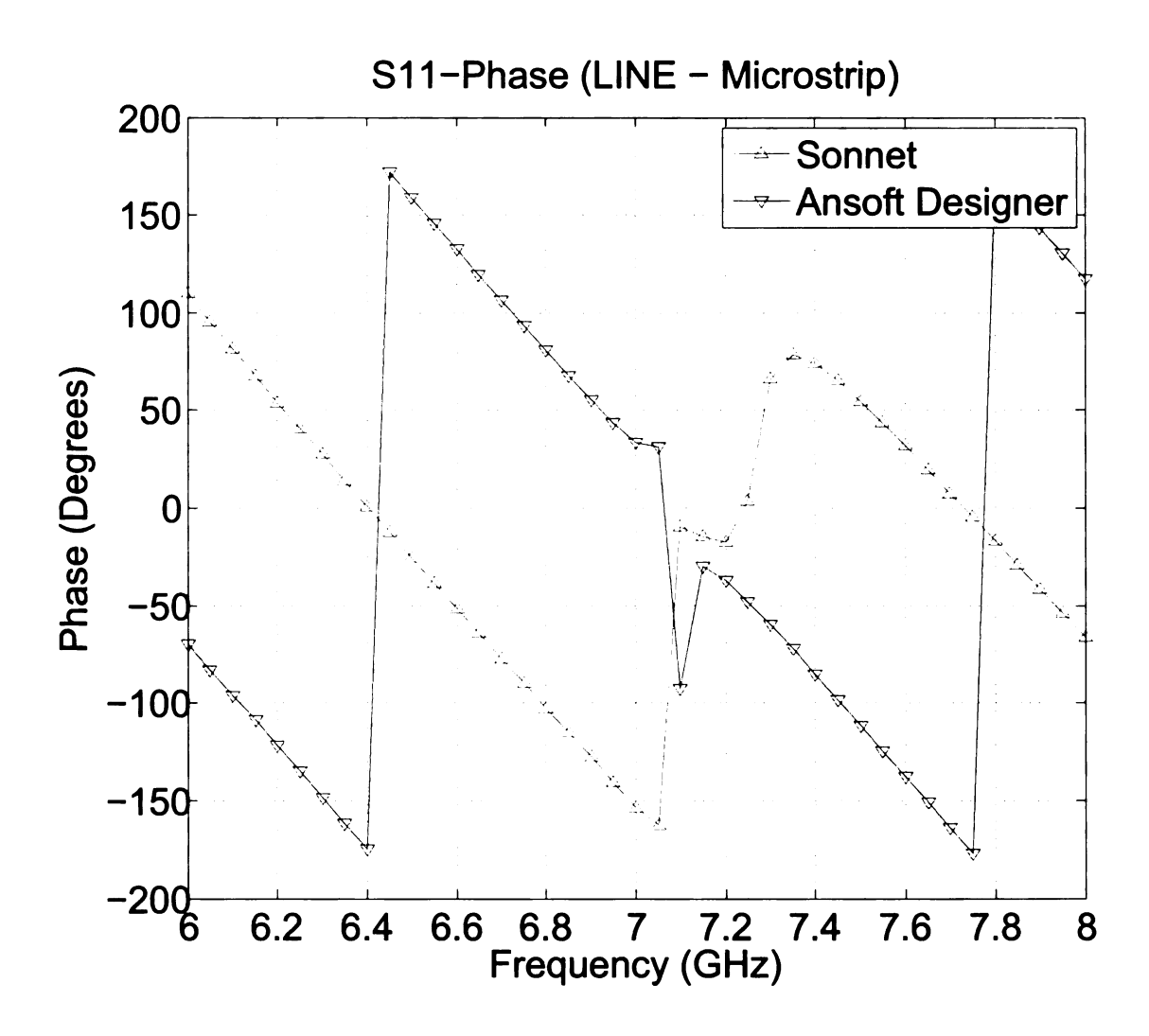


Figure 4.28. Phase of reflection coefficient for Line standard of the microstrip (Sonnet vs. Ansoft Designer)

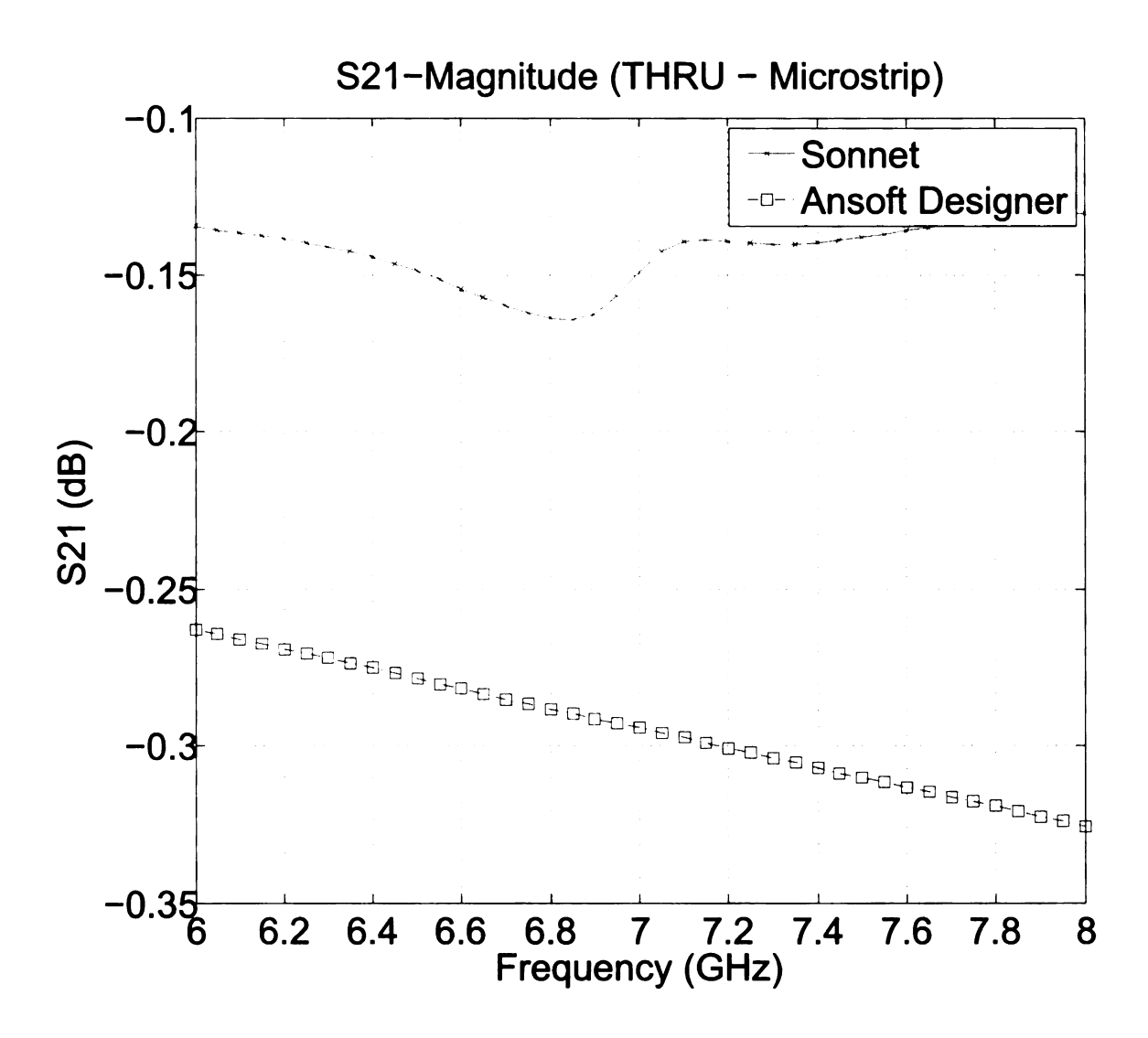


Figure 4.29. Magnitude of transmission coefficient for *Thru* standard of the microstrip (Sonnet vs. Ansoft Designer)

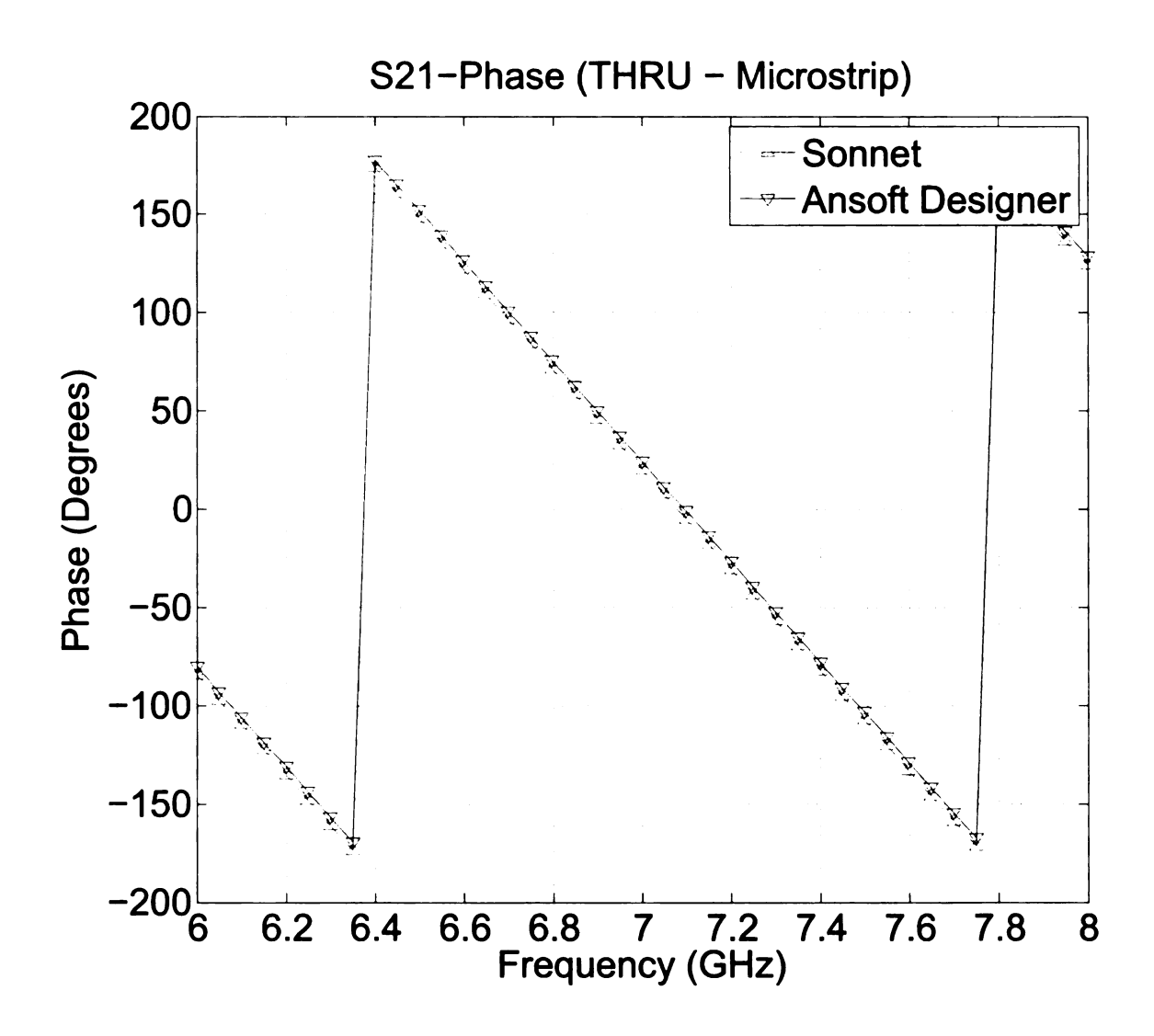


Figure 4.30. Phase of transmission coefficient for *Thru* standard of the microstrip (Sonnet vs. Ansoft Designer)

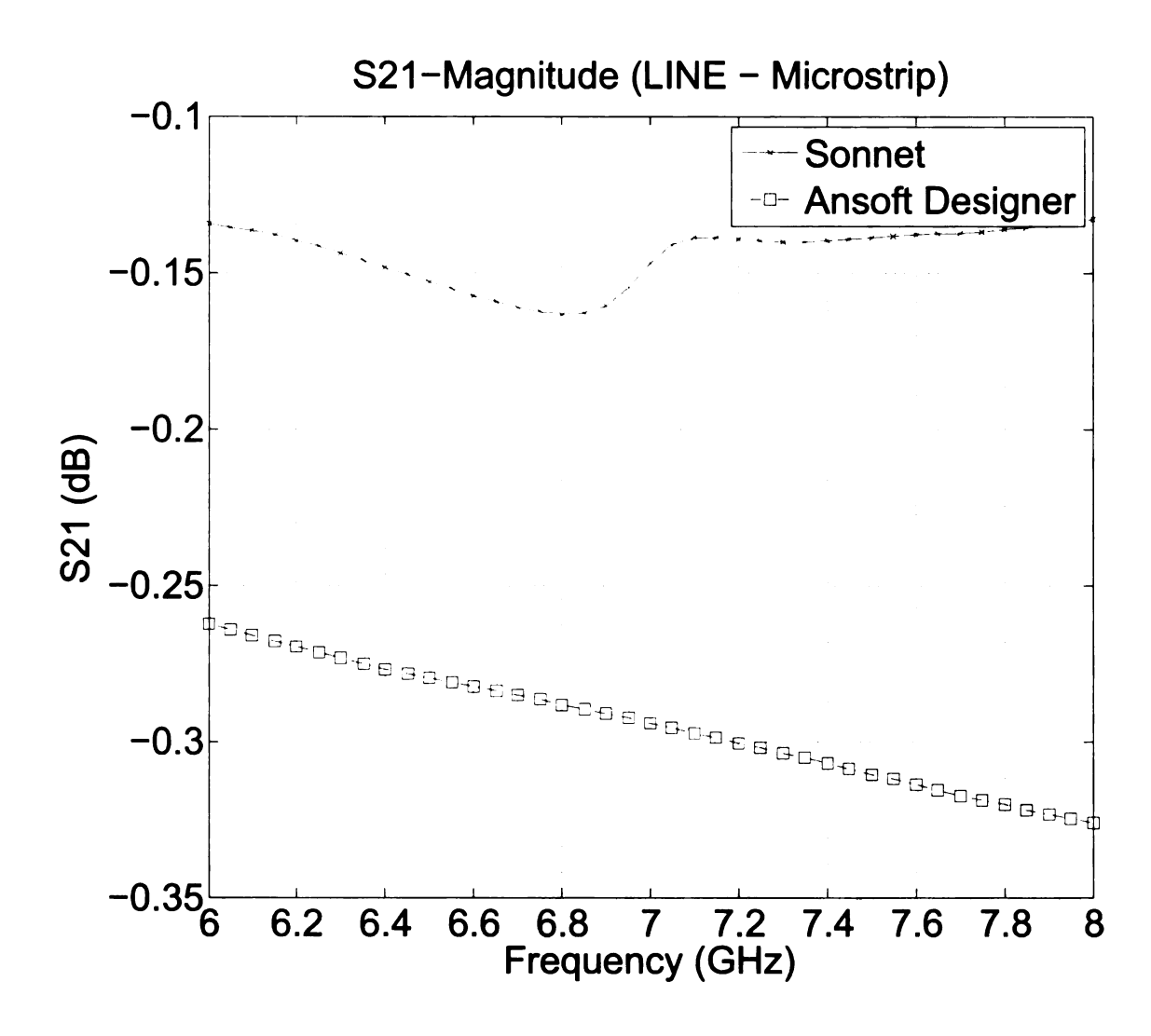


Figure 4.31. Magnitude of transmission coefficient for *Line* standard of the microstrip (Sonnet vs. Ansoft Designer)

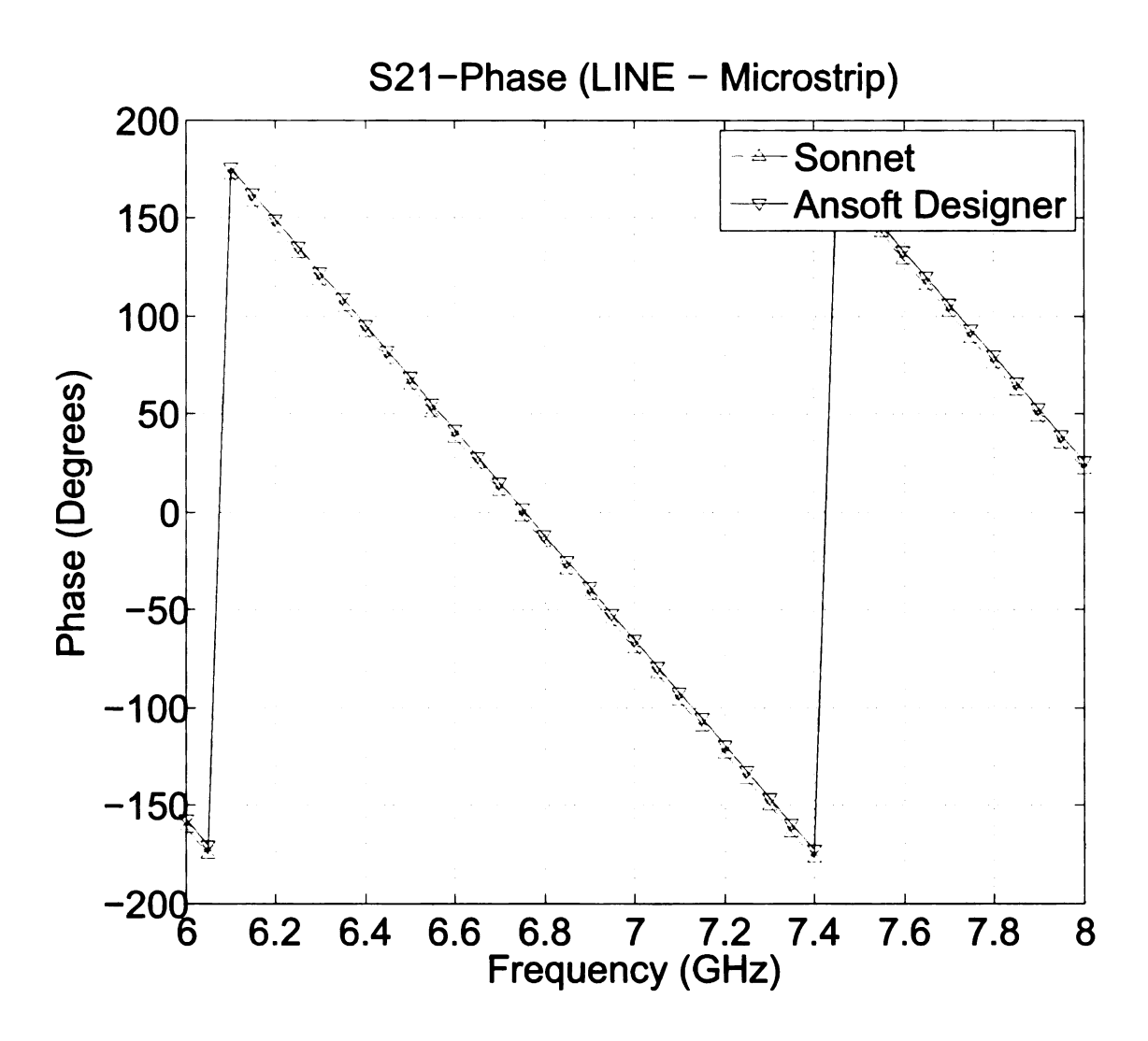


Figure 4.32. Phase of transmission coefficient for *Line* standard of the microstrip (Sonnet vs. Ansoft Designer)

4.4.3 Modeling the Negative Impedance Converter

Referring back to Section 3.2.1.3, the S-parameters of the NIC will be modeled according to the ABCD-parameters of the composite system of the microstrip and the NIC such that the parameter Z shown in Figure 3.14 represents the series impedance of the two-port network corresponding to the input impedance of the NIC, i.e., $Z = Z_{in,NIC} = -kZ_L = -\frac{R_2}{R_1}Z_L$. The reason of doing this is that the composite system is a cascaded network of two-port networks. The S-parameters of the composite system can be found using (3.48) and (3.55) for the second stage of the de-embedding process

$$[\mathbf{S_{comp}}] = \frac{\begin{bmatrix} \frac{Z_{in}}{50} & 2\\ 2 & \frac{Z_{in}}{50} \end{bmatrix}}{2 + \frac{Z_{in}}{50}} = \begin{bmatrix} \frac{Z_{in}}{Z_{in} + 100} & \frac{100}{Z_{in} + 100}\\ \frac{100}{Z_{in} + 100} & \frac{Z_{in}}{Z_{in} + 100} \end{bmatrix}$$
(4.33)

where $k=\frac{R_2}{R_1}$, $\omega=2\pi f$, $Z_{in,cap}=-\frac{k}{j\omega C}$ for the negative capacitor shown in Figure 4.33, and $Z_{in,ind}=-jk\omega L$ for the negative inductor shown in Figure 4.34. For simplicity, the values of R_2 and R_1 will be the same (e.g., $R_2=R_1=1$ kiloohm (k Ω)) for both the negative capacitor and negative inductor making k=1. This will make $Z_{in,cap}=-\frac{1}{j\omega C}$ and $Z_{in,ind}=-j\omega L$. The value of the capacitor is 10 picofarads (pF) and the value of the inductor is 0.1 nanohenrys (nH). Table 4.1 gives values of Z_{in} for the negative capacitor while Table 4.2 gives values of Z_{in} for the negative inductor. All tables and figures are observed in the C-band frequency range in 50 MHz increments.

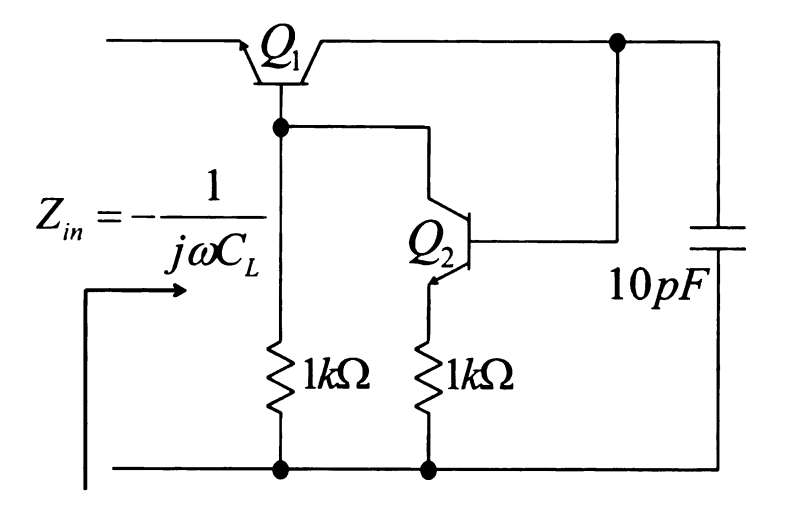


Figure 4.33. Negative impedance converter with capacitively terminated load

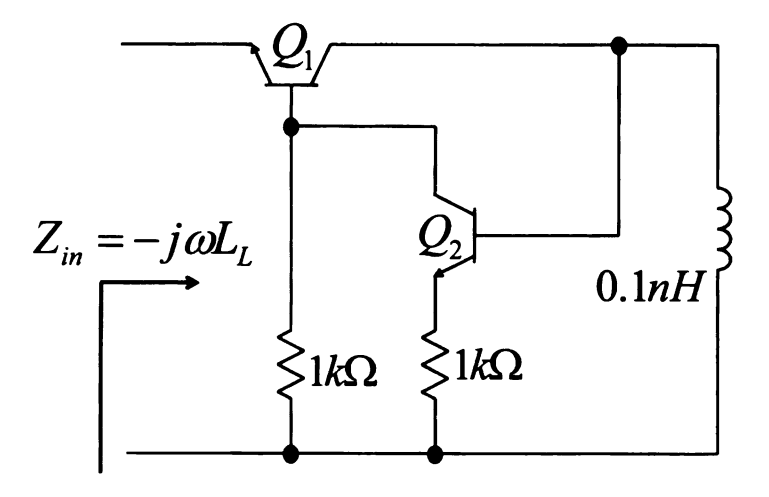


Figure 4.34. Negative impedance converter with inductively terminated load

Frequency (GHz)	$Z_{in} = -\frac{1}{j\omega C_L} (\Omega)$	Frequency (GHz)	$Z_{in} = -\frac{1}{j\omega C_L} \ (\Omega)$
6	j2.65258	7	j2.27364
6.05	j2.63066	7.05	j2.25752
6.1	j2.6091	7.1	j2.24162
6.15	j2.58789	7.15	j2.22594
6.2	j2.56702	7.2	j2.21049
6.25	j2.54648	7.25	j2.19524
6.3	j2.52627	7.3	j2.1802
6.35	j2.50638	7.35	j2.16537
6.4	j2.4868	7.4	j2.15074
6.45	j2.46752	7.45	j2.13631
6.5	j2.44854	7.5	j2.12207
6.55	j2.42985	7.55	j2.10801
6.6	j2.41144	7.6	j2.09414
6.65	j2.39331	7.65	j2.08046
6.7	j2.37545	7.7	j2.06695
6.75	j2.35785	7.75	j2.05361
6.8	j2.34051	7.8	j2.04045
6.85	j2.32343	7.85	j2.02745
6.9	j2.30659	7.9	j2.01462
6.95	j2.29	7.95	j2.00195
7	j2.27364	8	j1.98944

Table 4.1. Values of Z_{in} for negative capacitor with load capacitance of 10 pF in C-band

Frequency (GHz)	$Z_{in} = -j\omega L_L \ (\Omega)$	Frequency (GHz)	$Z_{in} = -j\omega L_L \ (\Omega)$
6	-j3.769911	7	-j4.39823
6.05	-j3.801327	7.05	-j4.429646
6.1	-j3.832743	7.1	-j4.461062
6.15	-j3.864159	7.15	-j4.492477
6.2	-j3.895575	7.2	-j4.523893
6.25	-j3.926991	7.25	-j4.555309
6.3	-j3.958407	7.3	-j4.586725
6.35	-j3.989823	7.35	-j4.618141
6.4	-j4.021239	7.4	-j4.649557
6.45	-j4.052655	7.45	-j4.680973
6.5	-j4.08407	7.5	-j4.712389
6.55	-j4.115486	7.55	-j4.743805
6.6	-j4.146902	7.6	-j4.775221
6.65	-j4.178318	7.65	-j4.806637
6.7	-j4.209734	7.7	-j4.838053
6.75	-j4.24115	7.75	-j4.869469
6.8	-j4.272566	7.8	-j4.900885
6.85	-j4.303982	7.85	-j4.9323
6.9	-j4.335398	7.9	-j4.963716
6.95	-j4.366814	7.95	-j4.995132
7	-j4.39823	8	-j5.026548

Table 4.2. Values of Z_{in} for negative inductor with load inductance of 0.1 nH in C-band

4.5 Comparing Computational Results with Simulated Results

The TRL calibration technique will be conducted for the first stage of the deembedding process by substituting (4.14) into (3.56) and (4.31) into (3.51) to obtain the following relation

$$[\mathbf{T_{comp}}] = [\mathbf{T_A}] \cdot [\mathbf{T_{DUT}}] \cdot [\mathbf{T_A}] \tag{4.34}$$

However, since the DUT of the first stage of de-embedding is the composite system in the second stage, the test fixture connectors are modeled using (4.31), and the measurements of the composite system are given by (4.33), the S-parameters do not need to be found since computational analysis produces the same result. Remember, the first stage of de-embedding moves the reference plane from the ends of the test port cables to the edge of the composite system.

The second stage of de-embedding undergo TRL calibration as well. This time connectors A and B (the half-length microstrips) are modeled by equation (4.32) or using Sonnet for more accurate analysis. Referring back to microstrip simulations displayed in Figures 4.23 to 4.42, the S-parameters of the microstrip will be used to conduct the TRL calibration technique for the second stage. The NIC is represented by (4.33). Following the procedure detailed in Section 3.2.2 and simplified in Section 4.3, the S-parameters of the NIC can be evaluated using (4.25). The figures and tables mentioned in Section 4.4.1 model the S-parameters for the negative capacitor and negative inductor examined in the C-band frequency range in 50 MHz increments.

In order to check if the results are accurate, a parameter study is performed in MATLAB comparing simulated data of the half-length microstrips done in Sonnet and Ansoft Designer. The simulated data will then be put into the theoretical model obtained in (4.33). First the S-parameters of a full-length microstrip ($\ell = 150$ mm) were compared to the S-parameters of two half-length microstrips ($\ell_A = 75$ mm)

cascaded together in Sonnet and Ansoft Designer. It was concluded that the full-length microstrip produced the same results as the cascaded half-length microstrips for both simulation programs. It also shows that the S-parameters of the cascaded system using the simulated data from Sonnet and Ansoft designer produce similar results when they are compared against each other. This is shown in Figures 4.35 to 4.38.

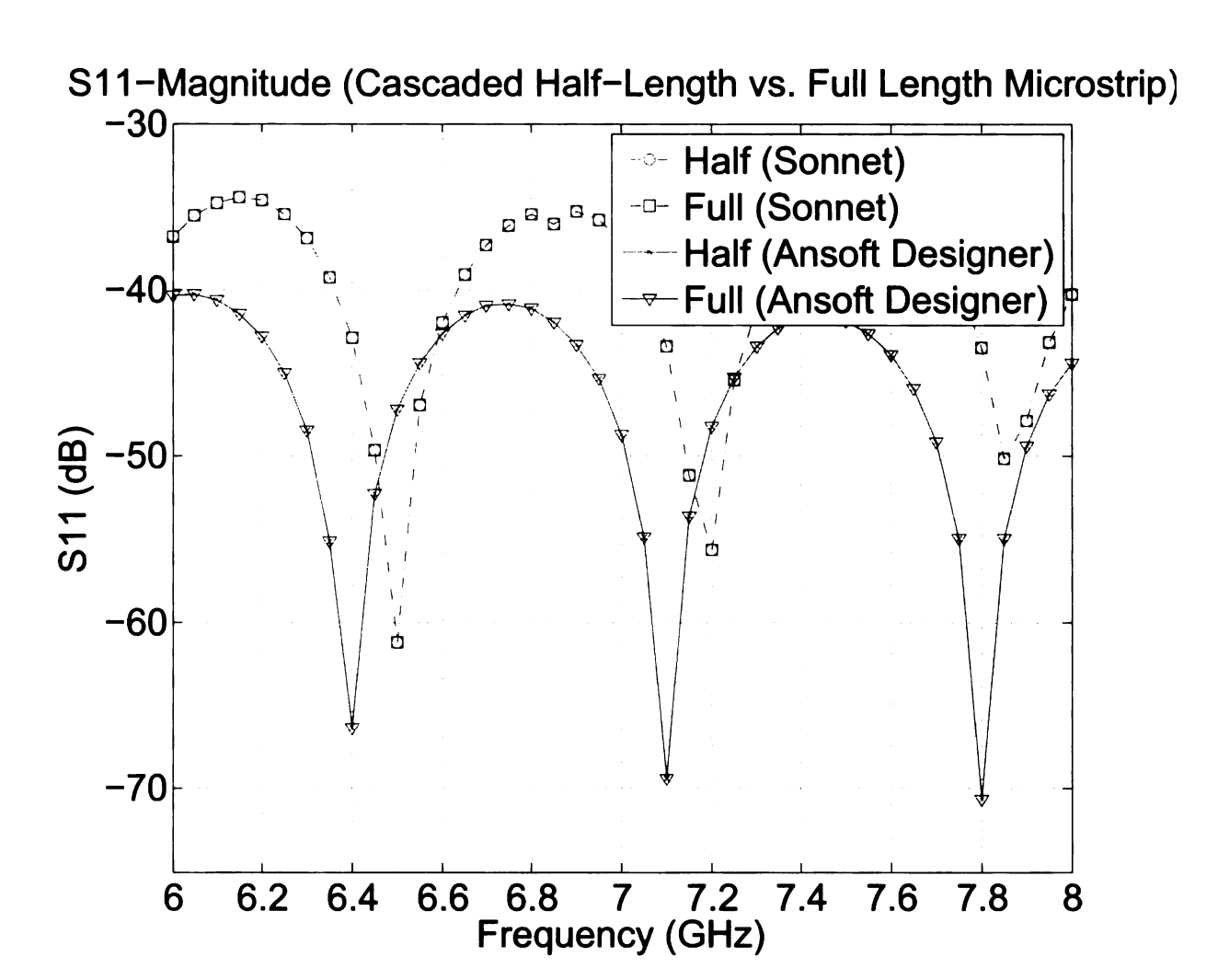


Figure 4.35. Magnitude of reflection coefficient of full-length microstrip vs. cascaded half-length microstrips (Sonnet vs. Ansoft Designer)

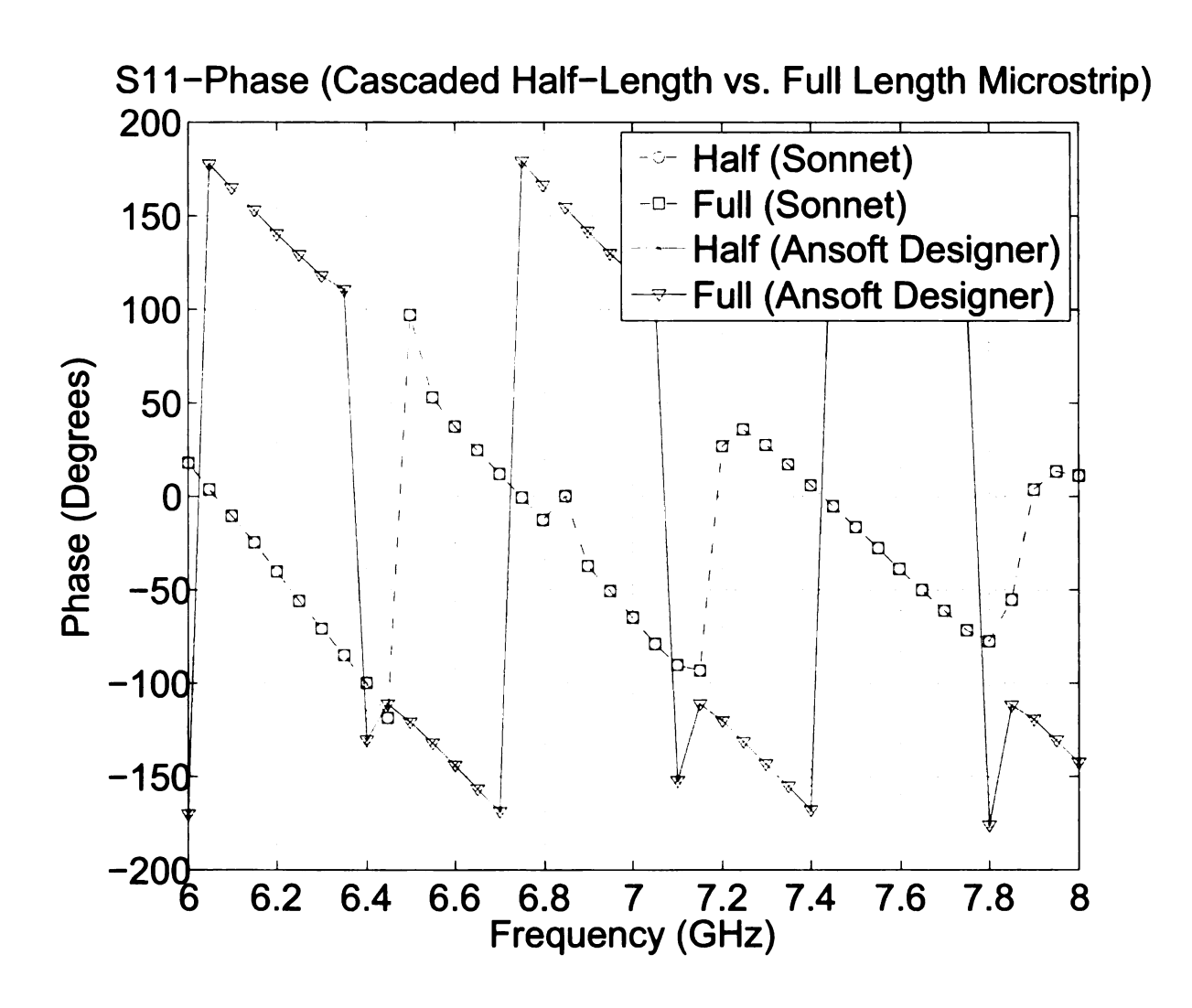


Figure 4.36. Phase of reflection coefficient of full-length microstrip vs. cascaded half-length microstrips (Sonnet vs. Ansoft Designer)

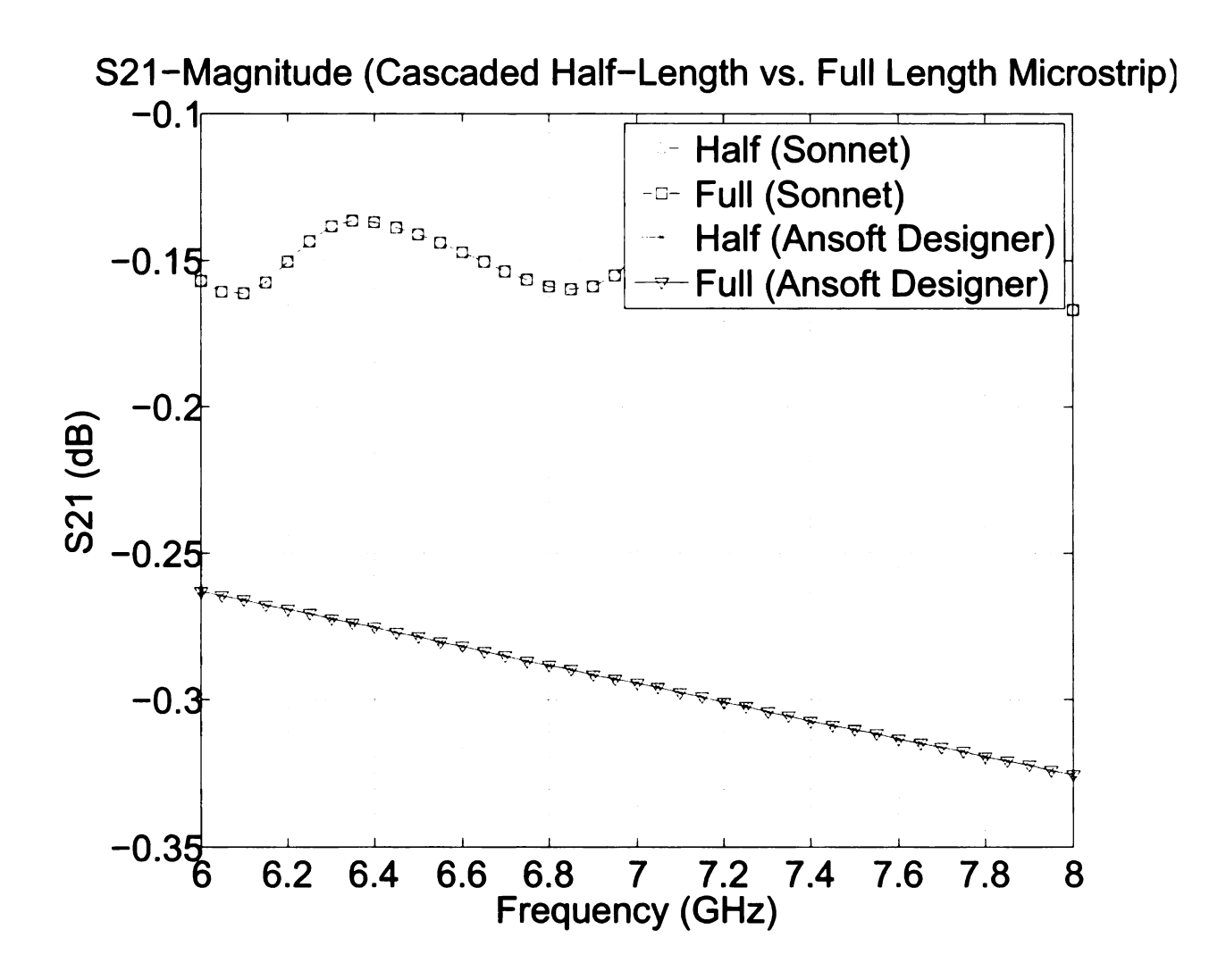


Figure 4.37. Magnitude of transmission coefficient of full-length microstrip vs. cascaded half-length microstrips (Sonnet vs. Ansoft Designer)

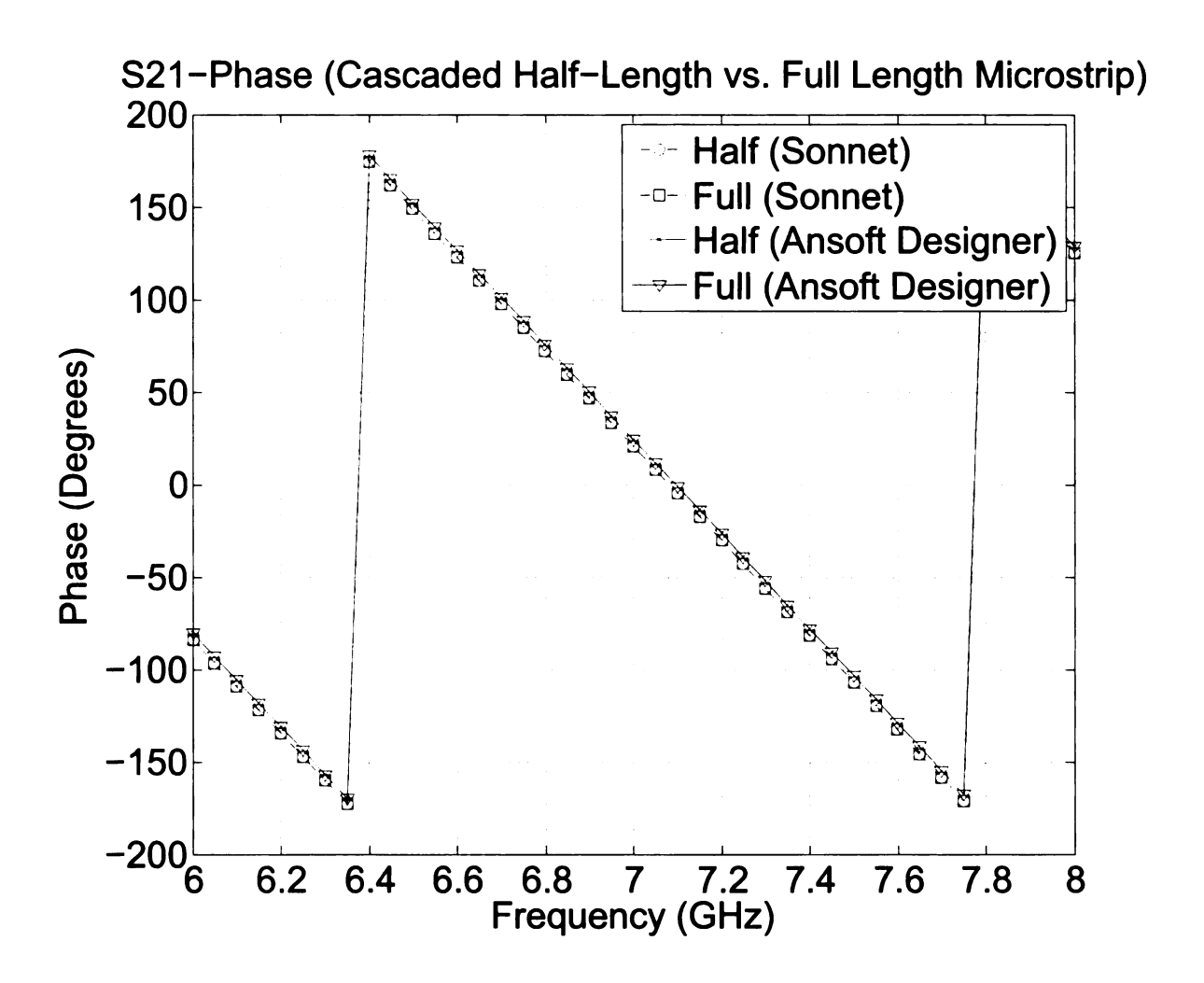


Figure 4.38. Phase of transmission coefficient of full-length microstrip vs. cascaded half-length microstrips (Sonnet vs. Ansoft Designer)

Using (4.15), the half-lengths modeled in Sonnet were created to produce a cascaded network of a half-length microstrip, a zero-length line, and another half-length microstrip. The computed S-parameters were compared to the cascaded network of a half-length microstrip, a zero-length reactive component, and another half-length microstrip modeled in Ansoft Designer. Examining Figures 4.23 to 4.32, it is shown that the ranges that the S-parameters for the TRL calibrations for both types of models (Sonnet vs. Ansoft Designer) are nearly identical despite that fact that the trends of the transmission coefficients being different. The reflection coefficients for both models do have similar ranges and trends.

Finally, a parameter study of components in the structure (half-length microstrip, active component, half-length microstrip) were performed. Several components were used: a 50- Ω resistor, a 75- Ω resistor, a 100- Ω resistor, a 10-pF capacitor, and a 0.1-nH inductor. Then, the reactive component values were varied from positive to negative (e.g. the capacitor was varied from -10 pF to 10pF in 4 pF increments and the inductor was varied from -0.1 nH to 0.1 nH in 0.04 nH increments). The following figures display the behavior of the cascaded system using resistive and reactive components.

Figures 4.39 to 4.50 display the S-parameters of the cascaded network with the $50\text{-}\Omega$, $75\text{-}\Omega$, and $100\text{-}\Omega$ resistors using the half-length microstrips modeled in Sonnet and Ansoft Designer. Figures 4.51 to 4.54 display the S-parameters of the cascaded network with the 10-pF capacitor and Figures 4.55 to 4.58 display the S-parameters of the cascaded network with the 0.1-nH inductor using the half-length microstrips modeled in Sonnet and Ansoft Designer. Figures 4.59 to 4.62 display the S-parameters of the cascaded network with the -10-pF capacitor and Figures 4.63 to 4.66 display the S-parameters of the cascaded network with the -0.1-nH inductor using the half-length microstrips modeled in Sonnet and Ansoft Designer using (4.33) in MATLAB to model the NIC.

The purpose of conducting the parameter study is to analyze how the cascaded system behaves as the active component values vary from impedance to positive reactance to negative reactance. Another thing it does is distinguish a negative capacitor with a positive inductor and a negative inductor with a positive capacitor. Equations (4.35) and (4.36) establish the relationships for each of them.

$$Z_{NIC,cap} = -\frac{1}{j\omega C}$$

$$Z_{ind} = j\omega L \tag{4.35}$$

$$Z_{NIC,ind} = -j\omega L$$

$$Z_{cap} = \frac{1}{j\omega C}$$
(4.36)

The key difference between the negative capacitor and the positive inductor is that the frequency relationships of the impedance functions are inverses of each other (e.g., the frequency of the negative capacitor is inversely proportional to its input impedance while the frequency of the positive inductor is proportional to its impedance). Similarly, the frequency relationships of the impedance functions for the negative inductor and positive capacitor are opposite when they are compared to each other. This is in spite of the fact that the phase for each case is the same.

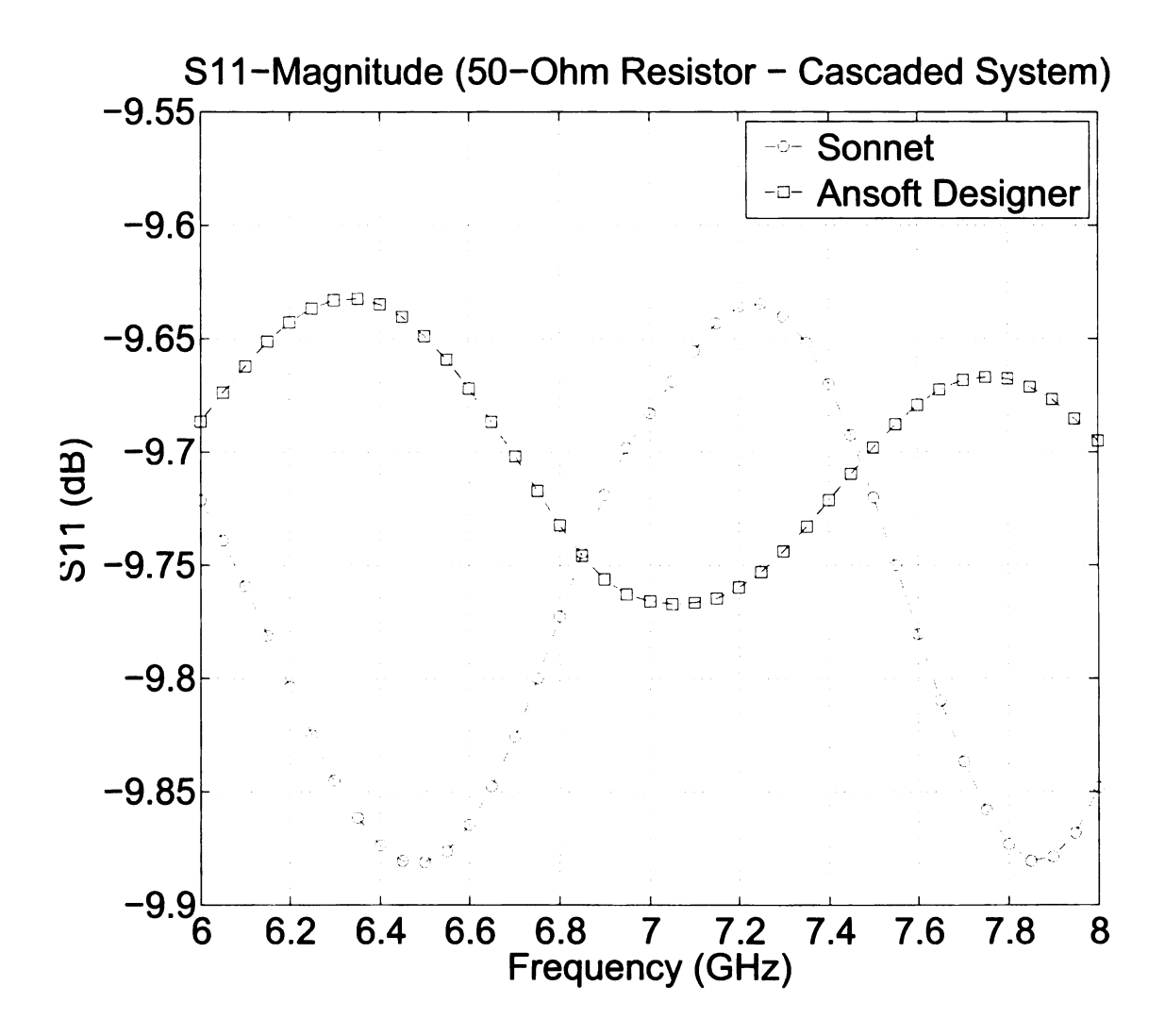


Figure 4.39. Magnitude of reflection coefficient of cascaded half-length microstrips with $50-\Omega$ resistor in between (Sonnet vs. Ansoft Designer)

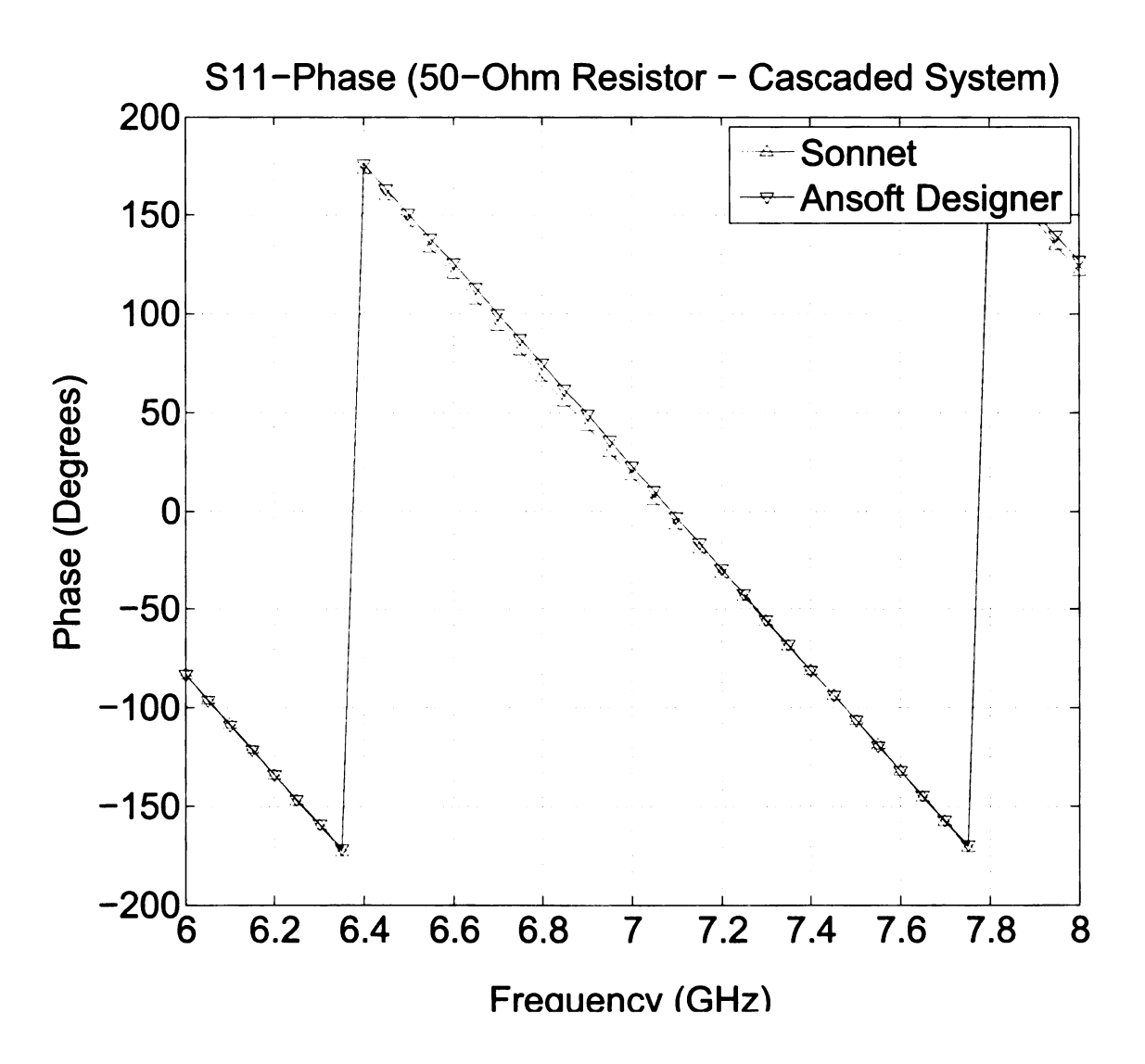


Figure 4.40. Phase of reflection coefficient of cascaded half-length microstrips with $50-\Omega$ resistor in between (Sonnet vs. Ansoft Designer)

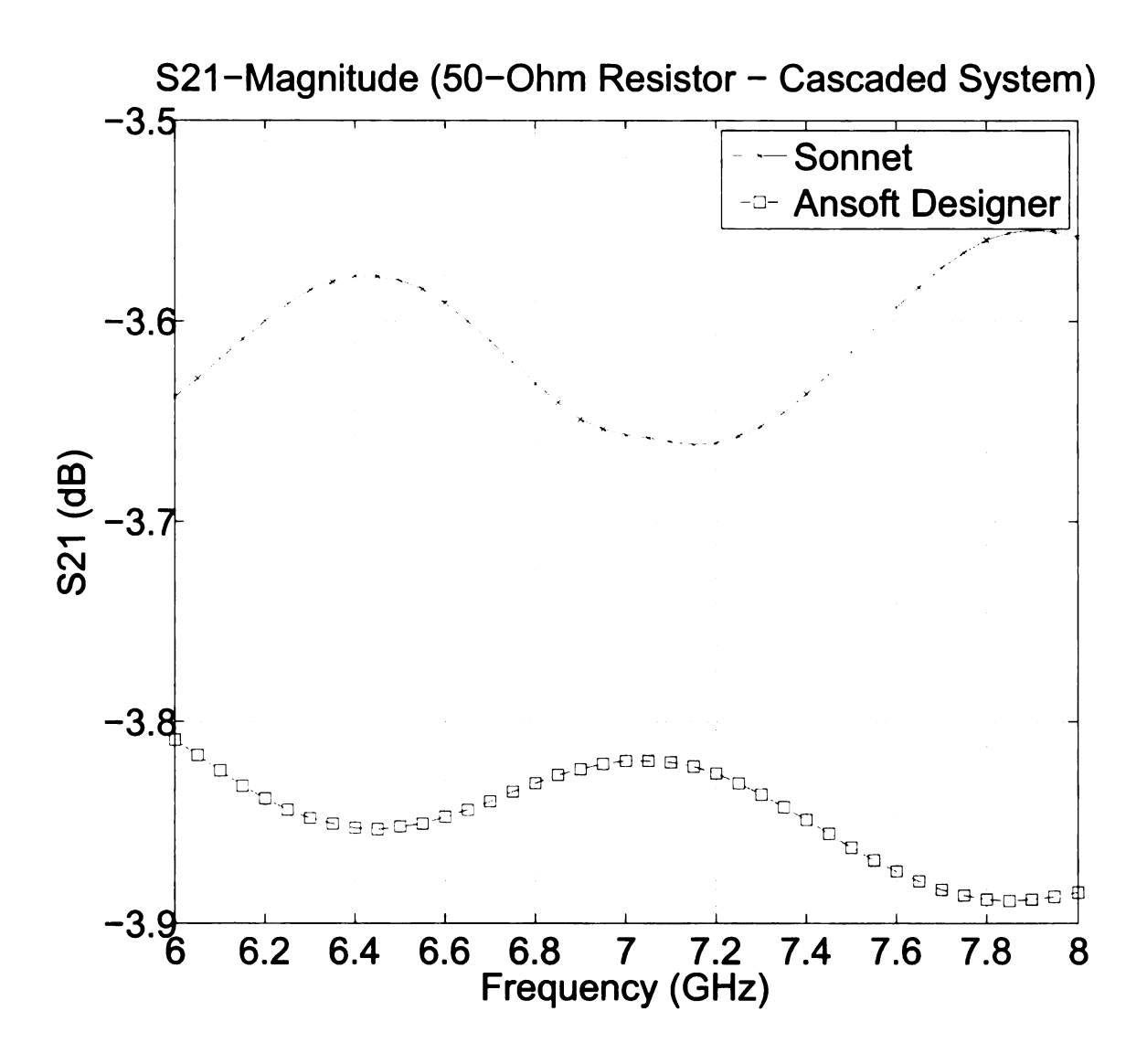


Figure 4.41. Magnitude of transmission coefficient of cascaded half-length microstrips with $50-\Omega$ resistor in between (Sonnet vs. Ansoft Designer)

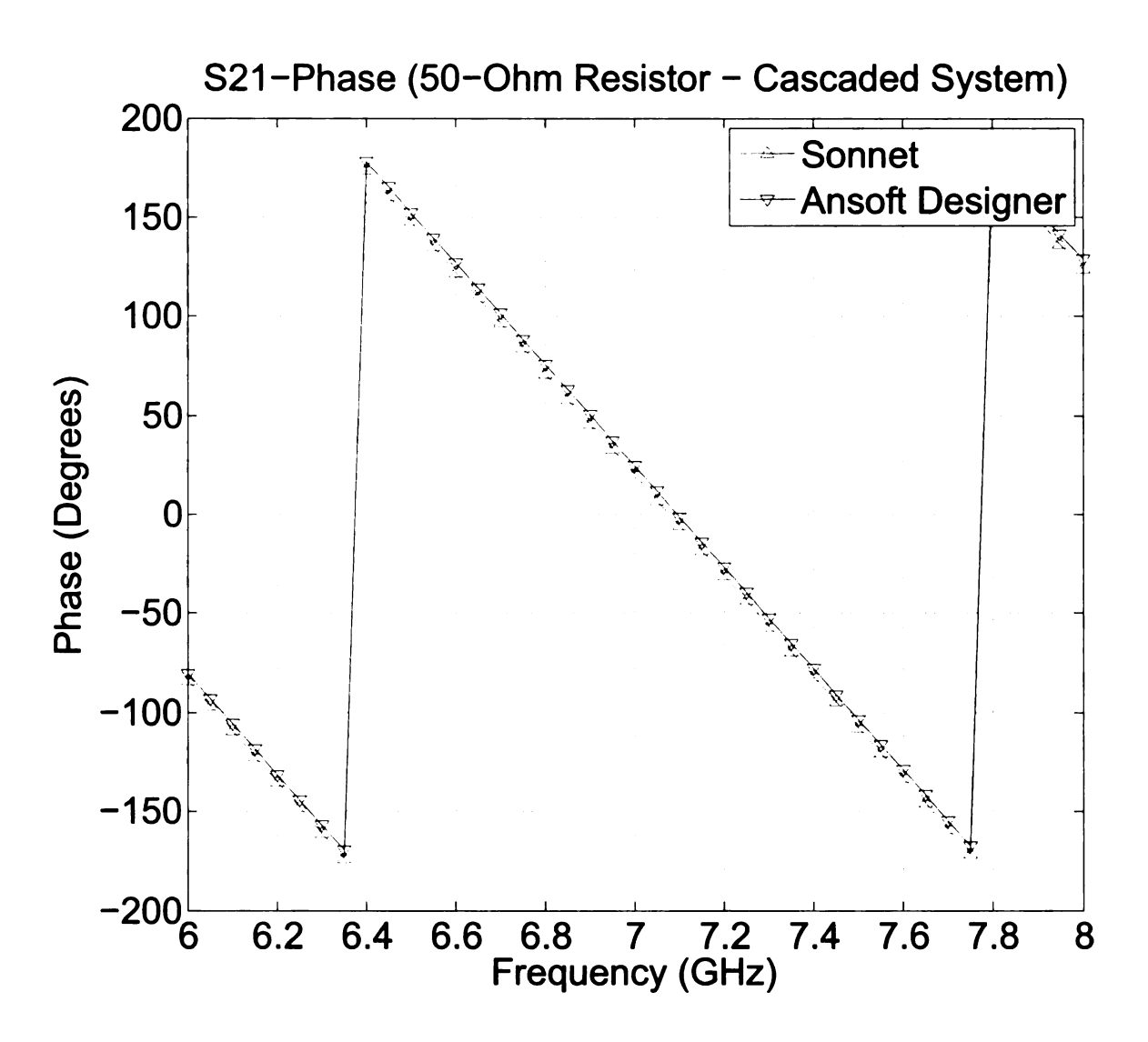


Figure 4.42. Phase of transmission coefficient of cascaded half-length microstrips with $50-\Omega$ resistor in between (Sonnet vs. Ansoft Designer)

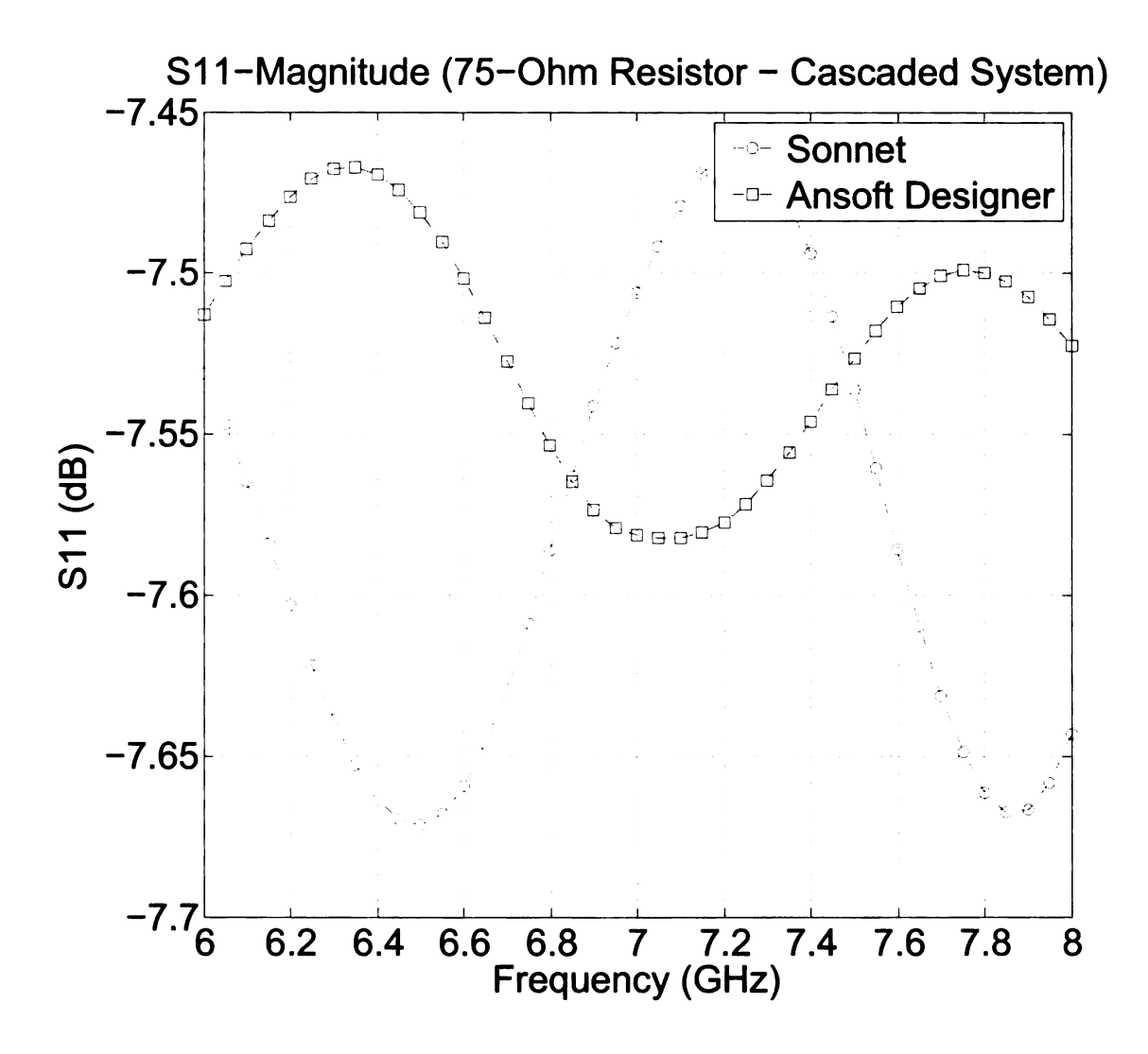


Figure 4.43. Magnitude of reflection coefficient of cascaded half-length microstrips with 75- Ω resistor in between (Sonnet vs. Ansoft Designer)

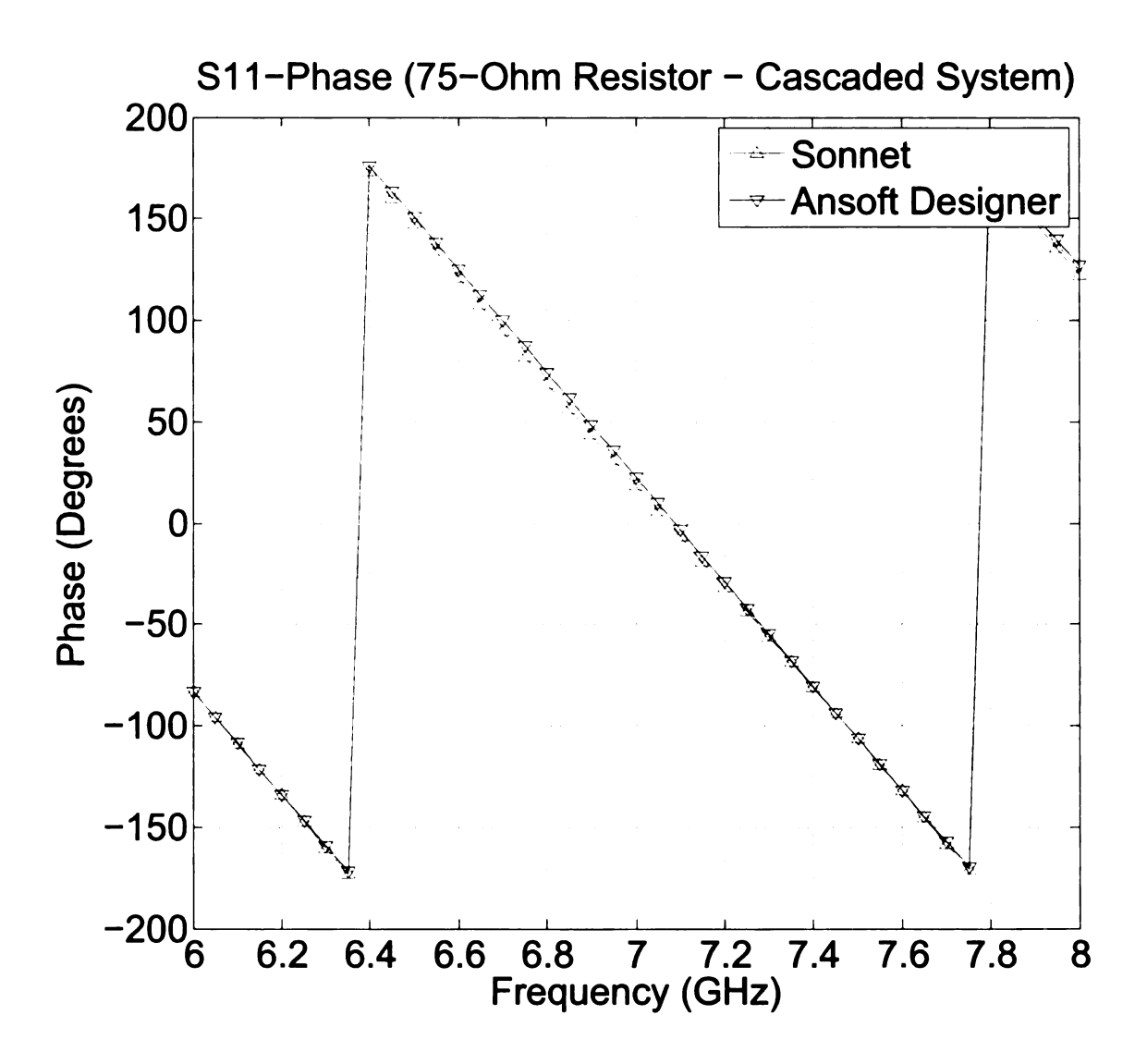


Figure 4.44. Phase of reflection coefficient of cascaded half-length microstrips with 75- Ω resistor in between (Sonnet vs. Ansoft Designer)

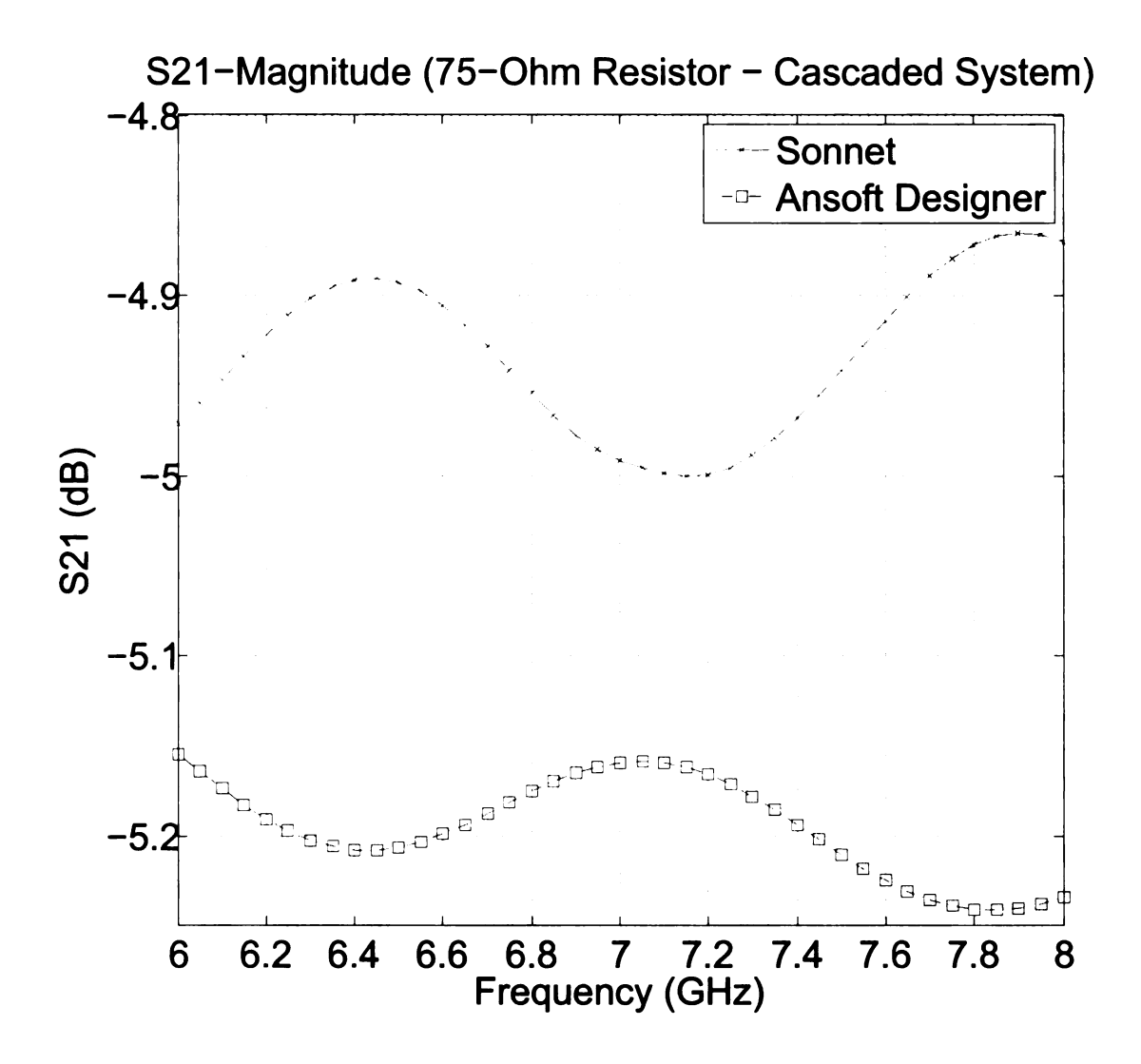


Figure 4.45. Magnitude of transmission coefficient of cascaded half-length microstrips with 75- Ω resistor in between (Sonnet vs. Ansoft Designer)

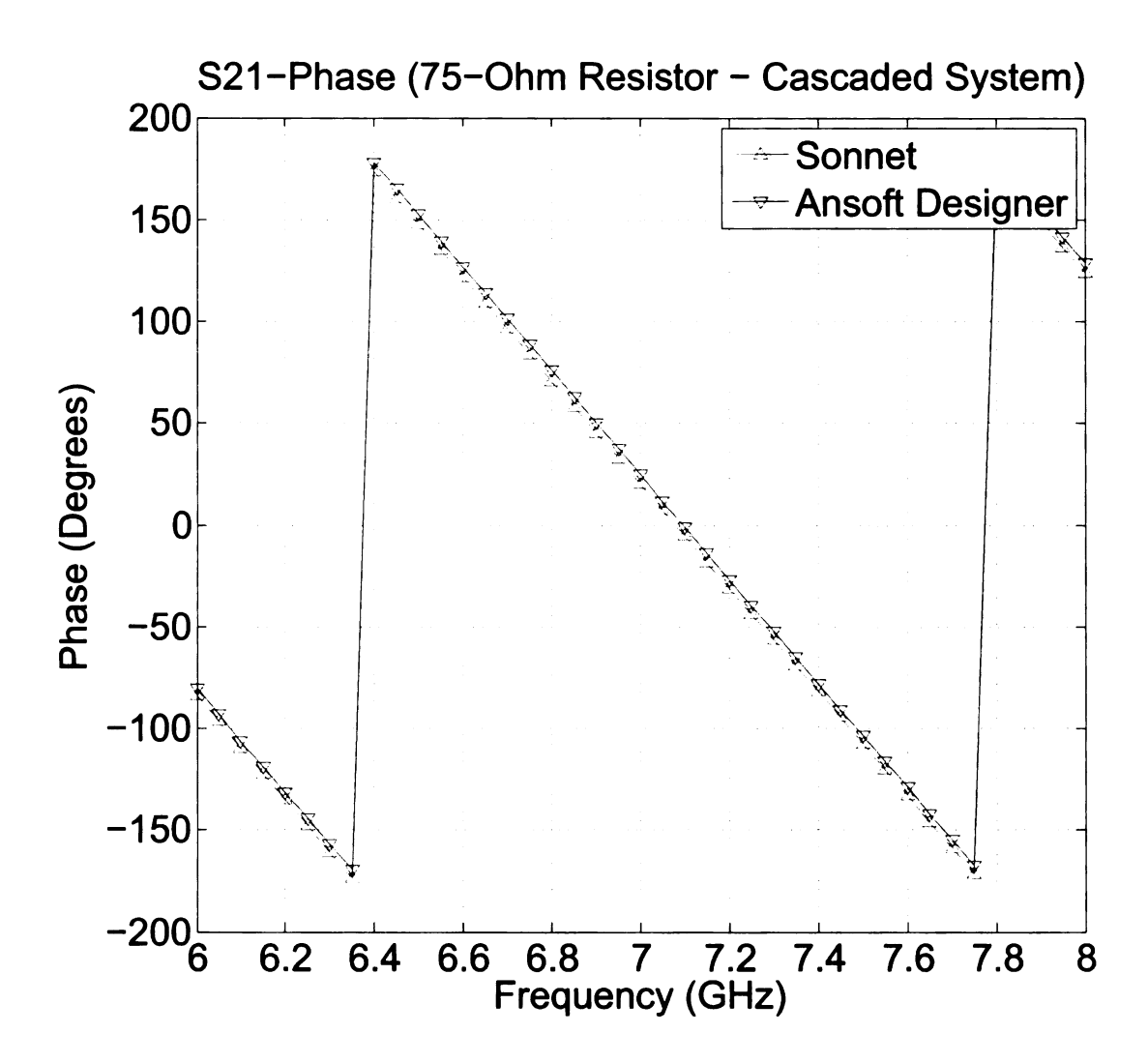


Figure 4.46. Phase of transmission coefficient of cascaded half-length microstrips with 75- Ω resistor in between (Sonnet vs. Ansoft Designer)

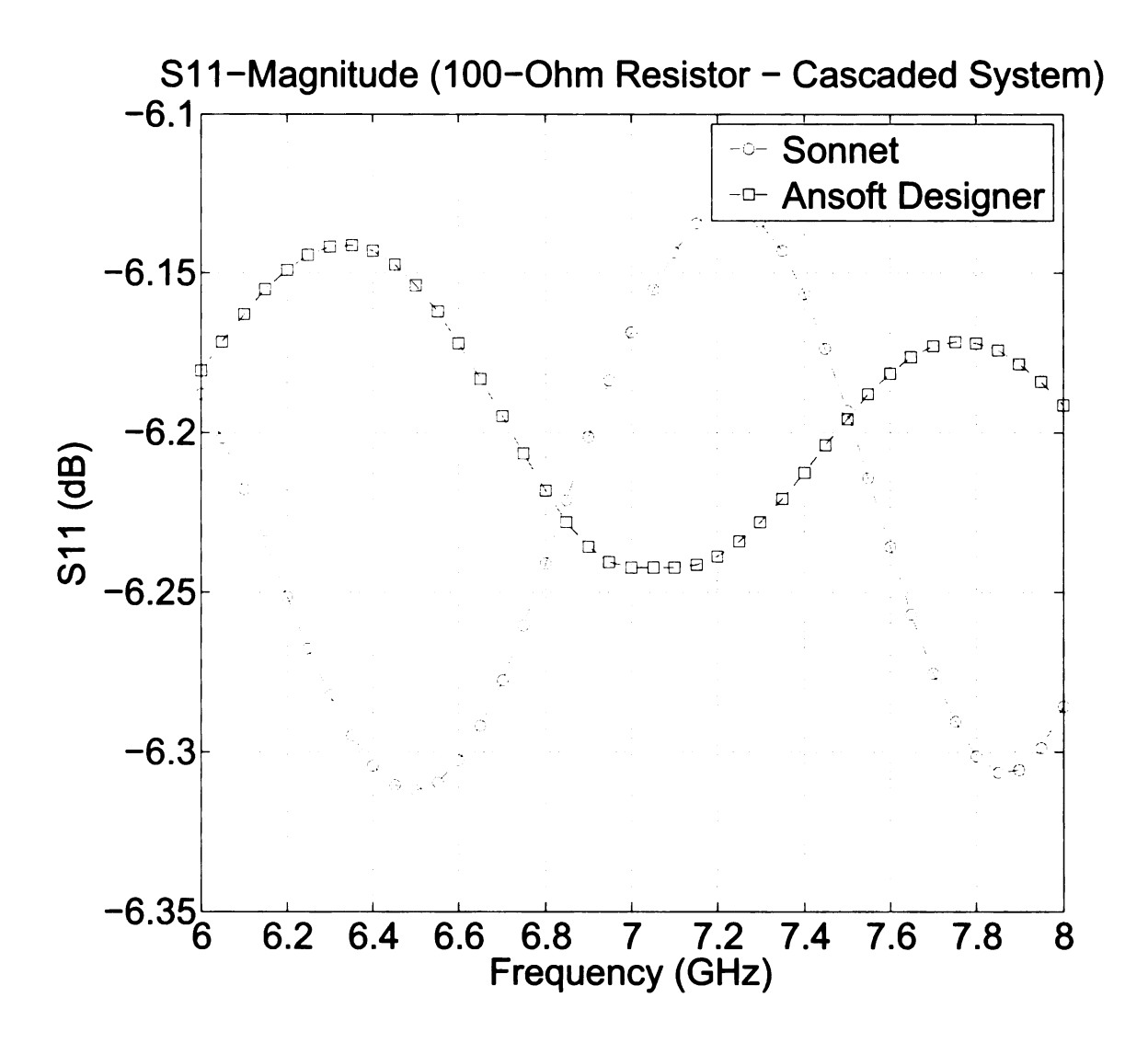


Figure 4.47. Magnitude of reflection coefficient of cascaded half-length microstrips with $100-\Omega$ resistor in between (Sonnet vs. Ansoft Designer)

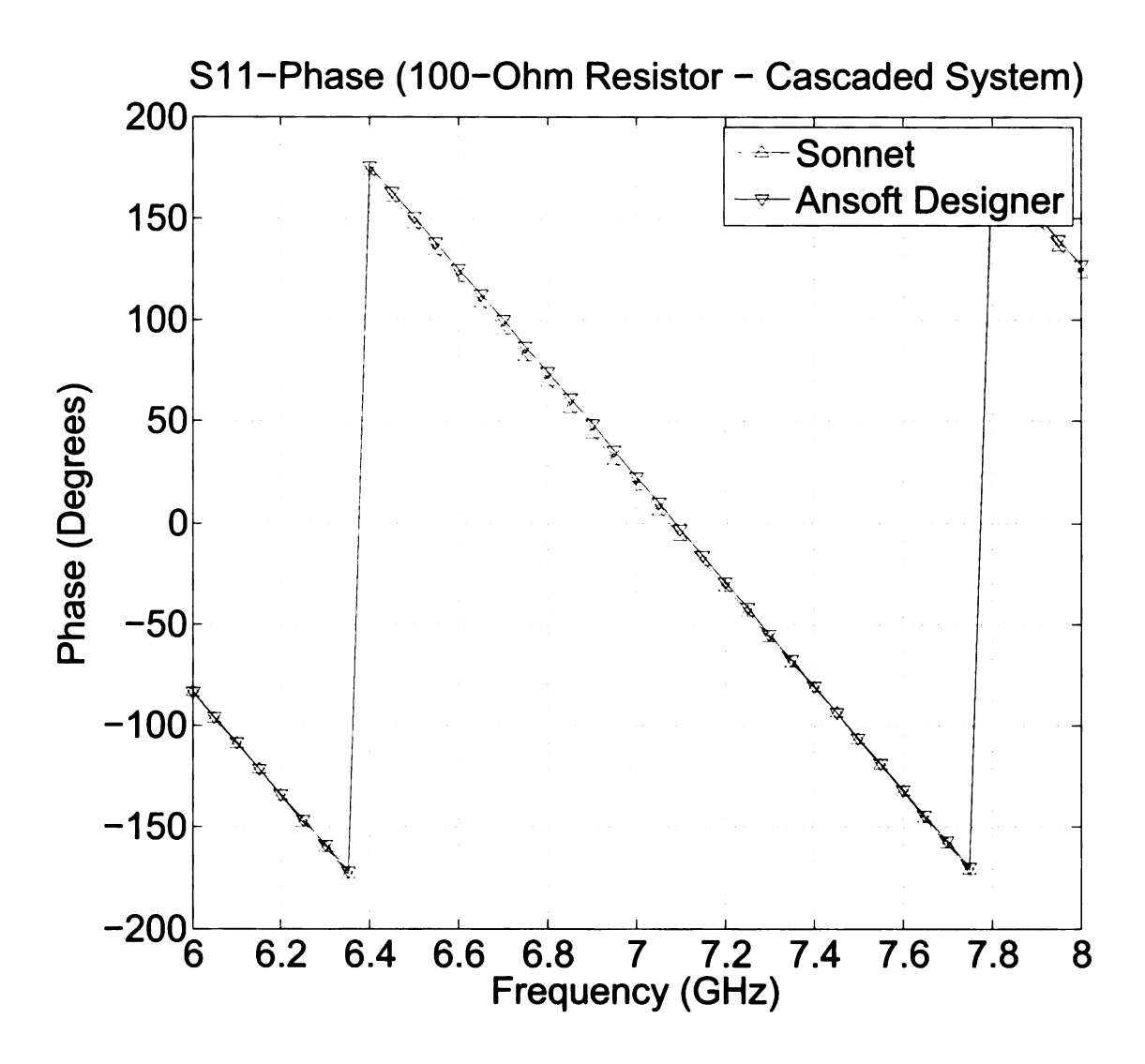


Figure 4.48. Phase of reflection coefficient of cascaded half-length microstrips with $100-\Omega$ resistor in between (Sonnet vs. Ansoft Designer)

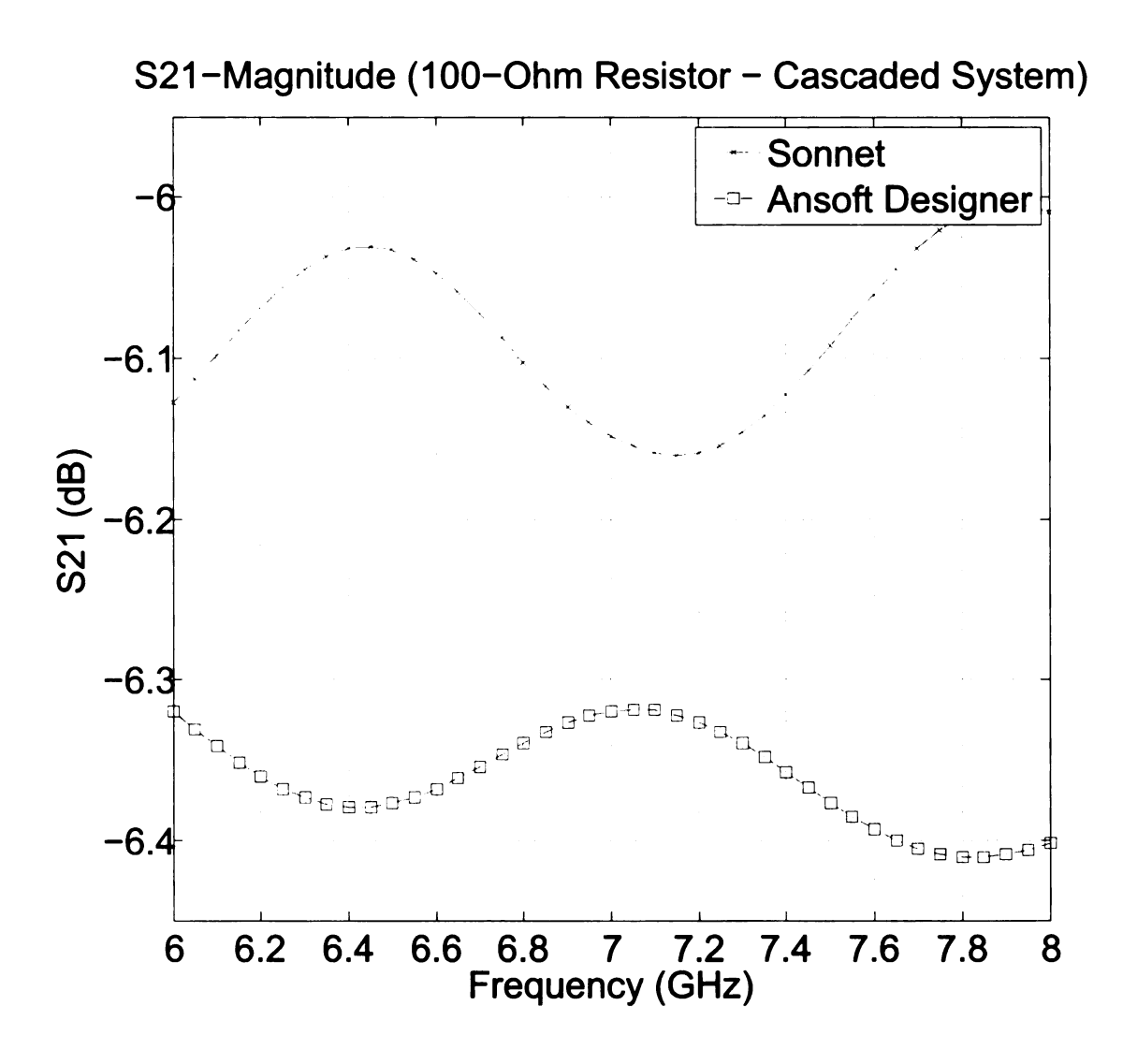


Figure 4.49. Magnitude of transmission coefficient of cascaded half-length microstrips with $100-\Omega$ resistor in between (Sonnet vs. Ansoft Designer)

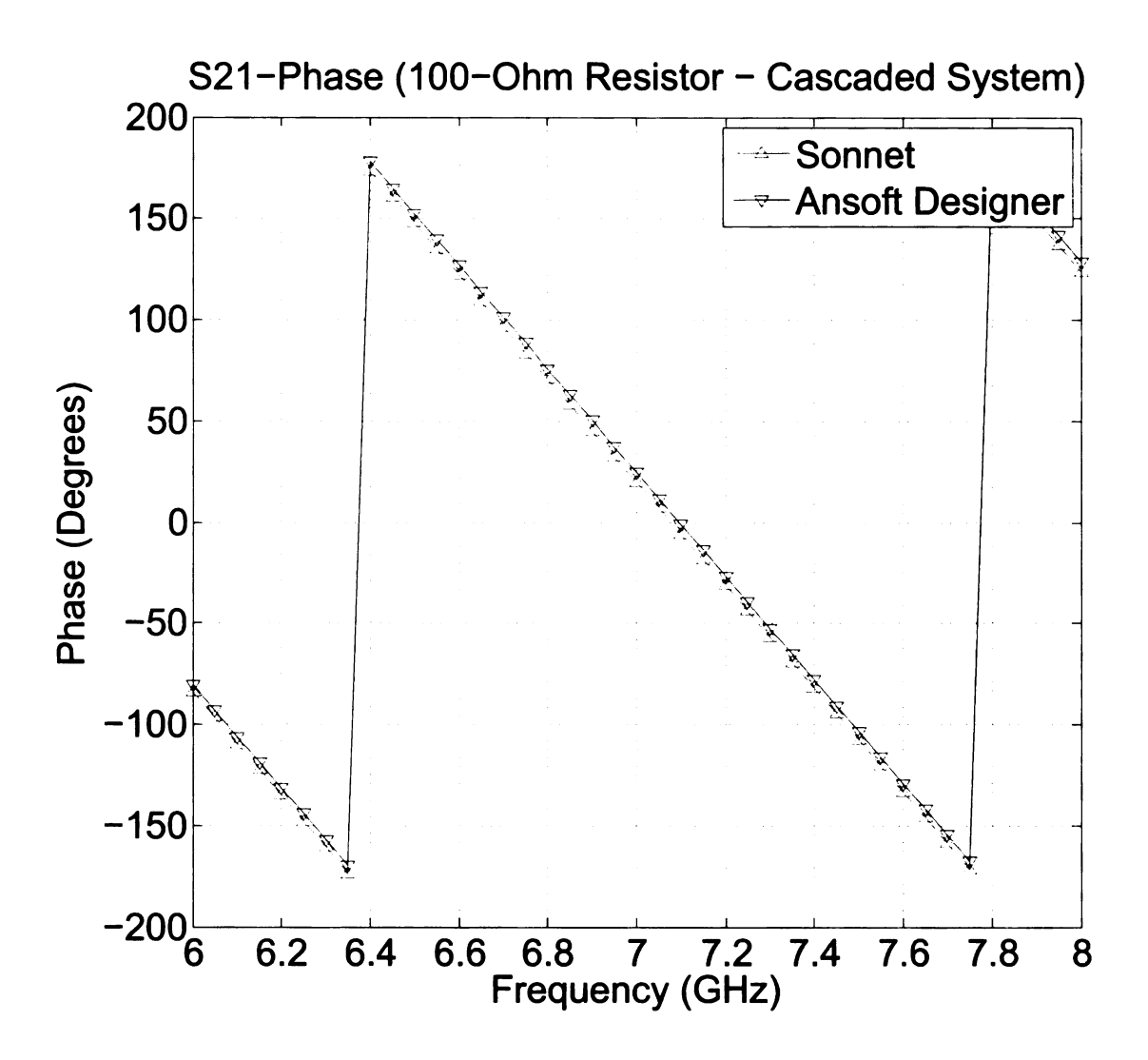


Figure 4.50. Phase of transmission coefficient of cascaded half-length microstrips with $100-\Omega$ resistor in between (Sonnet vs. Ansoft Designer)

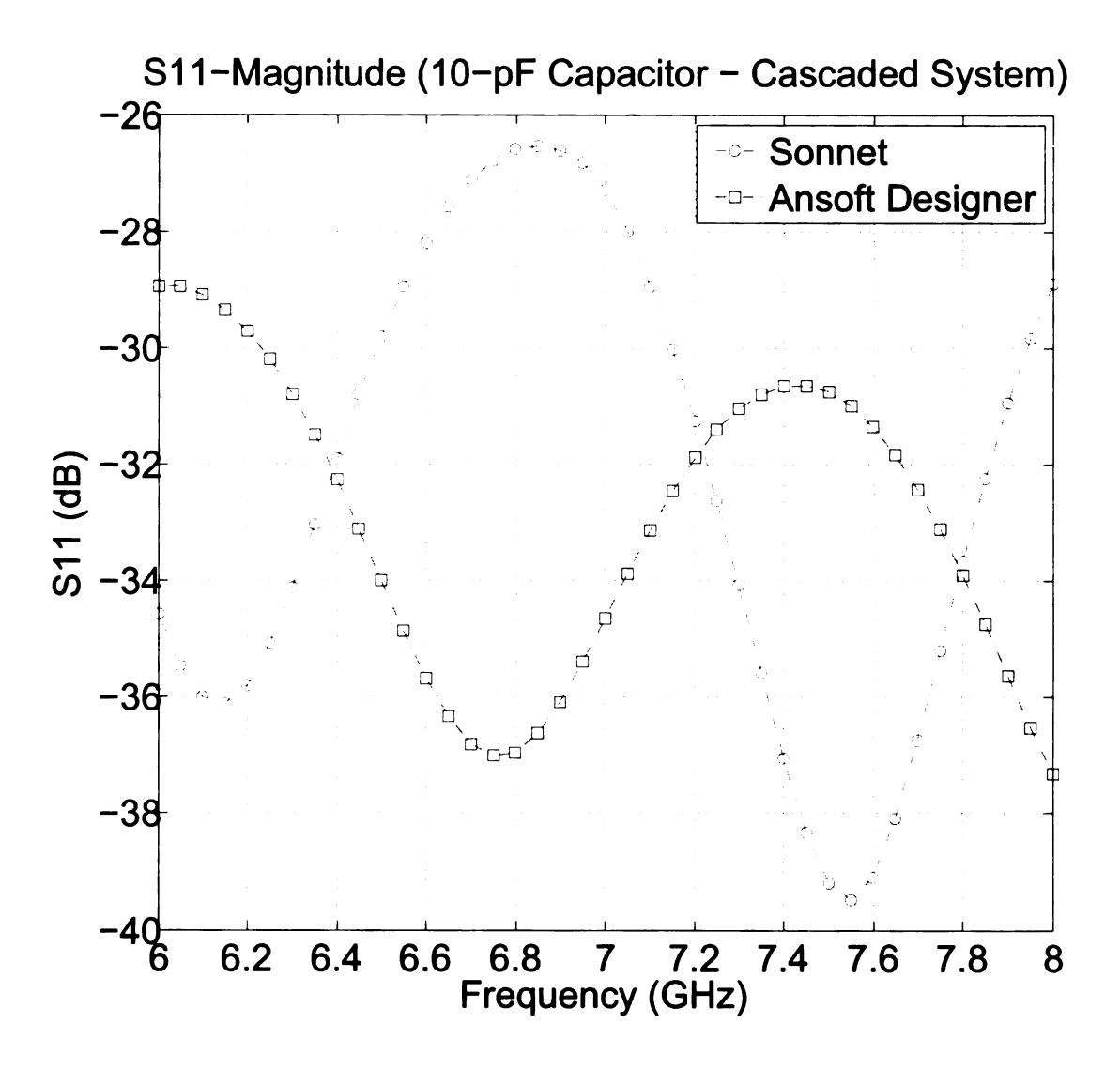


Figure 4.51. Magnitude of reflection coefficient of cascaded half-length microstrips with 10-pF capacitor in between (Sonnet vs. Ansoft Designer)

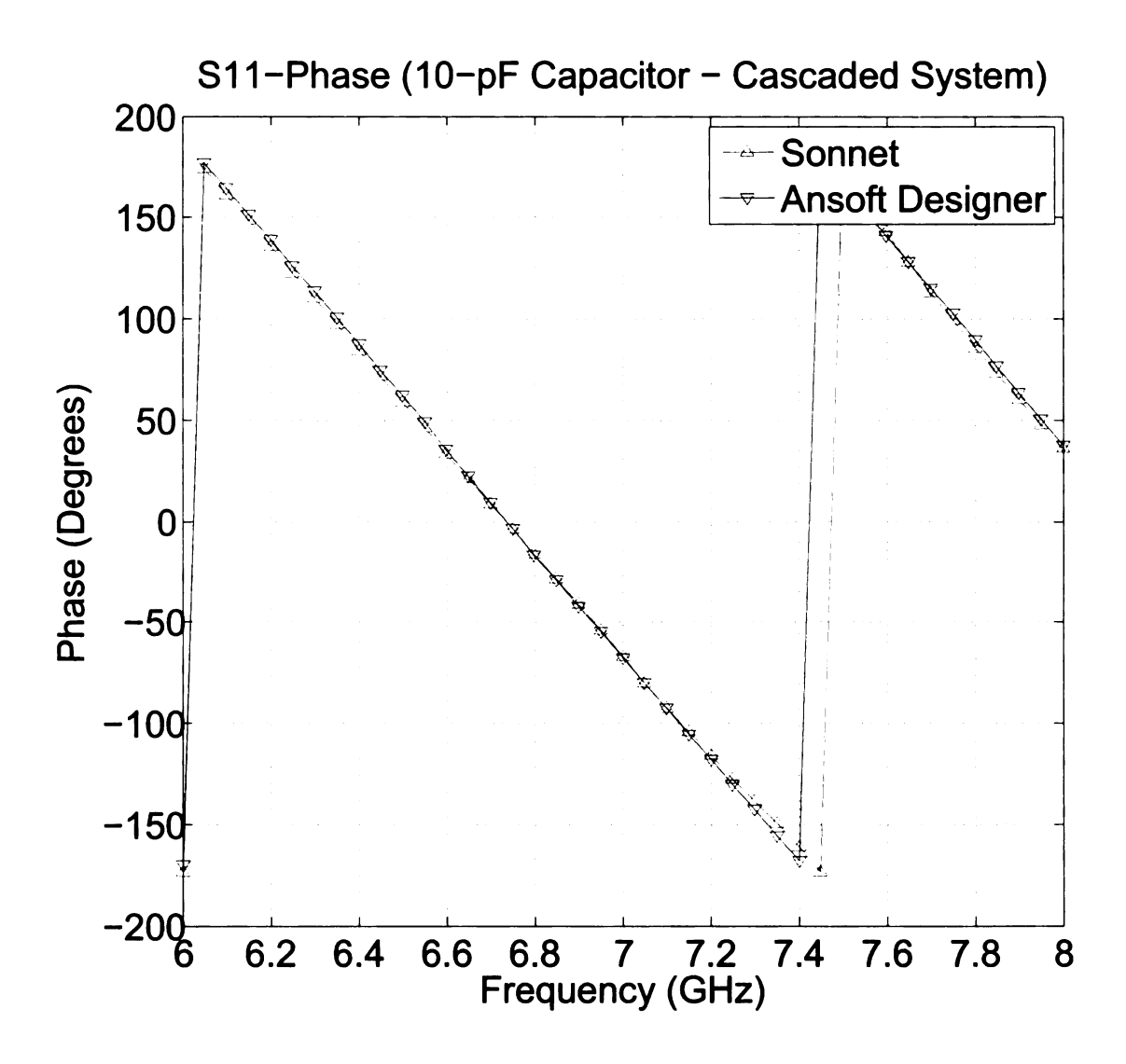


Figure 4.52. Phase of reflection coefficient of cascaded half-length microstrips with 10-pF capacitor in between (Sonnet vs. Ansoft Designer)

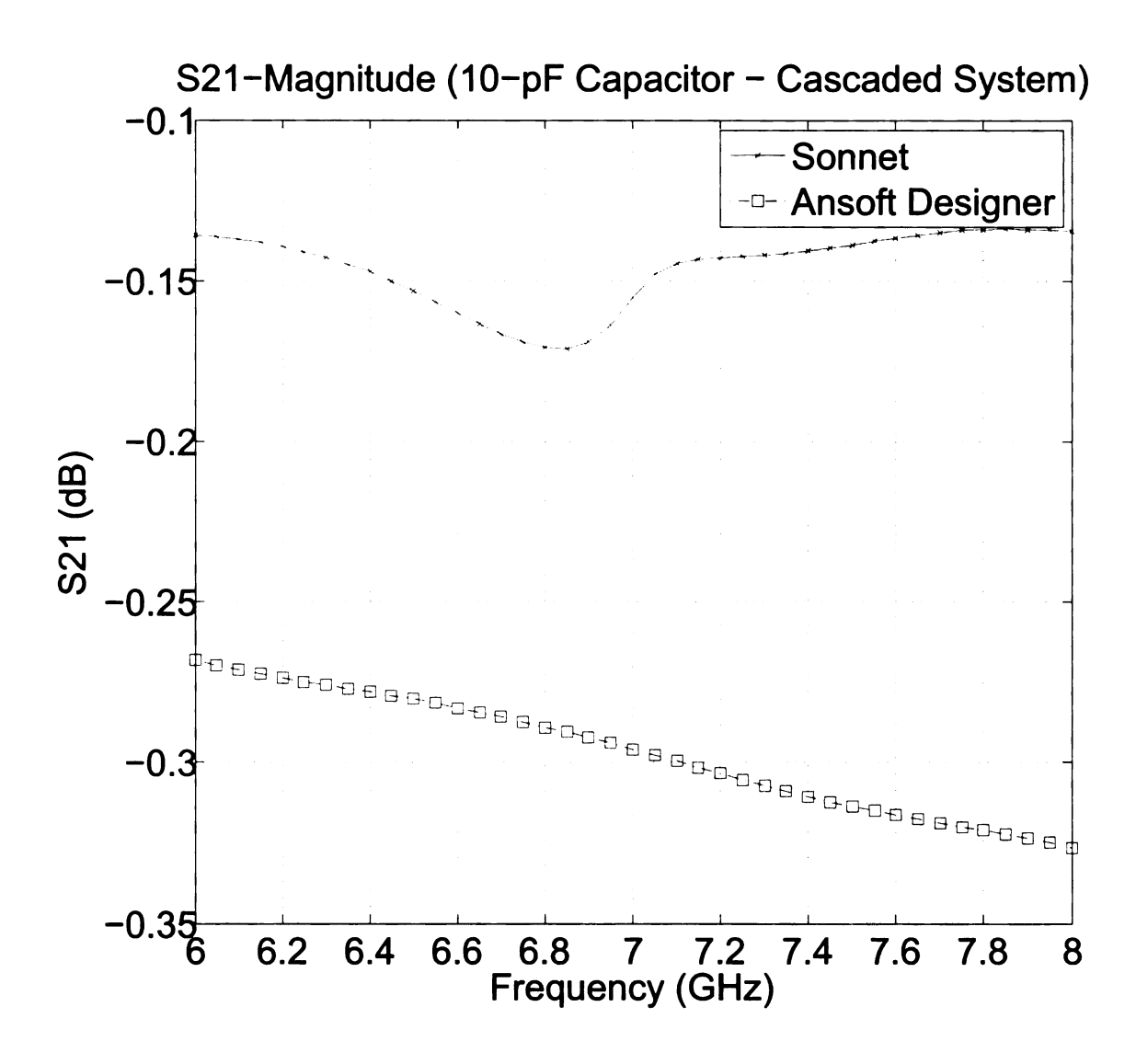


Figure 4.53. Magnitude of transmission coefficient of cascaded half-length microstrips with 10-pF capacitor in between (Sonnet vs. Ansoft Designer)

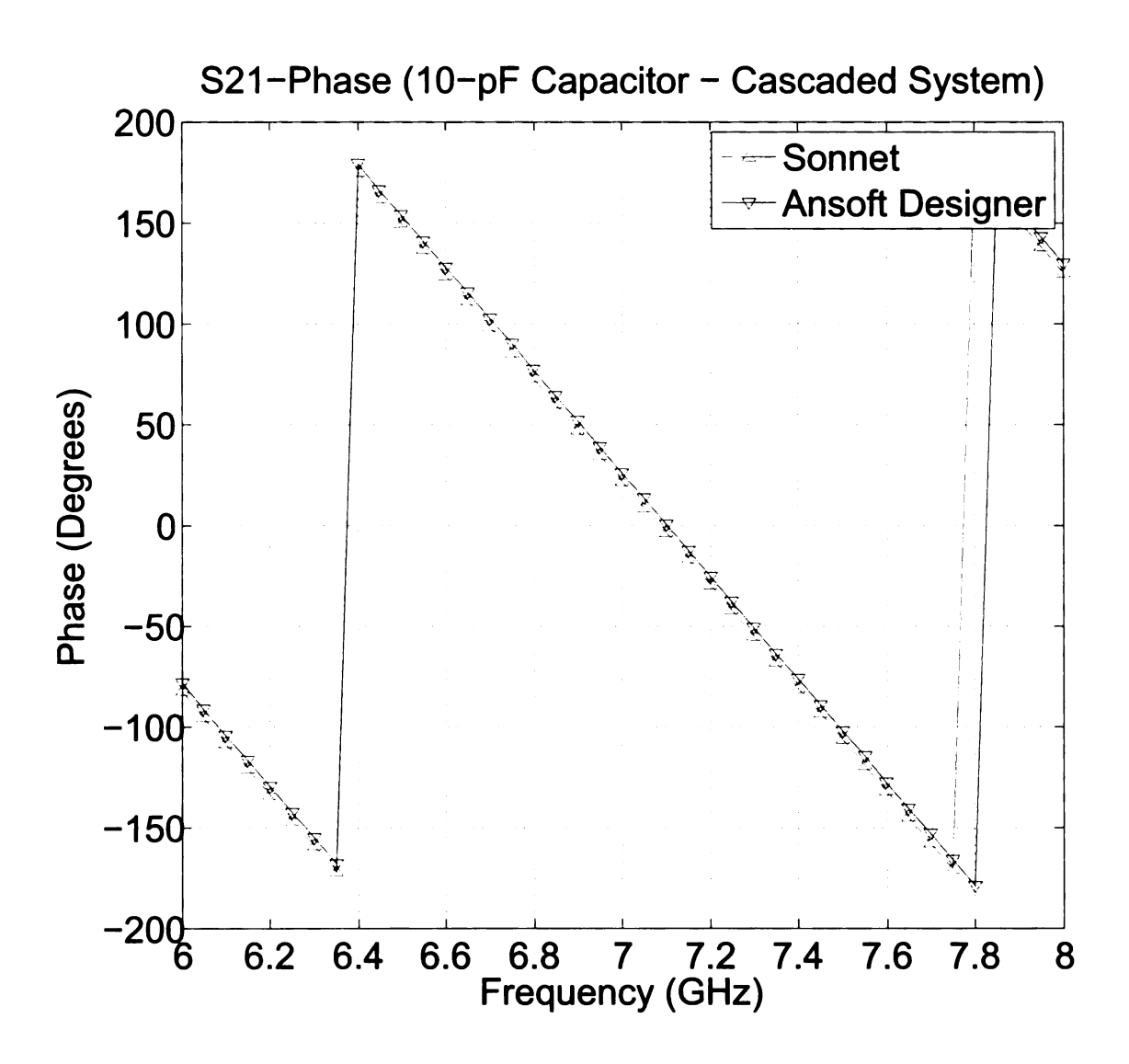


Figure 4.54. Phase of transmission coefficient of cascaded half-length microstrips with 10-pF capacitor in between (Sonnet vs. Ansoft Designer)

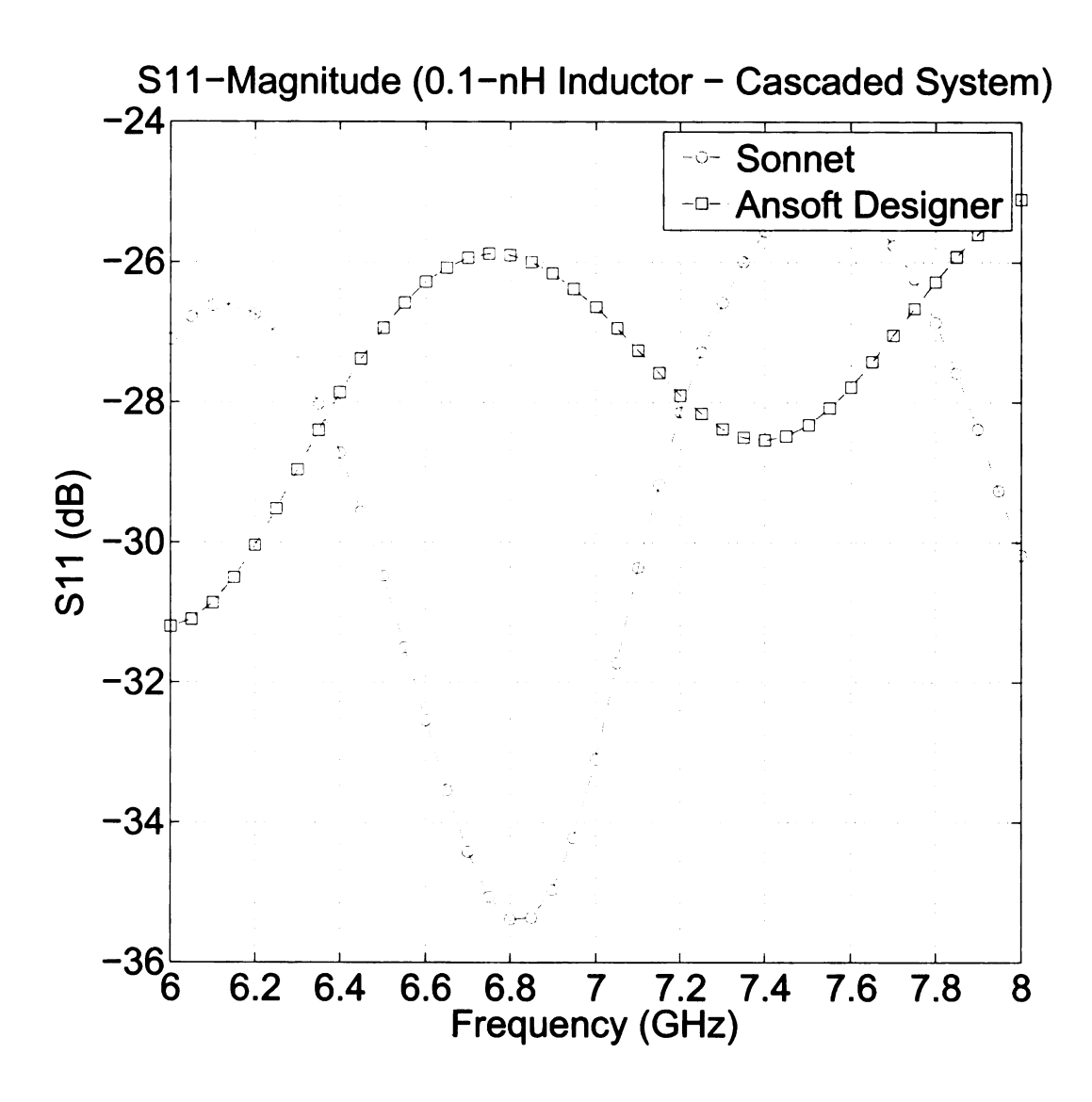


Figure 4.55. Magnitude of reflection coefficient of cascaded half-length microstrips with 0.1-nH inductor in between (Sonnet vs. Ansoft Designer)

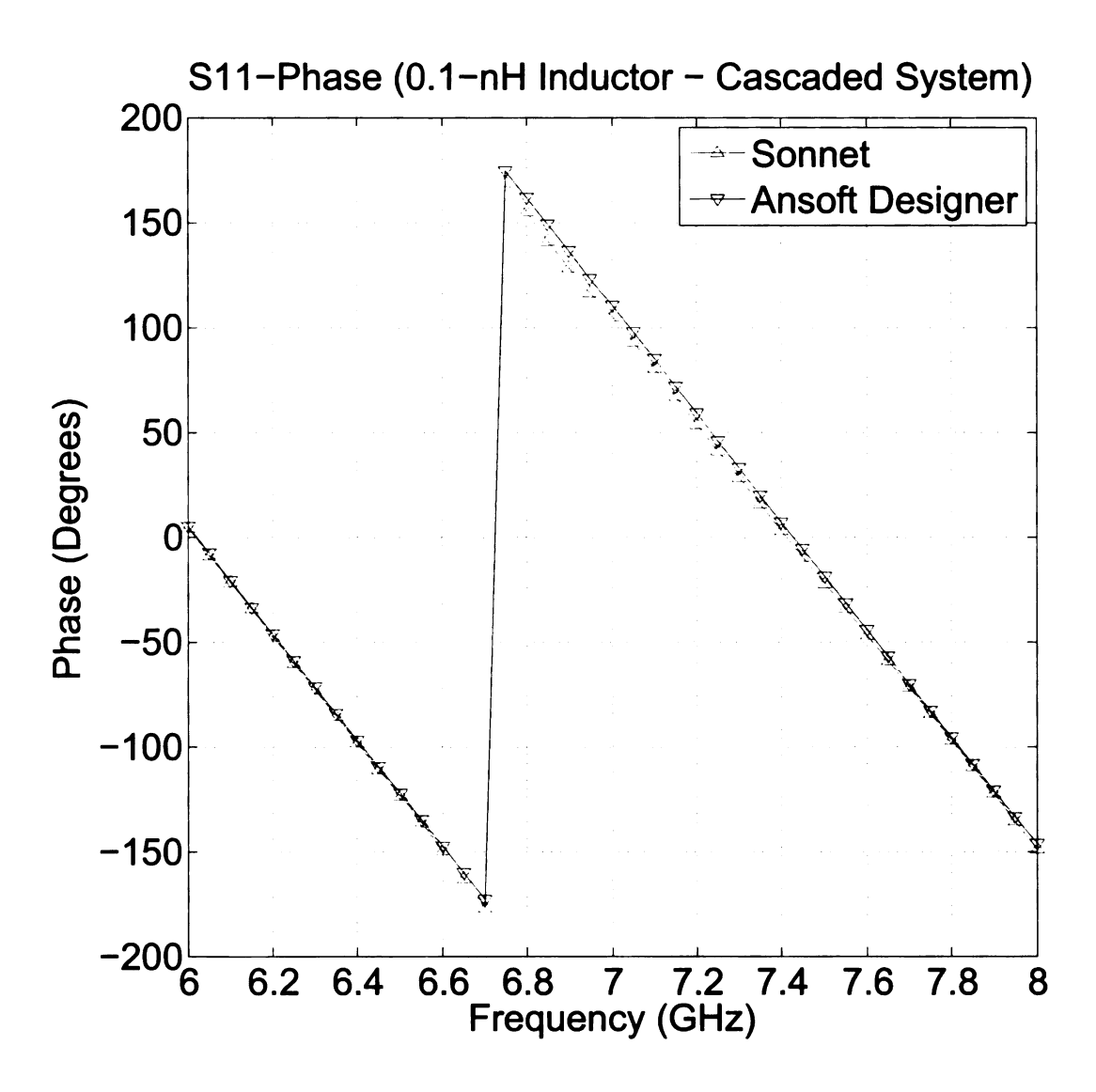


Figure 4.56. Phase of reflection coefficient of cascaded half-length microstrips with 0.1-nH inductor in between (Sonnet vs. Ansoft Designer)

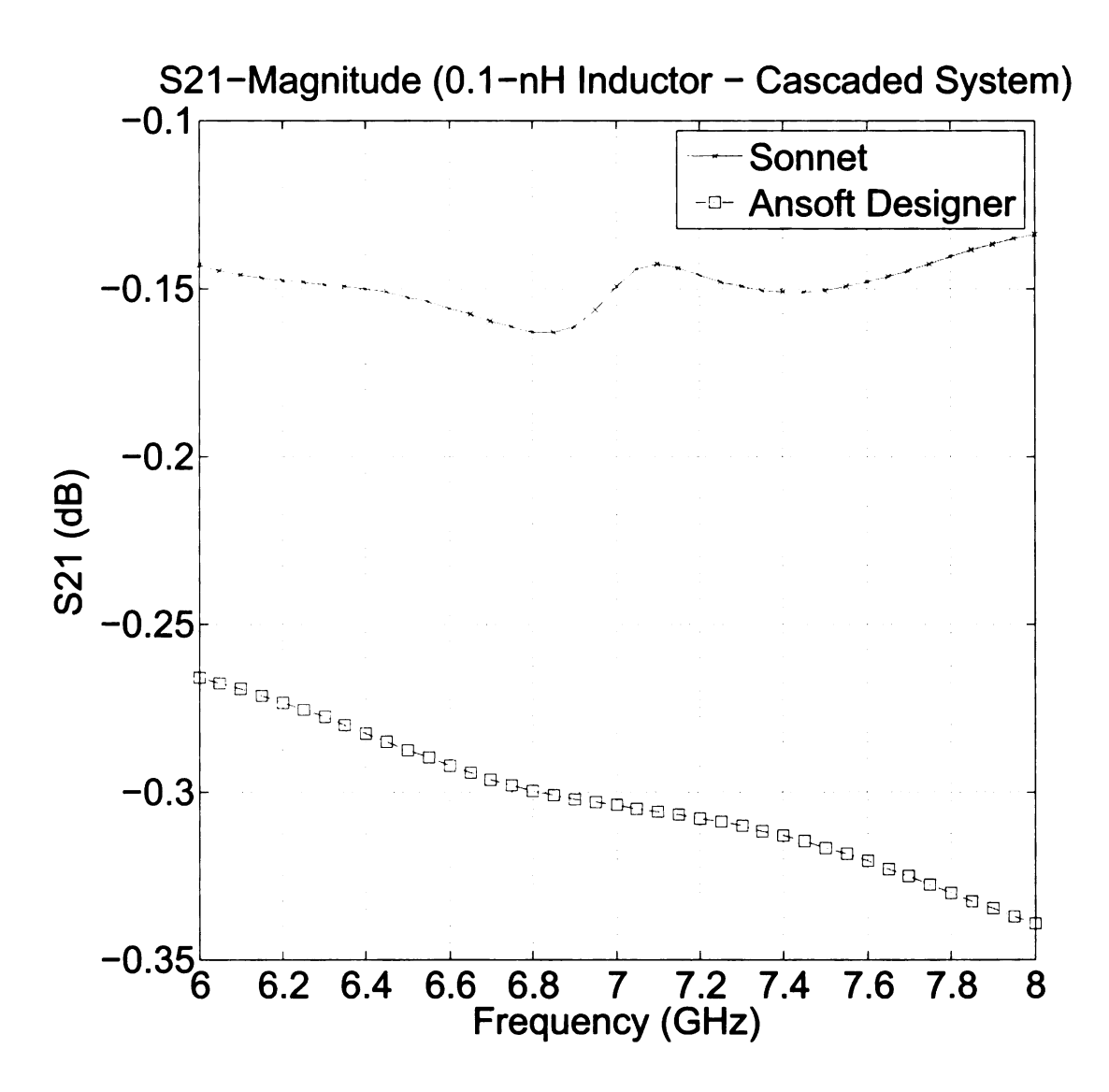


Figure 4.57. Magnitude of transmission coefficient of cascaded half-length microstrips with 0.1-nH inductor in between (Sonnet vs. Ansoft Designer)

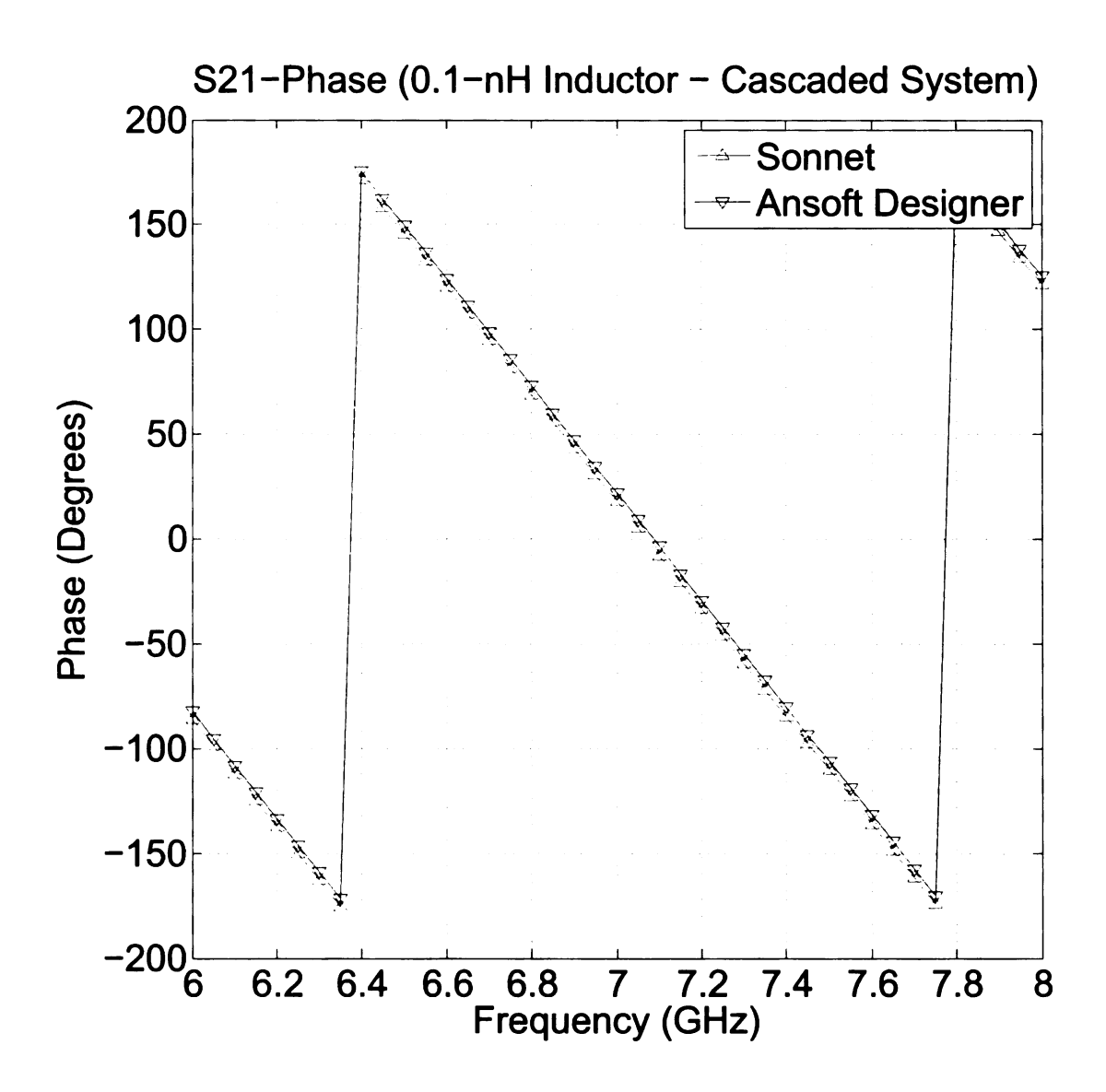


Figure 4.58. Phase of transmission coefficient of cascaded half-length microstrips with 0.1-nH inductor in between (Sonnet vs. Ansoft Designer)

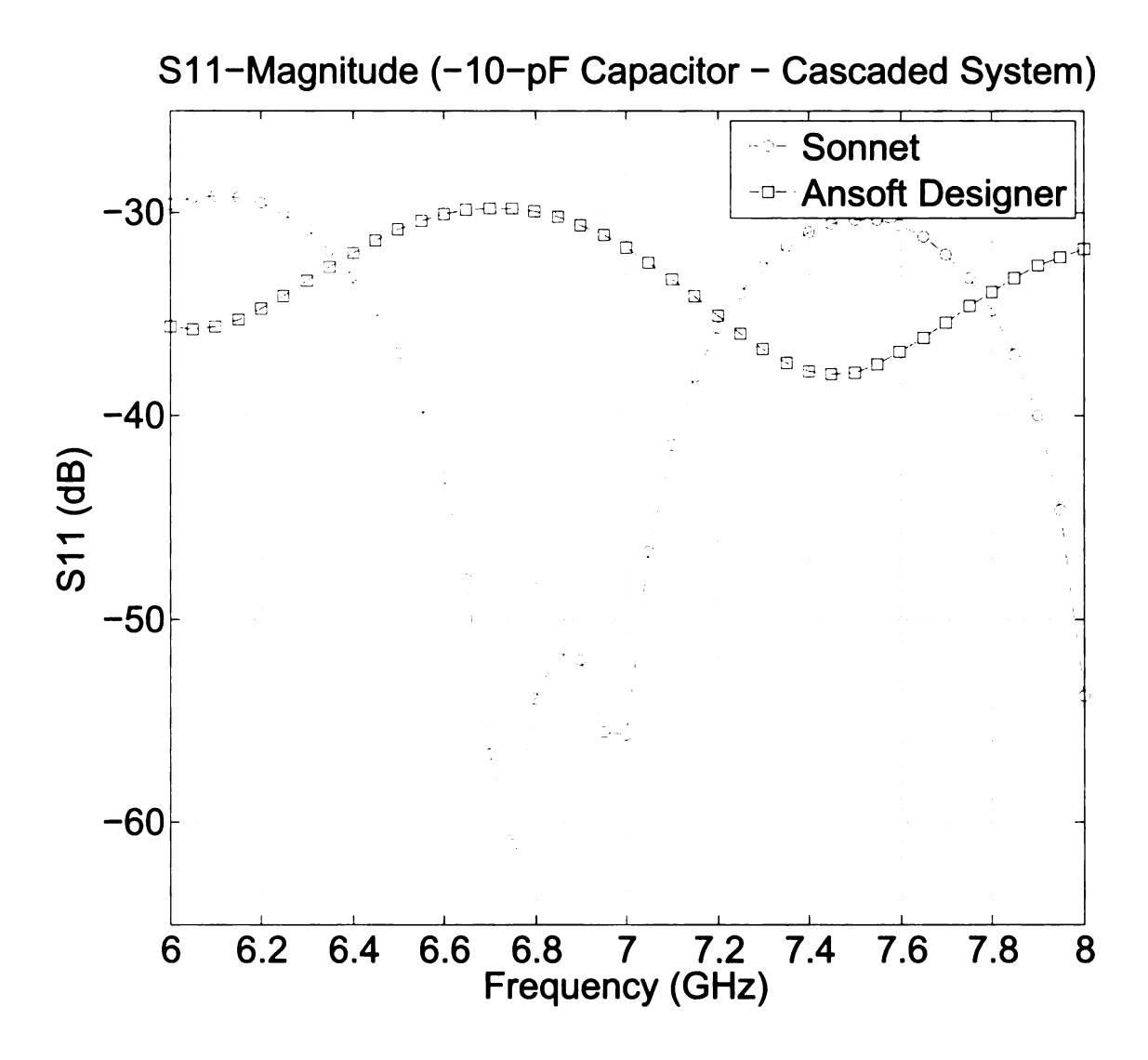


Figure 4.59. Magnitude of reflection coefficient of cascaded half-length microstrips with -10-pF capacitor in between (Sonnet vs. Ansoft Designer)

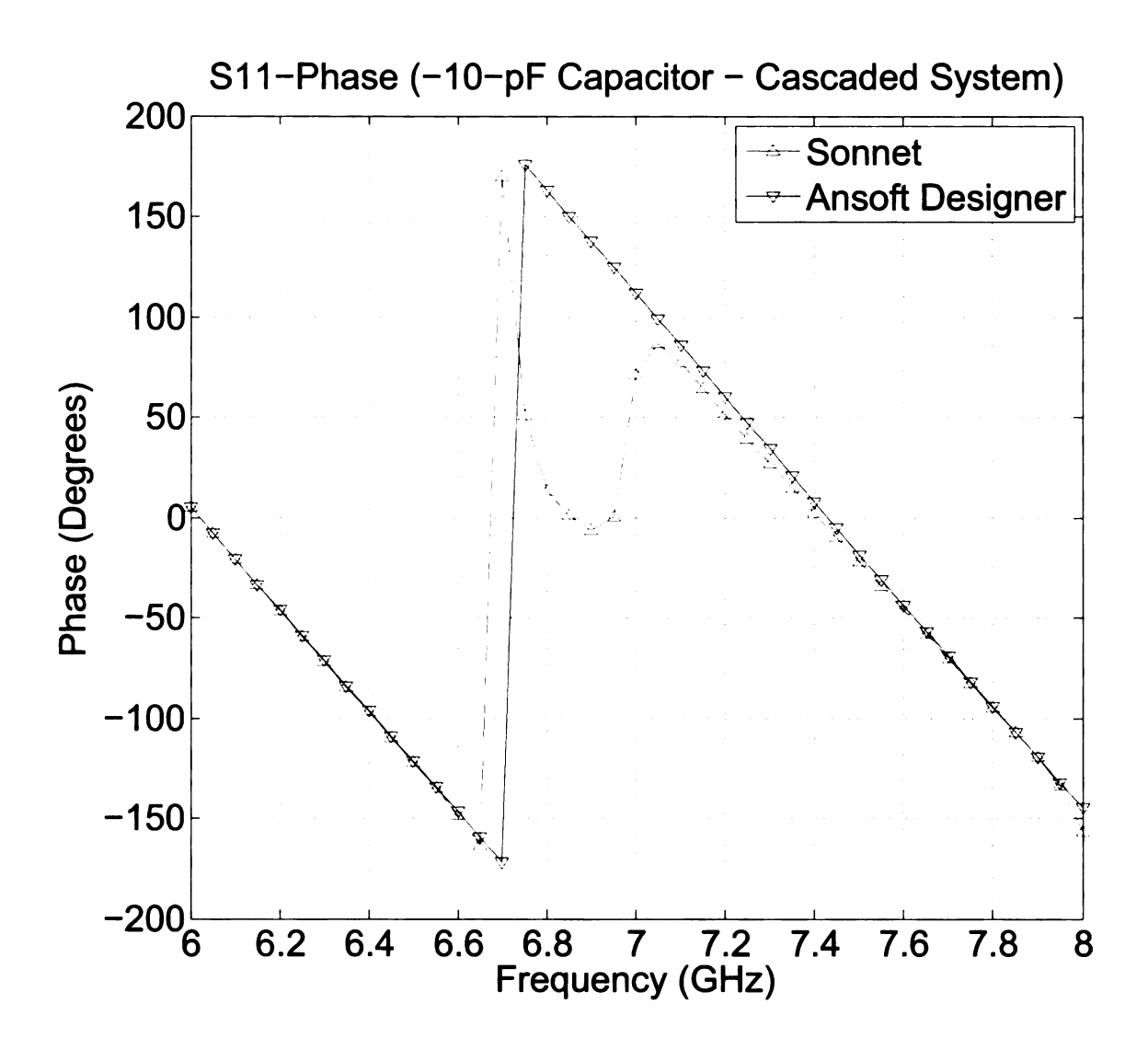


Figure 4.60. Phase of reflection coefficient of cascaded half-length microstrips with -10-pF capacitor in between (Sonnet vs. Ansoft Designer)

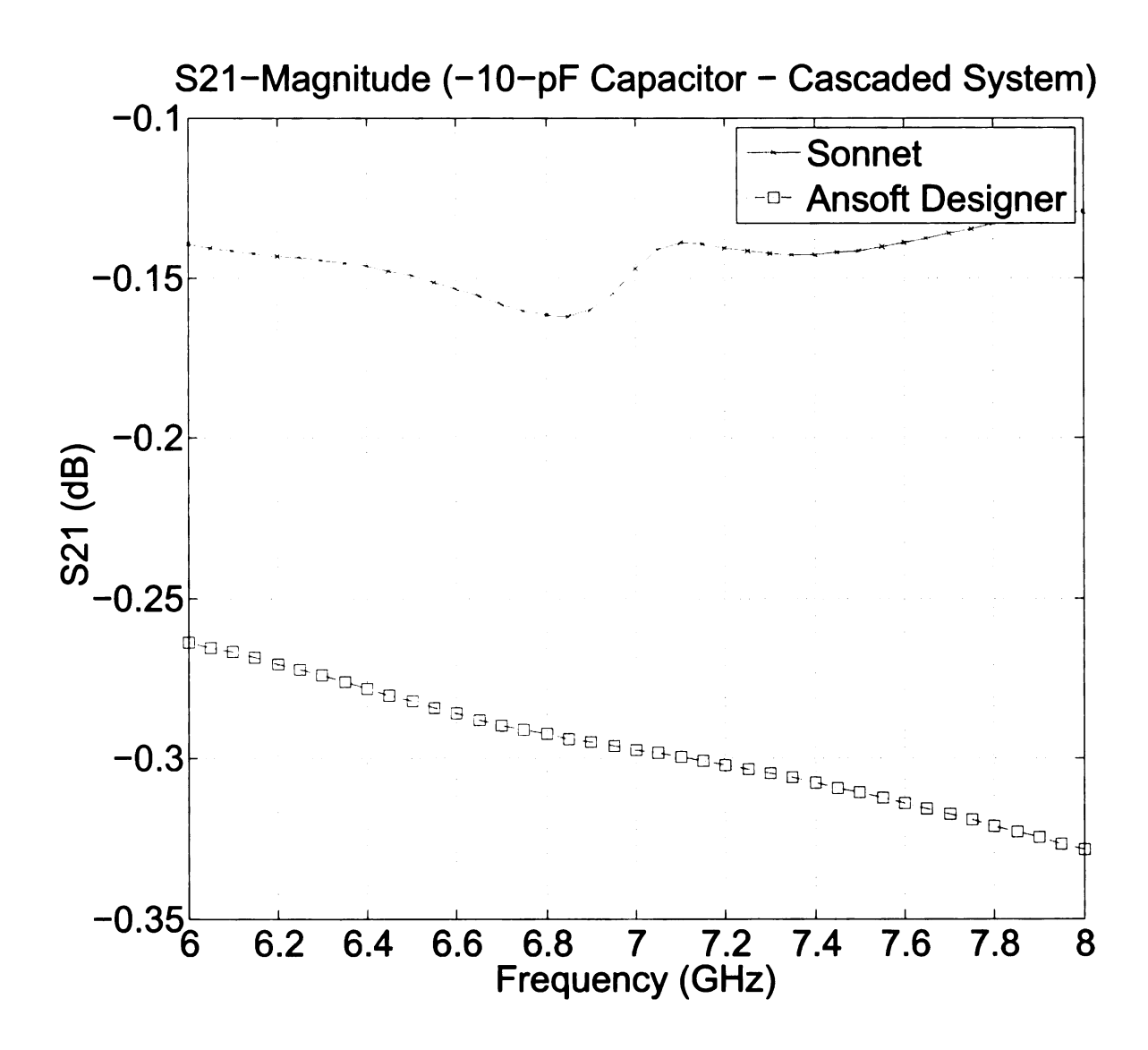


Figure 4.61. Magnitude of transmission coefficient of cascaded half-length microstrips with -10-pF capacitor in between (Sonnet vs. Ansoft Designer)

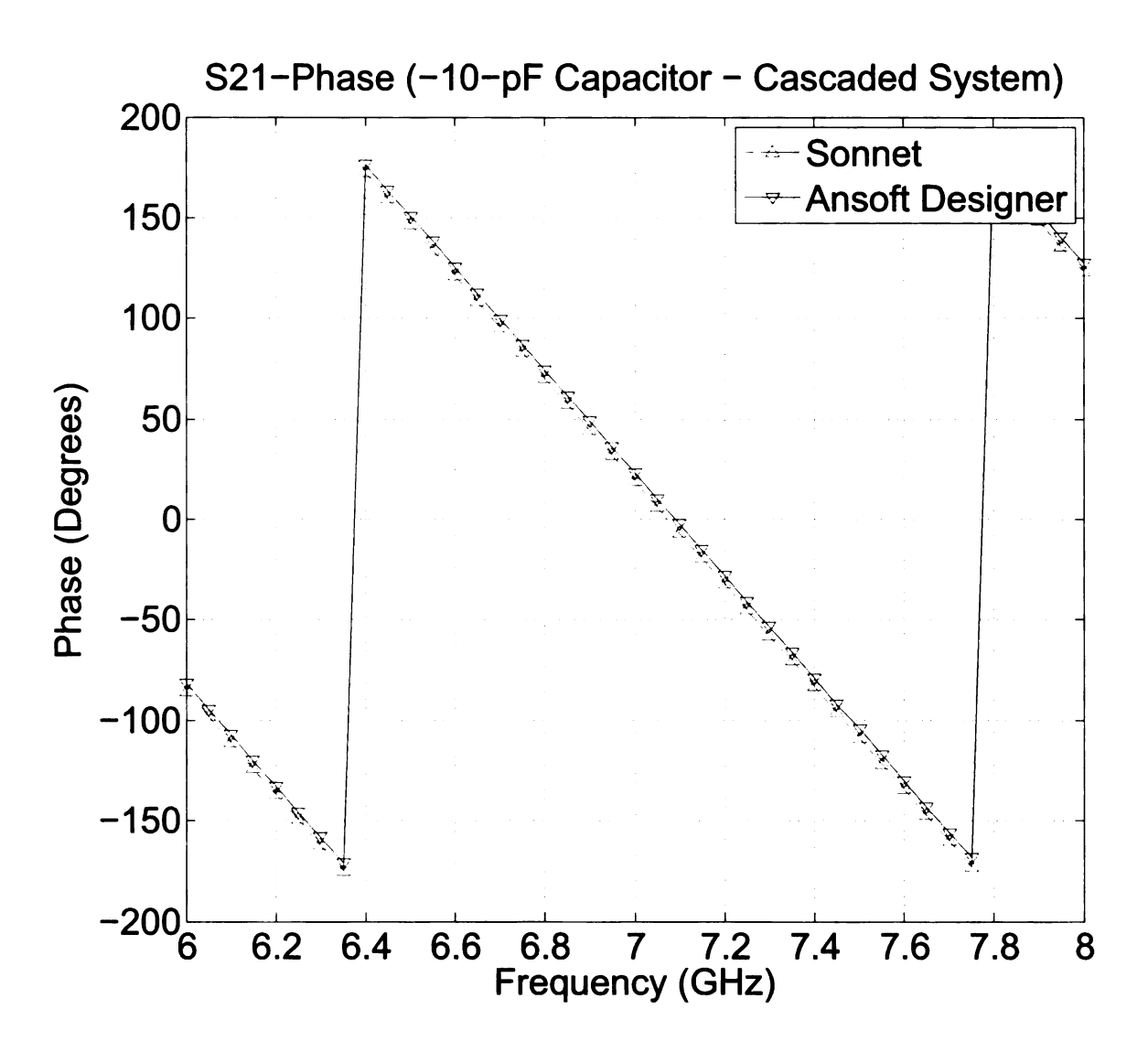


Figure 4.62. Phase of transmission coefficient of cascaded half-length microstrips with -10-pF capacitor in between (Sonnet vs. Ansoft Designer)

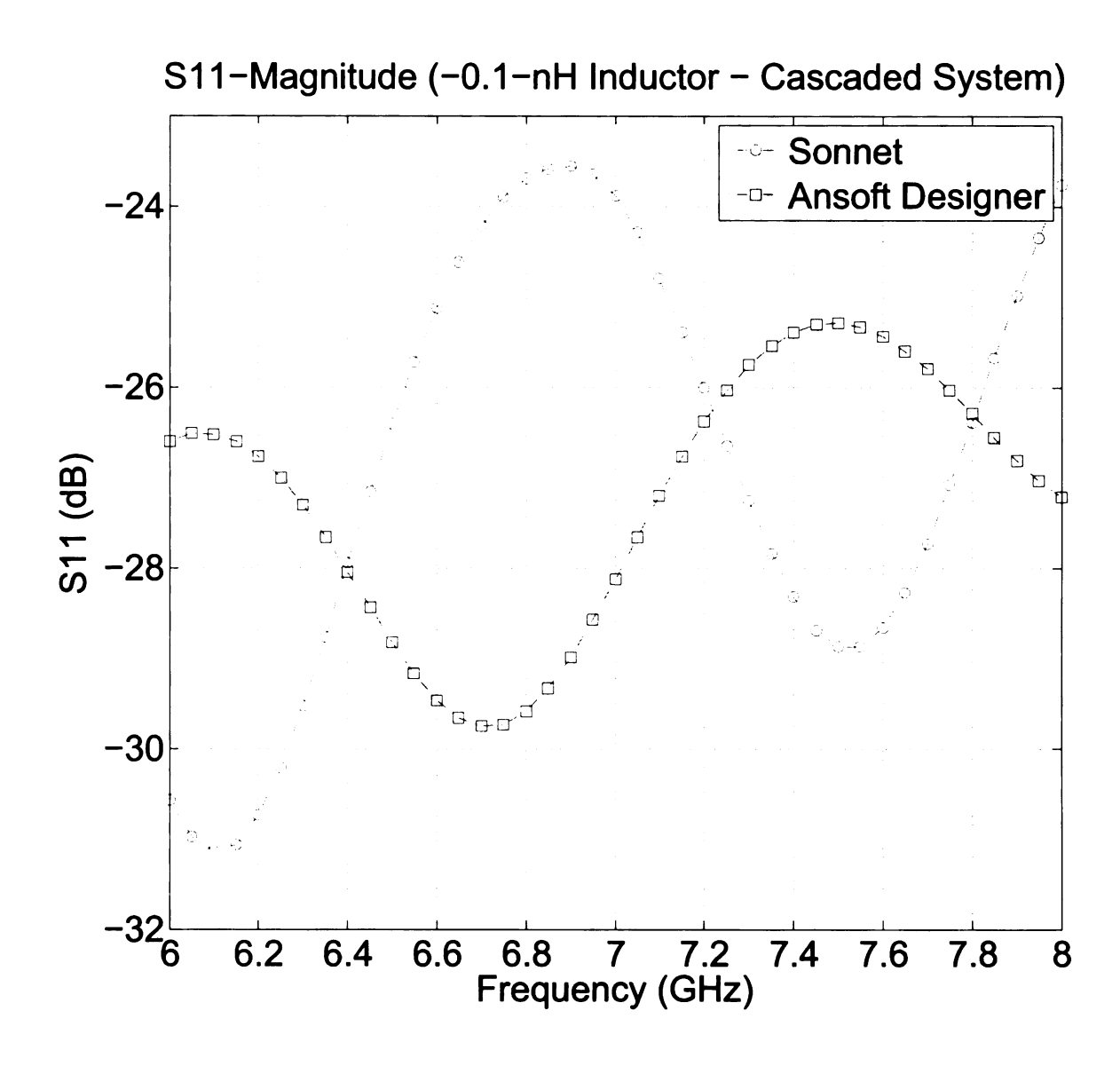


Figure 4.63. Magnitude of reflection coefficient of cascaded half-length microstrips with -0.1-nH inductor in between (Sonnet vs. Ansoft Designer)

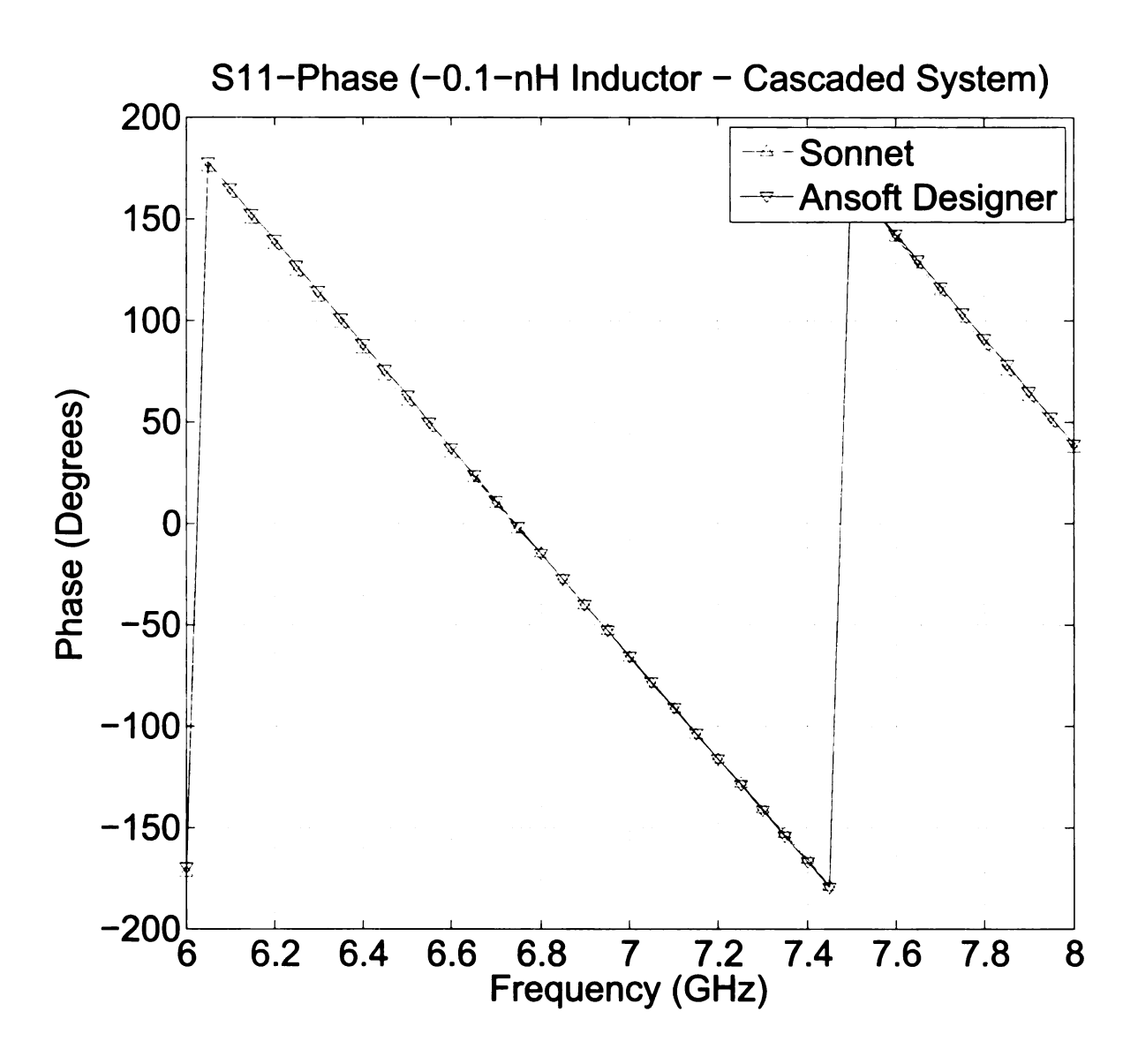


Figure 4.64. Phase of reflection coefficient of cascaded half-length microstrips with -0.1-nH inductor in between (Sonnet vs. Ansoft Designer)

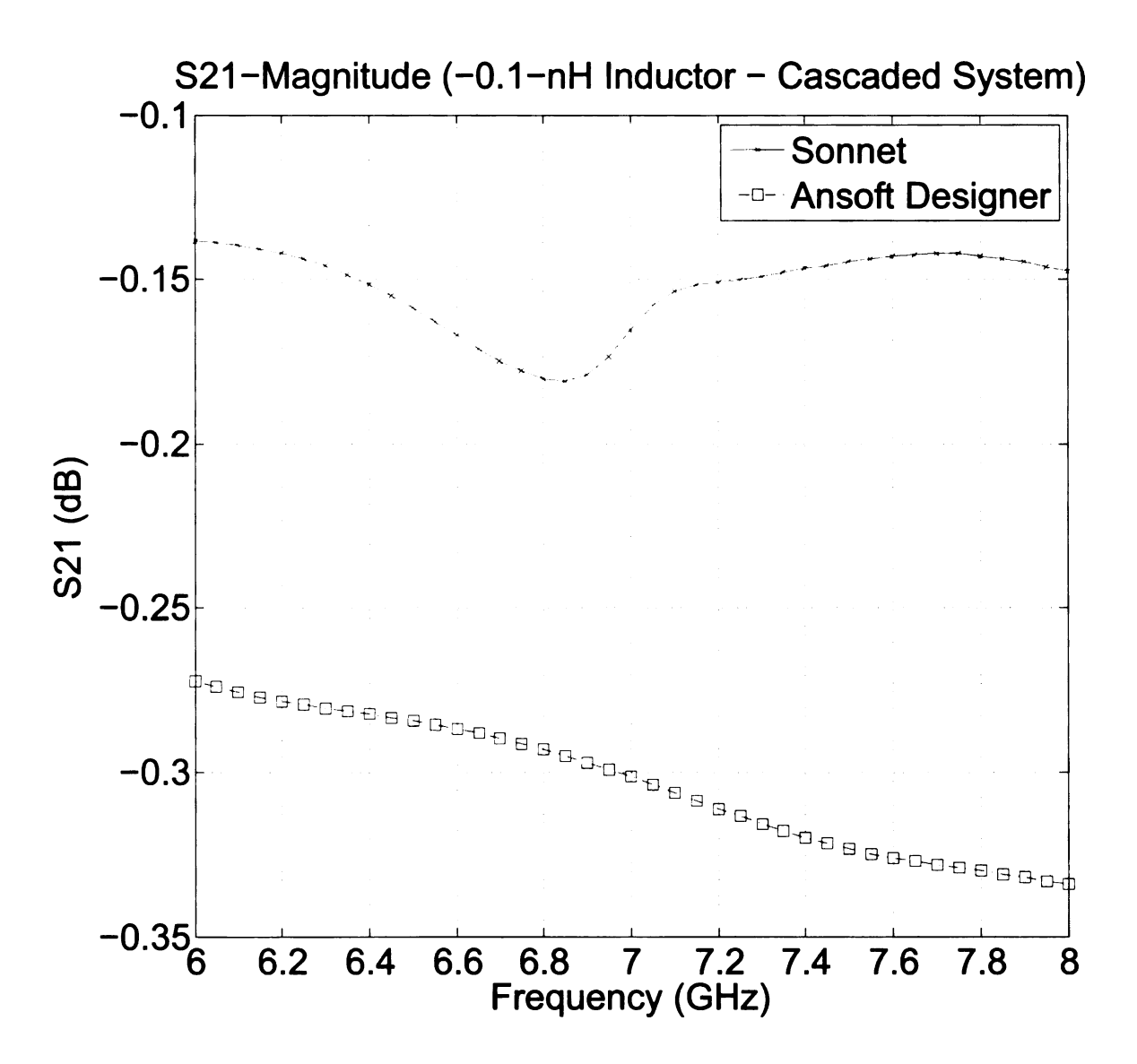


Figure 4.65. Magnitude of transmission coefficient of cascaded half-length microstrips with -0.1-nH inductor in between (Sonnet vs. Ansoft Designer)

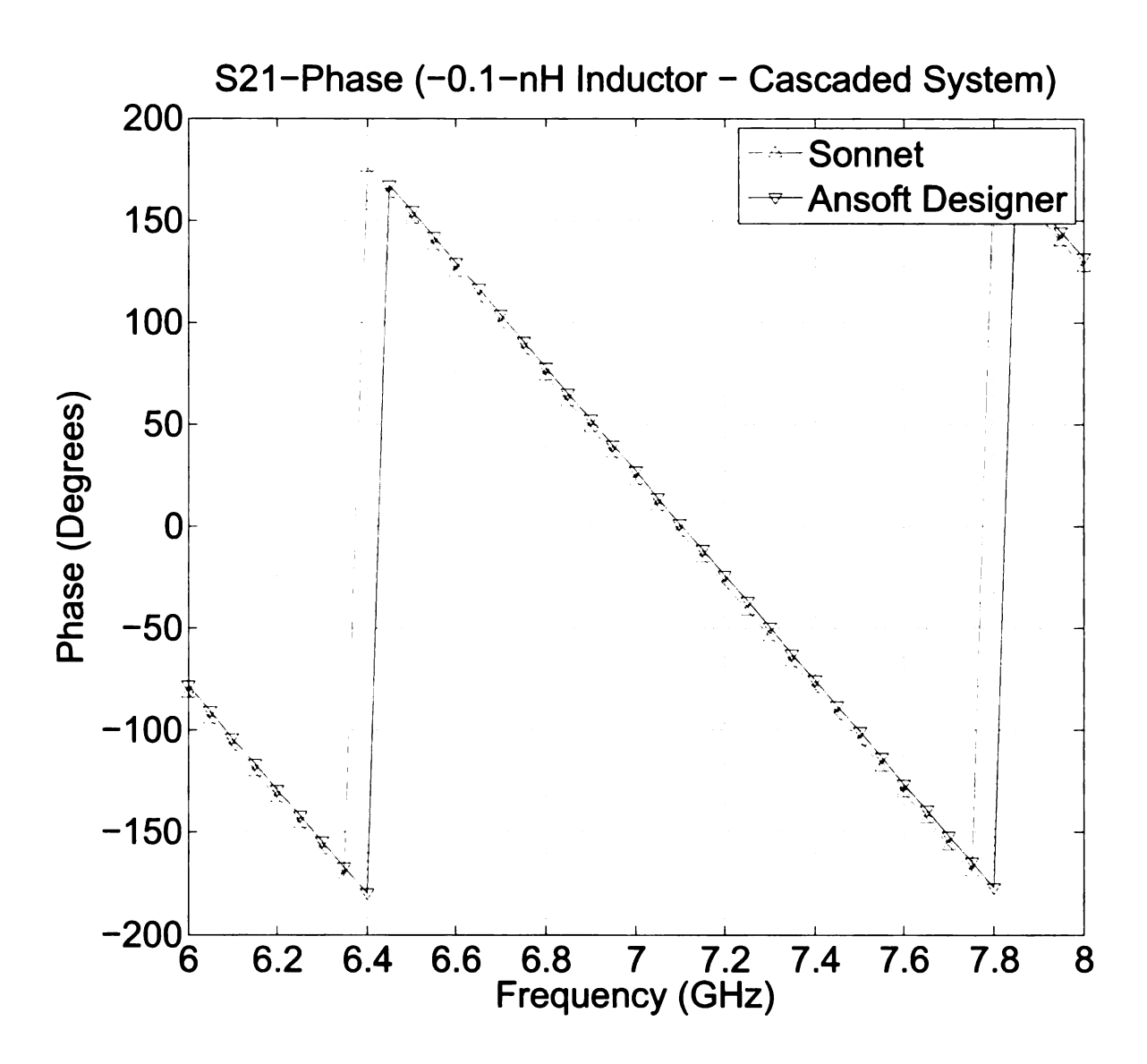


Figure 4.66. Phase of transmission coefficient of cascaded half-length microstrips with -0.1-nH inductor in between (Sonnet vs. Ansoft Designer)

The trends for the cascaded networks including the resistor, capacitor and inductor are similar using the half-length microstrips modeled in Sonnet and Ansoft Designer. The general trend for the resistor is that the reflection coefficient increases as the resistance increases. The opposite trend is true for the transmission coefficient as the resistance increases. For the reactive components (e.g., capacitor and inductor), there is little reflection while there is nearly complete transmission.

Figures 4.67 to 4.74 shows a parameter study of reactive components in the cascaded network. The reactive component used for Figures 4.67 to 4.70 and 4.71 to 4.74 is a capacitor and an inductor, respectively. The values of the reactive components were varied from positive to negative and the trends of the S-parameters as the reactance transitions from positive to negative is displayed in these figures.

For the following figures for the capacitor, the reflection coefficient increases in magnitude as the capacitance decreases from its nominal value of 10 pF to 0 pF and decreases in magnitude as the capacitance decreases from 0 to -10 pF. The transmission coefficient decreases in magnitude as the capacitance decreases from its nominal value of 10 pF to 0 pF and increases in magnitude as the capacitance decreases from 0 to -10 pF. For the following figures for the inductor, the reflection coefficient decreases in magnitude as the inductance decreases from its nominal value of 0.1 nH to 0 nH and increases in magnitude as the inductance decreases from 0 to -0.1 nH. The transmission coefficient increases in magnitude as the inductance decreases from its nominal value of 0.1 nH to 0 nH and decreases in magnitude as the inductance decreases from 0 to -0.1 nH. It should be noted that 0 pF denotes an open circuit and 0 nH represents a short circuit. The phase of the reflection coefficient and transmission coefficient relatively remains the same for both the capacitor and inductor as it transitions from positive to negative reactance. The half-length microstrips modeled in Sonnet were used in this parameter study because it produces results that will be similar to experimental data.

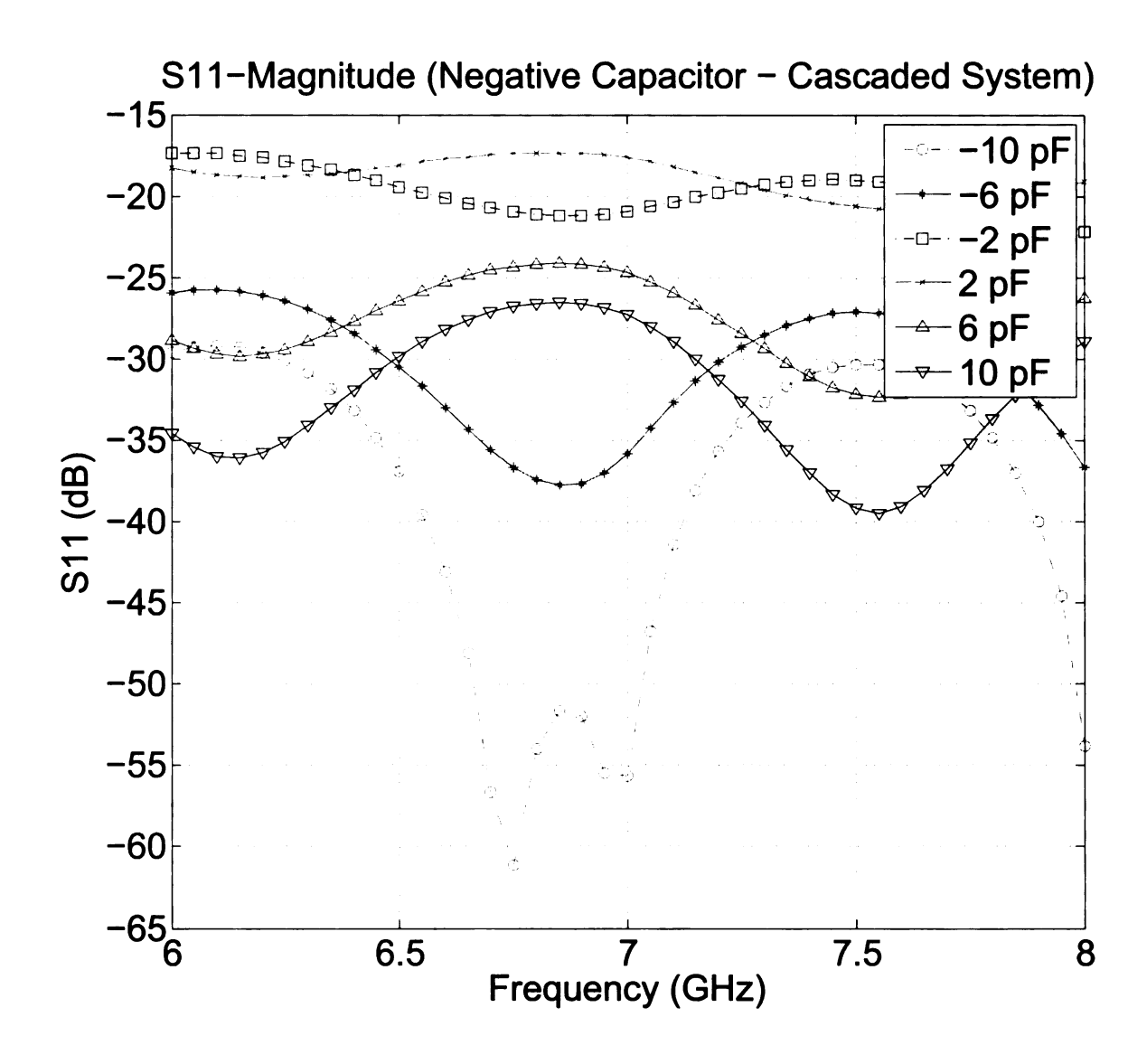


Figure 4.67. Magnitude of reflection coefficient of parameter study of cascaded system with capacitor varied from 10 pF to -10 pF

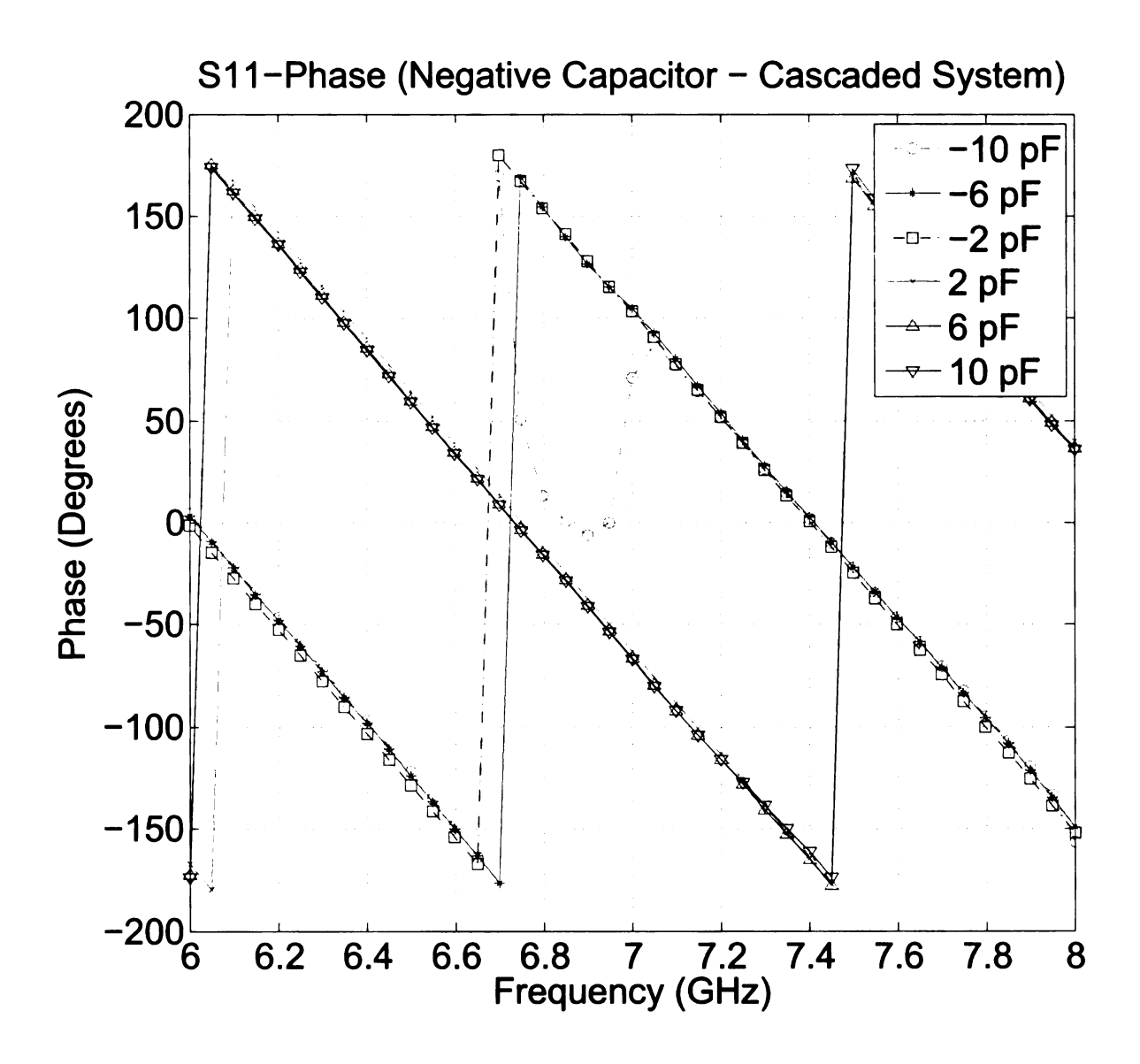


Figure 4.68. Phase of reflection coefficient of parameter study of cascaded system with capacitor varied from 10 pF to -10 pF

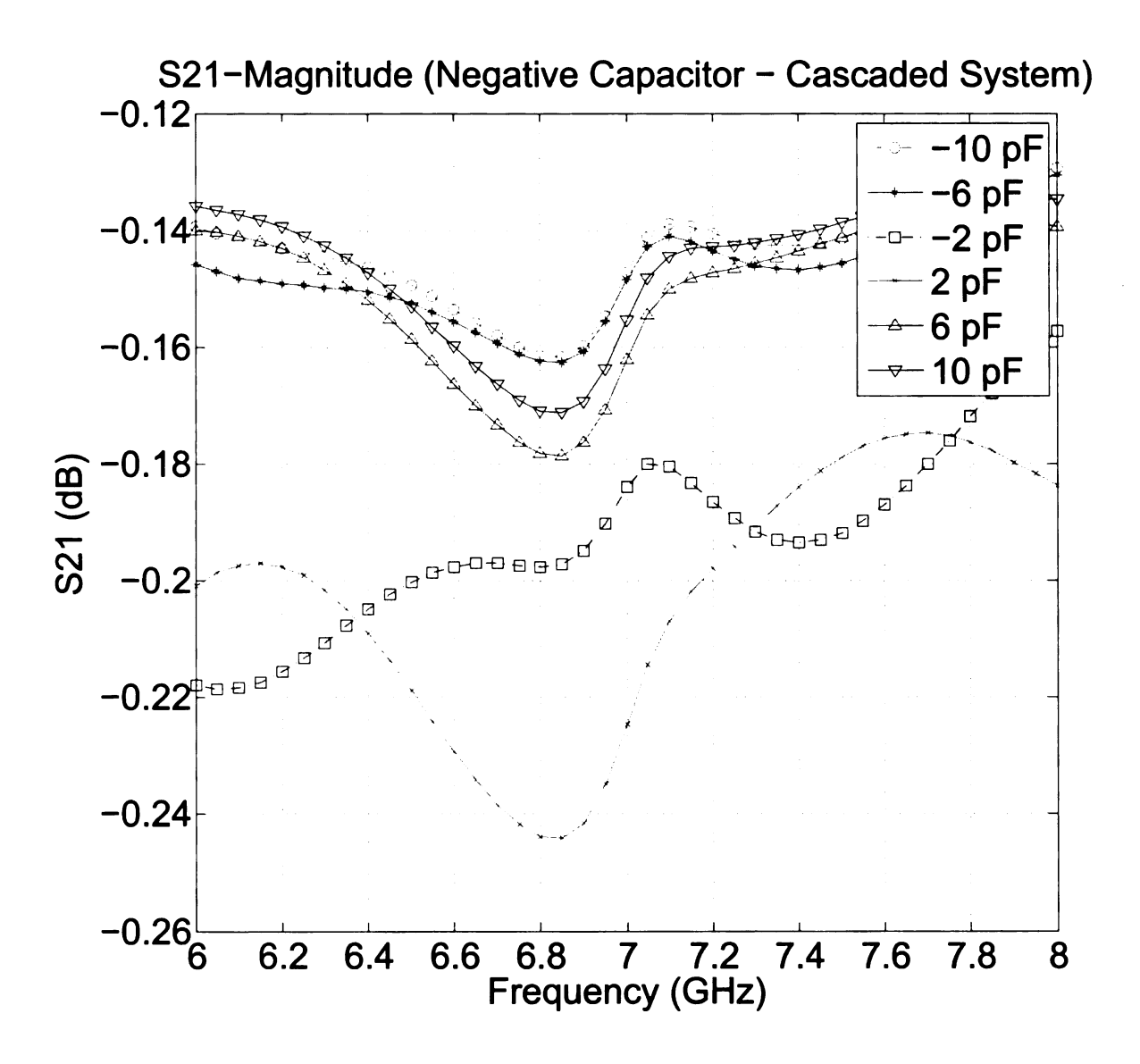


Figure 4.69. Magnitude of transmission coefficient of parameter study of cascaded system with capacitor varied from 10 pF to -10 pF

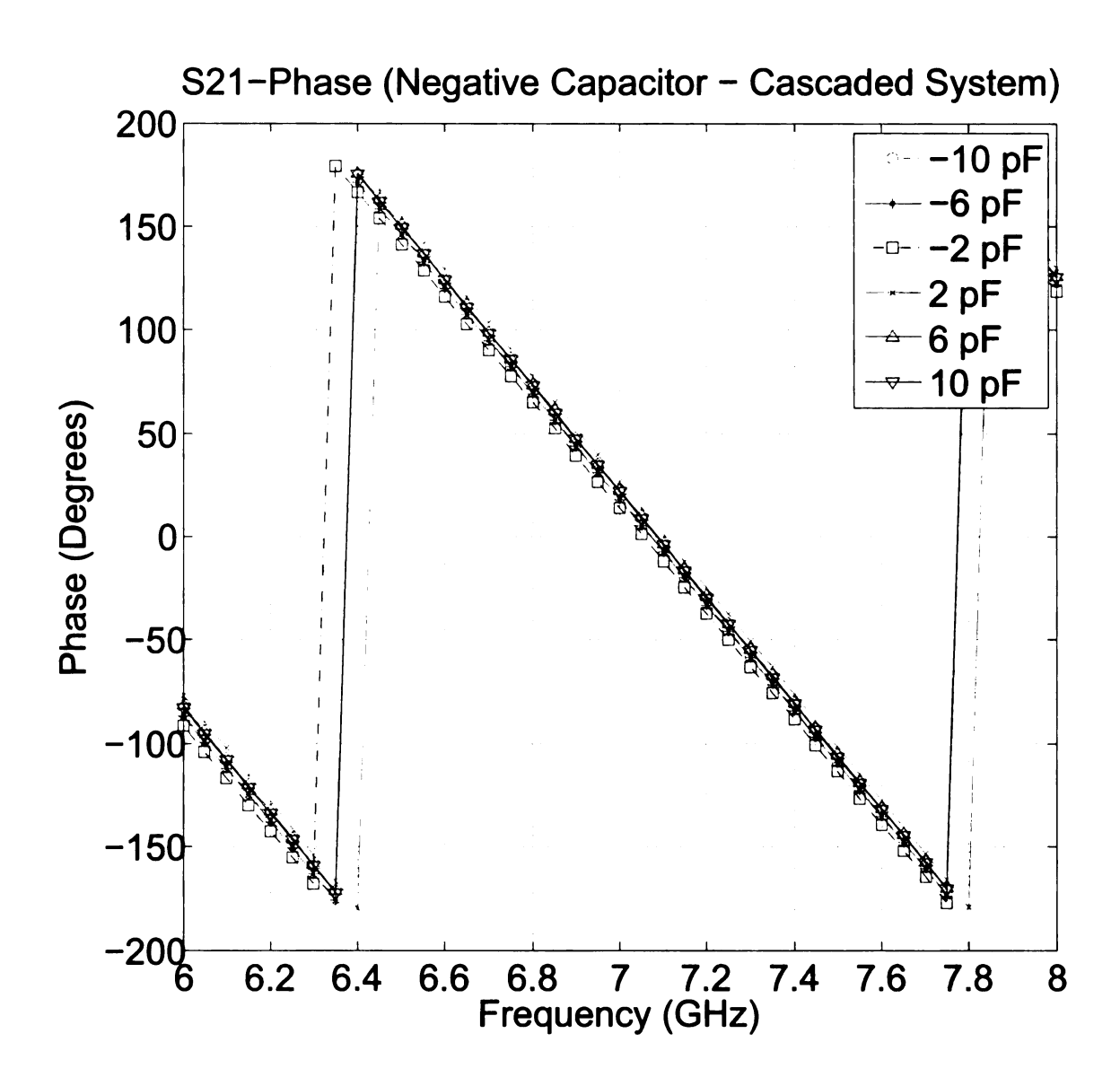


Figure 4.70. Phase of transmission coefficient of parameter study of cascaded system with capacitor varied from 10 pF to -10 pF

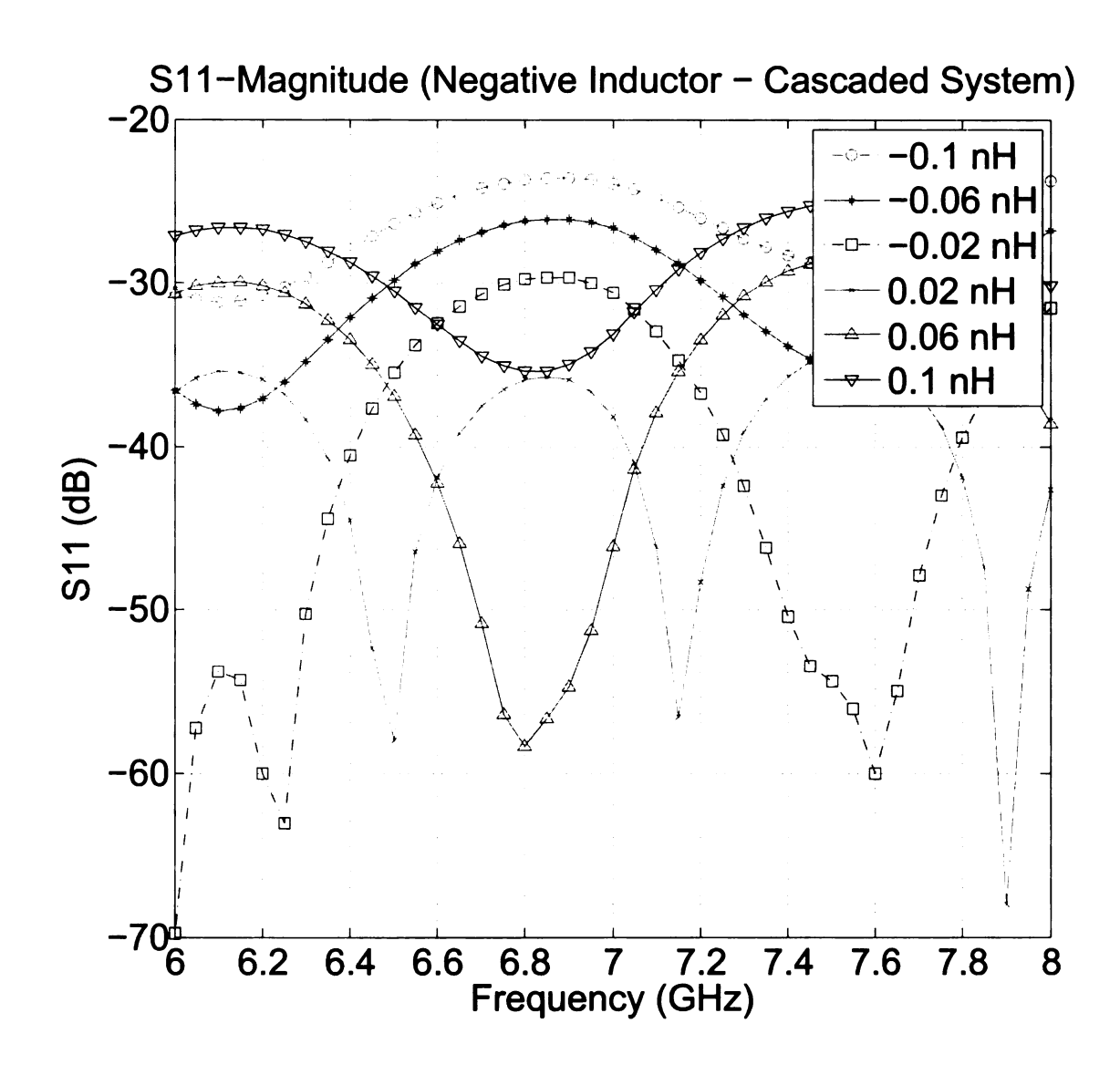


Figure 4.71. Magnitude of reflection coefficient of parameter study of cascaded system with inductor varied from $0.1~\mathrm{nH}$ to $-0.1~\mathrm{nH}$

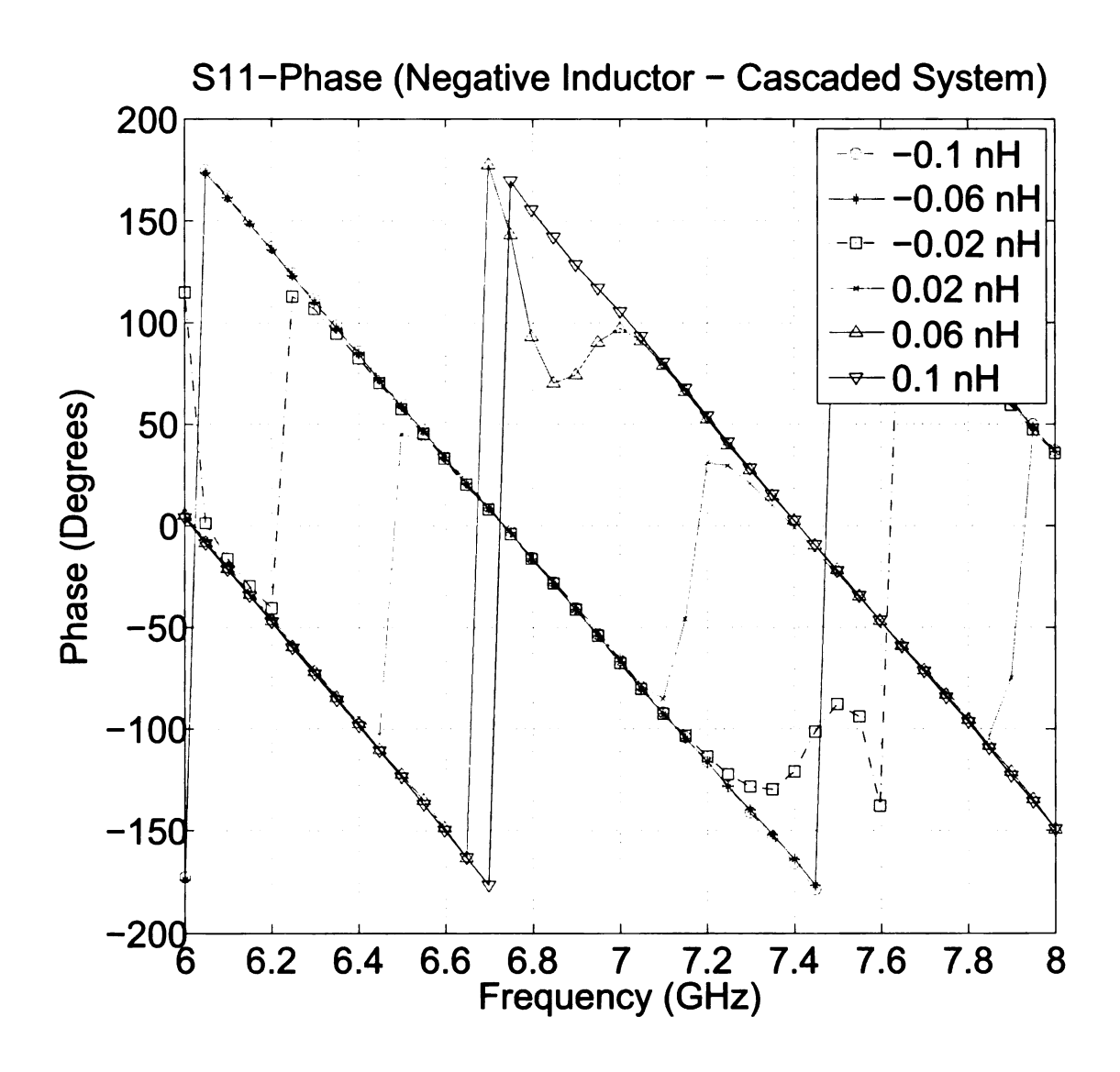


Figure 4.72. Phase of reflection coefficient of parameter study of cascaded system with inductor varied from $0.1~\mathrm{nH}$ to $-0.1~\mathrm{nH}$

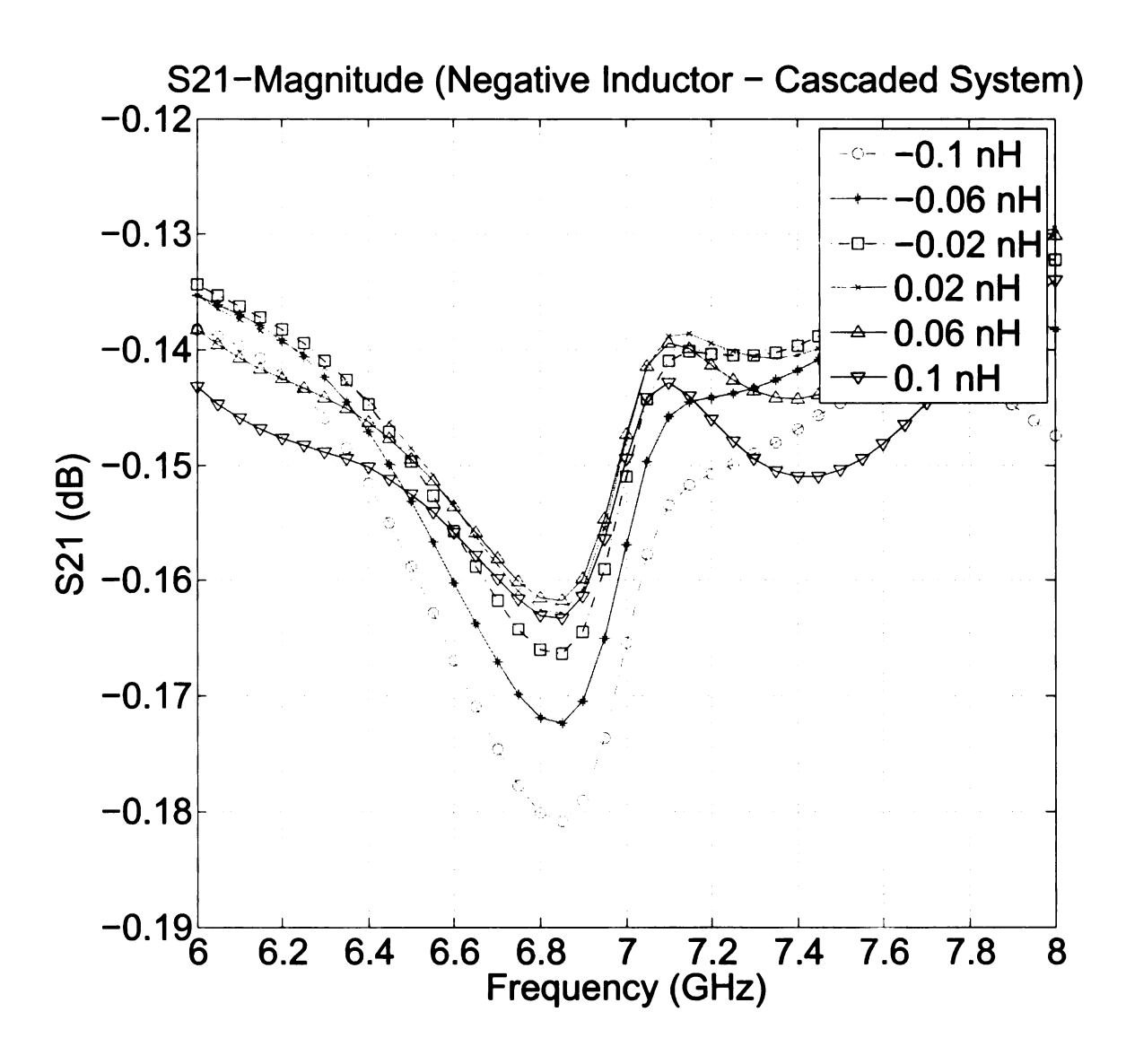


Figure 4.73. Magnitude of transmission coefficient of parameter study of cascaded system with inductor varied from $0.1~\mathrm{nH}$ to $-0.1~\mathrm{nH}$

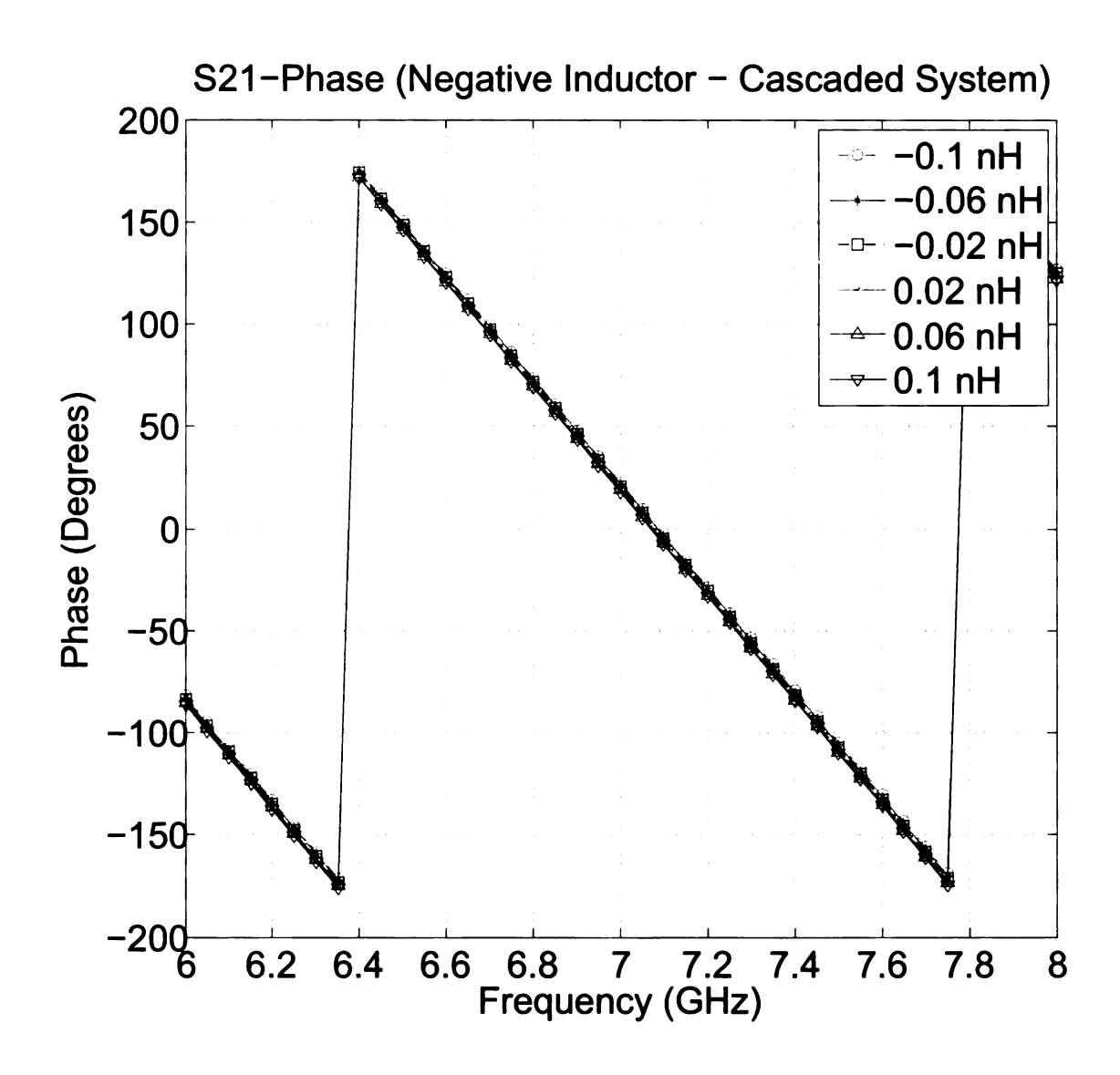


Figure 4.74. Phase of transmission coefficient of parameter study of cascaded system with inductor varied from $0.1~\mathrm{nH}$ to $-0.1~\mathrm{nH}$

CHAPTER 5

CONCLUSIONS AND FUTURE WORK

The purpose of this thesis is to analyze the behavior of a negative impedance converter attached to a microstrip transmission line in the C-band frequency bandwidth. This required modeling the NIC such that it operated in this frequency range. Using microwave network analysis, Fosters reactance theorem, and circuit analysis, non-Foster circuits can be realized with NICs. The non-Foster circuit that was observed was a grounded, voltage inversion, open-circuit stable NIC. This NIC was modeled using bipolar-junction transistors in such a way that it would be able to operate in the frequency bandwidth of interest and have it produce at optimal performance. In this particular case, the main transistor operated in the common-base configuration to reduce instabilities inherent for BJTs. Another transistor operating in the common-emitter configuration was present in the non-Foster circuit, but its purpose was to bias the voltage at its output to be in phase with the input voltage of the overall circuit.

The two-stage de-embedding process by the way of *Thru-Reflect-Line* calibration was needed to measure the S-parameters of the NIC without any effects from the microstrip, test fixture, and test port cables. The first stage removed the measurements of the test fixture and recorded only the data of the composite system of the NIC attached to the microstrip. The second stage removed the measurements of the microstrip and tabulated information of only the NIC. Transmission line theory, microstrip circuit analysis, and microwave network analysis involving scattering and transmission parameters were required to perform the TRL calibration technique standards.

Once all the individual components of the entire system have been modeled in

Sonnet and Ansoft Designer, computational analysis was performed to analyze how the NICs would behave at high frequencies. The NICs that were observed were a negative capacitor and a negative inductor. A parameter study of components embedded within the half-length microstrips designed in Sonnet was performed to observe how the cascaded network would perform. A $50-\Omega$ resistor, a $75-\Omega$ resistor, a $100-\Omega$ resistor, a 10-pF capacitor, and a 10-nH inductor were used to conduct this study. Then, the reactive component values were varied from positive to negative values to see the trends of the performance of the cascaded network. This helped distinguish a negative capacitor from a positive inductor and a negative capacitor from a positive capacitor.

Significant work still needs to be done with this project. Future work to consider is use additional circuit simulation software programs such as Agilent ADS (Advanced Design System) or Ansoft HFSS (High Frequency Structural Simulator) to analyze how the NIC circuit will interact with the half-length microstrips. This will help the experimentalist observe how the NIC will perform using silicon-germanium transistors as they produce lower noise, higher amplification, and need less power to achieve maximum performance at high frequencies compared to silicon transistors.

The circuit will be built and tested using the TRL calibration procedure outlined in [19] comparing all simulated models and the computational information evaluated in MATLAB. In addition, the characteristic impedances of the Anritsu 3680-20 Universal Test Fixture and the test port cables of the VNA (in this case the HP 8510 vector network analyzer) need to be measured to construct a better model of connectors A and B for the calibration method. Also, the TRL calibration procedure needs to be performed on the VNA outlined in [19].

BIBLIOGRAPHY

BIBLIOGRAPHY

- [1] J.T. Aberle and R. Loepsinger-Romak, "Antennas with Non-Foster Matching Networks," 1st Edition, Morgan and Claypool, 2007.
- [2] E.J. Rothwell and M.J. Cloud, *Electromagnetics*, CRC Press, Boca Raton, Florida, 2001.
- [3] R.F. Harrington, Time-Harmonic Electromagnetic Fields, McGraw-Hill, New York, 1961.
- [4] C.A. Balanis, Advanced Engineering Electromagnetics, 1st edition, Wiley, N.Y., 1989.
- [5] D.M. Pozar, Microwave Engineering, 3rd Edition, Wiley, N.Y., 2005.
- [6] J.L. Merill, "Theory of the Negative Impedance Converter, Bell System Technical Journal, Vol. 30, pp. 88109, Jan. 1951.
- [7] S.E. Sussman-Fort, "Matching Network Design Using Non-Foster Impedances," International Journal of RF and Microwave Computer-Aided Engineering, Volume 16, Issue 2, pp. 135 - 142, Published Online (IEEE Explore): Feb. 8, 2006, Copyright 2006 Wiley Periodicals, Inc. [Accessed: July 2, 2007].
- [8] S.E. Sussman-Fort, "Gyrator-based Biquad Filters and Negative Impedance Converters for Microwaves," International Journal of RF and Microwave Computer-Aided Engineering, Volume 8, Issue 2, Pages 86 101, Published Online: December 7, 1998, Wiley, [Accessed: July 6, 2007].
- [9] S.E. Sussman-Fort, "Matching Network Design Using Non-Foster Impedances" Powerpoint Presentation, International Journal of RF and Microwave Computer-Aided Engineering, Volume 16, Issue 2, pp. 135 - 142, Published Online (IEEE Explore): Feb. 8, 2006, Copyright 2006 Wiley Periodicals, Inc. [Accessed: July 2, 2007].
- [10] R.F. Pierret, Semiconductor Device Fundamentals, Addison-Wesley, 1996.
- [11] M.N. Horenstein, Microelectronic Circuits and Devices, 2nd Edition, Prentice Hall, N.J., 1996.
- [12] P. Horowitz and W. Hill, The Art of Electronics, 2nd Edition, Cambridge, 1989.

- [13] J.G. Linvill, "Transistor Negative-Impedance Converters," Proceedings of the IRE, Vol. 41, Issue 6, pp. 725-729, June 1953, Published Online (IEEE Explore) [Accessed: July 3, 2007].
- [14] J. Popovic and A. Pavasovic, "Voltage-driven negative impedance converter based on the modified Fabre-Normand CMOS current conveyor," 24th International Conference on Microelectronics, May 16-19, 2004, Volume: 2, pp. 543-546, Published Online (IEEE Explore): July 19, 2004 [Accessed: September 10, 2007].
- [15] R.L. Brennan, T.R. Viswanathan, and J.V. Hanson, "The CMOS Negative Impedance Converter," IEEE Journal of Solid-State Circuits, Volume 23, Issue 5, October 1988, pp. 1272-1275, Posted Online (IEEE Explore): August 6, 2002 [Accessed: July 3, 2007].
- [16] "Agilent De-embedding and Embedding S-Parameter Networks Using a Vector Network Analyzer," Agilent Application Note 1364-1, May 2004.
- [17] "Agilent Network Analysis Applying the 8510 TRL Calibration for Non-Coaxial Measurements," Agilent Product Note 8510-8A, July 2006.
- [18] P. Barba, "Numerical S-parameter and characterization of Inhomogeneously Filled Waveguides," Ph.D. Dissertation, Michigan State University, East Lansing, MI, 2006.
- [19] R. Franklin, "Microwave Test Flxture Characterization De-embedding Techniques Manual," Directed Study, University of Michigan, Ann Arbor, MI, 1990.
- [20] D. Schrader, Microstrip Circuit Analysis, Prentice Hall, 1995.
- [21] P. J. Matthews and J. J. Song, "RF Impedance Measurement Calibration," LS Note 223, Argone National Laboratory, IL, Feb. 12, 1993.
- [22] G. F. Engen, C. A. Hoer, "Thru-Refect-Line: An Improved Technique for Calibrating the Dual Six-Port Automatic Network Analyzer," IEEE Trans. Microwave Theory Tech., Volume 27, Issue 12, pp. 987-993, Dec. 1979.
- [23] "Anritsu 3680 Series Universal Test Fixture Operation and Maintenance Manual," U.S. Patent No. 5,017,865, Anritsu Company, June 1998.
- [24] R. Wang, "Bipolar Junction Transistor (BJT)," Introduction to Electrical Engineering (E84): Chapter 4 Lecture Notes, Harvey Mudd College, Claremont, CA, http://fourier.eng.hmc.edu/e84/lectures/ch4/node3.html, Page Updated: January 9, 2008 [Accessed Online: March 3, 2008].

